A Multi-faceted Approach for Targeting Metabolic and EMT Networks in Breast Cancer Cells

A Thesis

Submitted in Partial Fulfillment of the Requirements for the Degree of

DOCTOR OF PHILOSOPHY

By

Thirukumaran K

(Roll no. – 206106023)

Indian Institute of Technology Guwahati

Department of Biosciences & Bioengineering

Indian Institute of Technology Guwahati

Guwahati, 781039, Assam, India

DEDICATED TO MY FAMILY & FRIENDS

DECLARATION

I hereby declare that the results and discussions embodied in the thesis titled "**A Multi-faceted Approach for Targeting Metabolic and EMT Networks in Breast Cancer Cells"** are the outcome of research work carried out by me under the supervision of Prof. Siddhartha Sankar Ghosh, Department of Biosciences & Bioengineering, Indian Institute of Technology Guwahati, Guwahati, Assam, India for the award of the degree of Doctor of Philosophy. To the best of my knowledge and belief, the present thesis has not been submitted for any degree, diploma, associateship etc. of any Institute or University elsewhere.

Date: 25.02.2025

Place: Guwahati

Thirukumaran K

Roll number: 206106023

INDIAN INSTITUTE OF TECHNOLOGY GUWAHATI

DEPARTMENT OF BIOSCIENCES AND BIOENGINEERING

CERTIFICATE

This is to certify that this thesis entitled "**A Multi-faceted Approach for Targeting Metabolic and EMT Networks in Breast Cancer Cells**" has been submitted by **Thirukumaran K** (Roll No. **206106023**) to **Indian Institute of Technology Guwahati** for the award of the degree of **Doctor of Philosophy** in Department of Biosciences and Bioengineering**.** This thesis is a record of the bonafide research work carried out by him during his degree tenure. The findings presented here are purely derived from his own research work. He has meticulously performed the research and has been ardently adherent of lab protocols. This work in parts or as a whole is novel and is not been produced in any previous diploma or degree.

Date: 25.02.2025

Place: Guwahati

Prof. Siddhartha Sankar Ghosh

(Thesis Supervisor)

Acknowledgement

"*The roots of all goodness lie in the soil of appreciation for others*."

– Dalai Lama

I am deeply grateful to everyone who has supported me throughout my doctoral journey, without whom this thesis would not have been possible. First and foremost, I would like to express my sincere gratitude to my supervisor, **Prof. Siddhartha Sankar Ghosh**, for his invaluable guidance, encouragement, and unwavering belief in my potential. His mentorship has been pivotal to both my professional growth and my ability to overcome the challenges of this research. I am also grateful to my doctoral committee members, **Prof. Biplab Bose (Chairperson), Prof. Senthil Kumar S,** and **Prof. Lal Mohan Kundu**, for their insightful feedback, constructive critiques, and constant support. Their expertise and thoughtful recommendations have been instrumental in shaping this work. I would like to acknowledge the Department of Biosciences and Bioengineering (BSBE), Centre for Nanotechnology, Central Instrumentation Facility (CIF), and Param-Ishan HPC facility for providing the infrastructure and resources necessary to conduct this research.

A special thanks to my seniors, **Dr. Anitha T. Simon, Dr. Rajib Shome, Dr. Debashree Debasmita, Dr. Plaboni Sen, Dr. Muktashree Saha, Dr. Konika Choudhury,** and **Dr. Arupam Patra**. Their encouragement, insightful discussions, and camaraderie made this journey smoother and more enriching. My heartfelt appreciation extends to my lab members, **Shilpi, Arisha, Basab, Dheepika, Pijush, Parijat, Hirak, Sayantani Mukhopadhyay, Sawna, Sayantani Biswas, Sujisha, Haseena, Sailayee** and **Pratik.** Their teamwork, humor, and dedication created a positive and inspiring lab environment that I will always cherish.

I am also grateful for the enduring support of my friends, **Shilpi, Bharathi, Pradeep, Kannan, Thilag, Shanmugam, Giri, Muthu Velan, Krishna Kumar, and Soumen**. Their friendship and support helped me stay balanced and motivated throughout this journey. I extend my heartfelt gratitude to **Tamil Sangam IITG**, a community that has been a home away from home. The warmth, camaraderie, and cherished experiences I gained through this vibrant community have been an invaluable part of my journey, making my time here truly memorable. A special mention goes to my brother, **Manibalan**, whose constant encouragement and belief in my abilities have always pushed me forward. Lastly, I am forever indebted to my **Family members** for their unwavering support, patience, and love. Their sacrifices and encouragement have been the foundation of my success, and I dedicate this achievement to them.

Thank you all for being part of this journey.

Thirukumaran

Table of Contents

Abstract

Breast cancer, marked by its molecular heterogeneity and complex pathophysiology, remains a global health challenge despite advancements in therapies such as surgery, chemotherapy, and targeted approaches. Aggressive subtypes like triple-negative breast cancer (TNBC) show high rates of metastasis and resistance to standard treatments, highlighting the need for novel therapeutic approaches. Drug repurposing—the use of existing drugs for new therapeutic applications—has emerged as a promising strategy in cancer treatment, offering established safety profiles and the potential to address unmet clinical needs. This thesis investigates a multi-faceted approach to breast cancer therapy, targeting the interconnected networks of altered cancer cell metabolism and epithelial-to-mesenchymal transition (EMT), processes central to cancer progression, therapy resistance, and metastasis.

Chapter 1 introduces the complexities of breast cancer, with an emphasis on the limitations of current therapies in treating aggressive subtypes. This chapter discusses the role of drug repurposing as a viable strategy to enhance treatment efficacy by repositioning existing drugs with potential anti-cancer properties. Through a detailed literature review, various repurposing methods—computational screening, network pharmacology, and validation via *in vitro* and *in vivo* studies—are examined. The chapter also considers approaches to maximize the efficacy of repurposed drugs through combination therapies and advanced drug delivery systems, establishing a strong foundation for therapeutic framework of this study.

Chapter 2 investigates a network-based approach to drug repurposing, focusing on EMT and metabolic targets within breast cancer cells. Network analysis identified key proteins—Insulin Receptor (IR), Integrin beta 1 (ITGB1), and CD36—associated with EMT and metabolic reprogramming in cancer. Computational screening of FDA-approved drugs revealed Pimozide and Ponatinib as potent inhibitors of these targets. Molecular docking and dynamics simulations, followed by MMPBSA binding free energy studies, highlighted their strong interactions with these proteins. Initial *in vitro* validation demonstrated that Pimozide had significant anti-proliferative effects on breast cancer cell lines,

including MCF7, MDA-MB-231, and MDA-MB-468, with further enhancement in EMT-induced cells. This section thus identifies potential drugs for repurposing and validates their impact on critical targets in breast cancer.

In Chapter 3, Pimozide and Ponatinib were combined to enhance their efficacy against breast cancer through a multicomponent molecular dynamics approach, aiming to simultaneously inhibit IR, ITGB1, and CD36. The synergistic action of the combination treatment was validated *in vitro* in both monolayer and 3D tumor spheroid models of MCF-7 and MDA-MB-231 cells. The combination induced approximately 40% apoptosis, with significant reductions in the expression of proteins critical for EMT and metabolic processes, including IR, p-IR, IRS-1, and p-AKT. Furthermore, the treatment reduced fatty acid uptake, lipid accumulation, cancer stemness, and cell migration, demonstrating broad anti-cancer effects. This chapter establishes the potential of combination therapies targeting multiple pathways to effectively combat aggressive breast cancer phenotypes.

In Chapter 4, a drug cocktail approach was employed to minimize metabolic load and potential toxicity by carefully selecting chemotherapy drugs whose metabolizing enzymes do not overlap with those of Pimozide. A combination of Epirubicin, SAHA, and Pimozide (ESP) was identified as a synergistic cocktail. Cytotoxicity studies demonstrated that the ESP combination significantly lowered the IC_{50} of Pimozide, with a 30-fold reduction in MCF-7 and a 6-fold reduction in MDA-MB-231 cell lines. Mechanistic studies showed increased ROS generation, higher cleaved PARP levels, and activation of p53 and p21, alongside reduced AKT signaling. This multi-drug approach also reduced cancer stemness, invasiveness, and lipid accumulation, confirming its effectiveness in reducing cancer cell viability while minimizing systemic toxicity. This chapter illustrates how tailored drug cocktails can enhance therapeutic outcomes in breast cancer by optimizing drug efficacy and reducing resistance.

Chapter 5 explores pH-responsive drug delivery as a targeted approach to improve the delivery and efficacy of repurposed drugs in the acidic tumor microenvironment. Pimozide was encapsulated within Zeolitic Imidazolate Framework-8 (ZIF-8) nanoparticles using a single-step method. Characterization studies verified successful encapsulation, and pH-sensitive release profiles showed that 84.13% of

Pimozide was released in pH 6 conditions, versus 37.47% at physiological pH. *In vitro* cytotoxicity assays demonstrated that the Pimozide-ZIF-8 composite retained anti-cancer activity while reducing systemic side effects. This targeted delivery approach underscores the potential of using pH-sensitive frameworks for controlled drug release in the tumor microenvironment, enhancing therapeutic potency and reducing toxicity.

Collectively, this thesis demonstrates that a multi-pronged strategy—combining drug repurposing, synergistic drug combinations, and targeted delivery systems—can overcome many of the challenges associated with current breast cancer therapies. By targeting both EMT and metabolic pathways, this work offers promising avenues for the development of more effective treatments for aggressive breast cancer subtypes. The findings lay the groundwork for future translational research, bringing novel, multi-targeted therapies closer to clinical application in breast cancer treatment.

भारतीय प्रौद्योगिकी संस्थान गुवाहाटी
Indian Institute of Technology Guwahati

List of Abbreviations

ADME	Absorption, Distribution, Metabolism, and Excretion
AFM	Atomic Force Microscopy
AKT	Protein Kinase B
ALT	Alanine Aminotransferase
AMPK	AMP-Activated Protein Kinase
ATP	Adenosine Triphosphate
BRAF	B-Raf Proto-Oncogene
CD36	Cluster of Differentiation 36
CDK4/6	Cyclin-Dependent Kinases 4 and 6
CTLA-4	Cytotoxic T-Lymphocyte-Associated Protein 4
cAMP	Cyclic Adenosine Monophosphate
DLC	Drug Loading Content
DLE	Drug Loading Efficiency
DCFDA	Dichlorofluorescin Diacetate
DMEM	Dulbecco's Modified Eagle Medium
DLS	Dynamic Light Scattering
DOCK	Docking
DNA	Deoxyribonucleic Acid
EGFR	Epidermal Growth Factor Receptor
EMBL	European Molecular Biology Laboratory
EMT	Epithelial-to-Mesenchymal Transition
ESP	Etoposide, Salinomycin, Pimozide
FASN	Fatty Acid Synthase
FDA	Food and Drug Administration
FE-SEM	Field Emission Scanning Electron Microscopy
FE-TEM	Field Emission Transmission Electron Microscopy
FITC	Fluorescein Isothiocyanate
FAT	Fatty Acid Transporter
FTIR	Fourier Transform Infrared Spectroscopy
GLS	Glutaminase
GLUT4	Glucose Transporter Type 4
GROMACS	Groningen Machine for Chemical Simulations
HER2	Human Epidermal Growth Factor Receptor 2
HK2	Hexokinase 2
HPLC	High-Performance Liquid Chromatography
HR+	Hormone Receptor-Positive
HTS	High-Throughput Screening
IC_{50}	Half Maximal Inhibitory Concentration

IR	Insulin Receptor
IRS-1	Insulin Receptor Substrate 1
ITGB1	Integrin Beta 1
LDHA	Lactate Dehydrogenase A
LC-MS	Liquid Chromatography-Mass Spectrometry
MAPK	Mitogen-Activated Protein Kinase
MCF-7	Michigan Cancer Foundation-7 (breast cancer cell line)
MDA-MB-231	Triple-negative breast cancer cell line
MDA-MB-468	Triple-negative breast cancer cell line
MET	Mesenchymal-Epithelial Transition Factor
MMPs	Matrix Metalloproteinases
MMPBSA	Molecular Mechanics Poisson–Boltzmann Surface Area
MOF	Metal-Organic Framework
mTOR	Mechanistic Target of Rapamycin
MTT	3-(4,5-Dimethylthiazol-2-yl)-2,5-Diphenyltetrazolium Bromide
NF-κB	Nuclear Factor Kappa B
NGS	Next-Generation Sequencing
NRF2	Nuclear Factor Erythroid 2-Related Factor 2
NPT	Isothermal-Isobaric Ensemble
NVT	Isothermal-Isochoric Ensemble
PCA	Principal Component Analysis
PDB	Protein Data Bank
PGI	Phosphoglucose Isomerase
PI	Propidium Iodide
PI3K	Phosphoinositide 3-Kinase
PKM2	Pyruvate Kinase M2
PPAR-γ	Peroxisome Proliferator-Activated Receptor Gamma
PPI	Protein–Protein Interaction
PR	Progesterone Receptor
p-AKT	Phosphorylated AKT
p-IR	Phosphorylated Insulin Receptor
QSAR	Quantitative Structure-Activity Relationship
RIPA	Radioimmunoprecipitation Assay
RMSD	Root Mean Square Deviation
RMSF	Root Mean Square Fluctuation
ROS	Reactive Oxygen Species
SAHA	Suberoylanilide Hydroxamic Acid
SNAI1	Snail Family Transcriptional Repressor 1
SOD2	Superoxide Dismutase 2
SPR	Surface Plasmon Resonance
STAT3	Signal Transducer and Activator of Transcription 3
SWISS	Swiss Institute of Bioinformatics Tools

TCA	Tricarboxylic Acid Cycle
TGF-β	Transforming Growth Factor Beta
TME	Tumor Microenvironment
TNBC	Triple-Negative Breast Cancer
UV	Ultraviolet
VEGF	Vascular Endothelial Growth Factor
WNT	Wingless-Related Integration Site
XRD	X-ray Diffraction
ZEB	Zinc Finger E-Box Binding Homeobox
ZIF-8	Zeolitic Imidazolate Framework-8

List of Figures

List of Tables

CHAPTER 1

Introduction and Review of Literature

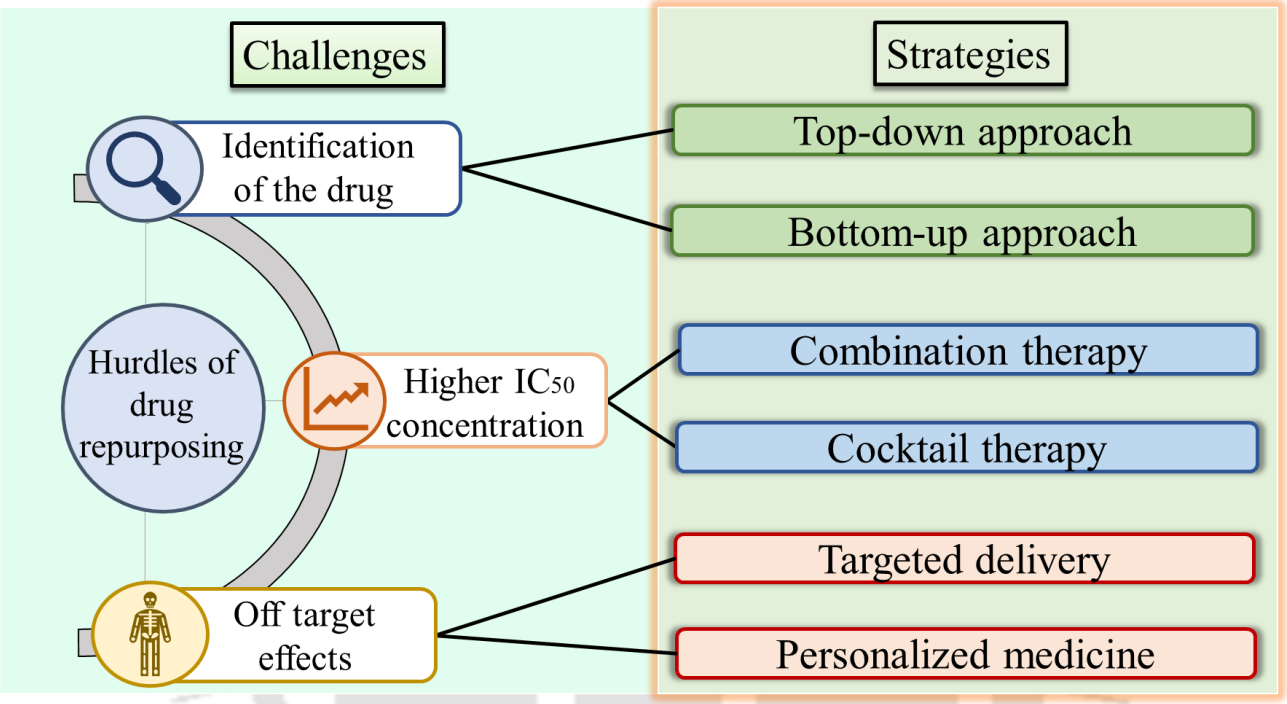

Chapter 1 introduces the clinical and molecular challenges of breast cancer, focusing on aggressive subtypes like TNBC. It reviews current treatment limitations and explores drug repurposing as a strategy to target altered metabolism and EMT in breast cancer, setting the stage for novel therapeutic approaches.

ACS Pharmacology & Translational Science, 2024
DOI: 10.1021/acsptsci.4c00545

CHAPTER 1

Introduction & Review of Literature

Breast cancer is a multifaceted disease characterized by its molecular heterogeneity and complex pathophysiology, making it a significant therapeutic challenge [1]. It remains one of the most common cancers affecting women worldwide, contributing to considerable morbidity and mortality [1]. The heterogeneity of breast cancer is evident at several levels, including genomic, transcriptomic, and epigenetic variations [2]. Genomic heterogeneity involves differences in DNA sequences, such as mutations, copy number alterations, and structural rearrangements. Transcriptomic heterogeneity reflects variations in gene expression profiles, while epigenetic heterogeneity includes changes in DNA methylation and histone modifications that regulate gene expression without altering the DNA sequence [2]. These variations contribute to the complex behavior of breast cancer, influencing its progression, response to treatment, and prognosis.

The primary molecular subtypes of breast cancer include hormone receptor-positive (HR+), human epidermal growth factor receptor 2-positive (HER2+), and triple-negative breast cancer (TNBC) [2]. HR+ cancers express estrogen receptors (ER) and progesterone receptors (PR), often responding to hormonal therapies [3, 4]. HER2+ cancers are characterized by the overexpression of the HER2 protein, targeted by specific therapies like trastuzumab. TNBC, which lacks ER, PR, and HER2 expression, is particularly aggressive and primarily treated with chemotherapy [3, 4]. Breast cancer progression involves several key processes, such as uncontrolled cell proliferation, evasion of apoptosis, angiogenesis, and metastasis [5, 6]. Aberrant cell division leads to tumor growth, while mechanisms that allow cancer cells to avoid programmed cell death contribute to their survival. Further, angiogenesis, the formation of new blood vessels, facilitates the supply of nutrients and oxygen to the growing tumor. Eventually, the spread of cancer cells to distant organs or metastasis accentuates breast cancer-related deaths and represents a significant challenge for effective treatment [5, 6].

Current treatment strategies for breast cancer include surgery, radiation therapy, chemotherapy, hormonal therapy, and targeted therapy (**Figure 1.1A**). Despite these options, several challenges persist in breast cancer therapy, such as developing resistance to standard treatments, thereby reducing their efficacy over time [7]. Further, the ability of cancer cells to spread to distant sites

complicates treatment and worsens the prognosis [8]. Chemotherapy and radiation therapy often cause significant side effects, impacting the quality of patient life [7]. Additionally, the diverse nature of breast cancer subtypes requires personalized treatment approaches, complicating the development of universal therapies.

Drug repurposing, also known as drug repositioning, has emerged as a promising strategy to address these challenges. It involves finding new therapeutic uses for existing drugs, leveraging their established safety profiles and known pharmacokinetics [9]. This strategy can reduce the time and cost associated with drug development (**Figure 1.1B**). In breast cancer treatment, several repurposed drugs, such as anti-diabetic drugs (e.g., Metformin), anti-inflammatory drugs (e.g., Aspirin), anti-microbial drugs (e.g., Doxycycline), anti-psychotic drugs (e.g., Pimozide), beta-blockers (e.g., Propranolol), anti-rheumatic drugs (e.g., methotrexate), and anti-alcoholism drugs (e.g., Disulfiram), have shown potential in overcoming limitations of conventional therapies, such as drug resistance, toxicity, and limited efficacy in certain subtypes [10 - 16]. By exploring the mechanisms through which these drugs exert their anti-cancer effects, researchers can identify novel therapeutic targets and develop combination therapies that enhance treatment efficacy while minimizing toxicity. This approach is particularly valuable in addressing the challenges posed by breast cancer heterogeneity, as it allows for the development of personalized treatment strategies that cater to the specific molecular characteristics of each subtype. While drug repurposing provides advantages like reduced development time and cost, it also faces challenges such as suboptimal targeting of cancer cells and regulatory requirements for re-evaluation in new therapeutic contexts, despite prior approval for other conditions.

In this study, particular emphasis is placed on cellular processes that can be effectively targeted by repurposed drugs, such as altered metabolism and epithelial-to-mesenchymal transition (EMT). Altered metabolism supports cancer cell survival and proliferation, while EMT contributes to metastasis and drug resistance. Targeting these processes offers a strategic approach to disrupting cancer progression. In addition, this work highlights advancements in drug repurposing for breast cancer, exploring innovative strategies for identifying new therapeutic uses for existing drugs. Furthermore, the current approaches to overcome the limitations of repurposed drugs, such as combination therapy and targeted delivery using nanoparticles, are also addressed to enhance their

efficacy and reduce toxicity. This comprehensive overview aims to highlight the potential of drug repurposing in developing effective and less toxic treatments for breast cancer.

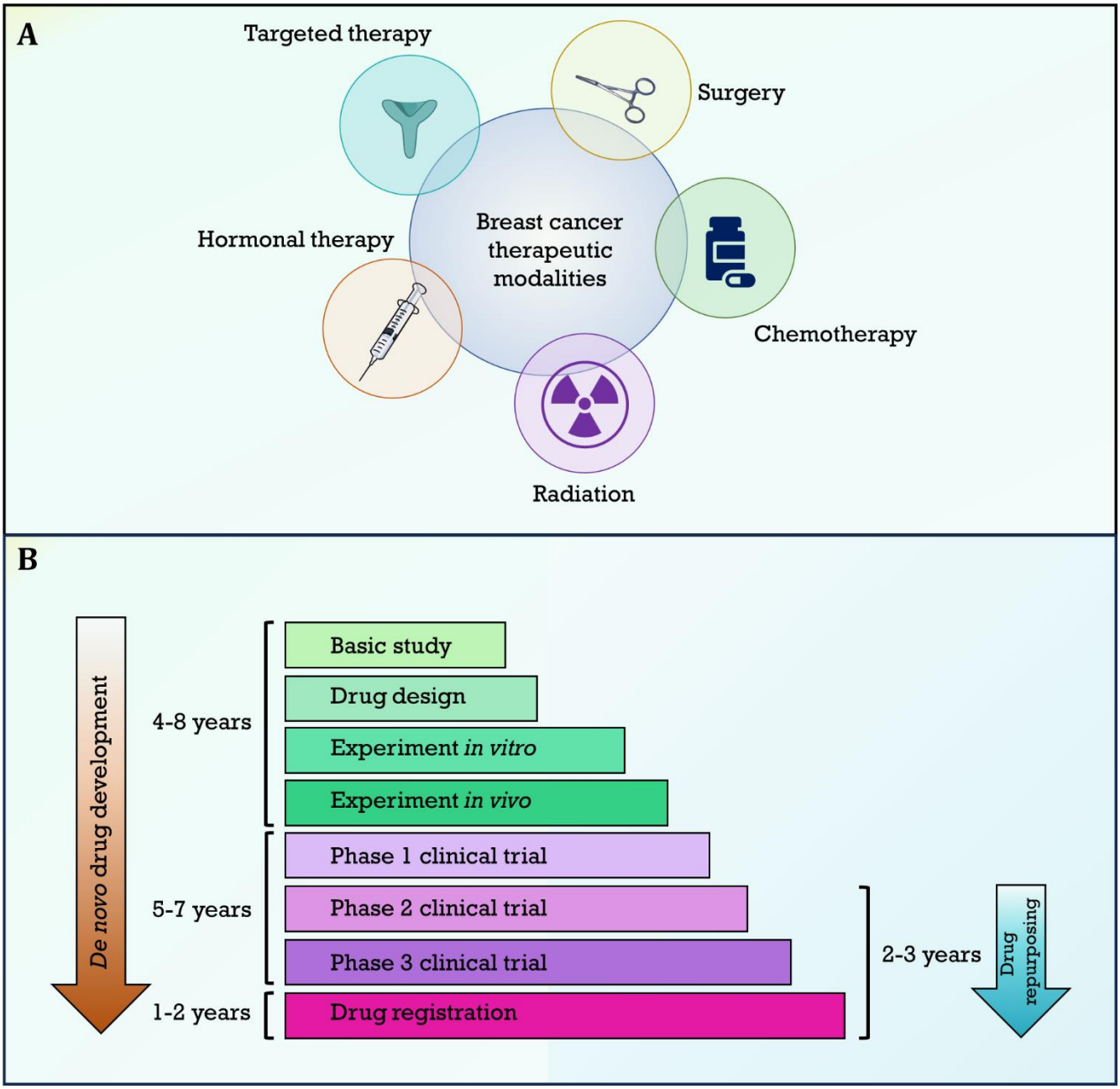

Figure 1.1: A) *Conventional therapeutic approaches for breast cancer treatment.* ***B)*** *Timeline of de novo drug development vs drug repurposing approach.* ***(****Reproduced with permission from Thirukumaran, K., et al. ACS Pharmacology & Translational Science, 2024. DOI: 10.1021/acsptsci.4c00545)*

1.1. Targeting Altered Metabolism and EMT Signaling in Breast Cancer

Breast cancer, like other cancers, is driven by several hallmarks that facilitate its growth, survival, and metastasis **(Table 1.1)**. Based on the latest literature, an illustration has been created to depict the heterogeneous nature of breast cancer and the associated hallmarks of the disease (**Figure 1.2**). These hallmarks include sustaining proliferative signaling through oncogenes such as HER2 and EGFR, evading growth suppressors by inactivating tumor suppressor genes like TP53 and RB1, resisting cell death by overexpressing anti-apoptotic proteins such as Bcl-2, enabling replicative immortality by upregulating telomerase, inducing angiogenesis through factors like VEGF to ensure a blood supply, and activating invasion and metastasis by altering cell adhesion molecules and enhancing motility [5]. Additional hallmarks include deregulating cellular energetics through metabolic reprogramming (altered metabolism), avoiding immune destruction by modulating immune checkpoints, and promoting genomic instability and mutation [5]. Among several hallmarks of cancer, altered metabolism, and EMT are particularly crucial in breast cancer progression and metastasis. Targeting these pathways represents a promising therapeutic strategy for combating breast cancer.

1.1.1. Altered Metabolism in Breast Cancer

Cancer cells exhibit metabolic reprogramming to support their rapid growth and proliferation. One of the most well-known metabolic alterations is the Warburg effect, where cancer cells preferentially utilize glycolysis, a process that breaks down glucose to produce energy in the absence of oxygen, even when oxygen is available [17]. Normally, cells rely on oxidative phosphorylation, a more efficient, oxygen-dependent process that occurs in the mitochondria. However, this metabolic shift in cancer cells not only provides quick energy but also generates essential biosynthetic precursors required for the rapid division and growth of tumor cells, contributing to their aggressiveness. [17]. Key enzymes involved in glycolysis, such as hexokinase 2 (HK2), pyruvate kinase M2 (PKM2), and lactate dehydrogenase A (LDHA), are often upregulated in breast cancer cells, making them potential therapeutic targets [18].

Additionally, breast cancer cells exhibit increased glutaminolysis, a process where glutamine is converted into glutamate and subsequently into alpha-ketoglutarate, feeding into the tricarboxylic acid (TCA) cycle to support anabolism and maintain redox balance [19]. Inhibitors of glutaminase (GLS), the enzyme that catalyzes the first step of glutaminolysis, have shown potential in

preclinical models of breast cancer [20]. Fatty acid synthesis is another metabolic pathway that is often dysregulated in breast cancer. Overexpression of fatty acid synthase (FASN), the enzyme responsible for *de novo* fatty acid synthesis, has been associated with poor prognosis [21]. Targeting FASN and other enzymes involved in lipid metabolism presents a promising approach to impairing cancer cell growth and survival.

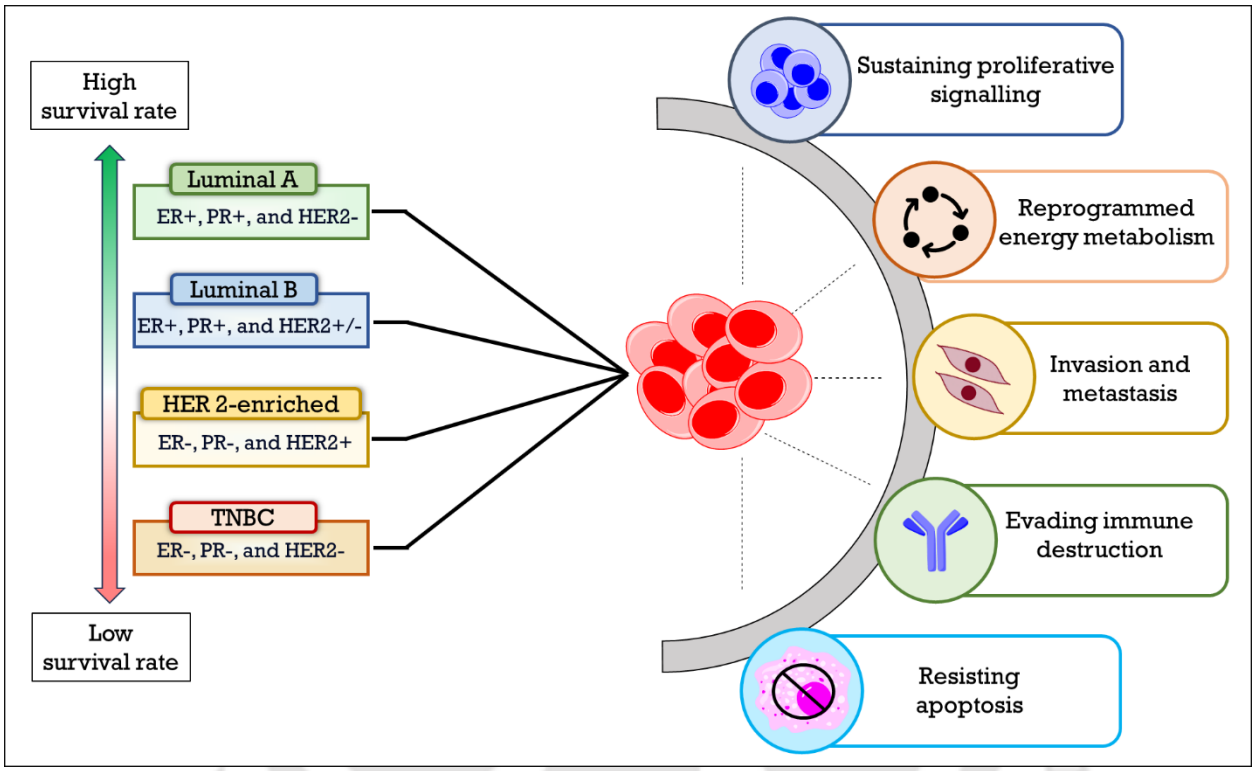

Figure 1.2: *Survival rate associated with the heterogeneous nature of breast cancer and the related hallmarks of the disease. (Reproduced with permission from Thirukumaran, K., et al. ACS Pharmacology & Translational Science, 2024. DOI: 10.1021/acsptsci.4c00545)*

1.1.2. EMT Signaling in Breast Cancer

EMT is a biological process through which epithelial cells lose their cell-cell adhesion properties and gain mesenchymal characteristics, enhancing their migratory and invasive capabilities. This process is critical for cancer metastasis, a hallmark of cancer that contributes significantly to cancer-related deaths [22]. EMT is regulated by several key transcription factors, including Snail, Slug, Twist, and ZEB1/2, which repress the expression of epithelial markers like E-cadherin and upregulate mesenchymal markers such as N-cadherin and vimentin. Signaling pathways such as

TGF-β, Wnt/β-catenin, Notch, and Hedgehog play pivotal roles in inducing and maintaining EMT [23]. These pathways are often aberrantly activated in breast cancer, leading to enhanced invasion, metastasis, and resistance to therapy. Targeting these pathways to inhibit EMT and reverse mesenchymal traits back to an epithelial state is an area of active research. For instance, inhibitors of TGF-β signaling (such as galunisertib) and Wnt/β-catenin signaling (like LGK974) have shown promise in preclinical studies [24, 25].

1.1.3. Interconnection Between Metabolism and EMT

There is growing evidence that metabolic reprogramming and EMT are interconnected processes that together drive cancer progression. For instance, EMT has been shown to induce metabolic changes that support the mesenchymal phenotype [26]. EMT transcription factors can regulate metabolic enzymes, altering pathways like glycolysis and fatty acid oxidation to favor cancer cell survival and dissemination. Conversely, metabolic changes can influence the EMT process [27]. For example, hypoxia-inducible factors (HIFs), which are stabilized under low oxygen conditions and promote glycolysis, can also activate EMT transcription factors, linking the metabolic state of the tumor microenvironment with EMT [28]. Given the interplay between these pathways, combined targeting of metabolism and EMT offers a strategic approach to disrupting breast cancer progression. Inhibiting key metabolic enzymes and signaling pathways involved in EMT could potentially reduce cancer cell proliferation, invasion, and metastasis, leading to improved therapeutic outcomes.

1.1.4. Potential Drug Targets

Identifying and targeting specific molecules involved in altered metabolism and EMT can provide novel therapeutic opportunities. Key drug targets in altered metabolism include glycolytic enzymes (e.g., HK2, PKM2, LDHA), glutaminase (GLS), and fatty acid synthase (FASN) [18, 21].

Glycolytic enzymes are critical for the Warburg effect, providing energy and biosynthetic precursors necessary for cancer cell proliferation [17]. HK2, PKM2, and LDHA are often overexpressed in cancer cells, making them attractive targets [29]. HK2 catalyzes the first step of glycolysis and is essential for glucose metabolism in cancer cells. Inhibitors of HK2, such as 2-deoxyglucose, have shown anti-cancer effects by reducing glycolysis and inducing apoptosis in

breast cancer cells. PKM2, an isoform of pyruvate kinase, promotes aerobic glycolysis and is involved in anabolic processes. Small molecule inhibitors targeting PKM2 can disrupt these metabolic pathways, inhibiting cancer cell growth. LDHA converts pyruvate to lactate, a key step in glycolysis, and its inhibition can reduce lactate production, affecting tumor microenvironment and cancer cell metabolism [18]. Glutaminase catalyzes the conversion of glutamine to glutamate, feeding into the TCA cycle. Breast cancer cells rely on glutaminolysis for energy and biosynthesis [19]. Inhibitors of GLS, such as CB-839, have shown promising results in preclinical models by disrupting glutamine metabolism, leading to reduced tumor growth and enhanced sensitivity to other treatments [30]. FASN is responsible for *de novo* lipid synthesis, which is crucial for rapidly dividing cancer cells. Overexpression of FASN is associated with poor prognosis in breast cancer. Targeting FASN can disrupt lipid metabolism, impairing cancer cell growth and survival. Orlistat, a known FASN inhibitor, has demonstrated anti-cancer effects in breast cancer models by reducing cell proliferation and inducing apoptosis [31].

In the context of EMT, drug targets include transcription factors (e.g., Snail, Slug, Twist, ZEB1/2) and signaling pathways (e.g., TGF-β, Wnt/β-catenin, Notch, Hedgehog) [32, 33]. Transcription factors like Snail, Slug, Twist, and ZEB1/2 are central regulators of EMT, controlling the expression of genes involved in cell adhesion, migration, and invasion [32]. Targeting these transcription factors can reverse EMT, reducing metastatic potential. For example, small molecules that inhibit Snail and Twist have been shown to restore epithelial characteristics and reduce invasion in breast cancer cells [23]. In addition, key signaling pathways such as TGF-β, Wnt/β-catenin, Notch, and Hedgehog are crucial for EMT induction and maintenance. Inhibitors of these pathways can block EMT and reduce metastasis [33]. Galunisertib, a TGF-β inhibitor, can suppress EMT and reduce metastatic spread [34]. LGK974, a Wnt/β-catenin inhibitor, can inhibit EMT and sensitize cancer cells to conventional therapies [25]. Notch pathway inhibitors, such as gamma-secretase inhibitors, have shown potential in reducing EMT and tumor growth in breast cancer models [35]. By targeting these critical molecules and pathways involved in altered metabolism and EMT, researchers can develop more effective therapeutic strategies for breast cancer.

Table 1.1: Hallmarks of Cancer and Corresponding Targeted and Repurposed Therapies

Hallmark	Pathways Involved	Molecular Targets	Examples of Targeted Therapies	Examples of Repurposed Drugs	References
Sustaining Proliferative Signaling	EGFR, HER2, MAPK, PI3K/AKT	EGFR, HER2, BRAF, PI3K	Trastuzumab, Cetuximab, Vemurafenib	Metformin (PI3K/AKT), Erlotinib (EGFR)	[10, 36, 37, 38, 39]
Evading Growth Suppressors	TGF-β, Rb, p53	TGF-βR, CDK4/6, MDM2	Palbociclib (CDK4/6), Nutlin-3 (MDM2)	Metformin (p53), Pioglitazone (CDK4/6)	[10, 40, 41, 42]
Resisting Cell Death	Bcl-2, p53, Apoptosis	Bcl-2, MDM2, Caspases	Venetoclax (Bcl-2), Navitoclax (Bcl-2)	Pimozide (p53), Metformin (p53)	[10, 43, 44]
Enabling Replicative Immortality	Telomerase, ALT	TERT, TRF2	Imetelstat (TERT)	Hydroxyurea (TERT)	[45, 46]
Inducing Angiogenesis	VEGF, HIF-1, Angiopoietins	VEGFR, PDGFR, Ang2	Bevacizumab (VEGF), Sunitinib (VEGFR)	Thalidomide (VEGF), Metformin (HIF-1)	[10, 47, 48, 49]
Activating Invasion and Metastasis	EMT, MMPs, Integrins	Snail, Slug, MMPs	Marimastat (MMPs), Galunisertib (TGF-β)	Metformin (EMT), Doxycycline (MMPs)	[10, 12, 34, 50]
Deregulating Cellular Energetics	Warburg effect, Glutaminolysis	HK2, GLS, LDHA	Lonidamine (HK2), CB-839 (GLS)	Metformin (Warburg effect), Dichloroacetate (LDHA)	[10, 51, 52, 53]
Avoiding Immune Destruction	PD-1/PD-L1, CTLA-4, IDO	PD-1, PD-L1, CTLA-4	Pembrolizumab (PD-1), Ipilimumab (CTLA-4)	Chloroquine (PD-L1)	[54, 55, 56]

1.2. Potential Drug Screening Methods for Repurposed Drugs

Historically, drug discovery and development were time-consuming and costly processes that primarily relied on serendipity and extensive *in vivo* testing. Before the advent of modern drug screening technologies, the identification of therapeutic agents was often based on empirical observations and trial-and-error methods. This approach led to the discovery of several important drugs, but it lacked precision and efficiency, resulting in long development times and high failure rates in clinical trials [57]. The advancement of technology and a deeper understanding of cancer biology made drug screening more systematic and efficient. The integration of high-throughput screening (HTS) technologies and computational methods has revolutionized drug discovery.

These technologies enable the rapid evaluation of thousands of compounds against specific cancer targets, significantly shortening the time required to identify promising candidates [58]. Moreover, the development of comprehensive drug databases and bioinformatics tools has facilitated the identification of potential repurposed drugs by leveraging existing data on drug-target interactions and molecular pathways [59, 60]. In the context of breast cancer, the impact of these modern drug screening methods has been profound. Traditional chemotherapy agents, while effective, often come with significant side effects and limitations. The identification of new therapeutic agents through advanced screening methods has led to the discovery of drugs that are more targeted and have fewer adverse effects. For instance, the repurposing of existing drugs such as Metformin and statins has opened new avenues for breast cancer treatment, offering additional options beyond conventional therapies [10].

Drug screening methods in breast cancer can indeed be approached using both top-down and bottom-up strategies. The application of both top-down and bottom-up approaches in drug screening enhances the ability to identify and validate repurposed drugs [61]. Top-down approaches leverage large-scale data analysis and experimental screening techniques to pinpoint potential candidates from existing drug libraries. This method is particularly advantageous for its speed and ability to handle vast amounts of data. In contrast, bottom-up approaches delve into the molecular and genetic mechanisms of breast cancer, allowing for a more targeted and precise identification of drug candidates based on specific aberrations within cancer cells. Combining these approaches not only broadens the scope of potential therapeutic agents but also enhances the understanding of their mechanisms of action. This integrated strategy is crucial for developing effective and personalized treatments for breast cancer, ultimately improving patient outcomes and expanding the arsenal of available therapies.

1.2.1. Top-Down Approaches

Top-down approaches typically start with existing drugs and screen them for new therapeutic applications against breast cancer. These methods often leverage large-scale data analysis and experimental screening techniques to identify candidate drugs. HTS, Drug Repositioning Databases, and Phenotypic Screening often fall under the top-down approaches (**Figure 1.3A**).

1.2.1.1. High-Throughput Screening:

HTS allows for the rapid screening of thousands of compounds to identify those with potential anti-cancer effects. Automated robotic systems and sophisticated detection methods are used to evaluate drug libraries against breast cancer cell lines [58]. For example, a study used HTS to screen a library of FDA-approved drugs and identified Metformin as a potential anti-cancer agent due to its ability to inhibit cancer cell proliferation [62]. Another HTS study identified itraconazole, an anti-fungal drug, as a potential inhibitor of angiogenesis in breast cancer by targeting the hedgehog signaling pathway [63].

1.2.1.2. Drug Repositioning Databases:

Computational databases such as DrugBank (https://go.drugbank.com/), Connectivity Map (CMap) (https://www.broadinstitute.org/connectivity-map-cmap), and LINCS L1000 (https://clue.io/) provide valuable resources for identifying repurposed drug candidates [64]. These databases compile extensive information on drug-target interactions, gene expression profiles, and molecular pathways. For instance, the CMap database was used to identify Pimozide as a potential breast cancer treatment by matching its gene expression profile to those of known anti-cancer drugs [65]. Similarly, DrugBank has facilitated the identification of Propranolol, a beta-blocker, as a potential repurposed drug for breast cancer due to its ability to reduce cell proliferation and induce apoptosis [66].

1.2.1.3. Phenotypic Screening:

This approach involves screening drugs based on observable cellular changes, such as alterations in cell morphology, viability, and apoptosis. Phenotypic screening can uncover drug candidates with unexpected mechanisms of action. An example is the identification of anti-cancer properties of thalidomide through its effects on angiogenesis and tumor growth in breast cancer models [67]. Another example is the use of phenotypic screening to identify Disulfiram, an anti-alcoholism drug, as an inhibitor of breast cancer stem cells by targeting the ALDH1 enzyme [68].

1.2.2. Bottom-Up Approaches

Bottom-up approaches begin with understanding the molecular and genetic underpinnings of breast cancer and use this information to identify potential drug candidates. These methods are

highly targeted and can reveal drugs with specific mechanisms of action. Genomic and Proteomic Profiling, Gene Expression-Based Screening, Molecular Docking, and Virtual Screening fall under the bottom-up approach of drug screening (**Figure 1.3B**).

1.2.2.1. Genomic and Proteomic Profiling:

Advanced techniques such as next-generation sequencing (NGS) and mass spectrometry are used to analyze the genetic and protein expression profiles of different cancer cells. These data sets can be found at different open access databases such as NCBI sequence database (GenBank) (https://www.ncbi.nlm.nih.gov/genbank/), EMBL (https://www.ebi.ac.uk/services/data-resources-and-tools?category=dna-rna), DNA Databank of Japan(https://www.ddbj.nig.ac.jp/index-e.html). By identifying key mutations and dysregulated pathways, researchers can match these with drugs that target these specific abnormalities. For instance, genomic profiling of breast cancer patients revealed mutations in the PI3K/AKT pathway, leading to the identification of PI3K inhibitors like Alpelisib as potential repurposed drugs [69]. Proteomic profiling has also been used to identify the anti-psychotic drug thioridazine as a potential repurposed drug for breast cancer by targeting cancer stem cells [70].

1.2.2.2. Molecular Docking and Virtual Screening:

Computational methods such as molecular docking and molecular dynamics simulation simulate the interaction between drugs and their target proteins. Virtual screening of large compound libraries can be used to predict the potent repurposed drugs against specific cancer-related proteins. The most commonly used open access tool for virtual screening is Auto-dock Vina which uses Monte Carlo simulation method. Apart from this, several tools are available for virtual screening such as DOVIS2.0, VSDocker, MPAD4, Ligen Docker-HT, GeauxDock, POAP and DOCK5,6. Virtual screening approach was used to identify Pimozide as a potential breast cancer treatment by predicting its binding to the Insulin receptor, Integrin beta 1 and CD36 [26]. Similarly, Niclosamide, an antihelminthic drug was identified as an inhibitor for the Wnt/β-catenin signaling pathway in breast cancer cells by utilizing molecular docking approach [71].

1.2.2.3. Gene Expression-Based Screening:

Gene expression signatures associated with breast cancer can be utilized to identify drugs that reverse these signatures, such as through tools like the GEO2R server. This method involves

comparing the gene expression profiles of treated and untreated cancer cells to identify drugs capable of normalizing aberrant gene expression. By analyzing large datasets of gene expression profiles, researchers can correlate specific signatures with drug response profiles, identifying potential therapeutic candidates. For instance, gene expression-based screening has identified atorvastatin as a drug that can downregulate oncogenic pathways in breast cancer cells, demonstrating the potential of this approach to pinpoint effective treatments [72]. Similarly, this approach was used to identify the anti-malarial drug chloroquine as a potential breast cancer treatment by reversing the expression of autophagy-related genes [56].

1.2.2.4. QSAR (Quantitative Structure-Activity Relationship)

QSAR models use statistical and computational techniques to predict the biological activity of compounds based on their chemical structure (https://www.3d-qsar.com/). By analyzing the relationship between chemical structure and biological activity, researchers can identify promising drug candidates for repurposing [73]. For example, QSAR models have been used to predict the anti-cancer potential of various compounds, leading to the identification of new uses for existing drugs. In breast cancer research, QSAR has been employed to identify small molecules that can inhibit specific targets like estrogen receptors, providing a computational approach to drug discovery. For instance, tamoxifen and raloxifene were identified as effective inhibitors of estrogen receptors through QSAR analysis [74].

1.2.2.5. Network Pharmacology

Network pharmacology involves the study of the complex interactions between drugs, targets, and biological networks. The most prominently used software for network analysis is Cytoscape (https://cytoscape.org/), which is an open source software platform for visualizing complex networks and integrating different type of attribute data.This approach can help identify multi-targeted therapies and understand the systemic effects of drug repurposing. By mapping the interactions between repurposed drugs and their multiple targets, researchers can predict their overall impact on cancer-related pathways [75]. For instance, network pharmacology has been used to identify drug combinations that target multiple signaling pathways in breast cancer, enhancing the therapeutic efficacy and reducing the likelihood of resistance. This holistic approach integrates data from genomics, proteomics, and metabolomics to provide a comprehensive view of drug actions. An example includes the use of network pharmacology to identify the anti-

inflammatory drug celecoxib and the anti-diabetic drug metformin as a combination therapy for targeting inflammation and metabolic pathways in cancer [76].

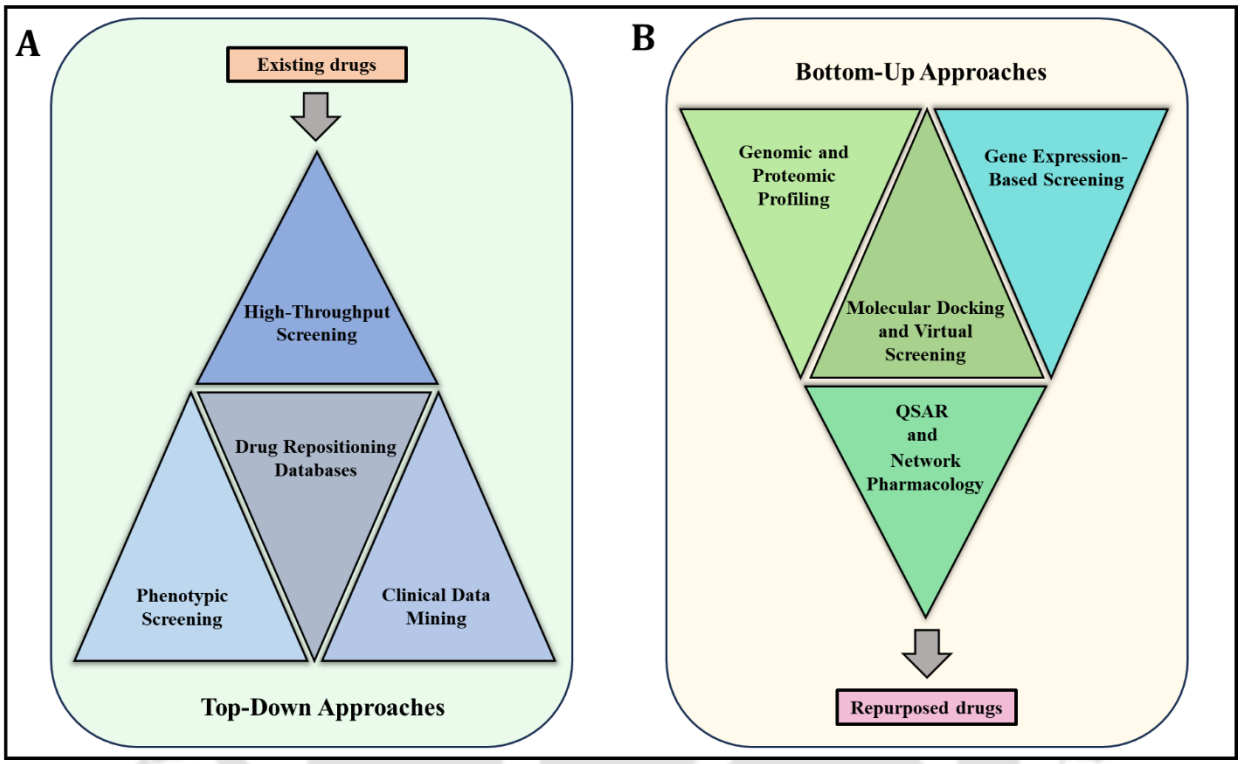

Figure 1.3: A) *Top-down approaches* ***B)*** *Bottom-up approaches of drug screening. (Reproduced with permission from Thirukumaran, K., et al. ACS Pharmacology & Translational Science, 2024. DOI: 10.1021/acsptsci.4c00545)*

1.2.3. Combination of Approaches

Combining top-down and bottom-up approaches can significantly enhance the identification and validation of repurposed drugs for breast cancer treatment. The integration of these methodologies allows for a comprehensive understanding of drug action, efficacy, and safety, ultimately leading to more effective therapeutic options. In the top-down approach, HTS is employed to identify potential drug candidates from large libraries of existing drugs. This method allows for the rapid assessment of thousands of compounds to determine their anti-cancer activity. For instance, HTS can identify drugs that inhibit cancer cell proliferation or induce apoptosis. An example of this is the discovery of Metformin, initially identified through HTS for its potential anti-cancer effects. Metformin, commonly used to treat type 2 diabetes, was found to inhibit the growth of breast

cancer cells in these high-throughput screens [62]. Once potential candidates are identified through the top-down approach, the bottom-up approach comes into play to validate and further characterize these drugs. This involves detailed genomic, proteomic, and metabolomic profiling to understand the mechanisms of action, target pathways, and potential biomarkers of response. For Metformin, subsequent genomic studies revealed its effects on the AMPK/mTOR signaling pathways in breast cancer cells. These studies showed that Metformin activates AMPK, leading to the inhibition of the mTOR pathway, which is critical for cancer cell growth and survival [10].

Such insights help in optimizing the use of repurposed drugs, determining the most effective dosages, and identifying patient populations that are most likely to benefit from the treatment. An integrated approach combining HTS and omics profiling was also used to identify the potential of Disulfiram, an anti-alcoholism drug, in breast cancer treatment [68]. Initially identified through HTS for its cytotoxic effects on breast cancer cells, Disulfiram was later studied using proteomic analysis. These studies showed that Disulfiram targets the ubiquitin-proteasome pathway, leading to the accumulation of misfolded proteins and subsequent cancer cell death [16]. Another example is the repurposing of the anti-malarial drug chloroquine [56]. HTS identified its potential to enhance the efficacy of existing breast cancer therapies. Genomic and proteomic profiling further revealed that chloroquine inhibits autophagy, a process that cancer cells utilize to survive under stress conditions, thereby sensitizing them to chemotherapy. Combining these approaches not only accelerates the drug discovery process but also enhances the precision of drug repurposing [77]. By leveraging the strengths of both methodologies, researchers can efficiently identify and develop repurposed drugs that target critical pathways in breast cancer. This integrative strategy leads to a better understanding of drug mechanisms, optimization of therapeutic regimens, and, ultimately, improved clinical outcomes for breast cancer patients. The comprehensive nature of this approach ensures that the most promising drug candidates are advanced to clinical trials, offering new hope for effective and less toxic breast cancer treatments.

1.3. Repurposed Drugs for Breast Cancer Therapy

Drug repurposing offers a promising approach to developing effective treatments for breast cancer by identifying new therapeutic uses for existing drugs. This strategy leverages the established safety profiles of these drugs, potentially accelerating the development of new cancer therapies. In breast cancer, repurposed drugs that target critical cellular processes, such as altered metabolism

and EMT, play a pivotal role in the regression of cancer progression, metastasis, and drug resistance [26]. This section explores various classes of repurposed drugs, their mechanisms of action, and their limitations.

1.3.1. Anti-Diabetic Drugs

Anti-diabetic drugs, primarily used to manage blood glucose levels, have been repurposed for their anti-cancer properties, particularly in targeting altered metabolic pathways in cancer cells. The most predominantly used anti-diabetic drug is Metformin, which inhibits mitochondrial complex I, reduces ATP production, and alters cellular energy status [78]. It is also repurposed in several cancers, including breast cancer, to suppress cancer cell proliferation. A clinical study demonstrated that Metformin combined with chemotherapy improved the overall survival rate of diabetic breast cancer patients compared to those receiving chemotherapy alone [79]. The study highlighted the potential of Metformin to enhance the efficacy of conventional treatments by targeting cancer metabolism. However, the anti-cancer efficacy of Metformin is limited by its low potency at standard doses used for diabetes treatment.

Pioglitazone, another anti-diabetic drug, activates PPAR-gamma to impair glucose and lipid metabolism. Its repurposing in breast cancer is based on its ability to modulate the tumor microenvironment and inhibit cancer cell proliferation [42]. Studies have reported that Pioglitazone can effectively reduce tumor growth in combination with other therapies [80]. Possible limitations of Pioglitazone include potential cardiovascular risks and weight gain. Rosiglitazone is also a PPAR-gamma agonist that has been explored for its anti-tumor effects, particularly in hormone receptor-positive breast cancer. Studies have indicated that Rosiglitazone can inhibit cell growth and induce apoptosis through the NF-κB pathway in breast cancer. However, its use is limited due to concerns about cardiovascular side effects [81].

1.3.2. Anti-Psychotic Drugs

Anti-psychotic drugs, traditionally used to treat psychiatric disorders, have shown potential in targeting cancer cell proliferation and metastasis by modulating various signaling pathways involved in cancer progression and EMT [26]. Pimozide, traditionally used as an anti-psychotic, targets several signaling pathways implicated in cancer progression, including those involved in metabolism and EMT. A Plethora of studies demonstrated that Pimozide inhibits cell proliferation

in breast cancer cell lines and effectively targets EMT-induced cells by targeting the Warburg effect, fatty acid metabolism, and p53 expression [13].

Another anti-psychotic drug, Thioridazine, originally targets dopamine receptors and has been shown to induce apoptosis in cancer stem cells by disrupting the Wnt/β-catenin signaling pathway [70]. Clinical studies indicate that Thioridazine can enhance the efficacy of standard chemotherapies when used in combination [82]. Its use is limited by side effects such as sedation and cardiotoxicity. In addition, Chlorpromazine, formerly used for schizophrenia treatment, has demonstrated potential in inhibiting breast cancer cell growth by modulating various signaling pathways, including cAMP phosphodiesterase and calmodulin-dependent pathways. Studies have shown that Chlorpromazine can sensitize cancer cells to chemotherapy, improving treatment outcomes [83]. The limitations of Chlorpromazine include its side effects on the central nervous system and potential for drug interactions.

1.3.3. Anti-Microbial Drugs

Anti-microbial drugs are designed to combat infections by several microorganisms. It has also shown promise in targeting various cancer-related pathways, thereby offering potential repurposed treatments for breast cancer [84]. Doxycycline, an antibiotic that inhibits bacterial protein synthesis, has been repurposed to target mitochondrial biogenesis and cancer cell proliferation [12]. Studies have shown that Doxycycline can inhibit breast cancer cell growth via PAR1/NF-κB/miR-17/E-cadherin pathway and sensitize cells to chemotherapy [85]. However, its long-term use can lead to antibiotic resistance and adverse effects on the gut microbiome. Itraconazole, an anti-fungal agent, inhibits the Hedgehog signaling pathway, which is implicated in cancer stem cell maintenance and EMT [86]. Clinical trials have demonstrated the potential of itraconazole to enhance the efficacy of standard chemotherapeutics in breast cancer. Its use is limited by hepatotoxicity and drug interactions at higher doses. In addition, Metronidazole, used to treat bacterial and protozoal infections, has been shown to induce DNA damage and apoptosis in cancer cells [87]. Evidence suggests that Metronidazole can enhance the effects of radiotherapy in breast cancer treatment. However, its neurotoxic side effects at high doses restrict its application in oncology [88].

1.3.4. Beta-Blockers

Beta-blockers are primarily used to manage cardiovascular conditions. In the case of cancer treatment, it demonstrated potential in inhibiting cancer cell proliferation and metastasis by modulating the adrenergic signaling pathway [89]. Propranolol (non-selective beta-blocker) has been repurposed to inhibit breast cancer cell proliferation and angiogenesis by blocking beta-adrenergic receptors. Clinical studies have indicated that Propranolol can reduce tumor growth and improve survival rates in breast cancer patients [66, 90]. However, its use is limited by potential cardiovascular side effects. Also, Metoprolol, a selective beta-1 blocker, has shown potential in reducing breast cancer cell proliferation and migration. Research suggests that Metoprolol can enhance the effects of conventional chemotherapeutics. However, its application is constrained by its primary function in cardiovascular management, requiring careful monitoring of cardiac function [91]. Atenolol, another selective beta-1 blocker, has been shown to inhibit cancer cell proliferation and metastasis. Studies indicate that Atenolol can reduce the invasive properties of breast cancer cells [92]. However, its anti-cancer efficacy is limited by its cardiovascular side effects and the need for high doses to achieve therapeutic effects in cancer treatment [91].

1.3.5. Anti-Rheumatic Drugs

Anti-rheumatic drugs are commonly used to treat inflammatory conditions. In addition, it also has been repurposed for its potential to modulate immune responses and inhibit cancer progression [93]. Methotrexate, an anti-rheumatic drug that inhibits dihydrofolate reductase, has been repurposed to target rapidly dividing cancer cells. Clinical studies have shown that methotrexate, combined with other chemotherapeutics, can enhance treatment efficacy in breast cancer. However, its use is limited by significant toxicities, including myelosuppression and hepatotoxicity [93]. Leflunomide is known for its inhibitory activity against dihydroorotate dehydrogenase. In addition, it also has been explored for its tyrosine kinase inhibitor activity and has shown potential in suppressing breast cancer cell proliferation and inducing apoptosis. Preclinical studies suggest that leflunomide can enhance the effects of conventional chemotherapeutics [94]. However, its hepatotoxicity and immunosuppressive effects limit its widespread use in cancer therapy. Sulfasalazine is used to treat inflammatory bowel disease and rheumatoid arthritis. It has been repurposed to target breast cancer cell proliferation due to the inhibitory activity against the NF-κB signaling pathway [95]. Research indicates that sulfasalazine

can reduce tumor growth and sensitize cancer cells to radiotherapy. However, its gastrointestinal side effects and potential for hypersensitivity reactions limit its application in oncology [96].

1.3.6. Anti-Alcoholism Drugs

Anti-alcoholism drugs, used to manage alcohol dependence, have been repurposed for their potential to inhibit cancer cell growth and metastasis. Disulfiram, an aldehyde dehydrogenase inhibitor, has been repurposed to target cancer stem cells and inhibit metastasis [16]. Clinical studies have demonstrated that Disulfiram, combined with copper, can induce apoptosis in breast cancer cells and enhance the efficacy of conventional treatments [97]. However, its use is limited by potential neurotoxicity and the need for careful patient monitoring. Naltrexone is used to reduce alcohol cravings by blocking opioid receptors. It has shown potential in inhibiting breast cancer cell proliferation and inducing apoptosis. Evidence suggests that naltrexone can enhance the effects of other anti-cancer agents. However, its primary use in addiction management limits its application in oncology without further clinical validation [98].

1.4. Limitations of Repurposed Drugs in Breast Cancer Treatment

Despite the promise of repurposed drugs in breast cancer treatment, several limitations hinder their effectiveness. One major challenge is the need for higher doses to achieve anti-cancer effects, which often exceed the doses used for their original indications. This can lead to increased toxicity and adverse effects [99]. For instance, Metformin, primarily used for diabetes, requires much higher doses to exhibit anti-cancer properties, potentially causing gastrointestinal disturbances and lactic acidosis [100]. Similarly, statins like atorvastatin need higher doses for anti-cancer efficacy, raising the risk of muscle toxicity and liver damage [101]. Another significant limitation is off-target effects. Repurposed drugs may interact with non-cancerous tissues, leading to unintended side effects. For example, the anti-psychotic drug pimozide, while showing potential in inhibiting breast cancer cell proliferation, can cause neurotoxic side effects at higher doses required for anti-cancer activity [102]. These off-target effects necessitate careful monitoring and management to balance efficacy and safety.

Bioavailability, pharmacokinetics and pharmacodynamics variability are also posing a challenge. Some repurposed drugs may not achieve sufficient concentrations in the tumor microenvironment due to poor absorption, rapid metabolism, or limited distribution. This can reduce their therapeutic

potential [103]. For instance, the anti-epileptic drug valproic acid has shown anti-cancer effects, but its bioavailability can be inconsistent, affecting its efficacy in cancer treatment [104]. In addition, differences in how the drug is absorbed, distributed, metabolized, and excreted in cancer patients compared to its original use can affect efficacy and safety [103]. For example, drugs like thalidomide, used for multiple myeloma, may exhibit different pharmacokinetic profiles in breast cancer patients, impacting their therapeutic outcomes.

Site-specific action is crucial for the effectiveness of cancer therapy. Many repurposed drugs do not effectively target cancer cells specifically, leading to systemic toxicity and reduced efficacy. For instance, Disulfiram, used for alcohol dependency, shows anti-cancer potential but can cause severe liver toxicity due to its non-specific action [105]. Achieving site-specific action remains a significant challenge in the repurposing of drugs for cancer therapy. Further, interaction with existing cancer treatments is also a concern. Repurposed drugs can interact with established cancer therapies, potentially leading to adverse effects or reduced efficacy. For example, combining a repurposed drug like Disulfiram with chemotherapy might result in drug-drug interactions, complicating treatment regimens and requiring careful consideration of dosing schedules and potential side effects [106]. Moreover, cancer cells can also develop resistance to repurposed drugs, limiting their long-term efficacy. For example, tamoxifen, originally an antiestrogen for breast cancer, faces resistance in many patients over time [107]. Similarly, Metformin may induce metabolic adaptations in cancer cells, reducing its long-term effectiveness [108]. This resistance further complicates the use of repurposed drugs in cancer treatment.

Apart from these biological limitations faced by the repurposed drugs, regulatory and approval challenges also pose significant hurdles. Repurposed drugs often face regulatory hurdles as they need to be re-evaluated for new indications [109]. This process can be time-consuming and costly, delaying their availability for cancer treatment. Pharmaceutical companies might lack the incentive to invest in clinical trials for repurposed drugs due to limited patent protection [109]. Further, intellectual property issues complicate the landscape. Since many repurposed drugs are off-patent, there is less financial motivation for pharmaceutical companies to invest in the necessary clinical trials and development. This lack of patent protection can hinder further research and commercial interest, limiting the advancement of repurposed drugs in cancer therapy [109].

1.5. Strategies to Overcome Limitations of Repurposed Drugs in Breast Cancer Treatment

The various limitations of repurposed drugs in breast cancer treatment have been addressed using several innovative strategies. These strategies aim to enhance the efficacy, specificity, and safety of repurposed drugs, ultimately improving patient outcomes.

1.5.1. Combination therapy

Combination therapy involves using repurposed drugs alongside conventional cancer treatments to enhance therapeutic efficacy and overcome resistance. This approach can potentiate the anti-cancer effects and reduce the required doses of individual drugs by targeting multiple pathways [110]. For example, clinical studies have shown that combining Metformin with standard chemotherapy improves overall survival rates in breast cancer patients. Metformin enhances the sensitivity of cancer cells to chemotherapy, reducing the required dose and associated side effects [76]. Similarly, atorvastatin, a statin drug, when combined with radiation therapy, has demonstrated enhanced anti-tumor effects in preclinical breast cancer models [111]. This combination improves radiation-induced DNA damage in cancer cells while protecting normal tissues.

1.5.2. Targeted Delivery Using Nanoparticles

Targeted delivery using nanoparticle-based systems can enhance the bioavailability and site-specific action of repurposed drugs [112]. These systems can deliver drugs directly to the tumor site, reducing systemic toxicity and improving therapeutic efficacy. For instance, Pimozide, an anti-psychotic drug encapsulated in nanoparticles, has shown increased accumulation in breast cancer cells, enhancing its anti-cancer activity while minimizing neurotoxic side effects [113]. Similarly, valproic acid, an anti-epileptic drug delivered through nanoparticles, has demonstrated improved bioavailability and targeted action against breast cancer cells in preclinical studies [114].

1.5.3. Personalized Medicine

Personalized medicine involves tailoring treatment based on the genetic, epigenetic, and molecular profile of the tumor [115]. This approach ensures that repurposed drugs are used in a manner that is most effective for the individual patient, reducing the risk of adverse effects and improving outcomes. For example, identifying biomarkers of tamoxifen resistance in breast cancer patients

allows for the use of alternative repurposed drugs or combination therapies that can bypass resistance mechanisms and improve treatment efficacy [115]. Genomic profiling can help identify breast cancer patients who are more likely to respond to Metformin based on the metabolic profile of the tumor, optimizing treatment outcomes [115].

1.5.4. Cocktail Therapy

Cocktail therapy involves the simultaneous use of multiple repurposed drugs that target distinct pathways within cancer cells. This strategy is designed to overcome resistance mechanisms, disrupt cancer progression more effectively, and achieve a synergistic therapeutic effect. By targeting multiple signaling or metabolic pathways, cocktail therapy reduces the chances of cancer cells adapting to treatment and enhances the overall anti-cancer efficacy [116]. The formation of an effective cocktail therapy relies on several approaches, including *in silico* computational screening, *in vitro* validation, and systematic dose optimization studies. However, an essential consideration in cocktail therapy is the toxicity and safety of the combined drugs, particularly if they are not metabolized efficiently within the body. Improper metabolism can lead to the accumulation of toxic intermediates, causing adverse effects and compromising patient safety [116]. For example, failure to adequately clear or metabolize one of the drugs in the combination may exacerbate systemic toxicity, leading to organ damage or severe side effects. Therefore, careful optimization of dosages, pharmacokinetic studies, and targeted delivery strategies are critical to ensure the safety and efficacy of cocktail therapies. For instance, the combination of bortezomib, lenalidomide, and thalidomide has demonstrated promising outcomes in preclinical studies, where each drug targets distinct pathways involved in cancer progression [116]. Such an approach highlights the importance of selecting drug combinations that complement each other's mechanisms of action, thereby enhancing therapeutic outcomes while minimizing resistance. Overall, cocktail therapy holds significant potential for improving cancer treatment efficacy, but its success relies on precise drug selection, dose optimization, and strategies to mitigate toxicity.

1.5.5. Drug Modifications and Reformulation

Modifying the chemical structure of repurposed drugs can enhance their pharmacokinetic properties and reduce toxicity. For instance, creating prodrugs that are metabolized into the active drug form, specifically within cancer cells, can increase specificity and reduce systemic side effects. An example is the reformulation of Disulfiram, an anti-alcoholism drug, into nanoparticle-

based systems that improve its delivery and reduce its liver toxicity while maintaining its anti-cancer properties [106].

1.5.6. Biomarker-Driven Approaches

Using biomarkers to identify patients who are most likely to benefit from specific repurposed drugs can optimize treatment efficacy. Biomarker-driven approaches can help select patients with specific genetic or molecular profiles that make them more responsive to particular therapies [117]. For example, identifying HER2-positive breast cancer patients who are likely to respond to certain repurposed drugs can tailor treatment plans more effectively [117].

1.5.7. Immunotherapy Combinations

Combining repurposed drugs with immunotherapy agents can enhance the anti-tumor immune response. For instance, Metformin has been shown to enhance the efficacy of immune checkpoint inhibitors by modulating the tumor microenvironment and increasing the infiltration of immune cells into tumors [118]. Such combinations can provide synergistic effects and improve overall treatment outcomes.

1.5.8. Regulatory and Approval Strategies

To address regulatory and intellectual property challenges, collaborative efforts between academia, industry, and regulatory bodies are crucial. Accelerated approval pathways and innovative trial designs can expedite the repurposing process [109]. Thalidomide repurposed for multiple myeloma, benefited from fast-track approval due to collaborative efforts that expedited clinical trials and regulatory reviews. Similar strategies can be applied to breast cancer repurposed drugs **(Table 1.2)**. By employing these strategies, the limitations associated with repurposed drugs in breast cancer treatment can be effectively addressed, paving the way for more effective and safer therapeutic options.

Table 1.2: *Repurposed Drugs for Breast Cancer: Mechanisms, Limitations, Strategies, and Identification Methods*

Category	Drug	Mechanism of Action	Method of Identification	Limitations	Strategies to Overcome Limitations	Reference
Anti-Psychotic Drugs	Pimozide	Inhibits dopamine receptors, targets EMT markers	In silico screening, molecular docking, *in vitro* validation	High doses are needed, and specificity issues	Combination therapy with Ponatinib, encapsulation in ZIF-8, PLGA nanoparticles	[13, 44, 113]
	Thioridazine	Inhibits dopamine receptors, targets cancer stem cells	Drug repositioning studies, *in vitro* assays	Off-target effects, cardiotoxicity	Dose optimization, targeted delivery systems	[70, 82]
	Olanzapine	Inhibits multiple receptors, modulates EMT	High-throughput screening, *in vitro* experiments	Weight gain, metabolic side effects	Use in combination with other cancer therapies, nanoformulations	[119, 120]
Anti-Fungal Drugs	Itraconazole	Inhibits Hedgehog signaling, angiogenesis	*In silico* analysis, *in vitro* studies	Limited cancer-specific targeting	Use in combination with chemotherapeutics, encapsulation in lipid nanoparticles.	[63, 86, 121]
	Ketoconazole	Inhibits CYP17, tGLI1, affects steroid synthesis	Retrospective clinical data analysis, *in vitro* assays	Off-target hormonal effects	Co-administration with hormonal therapy blockers	[122, 123]
	Fluconazole	Inhibits ergosterol synthesis, affects cell membrane	Virtual screening, *in vitro* validation	Low potency, resistance development	Higher dosing regimens, in combination with other anti-fungal agents	[124]
Anti-Malarial Drugs	Chloroquine	Inhibits autophagy, modulates immune response	*In silico* drug screening, clinical trial data	Retinal toxicity, limited efficacy at low doses	Combination with other chemotherapeutics used in controlled-release formulations	[56, 77]
	Hydroxy chloroquine	Inhibits autophagy, modulates immune response	Drug repositioning studies, *in vitro* validation	Retinal toxicity, low efficacy in monotherapy	Combination with chemotherapy or targeted therapies	[125]
	Artemisinin	Generates reactive oxygen species, induces apoptosis	Virtual screening, *in vitro* validation	Short half-life, resistance issues	Combination with standard cancer therapies, nanoparticle delivery systems	[126]
Anti-Diabetic Drugs	Metformin	Inhibits mTOR pathway, AMPK activation	Epidemiological studies, *in vitro* assays	Gastrointestinal side effects, lactic acidosis	Combination with other therapies, sustained-release formulations	[62, 76, 79]

	Pioglitazone	PPAR-γ agonist modulates glucose metabolism	Retrospective clinical studies, *in vitro* validation	Weight gain, cardiovascular risks	Combination with other anti-cancer drugs, dose optimization	[42, 80]
	Rosiglitazone	PPAR-γ agonist regulates gene expression	High-throughput screening, *in vitro* studies	Increased risk of heart failure, bone fractures	Combination therapy, dose reduction	[81]
Anti-Microbial Drugs	Doxycycline	Inhibits protein synthesis, anti-inflammatory	Drug repositioning studies, *in vitro* validation	Antibiotic resistance, gastrointestinal discomfort	Combination with radiotherapy	[12, 85]
	Azithromycin	Inhibits protein synthesis, anti-inflammatory	Epidemiological studies, *in vitro* assays	Antibiotic resistance, QT prolongation	Combination therapy, dose optimization	[127]
	Clarithromycin	Inhibits protein synthesis, modulates immune response	High-throughput screening, *in vitro* validation	Antibiotic resistance, hepatotoxicity	Combination with other therapies, dose adjustment	[129]
Beta-Blockers	Propranolol	Inhibits beta-adrenergic receptors, reduces angiogenesis	Epidemiological studies, *in vitro* assays	Bradycardia, hypotension	Combination with other therapies, targeted delivery	[66]
	Atenolol	Inhibits beta-adrenergic receptors, reduces tumor proliferation	Drug repositioning studies, *in vitro* validation	Bradycardia, fatigue	Combination with other anti-cancer drugs, dose optimization	[129]
Anti-Rheumatic Drugs	Methotrexate	Inhibits dihydrofolate reductase, reduces cell proliferation	Clinical studies, *in vitro* validation	Hepatotoxicity, myelosuppression	Combination with other anti-cancer agents, dose adjustment	[15]
	Sulfasalazine	Inhibits NF-κB pathway, reduces inflammation	Drug repositioning studies, *in vitro* assays	Gastrointestinal side effects, hypersensitivity	Combination therapy, targeted delivery systems	[95, 96]
Anti-Alcoholism Drugs	Disulfiram	Inhibits ALDH, induces oxidative stress	Drug repositioning studies, *in vitro* assays	Hepatotoxicity, neuropathy	Combination with other anti-cancer drugs, dose optimization	[97, 105, 106]
	Naltrexone	Opioid receptor antagonist modulates immune response	Epidemiological studies, *in vitro* validation	Nausea, hepatotoxicity	Combination therapy, targeted delivery	[98]

1.6. Key Features and Scope of Research

A thorough literature review on cancer metabolism, EMT signaling, and current therapeutic approaches for breast cancer highlights several promising research avenues. These insights provide a foundation for identifying novel therapeutic targets and strategies to overcome treatment resistance and metastasis.

- Construction of an interconnected EMT and metabolic network, and identification of potential target proteins.
- Identification and validation of potential repurposed drugs to target the interconnected network in breast cancer cells.
- Exploring the synergistic combination to enhance the efficacy of the repurposed drugs in breast cancer cells,
- Utilizing a pH-responsive carrier for precise drug release within the tumor microenvironment, minimizing systemic impact.

1.7. Objectives

- Identification of potential repurposed candidate drugs to target metabolic and EMT networks
- Experimental validations of the selected repurposed drugs on breast cancer cells using combination and cocktail therapeutic strategies
- Formulation of suitable nanocarriers for targeted release of the repurposed drug in tumor microenvironment mimicking condition.

1.8. Salient Outcomes of the Research

- **Identification of Effective Drug Combinations**: Pimozide and Ponatinib effectively inhibited IR, ITGB1, and CD36 pathways, demonstrating potential against breast cancer in monolayer and spheroid models.
- **Efficacy of ESP Cocktail**: ESP combination therapy significantly reduced the IC_{50} of Pimozide, enhancing apoptosis induction while targeting metabolic and oxidative stress pathways.

- **Synergy with ZIF-8 for Targeted Delivery**: Encapsulated Pimozide within ZIF-8 enabled controlled release and increased therapeutic impact specifically in the tumor environment mimic conditions.
- **Reduction in Cancer Stemness and Metastasis**: Combination therapies and ZIF-8 encapsulation effectively decreased cancer stemness and metastatic potential, addressing major resistance factors.

1.9. References

1. Sung, H., Ferlay, J., Siegel, R.L., Laversanne, M., Soerjomataram, I., Jemal, A., & Bray, F. (2021). Global cancer statistics 2020: GLOBOCAN estimates of incidence and mortality worldwide for 36 cancers in 185 countries. CA: A Cancer Journal for Clinicians, 71(3), 209-249. https://doi.org/10.3322/caac.21660
2. Polyak, K. (2011). Heterogeneity in breast cancer. Journal of Clinical Investigation, 121(10), 3786-3788. https://doi.org/10.1172/JCI60534
3. Miller, K. D., Nogueira, L., Mariotto, A. B., Rowland, J. H., Yabroff, K. R., Alfano, C. M., & Jemal, A. (2019). Cancer treatment and survivorship statistics, 2019. CA: A Cancer Journal for Clinicians, 69(5), 363-385. https://doi.org/10.3322/caac.21565
4. Turashvili, G., & Brogi, E. (2017). Tumor heterogeneity in breast cancer. Frontiers in Medicine, 4, 227. https://doi.org/10.3389/fmed.2017.00227
5. Hanahan, D., & Weinberg, R. A. (2000). The hallmarks of cancer. cell, 100(1), 57-70. https://doi.org/10.1016/s0092-8674(00)81683-9
6. Dai, X., Xiang, L., Li, T., & Bai, Z. (2016). Cancer hallmarks, biomarkers and breast cancer molecular subtypes. Journal of cancer, 7(10), 1281. https://doi.org/10.7150/jca.13141
7. Wang, J., & Wu, S. G. (2023). Breast cancer: an overview of current therapeutic strategies, challenge, and perspectives. Breast Cancer: Targets and Therapy, 721-730. https://doi.org/10.2147%2FBCTT.S432526
8. Martin, T. A., Ye, L., Sanders, A. J., Lane, J., & Jiang, W. G. (2013). Cancer invasion and metastasis: molecular and cellular perspective. In Madame Curie Bioscience Database [Internet]. Landes Bioscience.

9. Cha, Y., Erez, T., Reynolds, I. J., Kumar, D., Ross, J., Koytiger, G., & Laifenfeld, D. (2018). Drug repurposing from the perspective of pharmaceutical companies. British journal of pharmacology, 175(2), 168-180. https://doi.org/10.1111%2Fbph.13798
10. Shi, B., Hu, X., He, H., & Fang, W. (2021). Metformin suppresses breast cancer growth via inhibition of cyclooxygenase-2. Oncology Letters, 22(2), 1-14. https://doi.org/10.3892/ol.2021.12876
11. Liu, J., Zheng, F., Yang, M., Wu, X., & Liu, A. (2021). Effect of aspirin use on survival benefits of breast cancer patients: A meta-analysis. Medicine, 100(33), e26870. https://doi.org/10.1097/md.0000000000026870
12. Zhang, L., Xu, L., Zhang, F., & Vlashi, E. (2017). Doxycycline inhibits the cancer stem cell phenotype and epithelial-to-mesenchymal transition in breast cancer. Cell Cycle, 16(8), 737-745. https://doi.org/10.1080%2F15384101.2016.1241929
13. Kandasamy, T., Sarkar, S., Sen, P., Venkatesh, D., & Ghosh, S. S. (2024). Concurrent inhibition of IR, ITGB1, and CD36 perturbated the interconnected network of energy metabolism and epithelial-to-mesenchymal transition in breast cancer cells. Journal of Cellular Biochemistry. https://doi.org/10.1002/jcb.30574
14. Fjæstad, K. Y., Rømer, A. M. A., Goitea, V., Johansen, A. Z., Thorseth, M. L., Carretta, M., & Madsen, D. H. (2022). Blockade of beta-adrenergic receptors reduces cancer growth and enhances the response to anti-CTLA4 therapy by modulating the tumor microenvironment. Oncogene, 41(9), 1364-1375. https://doi.org/10.1038/s41388-021-02170-0
15. Yang, V., Gouveia, M. J., Santos, J., Koksch, B., Amorim, I., Gärtner, F., & Vale, N. (2020). Breast cancer: insights in disease and influence of drug methotrexate. RSC Medicinal Chemistry, 11(6), 646-664. https://doi.org/10.1039/D0MD00051E
16. Wang, L., Yu, Y., Zhou, C., Wan, R., & Li, Y. (2022). Anti-cancer effects of Disulfiram: A systematic review of in vitro, animal, and human studies. Systematic Reviews, 11(1), 109. https://doi.org/10.1186%2Fs13643-021-01858-4
17. Liberti, M. V., & Locasale, J. W. (2016). The Warburg effect: how does it benefit cancer cells?. Trends in biochemical sciences, 41(3), 211-218. https://doi.org/10.1016%2Fj.tibs.2015.12.001

18. Shegay, P. V., Shatova, O. P., Zabolotneva, A. A., Shestopalov, A. V., & Kaprin, A. D. (2023). Moonlight functions of glycolytic enzymes in cancer. Frontiers in Molecular Biosciences, 10, 1076138. https://doi.org/10.3389%2Ffmolb.2023.1076138
19. Yoo, H. C., Yu, Y. C., Sung, Y., & Han, J. M. (2020). Glutamine reliance in cell metabolism. Experimental & molecular medicine, 52(9), 1496-1516. https://doi.org/10.1038/s12276-020-00504-8
20. Wang, Z., Liu, F., Fan, N., Zhou, C., Li, D., Macvicar, T., ... & Zhao, Y. (2020). Targeting glutaminolysis: new perspectives to understand cancer development and novel strategies for potential target therapies. Frontiers in oncology, 10, 589508. https://doi.org/10.3389%2Ffonc.2020.589508
21. Fhu, C. W., & Ali, A. (2020). Fatty acid synthase: an emerging target in cancer. Molecules, 25(17), 3935. https://doi.org/10.3390%2Fmolecules25173935
22. Ribatti, D., Tamma, R., & Annese, T. (2020). Epithelial-mesenchymal transition in cancer: a historical overview. Translational oncology, 13(6), 100773. https://doi.org/10.1016%2Fj.tranon.2020.100773
23. Serrano-Gomez, S. J., Maziveyi, M., & Alahari, S. K. (2016). Regulation of epithelial-mesenchymal transition through epigenetic and post-translational modifications. Molecular cancer, 15, 1-14. https://doi.org/10.1186%2Fs12943-016-0502-x
24. Herbertz, S., Sawyer, J. S., Stauber, A. J., Gueorguieva, I., Driscoll, K. E., Estrem, S. T., & Lahn, M. M. (2015). Clinical development of galunisertib (LY2157299 monohydrate), a small molecule inhibitor of transforming growth factor-beta signaling pathway. Drug design, development and therapy, 4479-4499. https://doi.org/10.2147/dddt.s86621
25. Liu, J., Pan, S., Hsieh, M. H., Ng, N., Sun, F., Wang, T., & Harris, J. L. (2013). Targeting Wnt-driven cancer through the inhibition of Porcupine by LGK974. Proceedings of the National Academy of Sciences, 110(50), 20224-20229. https://doi.org/10.1073/pnas.1314239110
26. Kandasamy, T., Sen, P., & Ghosh, S. S. (2022). Multi-targeted drug repurposing approach for breast cancer via integrated functional network analysis. Molecular informatics, 41(8), 2100300. https://doi.org/10.1002/minf.202100300

27. Cha, Y. H., Yook, J. I., Kim, H. S., & Kim, N. H. (2015). Catabolic metabolism during cancer EMT. Archives of pharmacal research, 38, 313-320. https://doi.org/10.1007/s12272-015-0567-x
28. Tam, S. Y., Wu, V. W., & Law, H. K. (2020). Hypoxia-induced epithelial-mesenchymal transition in cancers: HIF-1α and beyond. Frontiers in oncology, 10, 486. https://doi.org/10.3389/fonc.2020.00486
29. Wang, H., Peng, R., Chen, X., Jia, R., Huang, C., Huang, Y., & Guo, G. (2018). Effect of HK2, PKM2 and LDHA on Cetuximab efficacy in metastatic colorectal cancer. Oncology letters, 15(4), 5553-5560. https://doi.org/10.3892/ol.2018.8005
30. Varghese, S., Pramanik, S., Williams, L. J., Hodges, H. R., Hudgens, C. W., Fischer, G. M., & Vashisht Gopal, Y. N. (2021). The glutaminase inhibitor CB-839 (telaglenastat) enhances the antimelanoma activity of T-cell–mediated immunotherapies. Molecular cancer therapeutics, 20(3), 500-511. https://doi.org/10.1158/1535-7163.mct-20-0430
31. Browne, C. D., Hindmarsh, E. J., & Smith, J. W. (2006). Inhibition of endothelial cell proliferation and angiogenesis by orlistat, a fatty acid synthase inhibitor. The FASEB journal, 20(12), 2027-2035. https://doi.org/10.1096/fj.05-5404com
32. Seo, J., Ha, J., Kang, E., & Cho, S. (2021). The role of epithelial–mesenchymal transition-regulating transcription factors in anti-cancer drug resistance. Archives of pharmacal research, 44, 281-292. https://doi.org/10.1007/s12272-021-01321-x
33. Jonckheere, S., Adams, J., De Groote, D., Campbell, K., Berx, G., & Goossens, S. (2022). Epithelial-mesenchymal transition (EMT) as a therapeutic target. Cells Tissues Organs, 211(2), 157-182. https://doi.org/10.1159/000512218
34. Yingling, J. M., McMillen, W. T., Yan, L., Huang, H., Sawyer, J. S., Graff, J., & Driscoll, K. E. (2018). Preclinical assessment of galunisertib (LY2157299 monohydrate), a first-in-class transforming growth factor-β receptor type I inhibitor. Oncotarget, 9(6), 6659. https://doi.org/10.18632/oncotarget.23795
35. Sen, P., & Ghosh, S. S. (2023). γ-Secretase inhibitor potentiates the activity of suberoylanilide hydroxamic acid by inhibiting its ability to induce epithelial to mesenchymal transition and stemness via Notch pathway activation in triple-negative breast cancer cells. ACS Pharmacology & Translational Science, 6(10), 1396-1415. https://doi.org/10.1021/acsptsci.3c00099

36. Bradley, R., Braybrooke, J., Gray, R., Hills, R., Liu, Z., Peto, R., & Swain, S. M. (2021). Trastuzumab for early-stage, HER2-positive breast cancer: a meta-analysis of 13 864 women in seven randomised trials. The Lancet Oncology, 22(8), 1139-1150. https://doi.org/10.1016/s1470-2045(21)00288-6
37. Sabatier, R., Lopez, M., Guille, A., Billon, E., Carbuccia, N., Garnier, S., & Bertucci, F. (2019). High response to cetuximab in a patient with EGFR-amplified heavily pretreated metastatic triple-negative breast cancer. JCO precision oncology, 3, 1-8. https://doi.org/10.1200/po.18.00310
38. Dai, Y., Yang, L., Sakandar, A., Zhang, D., Du, F., Zhang, X., & Wen, Q. (2022). Vemurafenib inhibits immune escape biomarker BCL2A1 by targeting PI3K/AKT signaling pathway to suppress breast cancer. Frontiers in Oncology, 12, 906197. https://doi.org/10.3389/fonc.2022.906197
39. Singh, G. K., Bajpai, J., Joshi, S., Prabhash, K., Choughule, A., Patil, A., & Badwe, R. A. (2020). Excellent response to erlotinib in breast carcinoma with rare EGFR mutation—a case report. ecancermedicalscience, 14. https://doi.org/10.3332/ecancer.2020.1092
40. Serra, F., Lapidari, P., Quaquarini, E., Tagliaferri, B., Sottotetti, F., & Palumbo, R. (2019). Palbociclib in metastatic breast cancer: current evidence and real-life data. Drugs in context, 8. https://doi.org/10.7573/dic.212579
41. Ye, D. J., Kwon, Y. J., Baek, H. S., Cho, E., Kwon, T. U., & Chun, Y. J. (2019). Combination treatment with auranofin and nutlin-3a induces synergistic cytotoxicity in breast cancer cells. Journal of Toxicology and Environmental Health, Part A, 82(10), 626-637. https://doi.org/10.1080/15287394.2019.1635934
42. Jiao, X. X., Lin, S. Y., Lian, S. X., Qiu, Y. R., Li, Z. H., Chen, Z. H., & Hu, G. H. (2020). Inhibition of the breast cancer by PPARγ agonist pioglitazone through JAK2/STAT3 pathway. Neoplasma, 67(4). https://doi.org/10.4149/neo_2020_190805n716
43. Pullarkat, V. A., Lacayo, N. J., Jabbour, E., Rubnitz, J. E., Bajel, A., Laetsch, T. W., & Stock, W. (2021). Venetoclax and navitoclax in combination with chemotherapy in patients with relapsed or refractory acute lymphoblastic leukemia and lymphoblastic lymphoma. Cancer discovery, 11(6), 1440-1453. https://doi.org/10.1158/2159-8290.cd-20-1465

44. Li, J., Qu, P., Zhou, X. Z., Ji, Y. X., Yuan, S., Liu, S. P., & Zhang, Q. G. (2022). Pimozide inhibits the growth of breast cancer cells by alleviating the Warburg effect through the P53 signaling pathway. Biomedicine & Pharmacotherapy, 150, 113063. https://doi.org/10.1016/j.biopha.2022.113063
45. Koziel, J. E., & Herbert, B. S. (2015). The telomerase inhibitor imetelstat alone, and in combination with trastuzumab, decreases the cancer stem cell population and self-renewal of HER2+ breast cancer cells. Breast cancer research and treatment, 149, 607-618. https://doi.org/10.1007/s10549-015-3270-1
46. Alavi, S. E., Esfahani, M. K. M., Alavi, F., Movahedi, F., & Akbarzadeh, A. (2013). Drug delivery of hydroxyurea to breast cancer using liposomes. Indian Journal of Clinical Biochemistry, 28, 299-302. https://doi.org/10.1007%2Fs12291-012-0291-y
47. Montero, A. J., Escobar, M., Lopes, G., Glück, S., & Vogel, C. (2012). Bevacizumab in the treatment of metastatic breast cancer: friend or foe?. Current oncology reports, 14, 1-11. https://doi.org/10.1007%2Fs11912-011-0202-z
48. Korashy, H. M., Maayah, Z. H., Al Anazi, F. E., Alsaad, A. M., Alanazi, I. O., Belali, O. M., & Alshamsan, A. (2017). Sunitinib inhibits breast cancer cell proliferation by inducing apoptosis, cell-cycle arrest and DNA repair while inhibiting NF-κB signaling pathways. Anti-cancer research, 37(9), 4899-4909. https://doi.org/10.21873/anticanres.11899
49. Wang, X., Shen, Y., MengLv, L., Zhang, X., Yang, J., Wang, F., & Yang, J. (2020). Thalidomide suppresses breast cancer tumor growth by inhibiting tumor-associated macrophage accumulation in breast tumor-bearing mice. European Journal of Pharmaceutical Sciences, 151, 105302. https://doi.org/10.1016/j.ejps.2020.105302
50. Sparano, J. A., Bernardo, P., Stephenson, P., Gradishar, W. J., Ingle, J. N., Zucker, S., & Davidson, N. E. (2004). Randomized phase III trial of marimastat versus placebo in patients with metastatic breast cancer who have responding or stable disease after first-line chemotherapy: Eastern Cooperative Oncology Group trial E2196. Journal of Clinical Oncology, 22(23), 4683-4690. https://doi.org/10.1200/jco.2004.08.054
51. Huang, Y., Sun, G., Sun, X., Li, F., Zhao, L., Zhong, R., & Peng, Y. (2020). The potential of lonidamine in combination with chemotherapy and physical therapy in cancer treatment. Cancers, 12(11), 3332. https://doi.org/10.3390%2Fcancers12113332

52. Gross, M. I., Demo, S. D., Dennison, J. B., Chen, L., Chernov-Rogan, T., Goyal, B., & Bennett, M. K. (2014). Anti-tumor activity of the glutaminase inhibitor CB-839 in triple-negative breast cancer. Molecular cancer therapeutics, 13(4), 890-901. https://doi.org/10.1158/1535-7163.MCT-13-0870
53. Ko, L., & Allalunis-Turner, J. (2009). Investigation on the mechanism of dichloroacetate (DCA) induced apoptosis in breast cancer. Journal of Clinical Oncology, 27(15_suppl), e14637-e14637. https://doi.org/10.1200/jco.2009.27.15_suppl.e14637
54. Mathias, C., Kozak, V. N., Magno, J. M., Baal, S. C. S., Dos Santos, V. H. A., Ribeiro, E. M. D. S. F., & Carvalho de Oliveira, J. (2023). PD-1/PD-L1 Inhibitors Response in Triple-Negative Breast Cancer: Can Long Noncoding RNAs Be Associated?. Cancers, 15(19), 4682. https://doi.org/10.3390%2Fcancers15194682
55. Page, D. B., Beal, K., Linch, S. N., Spinelli, K. J., Rodine, M., Halpenny, D., & McArthur, H. L. (2022). Brain radiotherapy, tremelimumab-mediated CTLA-4-directed blockade+/− trastuzumab in patients with breast cancer brain metastases. NPJ Breast Cancer, 8(1), 50. https://doi.org/10.1038/s41523-022-00404-2
56. Zhang, Y., Cao, Y., Sun, X., Feng, Y., Du, Y., Liu, F., & Jin, F. (2017). Chloroquine (CQ) exerts anti-breast cancer through modulating microenvironment and inducing apoptosis. International immunopharmacology, 42, 100-107. https://doi.org/10.1016/j.intimp.2016.11.027
57. Singh, N., Vayer, P., Tanwar, S., Poyet, J. L., Tsaioun, K., & Villoutreix, B. O. (2023). Drug discovery and development: introduction to the general public and patient groups. Frontiers in Drug Discovery, 3, 1201419. https://doi.org/10.3389/fddsv.2023.1201419
58. Sliwoski, G., Kothiwale, S., Meiler, J., & Lowe, E. W. (2014). Computational methods in drug discovery. Pharmacological reviews, 66(1), 334-395. https://doi.org/10.1124%2Fpr.112.007336
59. Fink, T., Bruggesser, H., & Reymond, J. L. (2005). Virtual exploration of the small-molecule chemical universe below 160 daltons. Angewandte Chemie International Edition, 44(10), 1504-1508. https://doi.org/10.1002/anie.200462457
60. Fink, T., & Reymond, J. L. (2007). Virtual exploration of the chemical universe up to 11 atoms of C, N, O, F: assembly of 26.4 million structures (110.9 million stereoisomers) and analysis for new ring systems, stereochemistry, physicochemical properties,

compound classes, and drug discovery. Journal of chemical information and modeling, 47(2), 342-353. https://doi.org/10.1021/ci600423u

61. Kiriiri, G. K., Njogu, P. M., & Mwangi, A. N. (2020). Exploring different approaches to improve the success of drug discovery and development projects: a review. Future Journal of Pharmaceutical Sciences, 6, 1-12. https://doi.org/10.1186/s43094-020-00047-9
62. Mahfauz, M., Yuruker, O., & Kalkan, R. (2024). Repurposing Metformin as a potential anti-cancer agent using in silico technique. DARU Journal of Pharmaceutical Sciences, 1-7. https://doi.org/10.1007/s40199-024-00523-0
63. Dhorje, S., Lavhate, P., & Srivastav, A. (2020). In silico drug repurposing: An anti-fungal drug, itraconazole, repurposed as an anti-cancer agent using molecular docking. MGM Journal of Medical Sciences, 7(3), 110-118. https://link.gale.com/apps/doc/A633514299/AONE?u=anon~b62522ec&sid=googleScholar&xid=9ef0863e
64. Subramanian, A., Narayan, R., Corsello, S. M., Peck, D. D., Natoli, T. E., Lu, X., & Golub, T. R. (2017). A next generation connectivity map: L1000 platform and the first 1,000,000 profiles. Cell, 171(6), 1437-1452. https://doi.org/10.1016/j.cell.2017.10.049
65. Fortney, K., Griesman, J., Kotlyar, M., Pastrello, C., Angeli, M., Sound-Tsao, M., & Jurisica, I. (2015). Prioritizing therapeutics for lung cancer: an integrative meta-analysis of cancer gene signatures and chemogenomic data. PLoS computational biology, 11(3), e1004068. https://doi.org/10.1371/journal.pcbi.1004068
66. Zheng, B., Du, P., Zeng, Z., Cao, P., Ma, X., & Jiang, Y. (2024). Propranolol inhibits EMT and metastasis in breast cancer through miR-499-5p-mediated Sox6. Journal of Cancer Research and Clinical Oncology, 150(2), 59. https://doi.org/10.1007%2Fs00432-023-05599-w
67. Ege, N., Bouguenina, H., Tatari, M., & Chopra, R. (2021). Phenotypic screening with target identification and validation in the discovery and development of E3 ligase modulators. Cell chemical biology, 28(3), 283-299. https://doi.org/10.1016/j.chembiol.2021.02.011
68. Hothi, P., Martins, T. J., Chen, L., Deleyrolle, L., Yoon, J. G., Reynolds, B., & Foltz, G. (2012). High-throughput chemical screens identify Disulfiram as an inhibitor of human

glioblastoma stem cells. Oncotarget, 3(10), 1124. https://doi.org/10.18632/oncotarget.707

69. André, F., Ciruelos, E., Rubovszky, G., Campone, M., Loibl, S., Rugo, H. S., & Juric, D. (2019). Alpelisib for PIK3CA-mutated, hormone receptor–positive advanced breast cancer. New England Journal of Medicine, 380(20), 1929-1940. https://doi.org/10.1056/nejmoa1813904
70. Cheng, H. W., Liang, Y. H., Kuo, Y. L., Chuu, C. P., Lin, C. Y., Lee, M. H., & Huang, C. Y. (2015). Identification of Thioridazine, an anti-psychotic drug, as an antiglioblastoma and anti-cancer stem cell agent using public gene expression data. Cell death & disease, 6(5), e1753-e1753. https://doi.org/10.1038/cddis.2015.77
71. Morris, A., Pagare, P. P., Li, J., & Zhang, Y. (2022). Drug discovery efforts toward inhibitors of canonical Wnt/β-catenin signaling pathway in the treatment of cancer: A composition-of-matter review (2010–2020). Drug discovery today, 27(4), 1115-1127. https://doi.org/10.1016/j.drudis.2021.11.014
72. Foda, M. Y., Salem, M. L., AlAkwaa, F. M., & et al. (2024). Atorvastatin lowers breast cancer risk by reversing an early tumorigenic signature. Scientific Reports, 14, 17803. https://doi.org/10.1038/s41598-024-67706-2
73. Vilar, S., & Costanzi, S. (2012). Predicting the biological activities through QSAR analysis and docking-based scoring. Membrane protein structure and dynamics: Methods and Protocols, 271-284. https://doi.org/10.1007/978-1-62703-023-6_16
74. Sodero, A. C. R., Romeiro, N. C., Da Cunha, E. F. F., de Oliveira Magalhães, U., De Alencastro, R. B., Rodrigues, C. R., & Albuquerque, M. G. (2012). Application of 4D-QSAR studies to a series of raloxifene analogs and design of potential selective estrogen receptor modulators. Molecules, 17(6), 7415-7439. https://doi.org/10.3390/molecules17067415
75. Federico, A., Fratello, M., Scala, G., Möbus, L., Pavel, A., Del Giudice, G., & Greco, D. (2022). Integrated network pharmacology approach for drug combination discovery: a multi-cancer case study. Cancers, 14(8), 2043. https://doi.org/10.3390/cancers14082043
76. Cao, N., Lu, Y., Liu, J., Cai, F., Xu, H., Chen, J., & Zhuang, H. (2020). Metformin synergistically enhanced the anti-tumor activity of celecoxib in human non-small cell

lung cancer cells. Frontiers in Pharmacology, 11, 1094. https://doi.org/10.3389/fphar.2020.01094

77. Cufí, S., Vazquez-Martin, A., Oliveras-Ferraros, C., Corominas-Faja, B., Cuyàs, E., López-Bonet, E., ... & Menendez, J. A. (2013). The anti-malarial chloroquine overcomes primary resistance and restores sensitivity to trastuzumab in HER2-positive breast cancer. Scientific reports, 3(1), 2469. https://doi.org/10.1038/srep02469
78. Yang, M., Darwish, T., Larraufie, P., Rimmington, D., Cimino, I., Goldspink, D. A., & Gribble, F. M. (2021). Inhibition of mitochondrial function by metformin increases glucose uptake, glycolysis and GDF-15 release from intestinal cells. Scientific Reports, 11(1), 2529. https://doi.org/10.1038/s41598-021-81349-7
79. Essa, N. M., Salem, H. F., Elgendy, M. O., Gabr, A., Omran, M. M., Hassan, N. A., & Boshra, M. S. (2022). Efficacy of Metformin as adjuvant therapy in metastatic breast cancer treatment. Journal of Clinical Medicine, 11(19), 5505. https://doi.org/10.3390%2Fjcm11195505
80. Alqahtani, Q. H., Alkharashi, L. A., Alajami, H., Alkharashi, I., Alkharashi, L., & Alhinti, S. N. (2024). Pioglitazone enhances cisplatin's impact on triple-negative breast cancer: Role of PPARγ in cell apoptosis. Saudi Pharmaceutical Journal, 32(5), 102059. https://doi.org/10.1016%2Fj.jsps.2024.102059
81. Xu, B., Xing, A., & Li, S. (2022). The forgotten type 2 diabetes mellitus medicine: Rosiglitazone. Diabetology international, 13(1), 49-65. https://doi.org/10.1007%2Fs13340-021-00519-0
82. Ke, X. Y., Ng, V. W. L., Gao, S. J., Tong, Y. W., Hedrick, J. L., & Yang, Y. Y. (2014). Co-delivery of Thioridazine and doxorubicin using polymeric micelles for targeting both cancer cells and cancer stem cells. Biomaterials, 35(3), 1096-1108. https://doi.org/10.1016/j.biomaterials.2013.10.049
83. Kamgar-Dayhoff, P., & Brelidze, T. I. (2021). Multifaceted effect of Chlorpromazine in cancer: Implications for cancer treatment. Oncotarget, 12(14), 1406. https://doi.org/10.18632%2Foncotarget.28010
84. Pfab, C., Schnobrich, L., Eldnasoury, S., Gessner, A., & El-Najjar, N. (2021). Repurposing of anti-microbial agents for cancer therapy: what do we know?. Cancers, 13(13), 3193. https://doi.org/10.3390%2Fcancers13133193

85. Lamb, R., Fiorillo, M., Chadwick, A., Ozsvari, B., Reeves, K. J., Smith, D. L., & Lisanti, M. P. (2015). Doxycycline down-regulates DNA-PK and radiosensitizes tumor initiating cells: Implications for more effective radiation therapy. Oncotarget, 6(16), 14005. https://doi.org/10.18632/oncotarget.4159
86. Tsubamoto, H., Sonoda, T., Ikuta, S., Tani, S., Inoue, K., & Yamanaka, N. (2015). Combination chemotherapy with itraconazole for treating metastatic pancreatic cancer in the second-line or additional setting. Anti-cancer Research, 35(7), 4191-4196.
87. Sadowska, A., Prokopiuk, S., Miltyk, W., Surażyński, A., Konończuk, J., Sawicka, D., & Car, H. (2013). Metronidazole affects breast cancer cell lines. Advances in Medical Sciences, 58(1), 90-95. https://doi.org/10.2478/v10039-012-0070-2
88. Acharya, D. K. (1994). Role of Metronidazole in radiation therapy (a review of 717 cancer cases). Indian journal of medical sciences, 48(5), 111-116.
89. Coelho, M., Soares-Silva, C., Brandão, D., Marino, F., Cosentino, M., & Ribeiro, L. (2017). β-Adrenergic modulation of cancer cell proliferation: available evidence and clinical perspectives. Journal of cancer research and clinical oncology, 143, 275-291. https://doi.org/10.1007/s00432-016-2278-1
90. Xie, W. Y., He, R. H., Zhang, J., He, Y. J., Wan, Z., Zhou, C. F., & Liu, J. (2019). β-blockers inhibit the viability of breast cancer cells by regulating the ERK/COX-2 signaling pathway and the drug response is affected by ADRB2 single-nucleotide polymorphisms. Oncology Reports, 41(1), 341-350. https://doi.org/10.3892/or.2018.6830
91. Carnet Le Provost, K., Kepp, O., Kroemer, G., & Bezu, L. (2023). Trial watch: beta-blockers in cancer therapy. OncoImmunology, 12(1). https://doi.org/10.1080/2162402X.2023.2284486
92. Cakir, Y., Plummer, H. 3., Tithof, P. K., & Schuller, H. M. (2002). Beta-adrenergic and arachidonic acid-mediated growth regulation of human breast cancer cell lines. International journal of oncology, 21(1), 153-157 https://doi.org/10.3892/or.2018.6830
93. Yang, V., Gouveia, M. J., Santos, J., Koksch, B., Amorim, I., Gärtner, F., & Vale, N. (2020). Breast cancer: insights in disease and influence of drug methotrexate. RSC Medicinal Chemistry, 11(6), 646-664. https://doi.org/10.1039%2Fd0md00051e

94. C.L. Shapiro, Leflunomide in Previously Treated Metastatic Triple Negative Cancers https://ClinicalTrials.gov/show/NCT03709446 June 2020, 2021.
95. Hwang, N., & Chung, S. W. (2020). Sulfasalazine attenuates tamoxifen-induced toxicity in human retinal pigment epithelial cells. BMB reports, 53(5), 284. https://doi.org/10.5483%2FBMBRep.2020.53.5.041
96. Kerkhove, L., Geirnaert, F., Rifi, A. L., Law, K. L., Gutiérrez, A., Oudaert, I., & De Ridder, M. (2023). Repurposing sulfasalazine as a radiosensitizer in hypoxic human colorectal cancer. Cancers, 15(8), 2363. https://doi.org/10.3390%2Fcancers15082363
97. Kang, X., Jadhav, S., Annaji, M., Huang, C. H., Amin, R., Shen, J., & Chen, P. (2023). Advancing cancer therapy with copper/disulfiram nanomedicines and drug delivery systems. Pharmaceutics, 15(6), 1567. https://doi.org/10.3390%2Fpharmaceutics15061567
98. Liu, W. M., & Dalgleish, A. G. (2022). Naltrexone at low doses (LDN) and its relevance to cancer therapy. Expert review of anti-cancer therapy, 22(3), 269-274. https://doi.org/10.1080/14737140.2022.2037426
99. Weth, F. R., Hoggarth, G. B., Weth, A. F., Paterson, E., White, M. P., Tan, S. T., & Gray, C. (2024). Unlocking hidden potential: advancements, approaches, and obstacles in repurposing drugs for cancer therapy. British Journal of Cancer, 130(5), 703-715. https://doi.org/10.1038/s41416-023-02502-9
100. Peters, N., Jay, N., Barraud, D., Cravoisy, A., Nace, L., Bollaert, P. E., & Gibot, S. (2008). Metformin-associated lactic acidosis in an intensive care unit. Critical Care, 12, 1-5. https://doi.org/10.1186/cc7137
101. Meurer, L., & Cohen, S. M. (2020). Drug-induced liver injury from statins. Clinics in Liver Disease, 24(1), 107-119. https://doi.org/10.1016/j.cld.2019.09.007
102. Shaw, V., Srivastava, S., & Srivastava, S. K. (2021, January). Repurposing anti-psychotics of the diphenylbutylpiperidine class for cancer therapy. In Seminars in cancer biology (Vol. 68, pp. 75-83). Academic Press. https://doi.org/10.1016%2Fj.semcancer.2019.10.007
103. Li, Y., Meng, Q., Yang, M., Liu, D., Hou, X., Tang, L., & Bi, H. (2019). Current trends in drug metabolism and pharmacokinetics. Acta Pharmaceutica Sinica B, 9(6), 1113-1144. https://doi.org/10.1016%2Fj.apsb.2019.10.001

104. Klotz, U., & Antonin, K. H. (1977). Pharmacokinetics and bioavailability of sodium valproate. Clinical Pharmacology & Therapeutics, 21(6), 736-743. https://doi.org/10.1002/cpt1977216736
105. Askgaard, G., Friis, S., Hallas, J., Thygesen, L. C., & Pottegård, A. (2014). Use of Disulfiram and risk of cancer: a population-based case–control study. European journal of cancer prevention, 23(3), 225-232. https://doi.org/10.1097/cej.0b013e3283647466
106. Werlenius, K., Kinhult, S., Solheim, T. S., Magelssen, H., Löfgren, D., Mudaisi, M., & Jakola, A. S. (2023). Effect of Disulfiram and copper plus chemotherapy vs chemotherapy alone on survival in patients with recurrent glioblastoma: A randomized clinical trial. JAMA network open, 6(3), e234149-e234149. https://doi.org/10.1001/jamanetworkopen.2023.4149
107. Chang, M. (2012). Tamoxifen resistance in breast cancer. Biomolecules & therapeutics, 20(3), 256. https://doi.org/10.4062/biomolther.2012.20.3.256
108. Ben Sahra, I., Le Marchand-Brustel, Y., Tanti, J. F., & Bost, F. (2010). Metformin in cancer therapy: a new perspective for an old anti-diabetic drug?. Molecular cancer therapeutics, 9(5), 1092-1099. https://doi.org/10.1158/1535-7163.mct-09-1186
109. van der Pol, K. H., Aljofan, M., Blin, O., Cornel, J. H., Rongen, G. A., Woestelandt, A. G., & Spedding, M. (2023). Drug repurposing of generic drugs: challenges and the potential role for government. Applied Health Economics and Health Policy, 21(6), 831-840. https://doi.org/10.1007%2Fs40258-023-00816-6
110. Nouri, Z., Fakhri, S., Nouri, K., Wallace, C. E., Farzaei, M. H., & Bishayee, A. (2020). Targeting multiple signaling pathways in cancer: The rutin therapeutic approach. Cancers, 12(8), 2276. https://doi.org/10.3390/cancers12082276
111. Ricco, N., & Kron, S. J. (2023). Statins in cancer prevention and therapy. Cancers, 15(15), 3948. https://doi.org/10.3390%2Fcancers15153948
112. Yetisgin, A. A., Cetinel, S., Zuvin, M., Kosar, A., & Kutlu, O. (2020). Therapeutic nanoparticles and their targeted delivery applications. Molecules, 25(9), 2193. https://doi.org/10.3390%2Fmolecules25092193
113. Uddin, N., Elkordy, A., & Faheem, A. (2019). Fabrication and physicochemical characterisation of novel Pimozide loaded PLGA nanoparticles. British Journal of Pharmacy, 4(1). https://doi.org/10.5920/bjpharm.615

114. Shafighi, S., Zaefizadeh, M., Jaafari, B., Alivand, M. R., & Ghorbian, S. (2023). Synthesis of multifunctional nano-drug with targeted delivery for the synergistic pathway of various inducers on inhibition of breast cancer cell line. http://dx.doi.org/10.21203/rs.3.rs-3309260/v1
115. Krzyszczyk, P., Acevedo, A., Davidoff, E. J., Timmins, L. M., Marrero-Berrios, I., Patel, M., ... & Yarmush, M. L. (2018). The growing role of precision and personalized medicine for cancer treatment. Technology, 6(03n04), 79-100. https://doi.org/10.1142/s2339547818300020
116. Landgren, O., & Iskander, K. (2017). Modern multiple myeloma therapy: deep, sustained treatment response and good clinical outcomes. Journal of Internal Medicine, 281(4), 365-382. https://doi.org/10.1111/joim.12590
117. Neves Rebello Alves, L., Dummer Meira, D., Poppe Merigueti, L., Correia Casotti, M., do Prado Ventorim, D., Ferreira Figueiredo Almeida, J., & Drumond Louro, I. (2023). Biomarkers in breast cancer: an old story with a new end. Genes, 14(7), 1364. https://doi.org/10.3390%2Fgenes14071364
118. Abdelmoneim, M., Aboalela, M. A., Naoe, Y., Matsumura, S., Eissa, I. R., Bustos-Villalobos, I., & Kasuya, H. (2023). The impact of Metformin on tumor-infiltrated immune cells: preclinical and clinical studies. International Journal of Molecular Sciences, 24(17), 13353. https://doi.org/10.3390%2Fijms241713353
119. Karpel-Massler, G., Kast, R. E., Westhoff, M. A., Dwucet, A., Welscher, N., Nonnenmacher, L., & Halatsch, M. E. (2015). Olanzapine inhibits proliferation, migration and anchorage-independent growth in human glioblastoma cell lines and enhances temozolomide's antiproliferative effect. Journal of neuro-oncology, 122, 21-33. https://doi.org/10.1007/s11060-014-1688-7
120. Sanomachi, T., Suzuki, S., Kuramoto, K., Takeda, H., Sakaki, H., Togashi, K., & Kitanaka, C. (2017). Olanzapine, an atypical anti-psychotic, inhibits survivin expression and sensitizes cancer cells to chemotherapeutic agents. Anti-cancer research, 37(11), 6177-6188. https://doi.org/10.21873/anticanres.12067
121. El-Sheridy, N. A., El-Moslemany, R. M., Ramadan, A. A., Helmy, M. W., & El-Khordagui, L. K. (2021). Enhancing the in vitro and in vivo activity of itraconazole

against breast cancer using miltefosine-modified lipid nanocapsules. Drug delivery, 28(1), 906-919. https://doi.org/10.1080%2F10717544.2021.1917728

122. Doheny, D., Manore, S., Sirkisoon, S. R., Zhu, D., Aguayo, N. R., Harrison, A., & Lo, H. W. (2022). An FDA-approved anti-fungal, ketoconazole, and its novel derivative suppress tGLI1-mediated breast cancer brain metastasis by inhibiting the DNA-binding activity of brain metastasis-promoting transcription factor tGLI1. Cancers, 14(17), 4256. https://doi.org/10.3390%2Fcancers14174256
123. Harris, A. L., Cantwell, B. M., & Dowsett, M. (1988). High dose ketoconazole: endocrine and therapeutic effects in postmenopausal breast cancer. British journal of cancer, 58(4), 493-496. https://doi.org/10.1038/bjc.1988.247
124. Bae, S. H., Park, J. H., Choi, H. G., Kim, H., & Kim, S. H. (2018). Imidazole anti-fungal drugs inhibit the cell proliferation and invasion of human breast cancer cells. Biomolecules & therapeutics, 26(5), 494. https://doi.org/10.4062%2Fbiomolther.2018.042
125. Cook, K. L., Wärri, A., Soto-Pantoja, D. R., Clarke, P. A., Cruz, M. I., Zwart, A., & Clarke, R. (2014). Chloroquine inhibits autophagy to potentiate antiestrogen responsiveness in ER+ breast cancer. Clinical Cancer Research, 20(12), 3222-3232. https://doi.org/10.1158/1078-0432.ccr-13-3227
126. Augustin, Y., Staines, H. M., & Krishna, S. (2020). Artemisinins as a novel anti-cancer therapy: targeting a global cancer pandemic through drug repurposing. Pharmacology & Therapeutics, 216, 107706. https://doi.org/10.1016%2Fj.pharmthera.2020.107706
127. Lamb, R., Ozsvari, B., Lisanti, C. L., Tanowitz, H. B., Howell, A., Martinez-Outschoorn, U. E., & Lisanti, M. P. (2015). Antibiotics that target mitochondria effectively eradicate cancer stem cells, across multiple tumor types: treating cancer like an infectious disease. Oncotarget, 6(7), 4569. https://doi.org/10.18632/oncotarget.3174
128. Komatsu, S., Miyazawa, K., Moriya, S., Takase, A., Naito, M., Inazu, M., & Tomoda, A. (2012). Clarithromycin enhances bortezomib-induced cytotoxicity via endoplasmic reticulum stress-mediated CHOP (GADD153) induction and autophagy in breast cancer cells. International journal of oncology, 40(4), 1029-1039. https://doi.org/10.3892%2Fijo.2011.1317

129. Talarico, G., Orecchioni, S., Dallaglio, K., Reggiani, F., Mancuso, P., Calleri, A.,& Bertolini, F. (2016). Aspirin and Atenolol enhance metformin activity against breast cancer by targeting both neoplastic and microenvironment cells. Scientific reports, 6(1), 18673. https://doi.org/10.1038/srep18673

CHAPTER 2

Target Identification and Drug Screening

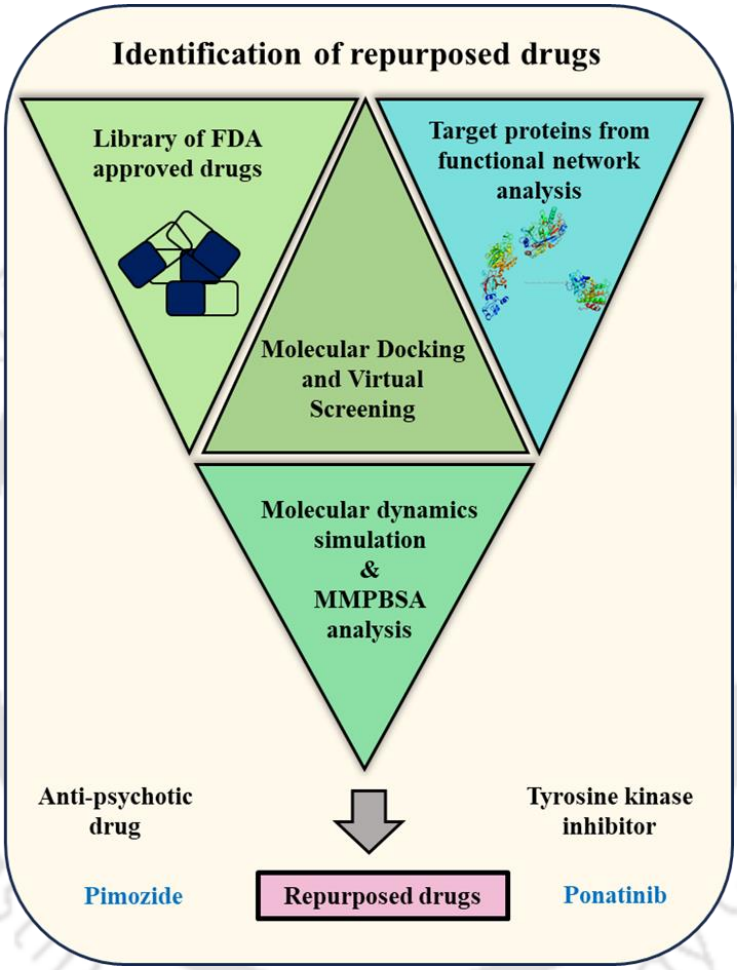

Chapter 2 identifies key target proteins (IR, ITGB1, CD36) and potential inhibitors using network analysis and computational screening, selecting Pimozide and Ponatinib as lead repurposed drugs. Their anti-cancer efficacy is validated through in vitro studies on breast cancer cell lines.

Molecular Informatics, 2022, 41(8), 2100300.

DOI: 10.1002/minf.202100300

CHAPTER 2

Target Identification and Drug Screening

2.1. Introduction

Breast cancer is one of the most common malignancies among urban women in India. As per the National cancer registry program, its annual surge is recorded to be approximately 2% compared to the other cancers, which stands at 0.68% over three years [1]. Over the last two decades, several researchers across the globe have contributed towards understanding the etiology of breast cancer with an aim to establish a suitable therapeutic module for obliterating the aggressive malignancy. However, the newly synthesized drugs' conversion into clinical use has been substantially reduced in the last few years. The reason behind the clinical attrition is not technical but the philosophy of rational drug discovery approach, especially the "one gene, one drug, one disease" paradigm. Even though the philosophy of rational drug design is followed for more than two decades to design a drug with lesser side effects, the clinical attrition rate of drugs challenges this approach [2].

Cancer is a complex disease with a highly synchronized network of growth driving signaling and metabolic pathways, which helps it to grow under stress conditions, escape from immune recognition, and facilitates its dissemination to other organs. Hence, the "one gene, one drug, one disease" paradigm needs to be altered with perturbation of the disease-causing network for cancer drug development. Moreover, the network biology analysis suggests that perturbation of disease-causing networks requires targeting multiple proteins in the network rather than individual protein(s) [3].

2.1.1Altered metabolism and EMT

Altered metabolism is one of the major hallmarks of cancer, whereby cancer cells rewire their metabolic pathways to fulfill the massive energy requirement for its rapid proliferation. Aerobic glycolysis is the well-established altered metabolism of glucose in cancer cells (i.e., Warburg effect). However, it is an inefficient way to produce ATPs. Therefore, to balance the reduced ATP production through aerobic glycolysis, cancer cells uptake more glucose and increase the rate of aerobic glycolysis [4]. On account of this metabolic rewiring, the cancer cells fulfill their energy requirement and increase their biomass production (such as essential fatty acids, lipids, nucleic acids, and amino acids) for their uncontrolled proliferation [5]. Research evidences suggest that

enzymes involved in the glycolysis pathway can drive EMT, thereby potentiating metastasis. [6] For example, the overexpression of phosphoglucose isomerase (PGI) involves stabilizing ZEB1 and ZEB2 via NF-kB signaling in breast cancer, and suppressing PGI leads to reverse MET in lung fibrosarcoma [6]. Similarly, aldose A (ALDOA), glyceraldehyde-3-phosphate dehydrogenase (GAPDH), and lactate dehydrogenase (LDH) also increases EMT via SNAI1 in several cancers [6].

Furthermore, EMT also triggers the metabolic rewiring in cancer cells. During EMT, the epithelial phenotypic cancer cells acquire mesenchymal properties and detach themselves from the extracellular matrices [5]. This transition causes detachment triggered ATP deficiency as a result of the reduced glucose uptake. Furthermore, after the mesenchymal transition, cancer cells undergo different phases of metastasis such as invasion, intravasation, circulation, extravasation, and colonization. In all these phases, the lesser availability of the nutrients and the higher amount of stress in the tumor microenvironment compels the cancer cells to rewire their metabolic pathways. Moreover, under this metabolic stress, the essential ATPs and biomass are generated from fatty acid oxidation and autophagy [5].

In this study, the altered metabolism and EMT (Epithelial to Mesenchymal Transition) signaling network of breast cancer has been substantially portrayed through networking followed by targeting. The interconnected functional associations of the genes involved in both the phenomenon are constructed based on the pathway studies. Furthermore, a list of FDA-approved drugs obtained from the Guide to pharmacology server was screened against the selected target proteins. The drugs having inhibitory activity against all the three target proteins were selected using molecular docking, molecular dynamic simulations, and binding free energy (MM-PBSA) studies. Moreover, *in-vitro* cell viability assay was carried out using the selected drug to validate the selected repurposed drug.

Therefore, repurposing an FDA-approved drug to target multiple proteins in the network will not only increase the efficacy of the treatment, but also reduce the time and capital required for the development of a novel drug.

2.2. Experimental Section

2.2.1. Functional network construction

The interconnection between the functional network of altered metabolism and EMT signaling was established by combining the pathways of central carbon metabolism in cancer (KEGG id: hsa05230), fatty acid digestion and absorption (KEGG id: hsa04975), fatty acid metabolism (KEGG id: hsa01212), and EMT signaling pathways (such as Wnt (KEGG id: hsa04310), TGF-β (KEGG id: hsa04350), PI3K/Akt (KEGG id: hsa04151), MAPK (KEGG id: hsa04010), NF-kB pathways (KEGG id: hsa04064)). The details of the above-mentioned pathways were downloaded from the KEGG pathway database (https://www.genome.jp/kegg/pathway.html). KEGG pathway database is a collection of pathway maps representing the molecular interactions and reactions of cellular pathways. The interconnection between the pathways was established with help of previously reported studies [7, 8, 9, 10, 11], which was further validated using the STRING v9.1 database (https://string-db.org) [12]. STRING (Search Tool for the Retrieval of Interacting Genes) provides the protein-protein interaction network derived from high throughput experimental data, analysis of co-expressed genes, database, and literature mining. Herein, the list of proteins present in the interconnected functional network was given as a query list in the STRING database. The maximum number of interactors in the network was limited to the query proteins only and the network type was set to full STRING network which provided both functional and physical association of the query proteins.

2.2.2. Microarray analysis

To appraise the significance of the selected genes (IR, ITGB1 & CD36) in cancer, the variation in the expression levels was analyzed in malignant versus normal cells, using the Oncomine database (https://www.oncomine.org/resource/login.html). The Oncomine is a cancer microarray expression database, wherein the expression analyses of numerous studies are log-transformed and median-centered for an individual array. It allows the user to perform multiple analysis based on their requirement. In this study, the analysis type and cancer type filters were used to retrieve the data pertaining to the gene of interest. Subsequently, the differential analysis of the gene expression level in a normal versus diseased state provided us with two significant datasets based on the study conducted by different groups of scientists across the world. Herein, each gene is assigned a rank, which is pertaining to their ranking in a particular dataset on account of their p-

value. The p-value signifies the differences between the groups specified for differential analysis. It is calculated by the database, which is based on the t-test statistics. Moreover, the ranking of the genes was used as an essential parameter to assess their significance in cancer.

2.2.3. Protein preparation

The three-dimensional coordinates of target proteins (Insulin receptor: PDB ID_4IBM, CD36: PDB ID_5LGD, ITGB1: PDB ID_4WK0) were downloaded from RCSB PDB database (https://www.rcsb.org/) in PDB format. The water molecules, ions, and small molecules were removed from the respective PDB structures using PyMol 2.3 (Schrodinger, LLC. 2010. The PyMOL Molecular Graphics System, Version 2.3.). Hydrogen atoms, charges were added to the PDB structure and the atom types were changed to AD4 using Autodock4 [13]. After the modifications, the structures were saved in pdbqt format and were further used for the docking studies.

2.2.4. Ligand preparation

The library of FDA-approved drugs was downloaded from the Guide to pharmacology server (https://www.guidetopharmacology.org/GRAC/LigandListForward?database=all) as SDF format. [14] The library contains 1293 FDA-approved drugs currently used for various diseases. The SDF format of all the ligands was converted into pdbqt format for Vina docking using Open Bable version 2.4.0 [15]. Based on literature studies Ceritinib (PubChem ID: 57379345) [16], Nobiletin (PubChem ID: 72344) [17], and Matrine (PubChem ID: 91466) [18] were selected as the control inhibitors for IR, CD36, and ITGB1, respectively. The control inhibitors were downloaded from PubChem in SDF format and were converted into pdbqt using Openbable. In addition, set of inhibitors with known inhibition values were downloaded (SDF format) from ChEMBL (https://www.ebi.ac.uk/chembl/) for each target protein CD36 and IR (no inhibitors available for ITGB1).

2.2.5. Virtual screening of FDA approved drugs

Virtual screening is an efficient method to predict the potent binding partners for target proteins. In this study AutoDock Vina 1.1.2 an open-source software was used for virtual screening of drug libraries. Vina considers the proteins as rigid and ligands as flexible during the virtual screening process [19]. The search box (size of X, Y, Z nm with center at Xc, Yc, Zc nm) for virtual screening was set to (size of 49.9834, 59.6378, 53.8160 nm with center at -3.9276, -6.8331, 16.947) for IR, (size of 47.2572, 30.7497, 55.0701 nm with center at -43.5045, -30.3028, 30.6686 nm) for CD36 and (size of 50.6492, 87.5371, 69.9574 nm with center at 20.8639, -2.9008, -52.0917 nm) for ITGB1. The physical interactions of drugs with target proteins were visualized and images were rendered using PyMol 2.3 (Schrodinger, LLC. 2010. The PyMOL Molecular Graphics System, Version 2.3.) and Discovery Studio Visualizer v20.1.0.19195.

2.2.6. Molecular dynamics simulation

Molecular dynamics simulation is an effective computational tool to study the behavioral changes of biomolecules such as proteins, nucleic acids, and lipids in a dynamic environment. The dynamic behavioral changes of target proteins upon binding of a drug molecule was analyzed with GROMACS 2019.6. The PDB structures of the proteins were converted into gmx format (gromacs format) using the CHARMM27 force field [20]. The topology of protein-drug complexes was generated by following Justin's gromacs tutorial [21]. The complexes were confined in a dodecahedron box with a distance of 1.0 nm from the box edge and the TIP3P water model was used to solvate the complex system. Na^+ ions and Cl^- ions were added to the solvated system based on the net charge using the "genion" module of gromacs. The energy of the system was minimized until the maximum force attained was lesser than 10kJ/mol using the steepest descent algorithm. The equal distribution of ions and solvents around the protein-drug complexes was confirmed by running the canonical ensemble (NVT equilibration) with a velocity-rescale thermostat and isobaric-isothermal ensemble (NPT equilibration) with Berendsen pressure coupling for 100 Pico-seconds. The reference temperature and pressure were set to 300 K and 1 atmosphere for NVT and NPT ensembles, respectively. The final MD run of equilibrated system was performed for 100 nanoseconds with two femto second (2 fs) time step. The analysis of root means square deviation (RMSD), root means square fluctuations (RMSF) and pair distance were done after the successful completion of MD simulation.

2.2.7. Binding free energy

The strength of the binding forces of protein-drug interactions was assessed in terms of free energies using MMPBSA (Molecular Mechanics Poisson-Boltzmann Surface Area) method. MM-PBSA is an extensively used method to calculate the binding free energy of protein-ligand complexes from MD trajectories. The snapshots of complex structures were extracted from MD trajectory file with 1 ns time intervals, and binding energies were calculated using g_mmpbsa gromacs function [22]. The Binding free energy ($\triangle G_{\text{bind}}$) of each complex were calculated using the following equation:

$$\triangle G_{\text{bind}} = \triangle EMM + \triangle GPBSA - \text{T}\triangle SMM$$

where $\triangle G_{\text{bind}}$ is the calculated average free energy, $\triangle EMM$ is the average molecular mechanics' energy, $\triangle GPBSA$ is the solvation free energy, and $\text{T}\triangle SMM$ represents the solute configuration entropy [23].

2.2.8. Cell lines and culture condition

The MCF7, MDAMB231, and MDAMB468 (human breast cancer cell lines) were purchased from the National Centre for Cell Science, Pune, India. It was cultured in Dulbecco's Modified Eagle Medium supplemented with L-glutamine, sodium pyruvate (Sigma-Aldrich, St. Louis, MI, USA), 10% FBS (fetal bovine serum) (Thermo Fisher Scientific, Waltham, MA, USA), sodium bicarbonate (Sigma-Aldrich), 100 U/ml Penicillin and 100 µg/ml Streptomycin (Thermo Fisher Scientific). The cells were maintained at 37 °C in humidified air containing 5% carbon dioxide. The protocol mentioned in the previous study was followed to induce EMT in MDA-MB-231 and MDA-MB-468 cell lines [24].

2.2.9. Cell viability assay

The cell viability was evaluated using [3-(4,5-dimethylthiazol-2-yl)-2,5-diphenyltetrazolium-bromide] MTT assay (HiMedia) in which the tetrazolium salt is reduced to purple-colored formazan by the respiring mitochondria of the living cells. A total of 5x10^3 cells/well in a 96-well plate were used to assess the dose-dependent cell viability of the treated cells with increasing concentrations of the drug, Pimozide (Purity >98% by TLC, Sigma-Aldrich, St. Louis, MI, USA). After 48 hours of treatment, 5 µl of MTT was directly added to the wells and was incubated for 1

hour 30 minutes at 37 °C under humidified conditions with 5% CO_2. The percentage cell viability was calculated by taking the absorbance of the formazan crystals dissolved in DMSO at 570 nm and the background measurement was normalized at 630nm using a microplate reader (Infinite 200 PRO, Tecan, Crailsheim, Germany). The data was normalized by taking the cell viability of the untreated cells as 100%. The cell viability (%) was determined using the formula:

$$Cell\ viability\ \% = \frac{[(Abs\ 570 - Abs\ 630)\ treated\ cells]}{[(Abs\ 570 - Abs\ 630)\ control\ cells]} * 100$$

Following this, the inhibitory concentration-50 (IC_{50}) values were determined from the sigmoidal dose-response curves using the GraphPad Prism (version 6.0.0 for Windows, GraphPad Software, San Diego, California USA, www.graphpad.com).

2.2.10. Reactive oxygen species (ROS) detection assay

The level of cellular reactive oxygen species plays an essential role in determining cell fate. Depending on the level and exposure to the ROS, a cell can enter into apoptosis or proliferation. The most commonly used method to detect the intracellular ROS level is using of cell-permeable ROS-sensitive fluorescent dye, 2′,7′-dichlorofluorescein diacetate (DCFDA). DCFDA is deacetylated by cellular esterase and converted into a non-fluorescent compound after entering the cell. This non-fluorescent form is later oxidized by several cellular reactive oxygen species and is converted to DCF (2′,7′-dichlorofluorescein). DCF is highly fluorescent and can be detected by fluorescent spectroscopy or flow cytometry. In this study, the cells are treated with Pimozide for 24 h and incubated with 2 µM DCFDA for 30 min. After incubation, cells were trypsinized and washed with PBS to remove excess DCFDA. Reactive oxygen species were analyzed using a CytoFLEX (Beckman Coulter) flow cytometer.

2.2.11. Statistical analysis

All the statistical analyses were carried out using the GraphPad Prism software. The experimental data were expressed as mean ± SEM. Additionally, a one-way ANOVA test was used to access the correlations among the groups. The p-value < 0.05 (*) is considered to be statistically significant, whereas p<0.001 (***) and p<0.0001 (****) are considered to be highly significant.

2.3. Results

2.3.1. Functional network analysis

The interconnected functional network of altered metabolism and EMT signaling was constructed based on the pathway studies. Herein, eight pathway networks were downloaded that comprised a total of 1182 genes, and each pathway is highly activated during a different phase of cancer progression. Aerobic glycolysis (Warburg effect) is highly activated at the initial stages of cancer when cancer cells require massive energy and biomass for uncontrolled proliferation, while fatty acid oxidation is highly activated during metastasis or invasive stage of cancer when cancer cells are unable to produce the biomass from glucose metabolism. This metabolic rewiring also affects the pathways that activate the EMT-related genes, such as PI3K/Akt, TGF-β, NF-kB, Wnt, and MAPK pathways. The metabolic and EMT signaling pathways are interconnected in such a way that they can mutually rewire each other based on the changes in the tumor microenvironment.

The interconnection between these pathways using previously reported studies was established [7, 8, 9, 10, 11]. The resulting interconnected functional network consists of 70 genes, which are directly involved in both cancer metabolism and EMT signaling (**Figure 2.1**). The established interconnected network was further validated using the STRING server. It provided us with the functional and physical association between these 70 genes. All the proteins in the network were found to be interconnected with one or more proteins either functionally or physically (**Figure 2.2**). Moreover, three target proteins (IR, CD36 & ITGB1) were selected from the network based on the criteria that targeting the combination of proteins should perturbate 100% of the interconnected network. Additionally, IR, CD36, and ITGB1 are cell surface receptors, which are the commencing point of the interconnected network and can easily be targeted.

Insulin receptor (IR), Integrin β1 (ITGB1), and CD36 (also known as fatty acid translocase (FAT)) are the three key players of glucose and fatty acid metabolism in breast cancer cells. They also activate the pathways that potentiates EMT such as PI3K/AKT, NF-kB, MAPK, TGFβ, and Wnt signaling pathways. IR is a 156 kDa tyrosine kinase receptor that mediates the pleiotropic effects of insulin or insulin-like growth factors (IGFs). The binding of insulin or insulin-like ligands activates the IR by autophosphorylation of tyrosine residues (amino acids 960, 953, and/or 972, 1146, 1151, 1152, 1316, and 1322) [25]. Activated IR phosphorylates IRS1 (Insulin receptor substrate 1) and promotes the translocation of GLUT4 to the cell membrane via PI3K/AKT

pathway. PI3K/AKT pathway also plays a crucial role in EMT activation by activating the transcription of EMT genes via mTORC1, GSK3β/β-catenin, and NF-kB pathways. It is reported that the expression of IR is 6 to 7-fold higher in breast cancer than the normal breast tissue [26]. This aberrant expression of IR causes the increased glucose uptake and glycolysis via GLUT4 to manage the excessive energy requirement for cancer cell proliferation. It also activates the transcription of EMT transcription factors via the Src/Ras/MAPK signaling pathway.

On other hand, ITGB1 is also involved in the increased glucose uptake and glycolysis via the FAK/PI3K/AKT pathway in breast cancer [27]. ITGB1 is a member of the integrin superfamily which has multiple functions like cell adhesion, proliferation, and migration. ITGB1 was reported to overexpress in many cancers and is known to facilitate EMT and metastasis [28]. It activates the transcription of EMT genes via the TGF-β/SMAD2/3/4 signaling pathway.

CD36 is a transmembrane glycoprotein that is involved in the translocation of free fatty acids from the extracellular region to the cytoplasm, also known as FA translocase (FAT), scavenger receptor class B type 2 (SR-B2), GP88, and platelet GPIV. It is widely expressed on the cell surface of dendritic cells (DCs), retinal epithelial cells, monocytes, microvascular endothelial cells (MVECs), adipocytes, platelets, microglial cells, and enterocytes [29]. At the initial stage of cancer, the expression level of CD36 is invariably low and it increases during metastasis [30]. This increased expression of CD36 during metastasis provides the energy source and precursor for cell proliferation via fatty acid oxidation. Apart from cancer metabolism, CD36 also interacts with several signaling pathways that activate EMT and metastasis [31]. Mostly, it activates epithelial to mesenchymal transition (EMT) causing genes via the Wnt/β-catenin signaling pathway.

Therefore, based on the interconnected network analysis, IR, ITGB1, and CD36 have a greater impact on cancer metabolism and EMT signaling, and targeting these three surface receptors might be a potent therapeutic approach for obliterating cancer.

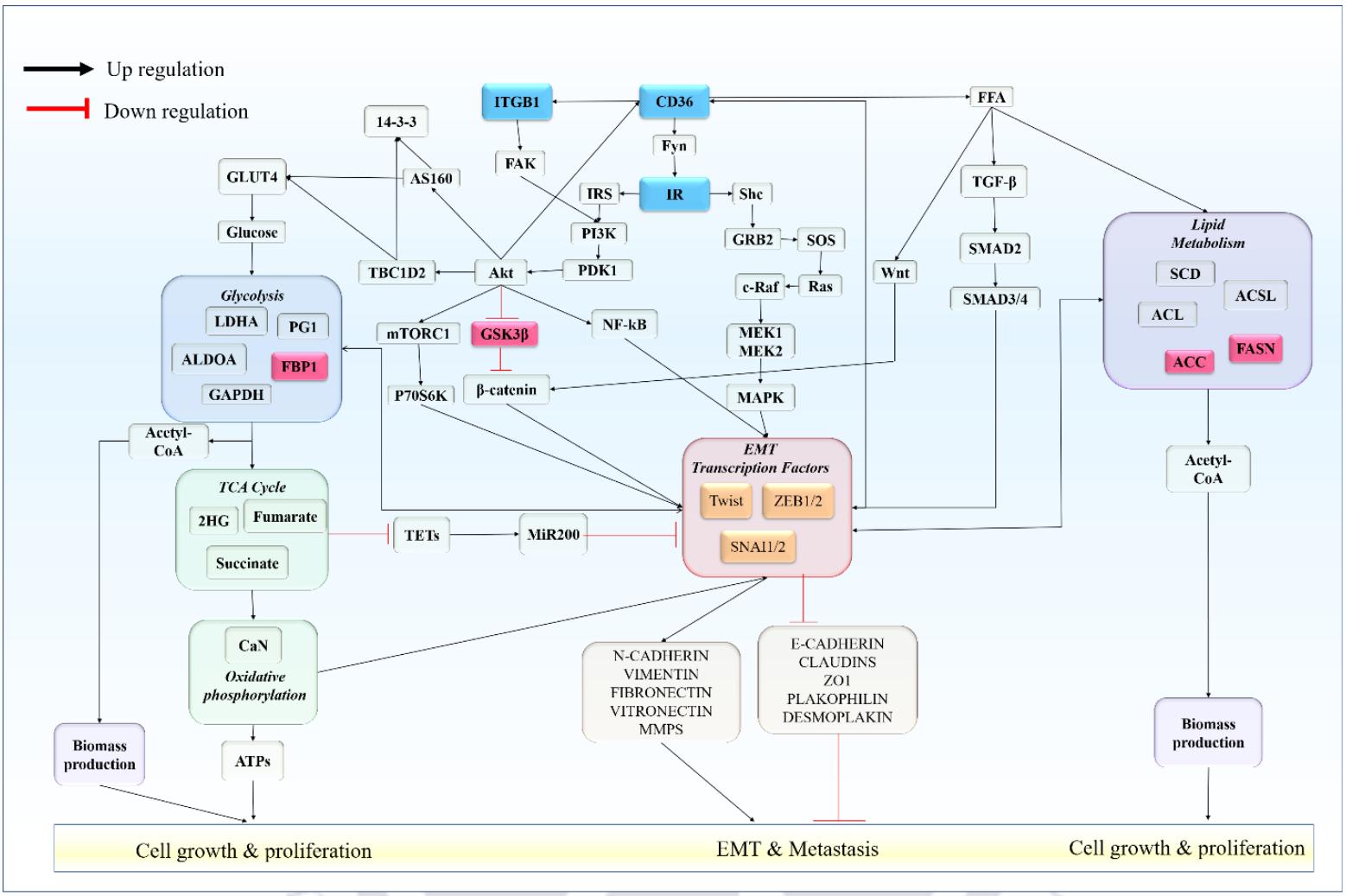

Figure 2.1: *Interconnected functional network of altered metabolism and EMT signaling. Boxes in blue color signifies the target proteins, red color indicates proteins involved in the downregulation of EMT transcription factors, while the other shades are involved in the upregulation of EMT and cell proliferation.*

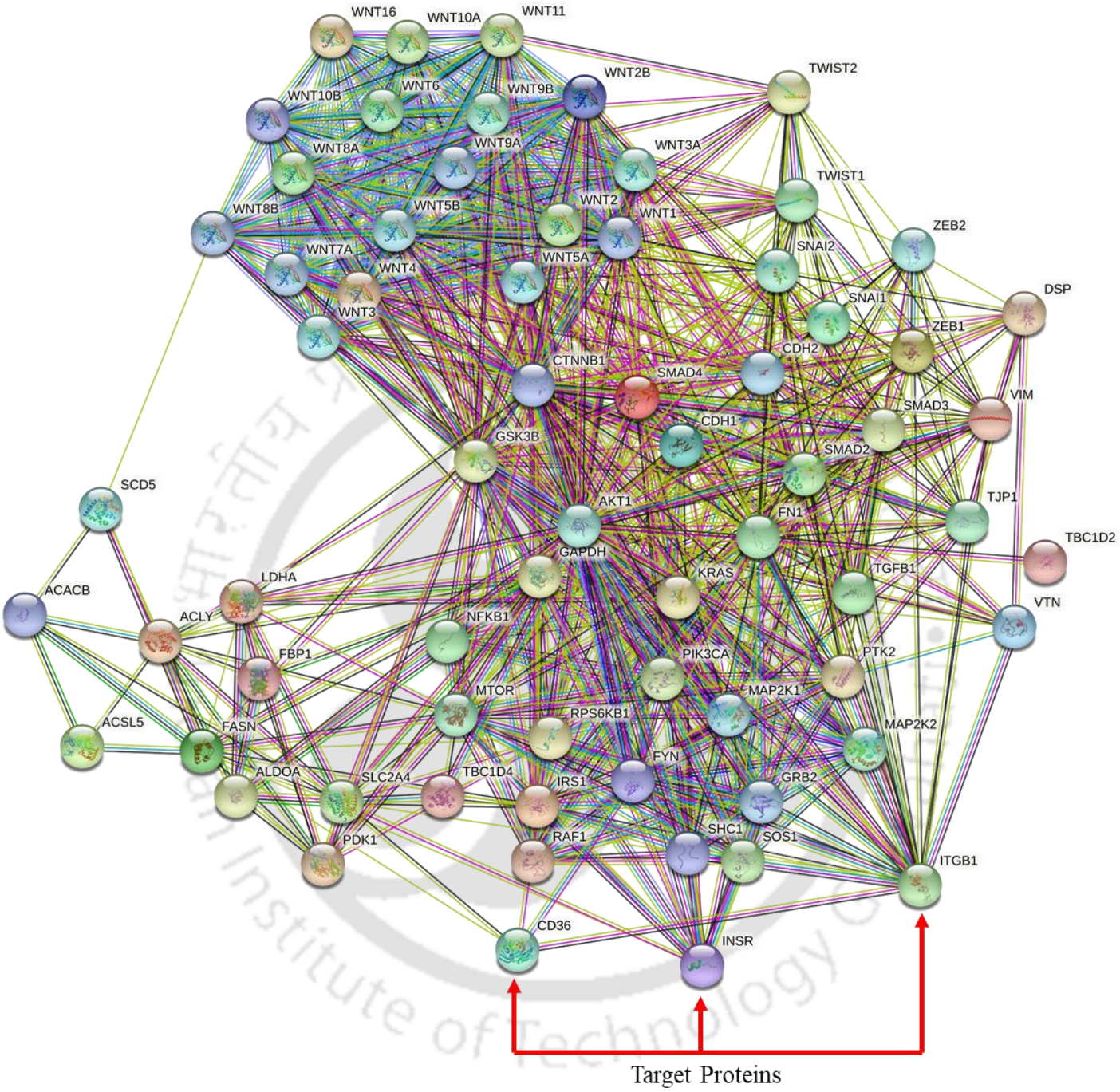

Figure* 2.2*: *Functional and physical association between the proteins of the interconnected functional network, validated by the STRING protein-protein interaction database.*

2.3.2. Microarray analysis

Based on the reports of various studies, the Oncomine database reveals the expression profile of the following genes (IR, ITGB1, and CD36) in various breast cancer subtypes, which are mentioned in **Table 2.1**. To ensure the significant difference in the expression pattern of the genes in cancer versus normal cells, the genes exhibiting a rank above 20% were considered significant. Microarray analysis revealed the overexpression of target proteins in various types of breast cancers and supported the target selection. Therefore, suggesting the fact that these three selected target proteins might be potential biomarkers of breast cancer.

Table 2.1: *Expression analysis of Target proteins in breast cancers by the Oncomine database*

Gene	Over-expression in breast cancer (Gene-rank)					Over-expression in breast cancer (Fold-change)				
	p-value	Fold change	Ranking %	Cancer Type	Group	p-value	Fold change	Ranking %	Cancer Type	Group
CD36	3.2E-13	1.632	8	Invasive Breast Carcinoma Stroma	Finak Breast [32]	3.2E-13	1.632	8	Invasive Breast Carcinoma Stroma	Finak Breast [32]
INSR	9.5E-4	1.48	5	Ductal Breast Carcinoma in situ Stroma	Ma Breast 4 [33]	0.06	2.634	11	Ductal Breast Carcinoma in-situ	Radvanyi Breast [35]
ITGB1	0.006	1.57	8	Invasive Ductal Breast Carcinoma Stroma	Karnoub Breast [34]	8.19E-6	2.519	32	Invasive Breast Carcinoma Stroma	Finak Breast [32]

2.3.3. Virtual screening studies

The library of 1293 approved drugs were screened against the respective target proteins (IR, CD36, and ITGB1), obtained from the PDB database. Ceritinib, Nobiletin, and Matrine, which were selected as the control inhibitors for IR, CD36, and ITGB1, respectively, and used to validate the docking studies. The virtual screening was performed using Autodock Vina, which provided us with more than 500 drugs with greater binding energy than the control inhibitors for each target protein. The predicted binding energy of Ceritinib, Nobiletin, and Matrine were -7.4, -8.2, and -6.3 Kcal/mol, respectively. Following this, top 50 ranked drugs were selected for each target protein and checked for the common drugs among them that will get bound to all three proteins. Seven FDA-approved drugs exhibit better binding scores than reference drugs on the three targets

(IR, CD36, and ITGB1). Among these seven drugs, four are being used as anticancer drugs (Capmatinib, Nilotinib, Radotinib, and Ponatinib), while two are being used as antipsychotic drugs (Risperidone and Pimozide) and one is being used to treat opioid-induced constipation (Naldemedine). Furthermore, these seven drug complexes were selected for further analysis. The binding energies, along with their binding interactors of the selected complexes are mentioned in **Table 2.2**. Additionally, the 2D interaction profile of the docked complexes is depicted in **Figure 2.3**. The dynamic behaviors of these seven drugs with target proteins were further analyzed with molecular dynamics simulation and binding free energy analysis.

Table 2.2: *Interaction details of selected drugs with target proteins predicted by Auto dock Vina.*

Drugs	Binding energies (kcal/mol)	No. of Hydrogen Bonds	Interacting amino-acid in Hydrogen bond	No. of Non-covalent interactions	Interacting amino-acids in the non-covalent interactions
Insulin Receptor (IR)					
Capmatinib	-10	1	SER1090	20	ILE1157, ASP1083, LEU1002, GLY1003, MET1139, VAL1010, MET1153, LYS1030, ASP1150, MET1076, ALA1028, VAL1060, MET1079, GLU1077, GLY1082, LEU1078, PRO1099, SER1086, HIS1081, TYR1087
Naldemedine	-9.3	0	-	18	TYR1087, HIS1081, SER1090, ASN1097, SER1086, ALA1080, ARG1000, ILE1157, MET1139, ASP1150, MET1076, VAL1060, GLU1077, LEU1078, MET1079, VAL1010, LEU1002, GLY1003
Nilotinib	-10.2	2	ASP1083, ASN1097	24	HIS1081, GLY1082, SER1090, TYR1087,

					VAL1060, GLU1077, ASP1150, MET1079, LEU1078, MET1138, LEU1002, ARG1089, ALA1095, ALA1028, MET1076, VAL1010, GLY1003, ILE1157, GLU1004, GLY1005, MET1153, SER1086, THR1154, TYR1158
Pimozide	-10.3	1	ASN1097	23	GLN1004, MET1153, GLY1005, ILE1157, THR1154, VAL1010, ASP1150, MET1076, VAL1060, GLU1077, ALA1028, MET1139, MET1079, LEU1078, LEU1002, GLY1082, HIS1081, PRO1099, TYR1087, SER1090, SER1086, GLY1003, ASP1083
Ponatinib	-9.3	3	SER1090, ASN1097, ASP1150	20	GLN1004, ILE1157, ASP1083, GLY1003, SER1086, TYR1087, MET1153, VAL1010, MET1139, LEU1002, GLY1082, HIS1081, MET1076, ALA1028, MET1079, ALA1080, PRO1099, VAL1060, GLU1077, LEU1078
Radotinib	-9.9	3	ASN1097, LEU1002, SER1086	18	SER1090, ARG1089, LEU1078, ARG1000, ALA1080, HIS1081, MET1079, GLY1082, MET1153, MET1076,

					ASP1150, ALA1028, MET1139, VAL1010, GLY1003, ASP1083, ILE1157, TYR1158
Risperidone	-9.7	1	MET1079	17	SER1090, ASN1097, SER1086, ASP1083, MET1139, MET1153, ASP1150, LEU1078, GLY1082, LEU1002, HIS1081, TYR1087, MET1076, VAL1060, ALA1028, GLU1077, VAL1010
CONTROL	-7.4	0	-	20	GLY1003, ASP1083, GLY1082, GLY1005, GLY1004, SER1086, ARG1000, ILE1157, MET1153, VAL1010, THR1154, MET1139, MET1079, LEU1002, ALA1080, ASN1097, SER1090, TYR1087, HIS1081, PRO1099
			CD36		
Capmatinib	-8.4	3	ASP250, SER268, SER269	16	PHE114, TYR212, ARG96, GLN116, LYS385, ALA251, PHE383, THR369, PHE266, LEU371, LEU295, ILE275, ASP270, ILE271, LEU387, PHE300
Naldemedine	-8.4	2	SER269, LYS334	22	ASP250, SER268, ARG96, LYS385, ARG63, ASN118, TYR204, PHE201, PRO203, THR207, PHE114, TYR212, CYS333, ASP209, ASP270, TYR238, TYR230, CYS272,

					LEU236, LYS231, PHE267, GLU116
Nilotinib	-8.6	5	SER269, ASP209, ASN118, THR207, ARG96	18	ILE341, GLN116, ALA252, VAL61, LYS334, TYS204, ASP250, SER268, ALA251, LYS385, PHE201, ASP270, TYR212, PHE114, PHE383, THR380, PRO203, PHE267
Pimozide	-8.2	0	-	24	LEU381, ILE422, LYS426, GLY423, GLY58, ASP250, THR380, ARG96, LYS385, SER268, PHE266, LEU371, ALA251, PHE383, VAL61, ALA252, THR57, SER253, TRP54, ALA50, LEU44, PHE379, ASN53, THR59
Ponatinib	-8.1	1	ALA252	23	ALA50, PHE379, ASN53, THR57, SER253, VAL61, PHE383, ARG96, ALA251, SER268, ASP250, ASP270, LEU387, ILE341, THR380, LEU371, THR59, PHE266, THR369, LYS385, LEU295, ILE271, ILE275
Radotinib	-8.5	2	LYS231, ARG96	21	TYR238, CYS333, TYR230, GLN116, ASP250, PHE114, TYR212, CYS272, ASP209, ALA208, GLY210, ALA251, THR207, ASN118, SER269, TYR204, ASP270, PHE267, SER268, LYS385, PHE266
Risperidone	-8.2	1	SER268	22	GLY326, PHE300, ARG273, ILE271, ASP270, ASP250, ILE341, SER342, VAL327, LEU328, LEU343, ILE275, LEU295, PHE266, LYS385, LEU387, LEU371, ARG386,

					THR369, ALA251, PHE383, ARG96
CONTROL	-6.3	1	ARG96	16	PHE266, PHE267, LEU371, ALA251, LYS385, SER268, ASP270, ALA252, PHE383, THR380, ASP250, SER269, THR59, THR57, VAL61, TYR212
			Integrin β1 (ITGB1)		
Capmatinib	-10.8	1	THR92	15	LYS23, GLU432, THR431, TYR121, PHE430, THR251, VAL250, ASN249, GLU89, GLU433, GLU435, LYS424, GLN97, LYS71, GLN98
Naldemedine	-10.9	1	GLU433	14	THR251, VAL250, ASN249, GLU432, TYR121, ILE94, GLN97, THR92, LYS73, PHE430, THR431, GLU89, PRO88, LYS71
Nilotinib	-11.5	3	LYS326, LYS329, GLU361	15	ALA336, SER357, SER335, VAL337, GLU365, ARG393, LEU364, PRO333, LEU428, ILE363, LYS394, SER396, ASN330, LEU331, LEU358
Pimozide	-12.1	1	GLU433	16	LYS71, GLN98, TYR121, THR431, ASN249, THR251, VAL250, PHE430, GLU89, ILE91, PRO88, THR92, ILE94, GLU432, GLN97, LYS424
Ponatinib	-11	1	SER357	15	VAL337, ALA336, LEU428, LEU358, PRO333, GLU365, VAL303, ILE363, GLU390, GLU361, LYS394, SER396, SER335, LYS329, ARG393
Radotinib	-11.5	2	ARG426, ASN310	16	ASN366, LEU428, GLY367, GLU308, LYS368, ILE363,

					ARG393, THR431, PHE430, GLU433, SER307, GLN304, VAL303, GLU432, PRO333, GLU365
Risperidone	-11.3	0		18	LYS71, LYS73, GLU97, THR92, GLU89, ILE91, PRO8, PRO122, TYR121, ASN249, THR251, GLY429, PHE430, VAL250, THR431, GLU432, GLU433
CONTROL	-8.2	0	-	11	ILE94, GLU432, GLU433, THR92, TYR121, LYS73, GLN97, ILE91, GLU89, PRO88, ASP90

A

CD 36

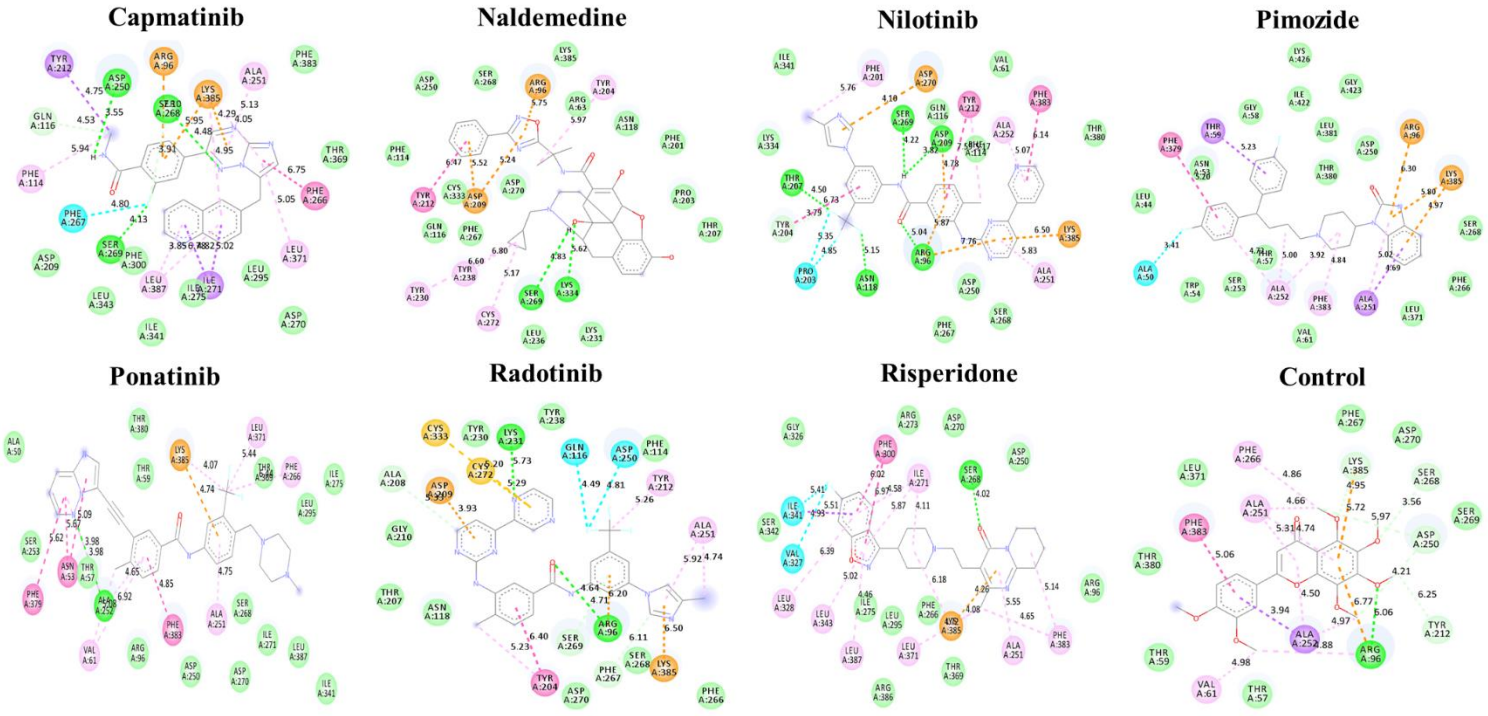

Figure 2.3: *Two-dimensional interaction profile of selected drug molecules with each target protein.* ***A)*** *CD36,* ***B)*** *Insulin Receptor,* ***C)*** *Integrin β1.*

2.3.3. Molecular dynamics studies

Molecular dynamics simulation is an improved method to predict the dynamic behavior of biomolecules in a solvated environment. It has been successfully used over a decade in protein structural studies as well as in the drug discovery field. In this study, a 100 ns simulation of target proteins with selected drug molecules was performed to check their interaction in the solvated system. The stability and strength of protein-drug interactions were analyzed based on RMSD (root means square deviation), RMSF (root means square fluctuations), and pair distance. The maximum, minimum, and average values of the above-mentioned parameters were calculated from MD trajectory files, which are tabulated in **Table 2.3**.

2.3.4. Stability analysis of protein-drug complexes

The stability of the target proteins upon drug binding was analyzed through backbone RMSDs and RMSF. The backbone deviation of target proteins with drugs and without drugs were extracted from MD trajectories and plotted against time (ns) (**Figure 2.4A**). The RMSD values of CD36 were stabilized between 0.1 to 0.15 nm after 3 ns. The CD36-capmatinib complex (0.1033 nm) showed less average RMSD than the apo-CD36 (0.1068 nm) and the rest of the drug complexes had greater average RMSD than apo-CD36. However, the observed maximum deviations of CD36-drug complexes were less than 0.2 nm or 2Å, which is a widely accepted range for protein molecules. The residual fluctuation of target proteins and complexes were also analyzed (**Figure 2.4A**). There was not much difference in the residual fluctuations of drug complexes and apo CD36 (**Figure 2.4B**). The maximum fluctuations were observed at the N-terminal and C-terminal residues, which is an expected outcome because of the loop nature of terminal regions. Both RMSD and RMSF analysis of CD36 clearly stated that the binding of these selected drugs does not affect the structural stability of CD36. Furthermore, the backbone RMSDs of IR was stabilized between 0.2 to 0.3 nm after 5 ns of simulation, however, the complexes ponatinib and control were deviated a bit more after 10^{th} ns and 25^{th} ns, respectively and stabilized between 0.35 to 0.4 nm (**Figure 2.4A**). There was also some deviation observed in the Nilotinib complex after 75^{th} ns (**Figure 2.4A**). The average RMSD of IR with drug bound state was comparatively more than the unbound state, however, it is less than the control drug except for ponatinib complex (0.02 nm more than control). The residual fluctuation analysis of IR with drug and without drug explained the reason for increased deviation in the complexes. The N-terminal and C-terminal region of IR

fluctuated more especially for ponatinib and control complexes (**Figure 2.4B**). The terminal regions of proteins were known to cause more fluctuation during the simulation and that caused the increased RMSD values of complex structures in IR. By keeping the RMSF data in mind, it can be infered that these selected drug molecules are able to bind to IR stably with minor fluctuation at terminal regions. In the case of ITGB1, the unbound state itself showed increased backbone RMSD (**Figure 2.4A**) because of the more loop and helix in nature. The complex of Naldemedine, Pimozide, Ponatinib, Radotinib and control shows less deviation in backbone RMSD than the unbound state of ITGB1. The backbone RMSDs of all the complexes were stabilized between 0.3 to 0.5 nm after 10 ns simulation, however, the ITGB1-risperidone complex was stabilized between 0.3 to 0.5 nm up to 40 ns and then shift to 0.8 to 1.0 nm. The residual fluctuation analysis of ITGB1 complexes showed that the fluctuations caused by the binding of drugs were more or less similar to the unbound state except for risperidone (**Figure 2.4B**). The binding of risperidone caused the fluctuation over half of the total residues of ITGB1 leading to two-fold fluctuations (**Table 2.3**). To conclude, all the selected drug molecules were shown to form stable complexes with ITGB1 except risperidone.

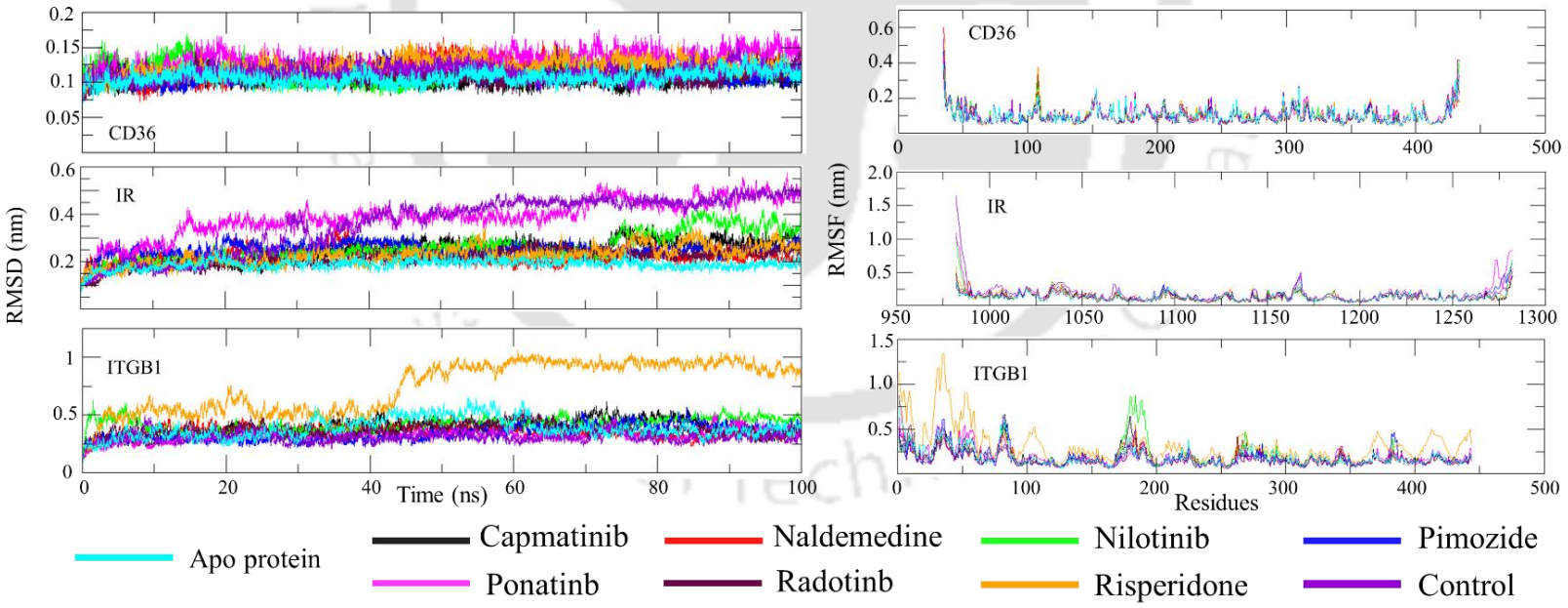

Figure 2.4: A) *Root means square deviation of target proteins upon binding of drug molecules over 100 ns.* ***B)*** *Root mean square fluctuation of target proteins in residual level over 100 ns. Target proteins were depicted in a different color with respect to the drug molecules.*

2.3.5. Contact analysis of drug complexes

The contact analysis between protein and drug helped us to understand the binding pattern of drug molecules and their strength of binding with target proteins. The pairing distance data of protein-drug complexes were extracted from MD trajectory and plotted against time (ns) (**Figure 2.5**). The pairing distance maintained by the selected drugs with all three target proteins were in the range between 0.1 nm to 0.3 nm (1Å to 3Å) and the average distance was less than 0.22 nm (2.2 Å) except for ITGB1 – control (Matrine) complex (2.232 nm or 22.32 Å) (**Table 2.3**). In this short range of pairing distance, all the interacting forces can act strongly and keep the drug molecule within the binding pocket for a long time. To support the pairing distance analysis, the snapshot of protein-drug complexes was also extracted with 20 ns time interval and depicted in **Figure 2.6**. It was observed that selected drug molecules were bound within the binding pocket throughout the 100 ns simulation, except the ITGB1 control inhibitor (Matrine). The contact time of Matrine with ITGB1 was very less with frequent detachment from ITGB1 for the whole simulation period. It is also observed that all the drug molecules share the same binding pocket of ITGB1 (Hinge region between β domain and Hybrid domain of ITGB1) except Ponatinib (binds to β domain). The control drug Matrine was initially bound to the hinge region and shifted to the β domain after 96th ns. The simulation time of the ITGB1- Matrine complex was further extended by 20 ns to check its contact time in the β domain. After 100th ns also the contact time of Martine was not stable as other drugs; it kept on changing the binding site often but within the β domain of ITGB1 (Data not shown). However, the stability of the ITGB1-Matrine complex was better than the unbound state (Figure 4), So based on the points mentioned above, Matrine may have the ability to bind with multiple binding sites of ITGB1.

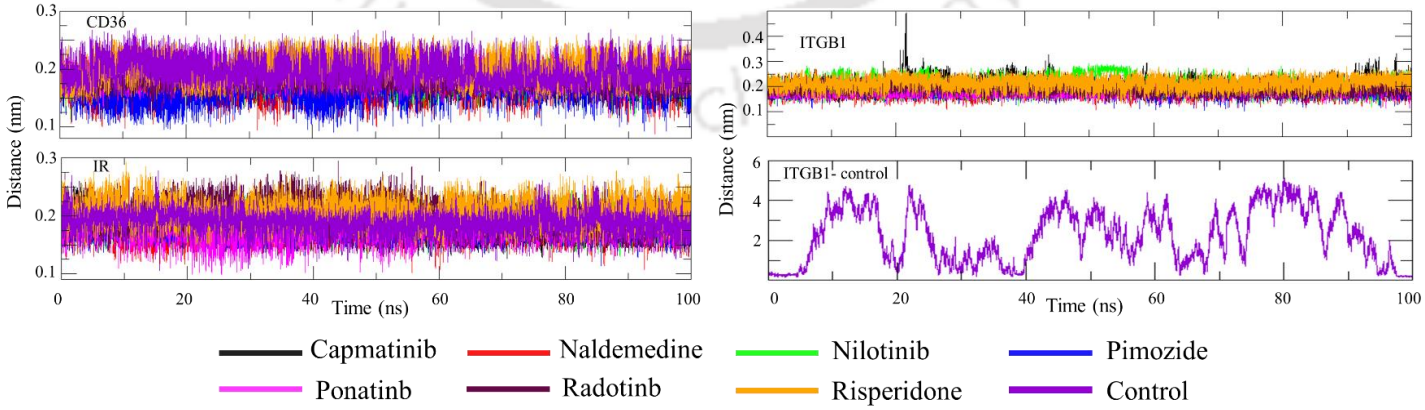

Figure 2.5: *Pair distance between target proteins and drug molecules over 100 ns simulation.*

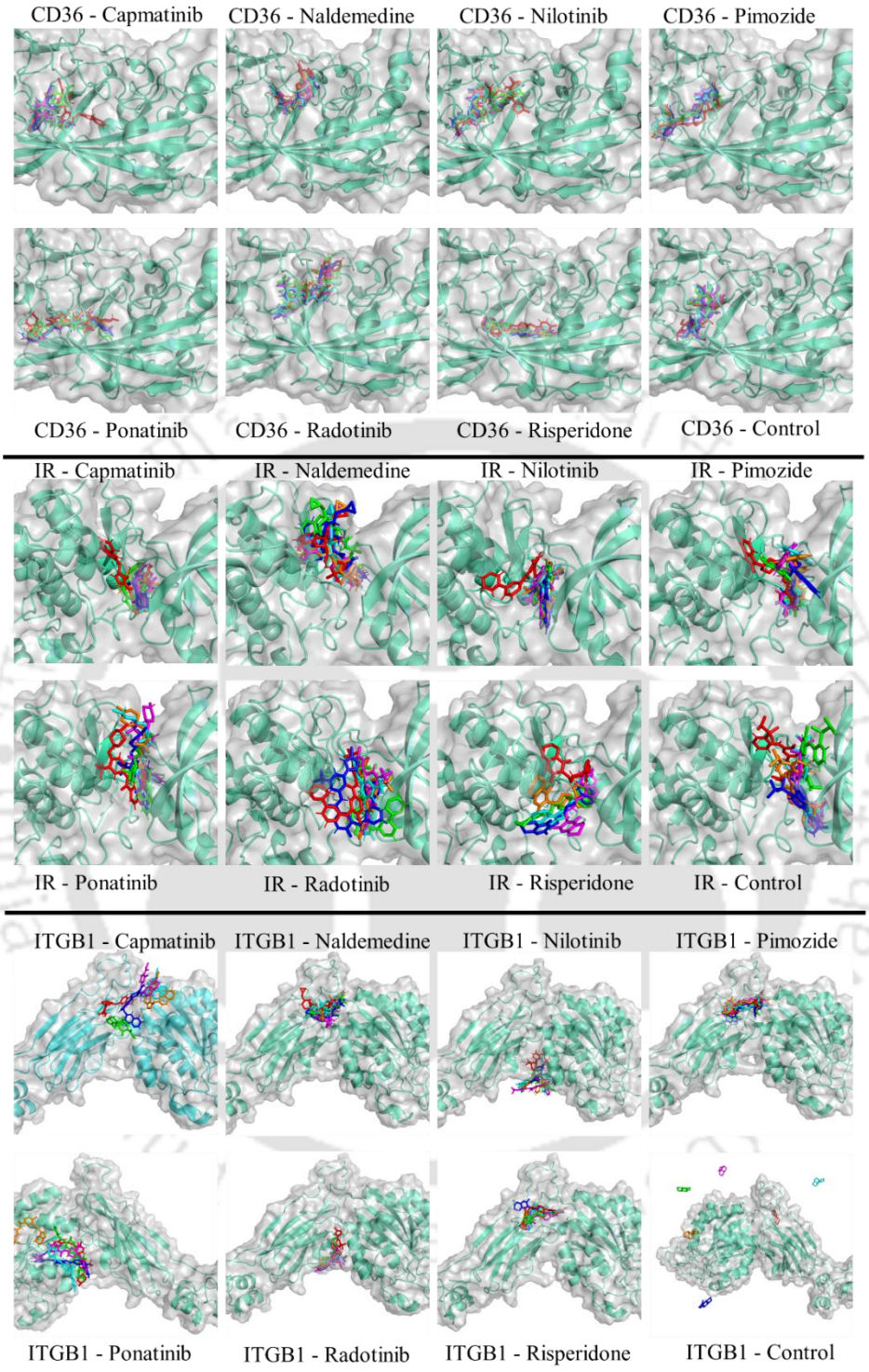

Figure 2.6: *Binding conformation of drug molecules in the binding pockets of target proteins with 20 ns time interval. The drug molecules are depicted in different colors inside the binding pocket based on the time frame, red- 0th ns, green-20th ns, blue- 40th ns, magenta- 60th ns, cyan- 80th ns, orange- 100th ns.*

Table 2.3: *The maximum, minimum, and average values of MD parameters of protein-drug complexes.*

Complex name	RMSD (nm)			RMSF (nm			Pair distance		
	Max	Min	Avg	Max	Min	Avg	Max	Min	Avg
Apo-CD36	0.1469	0.0299	0.1068	0.3909	0.0432	0.1004	---	---	---
Capmatinib	0.1356	0.0316	0.1033	0.3473	0.0402	0.0981	0.228	0.125	0.172
Naldemedine	0.1644	0.0303	0.1166	0.6007	0.0433	0.098	0.233	0.088	0.168
Nilotinib	0.1691	0.0324	0.1130	0.4056	0.043	0.1063	0.226	0.114	0.176
Pimozide	0.1476	0.0314	0.1095	0.469	0.0459	0.0995	0.236	0.091	0.168
Ponatinib	0.1752	0.0309	0.1309	0.4361	0.0476	0.1040	0.255	0.116	0.190
Radotinib	0.1540	0.0319	0.1087	0.4179	0.0405	0.0992	0.242	0.125	0.177
Risperidone	0.1620	0.0330	0.1226	0.524	0.0406	0.1021	0.261	0.129	0.203
Control	0.1622	0.0309	0.1136	0.5355	0.0452	0.1028	0.271	0.131	0.196
Apo-IR	0.2627	0.0339	0.1886	0.6879	0.0473	0.1261	---	---	---
Capmatinib	0.3582	0.0322	0.2449	0.4909	0.0436	0.1294	0.26	0.126	0.177
Naldemedine	0.3530	0.0309	0.2218	0.6617	0.0408	0.1270	0.244	0.102	0.181
Nilotinib	0.4216	0.0300	0.2627	1.0575	0.0419	0.1347	0.251	0.125	0.194
Pimozide	0.3241	0.0300	0.2514	0.5511	0.0532	0.1422	0.246	0.114	0.182
Ponatinib	0.5772	0.0310	0.3889	1.0892	0.0486	0.1575	0.248	0.099	0.175
Radotinib	0.2994	0.0310	0.2149	0.43	0.0437	0.13055	0.295	0.132	0.205
Risperidone	0.3435	0.0316	0.2269	0.5768	0.0425	0.1309	0.292	0.14	0.207
Control	0.5359	0.0318	0.3612	1.644	0.0474	0.1779	0.278	0.106	0.189
ITGB1	0.6532	0.0303	0.3865	0.8325	0.0576	0.1838	---	---	---
Capmatinib	0.6143	0.0324	0.3880	0.6612	0.0603	0.1877	0.494	0.119	0.208
Naldemedine	0.5104	0.0315	0.3541	0.8732	0.0564	0.1728	0.267	0.107	0.182
Nilotinib	0.6262	0.0346	0.4215	0.8703	0.072	0.1961	0.291	0.118	0.204
Pimozide	0.5667	0.0341	0.3445	0.6273	0.0573	0.1760	0.251	0.102	0.185
Ponatinib	0.5268	0.0333	0.3263	0.6245	0.0626	0.1875	0.258	0.115	0.176
Radotinib	0.5510	0.0325	0.3725	0.5444	0.0564	0.1656	0.258	0.132	0.194
Risperidone	1.0627	0.0329	0.7493	1.3398	0.0802	0.3157	0.279	0.135	0.214
Control	0.5036	0.0334	0.3066	0.5339	0.06	0.1666	5.133	0.162	2.232

2.3.6. Binding free energy analysis

Binding free energy of protein-drug interaction provided us with the details of intermolecular forces involved, such as Van der Waal's, electrostatic interaction, polar solvation, and nonpolar solvation energies. The binding free energy of protein-drug interactions was calculated using the MM-PBSA method. Among all interacting forces, electrostatic and van der Waal forces play an essential role in drug binding. Electrostatic force attracts the drug molecules to the binding pocket and van der Waal force aids to keep the drug molecule in the binding pocket [36]. The binding free energy of protein-drug complexes from MD trajectories was calculated with one ns time interval (**Table** 2.**4**). It was observed that Nilotinib and Radotinib had positive net binding energy with CD36 because their unfavorable polar solvation energy is higher than the favorable electrostatic and van der Waals energies. In most cases, the polar solvation energy was neutralized by electrostatic interactions [37]. By keeping all MD parameters and binding free energy data in mind, Nilotinib, Radotinib, and Risperidone were excluded from the potential multi-target drug list. The rest of the four drugs, Capmatinib, Pimozide, Nalmedine, and Ponatinib, showed greater binding free energy than the control sample in at least two proteins and moderate binding energy in other one protein (**Table 2.4**). These four drugs showed higher van der Waals energy than control in all three target proteins, which is essential for increased contact time with protein. It was observed that the control inhibitor of ITGB1 has much less van der Waals energy, which causes the detachment during the simulation (**Figure 2.6**). Given all these points, it is postulated that Capmatinib, Ponatinib, Pimozide, and Nalmedine can inhibit all three target proteins and perturbate the interconnected network.

Table 2.4: *Binding free energy analysis of protein-drug complexes by MM-PBSA method.*

	Van der Waals energy (kJ/mol)	**Electrostatic energy (kJ/mol)**	**Polar solvation energy (kJ/mol)**	**SASA energy (kJ/mol)**	**Binding energy (kJ/mol)**
CD36-Drug					
Capmatinib	-229.914	-73.135	240.007	-20.875	-83.918
Naldemedine	-262.087	-157.374	420.294	-26.522	-18.690
Nilotinib	-164.654	-805.202	1518.600	-27.627	521.117
Pimozide	-245.613	-96.757	293.151	-24.924	-74.137
Ponatinib	-267.220	-295.484	506.864	-26.662	-82.50
Radotinib	-224.628	-120.420	429.185	-25.165	58.972
Risperidone	-244.252	-42.850	212.782	-21.277	-95.557
Control	-206.761	-40.181	213.619	-21.173	-54.496
IR - Drug					
Capmatinib	-203.867	-37.650	137.994	-18.297	-121.821
Naldemedine	-207.535	-405.119	179.116	-19.432	-452.970
Nilotinib	-221.365	-16.227	92.452	-19.605	-164.745
Pimozide	-197.062	-1.534	62.774	-19.173	-154.995
Ponatinib	-240.360	-12.006	100.207	-21.474	-173.633
Radotinib	-157.175	-31.430	137.986	-16.228	-66.847
Risperidone	-137.635	-430.016	185.735	-13.964	-395.88
Control	-135.215	-481.954	299.99	-16.398	-303.567
ITGB1 - Drug					
Capmatinib	-99.475	-40.114	101.068	-10.282	-48.802
Naldemedine	-153.375	-88.747	151.010	-16.129	-107.242
Nilotinib	-43.322	-600.892	650.208	-10.530	-4.235
Pimozide	-177.323	-206.426	255.653	-18.657	-146.755
Ponatinib	-124.706	-446.764	272.930	-13.968	-312.507
Radotinib	-191.972	-31.086	193.416	-18.917	-48.558
Risperidone	-155.547	-137.265	196.685	-15.714	-111.841
Control	-4.213	-94.226	14.347	-0.639	-84.731

2.3.7. Cell viability assay

The computational approach used to select multi-target drugs was validated using an *in-vitro* cell viability assay. Pimozide was chosen to validate the computational results based on the postulation that demonstrating the anti-cancer activity by an anti-psychotic drug (Pimozide) would be a better validation than established anti-cancer drug. Three different breast cancer cell lines namely MCF-7, MDA-MB-231, and MDA-MB-468 was used to validate the *in-silico* findings. MCF7 is a hormone receptor-positive cell line that expresses estrogen receptor (ER), progesterone receptor (PR), and HER-2. On the other hand, MDA-MB-231 and MDA-MB-468 are triple-negative breast cancer that possesses the capability to transit from epithelial to mesenchymal phenotype upon EGF induction. In the present study, MCF7, MDAMB231, and MDAMB468 cell lines were treated with increasing concentrations of Pimozide to access their effect on cell viability. Also, the viability for the MDAMB231 and MDAMB468 cells treated with Pimozide was determined after the induction of EMT.

Following the MTT assay on the Pimozide treated cells, there was a significant dose-dependent decrease in cell viability (the IC_{50} values are depicted in **Figure 2.7**). Significant correlations were also observed in the EMT-induced TNBC (triple-negative breast cancer) cells, i.e., MDA-MB-468 and MDA-MB-231 (**Figure 2.7**). The IC_{50} values of EMT-induced cells were lower than the uninduced cell lines, which support our postulation that Pimozide has a role in EMT signaling. Other studies also reported the anti-proliferative effect of Pimozide on MCF7, MDA-MB231 and in combination with γ-radiation on MCF7 [38, 39]. Furthermore, Dakir et al. reported that treatment of MCF7 and MDA-MB-231 with Pimozide inhibits the AKT signaling [38]. Nevertheless, the detailed signaling mechanism of Pimozide on altered metabolism and EMT network will be ventured in upcoming chapters with *in-vitro* studies.

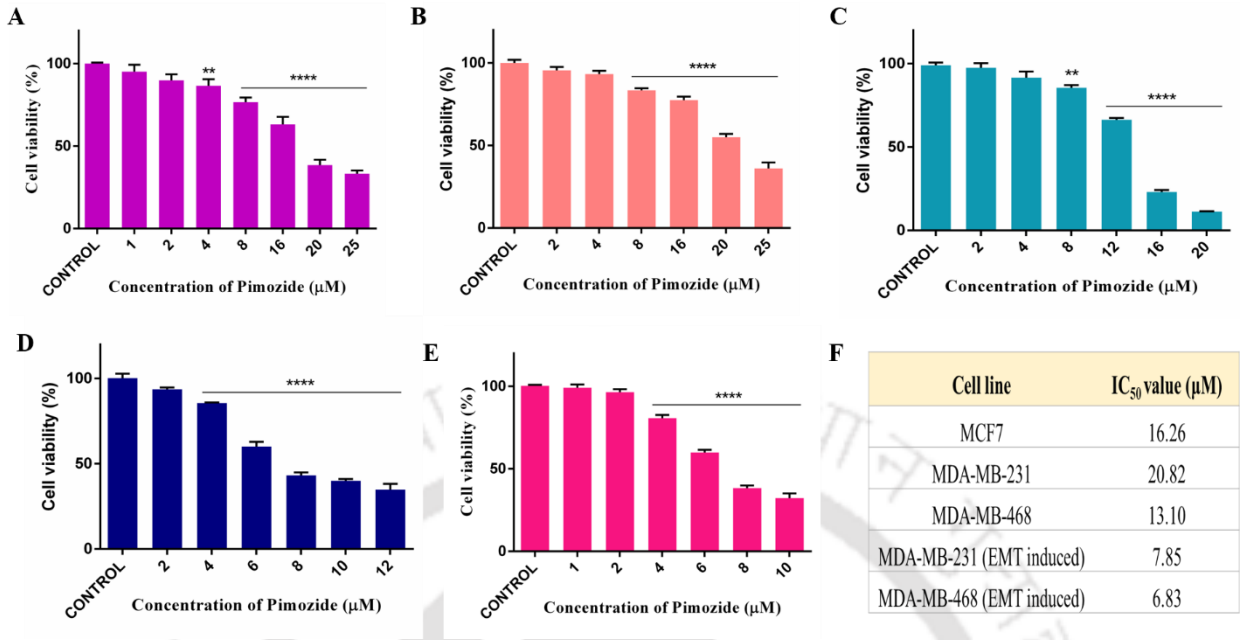

Cell line	IC_{50} value (µM)
MCF7	16.26
MDA-MB-231	20.82
MDA-MB-468	13.10
MDA-MB-231 (EMT induced)	7.85
MDA-MB-468 (EMT induced)	6.83

***Figure 2.7**: Graphical representation of the dose-dependent decrease in cell viability, after treatment with Pimozide for 48 h. **A)** MCF7, **B)** MDA-MB231, **C)** MDA-MB-468, **D)** EMT induced MDA-MB-231, **E)** EMT induced MDA-MB-468, and **F)** IC_{50} values of Pimozide on EMT induced and uninduced breast cancer cell lines. Results are represented as mean ± SEM p-value < 0.05 (*), p<0.01 (**), p<0.001 (***) and p<0.0001 (****).*

2.3.8. Reactive oxygen species (ROS) analysis

In addition to the cell viability assay, the cellular reactive oxygen species (ROS) generation in MCF7 and MDA-MB-231 cell lines was also analyzed. The level of intracellular ROS plays a vital role in defining cell fate, such as apoptosis or proliferation. In typical cases, intracellular accumulation of ROS causes various cellular damages through oxidation of proteins, lipids and nucleic acids, which eventually leads to apoptosis of cells. In some cases, it can also lead to abnormal proliferation and transformation of cells. The accumulation of intracellular ROS in MCF7 and MDA-MB-231 cell lines after being treated with IC_{50} concentration of Pimozide for 24 h was evaluated. ROS accumulation increases 2.36-fold in Pimozide treated MCF7 cells than the untreated MCF7 cells. Similarly, a 7.17-fold increase in MDA-MB-231 and a 6.79-fold increase in EMT induced MDA-MB-231 cell lines was observed upon Pimozide treatment (IC_{50} concentration) (**Figure 2.8**). Since ROS accumulation was studied with IC_{50} concentration of

Pimozide, it can be inferred that the increased ROS level in MCF7 and MDA-MB-231 might involve apoptosis rather than proliferation, which can be ascertained in further studies.

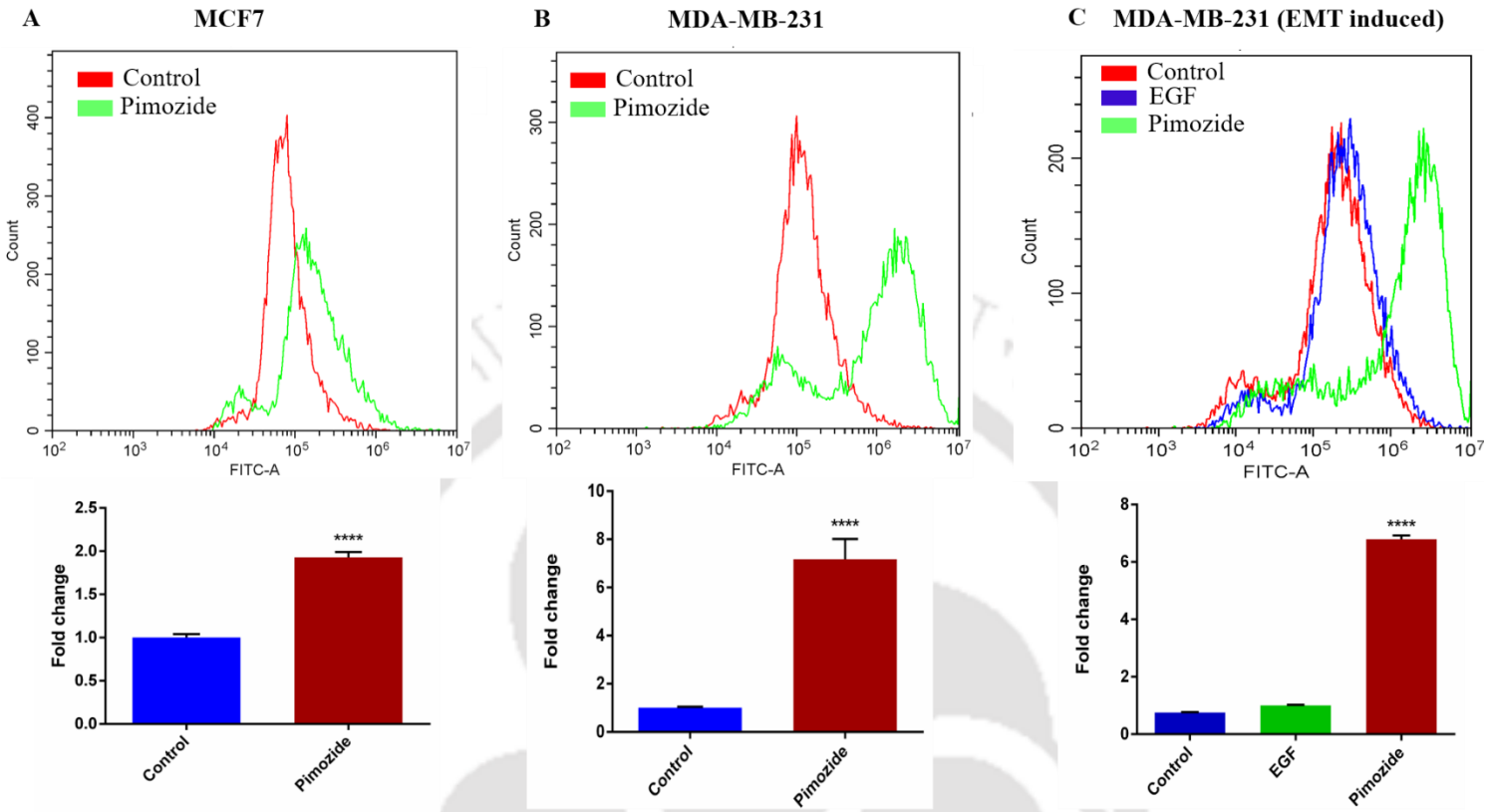

***Figure 2.8**: Graphical representation of the increased reactive oxygen species (ROS) upon treatment with Pimozide for 24 h. **A)** MCF7, **B)** MDA-MB231, **C)** EMT induced MDA-MB-231. Here 'control' represents the cell line without pimozide treatment and 'EGF' is EMT induced cell lines by EGF. Results are represented as mean ± SEM p<0.0001 (****).*

2.4. Discussion

In the pursuit of understanding and targeting key molecular drivers of breast cancer, this study constructed an interconnected functional network linking altered metabolism and EMT signaling. This approach highlighted the dynamic role that metabolic reprogramming plays across different cancer stages. Initially, aerobic glycolysis is predominant, supporting rapid cellular proliferation through the Warburg effect. This metabolic reliance on glucose gradually shifts as cancer progresses, with fatty acid oxidation becoming more dominant in metastatic stages. This shift provides the energy and resources required for EMT and invasiveness, emphasizing the adaptive

nature of cancer metabolism. The integration of EMT-activating pathways—such as PI3K/Akt, TGF-β, NF-κB, Wnt, and MAPK—reveals a robust, mutually reinforcing network where metabolic and signaling pathways co-evolve based on tumor microenvironmental cues, ultimately promoting metastasis.

The network analysis identified three critical nodes: insulin receptor (IR), integrin β1 (ITGB1), and CD36. These cell surface receptors are pivotal not only for metabolic regulation but also for EMT activation. The elevated expression of IR in breast cancer aligns with its role in facilitating glucose uptake and glycolysis through GLUT4 translocation, activating EMT-associated transcription factors via the PI3K/Akt pathway. This finding supports prior observations of overexpression of IR in breast cancer, which associates with increased glycolysis and enhanced invasiveness. Likewise, ITGB1 is known to contribute to EMT by promoting cell adhesion and migration through TGF-β/SMAD signaling, further substantiating its role in breast cancer progression. Function of CD36 in fatty acid translocation also aligns with its upregulation during metastatic phases, corroborating its dual role in supporting energy production via fatty acid oxidation and activating EMT through Wnt/β-catenin signaling. Together, IR, ITGB1, and CD36 present themselves as promising therapeutic targets due to their central roles in sustaining cancer metabolism and EMT processes. The microarray analysis further validated these targets by demonstrating their differential expression in various breast cancer subtypes compared to normal tissues. This validation supports the hypothesis that targeting these receptors could selectively impair cancer metabolism and EMT processes in tumor cells while sparing normal cells, especially given their lower expression in non-cancerous tissue.

Virtual screening provided an initial pool of FDA-approved drugs with high binding affinities to these targets, narrowing down to seven drugs with promising profiles. Notably, anticancer agents Capmatinib, Nilotinib, Radotinib, and Ponatinib, along with Pimozide and Risperidone—primarily used for psychiatric disorders—emerged as potential candidates. These drugs, especially the antipsychotics, indicate novel repurposing opportunities with a multifaceted impact on cancer metabolism and EMT pathways. For example, ability of Pimozide to target multiple components of the network holds potential in developing combination therapies to exploit dependency of cancer on specific metabolic and signaling pathways. The molecular dynamics simulations confirmed the stability of these selected drug-protein complexes, further affirming their potential

for robust interactions under physiological conditions. Although minor deviations were observed in some complexes, especially in terminal regions as seen in the IR-ponatinib complex and the ITGB1-risperidone complex, these fluctuations are consistent with expected protein dynamics, particularly in regions with flexible loops or helices. The stability of other complexes, with RMSD values within acceptable ranges, underscores the potential efficacy of these drugs in maintaining stable interactions within the binding pockets of target receptors. Binding free energy analyses using MM-PBSA revealed that electrostatic and Van der Waals interactions predominantly drive drug binding within the network. While most drugs displayed favorable binding energy profiles, a few, such as Nilotinib and Radotinib with CD36, exhibited fewer stable interactions due to high polar solvation energy. These findings highlight areas for potential refinement in drug selection or modifications to improve binding affinity.

Overall, this study provides a compelling basis for targeting IR, ITGB1, and CD36 as part of a therapeutic strategy that disrupts metabolic reprogramming and EMT in breast cancer. The identified drugs not only bind effectively to these receptors but also show promise in maintaining complex stability and specificity. By focusing on these interlinked pathways, these findings lay the groundwork for a therapeutic approach that could limit cancer progression by exploiting the reliance of cancer cells on metabolic flexibility and signaling pathway co-dependencies.

2.5. Conclusion

In recent therapeutic paradigm, targeting the hub of proteins that play crucial roles in multiple interconnected signaling pathways has been attributed as a better strategy in clinical cancer research. Herein, extensive network analysis establishes interconnected functional network of cancer metabolism and EMT signaling, where three proteins (IR, ITGB1 & CD36) evolved as the hub for drug targeting. Computational screening was carried out from the library of 1293 FDA-approved drugs for the selection of a “multi-target drug” to target this hub. Initially, seven drug candidates were selected from molecular docking studies, which were subsequently screened using MD simulation and binding free energy analysis. Finally, four FDA-approved drugs, namely Capmatinib, Ponatinib, Pimozide, and Naldemedine were selected, which might inhibit all three target proteins. Out of these four, Capmatinib and Ponatinib are known anti-cancer drugs, Naldemedine is used to treat opioid-induced constipation and Pimozide is an anti-psychotic drug. Leaving aside two anti-cancer drugs, experimental validation of the computational screening

results for repurposing Pimozide as an anti-cancer agent was quite informative. Interestingly, better efficacy with reduced IC_{50} values in EMT-induced breast cancer cell lines than the uninduced breast cancer cell lines of Pimozide was established. This *in-vitro* data supports the postulation that Pimozide has a role in the perturbation of the EMT signaling network. A detailed molecular understanding of impact of Pimozide on the interconnected network of altered metabolism and EMT signaling highlights its potential as a repurposed multi-target drug to combat aggressive cancer progression. In the upcoming chapters, the mechanisms of action of the repurposed drugs identified in this study was validated, utilizing a series of *in vitro* experiments to further elucidate their therapeutic potential.

2.6. References

1. Maurya, A. P., & Brahmachari, S. (2021). Current status of breast cancer management in India. Indian Journal of Surgery, 83(Suppl 2), 316-321. https://doi.org/10.1007/s12262-020-02388-4
2. Hopkins A. L. (2008). Network pharmacology: the next paradigm in drug discovery. Nature chemical biology, 4(11), 682–690. https://doi.org/10.1038/nchembio.118
3. Csermely, P., Agoston, V., & Pongor, S. (2005). The efficiency of multi-target drugs: the network approach might help drug design. Trends in pharmacological sciences, 26(4), 178–182. https://doi.org/10.1016/j.tips.2005.02.007
4. Fadaka, A., Ajiboye, B., Ojo, O., Adewale, O., Olayide, I., & Emuowhochere, R. (2017). Biology of glucose metabolization in cancer cells. Journal of Oncological Sciences, 3(2), 45-51. https://doi.org/10.1016/j.jons.2017.06.002
5. Cha, Y. H., Yook, J. I., Kim, H. S., & Kim, N. H. (2015). Catabolic metabolism during cancer EMT. Archives of pharmacal research, 38(3), 313–320. https://doi.org/10.1007/s12272-015-0567-x
6. Sciacovelli, M., & Frezza, C. (2017). Metabolic reprogramming and epithelial-to-mesenchymal transition in cancer. The FEBS journal, 284(19), 3132–3144. https://doi.org/10.1111/febs.14090
7. Coelho, B. P., Fernandes, C. F. L., Boccacino, J. M., Souza, M. C. D. S., Melo-Escobar, M. I., Alves, R. N., Prado, M. B., Iglesia, R. P., Cangiano, G., Mazzaro, G. R., & Lopes, M. H. (2020). Multifaceted WNT Signaling at the Crossroads Between Epithelial-Mesenchymal

Transition and Autophagy in Glioblastoma. Frontiers in oncology, 10, 597743. https://doi.org/10.3389/fonc.2020.597743

8. Yee, L. D., Mortimer, J. E., Natarajan, R., Dietze, E. C., & Seewaldt, V. L. (2020). Metabolic Health, Insulin, and Breast Cancer: Why Oncologists Should Care About Insulin. Frontiers in endocrinology, 11, 58. https://doi.org/10.3389/fendo.2020.00058
9. Nath, A., Li, I., Roberts, L. R., & Chan, C. (2015). Elevated free fatty acid uptake via CD36 promotes epithelial-mesenchymal transition in hepatocellular carcinoma. Scientific reports, 5, 14752. https://doi.org/10.1038/srep14752
10. Pan, J., Fan, Z., Wang, Z., Dai, Q., Xiang, Z., Yuan, F., Yan, M., Zhu, Z., Liu, B., & Li, C. (2019). CD36 mediates palmitate acid-induced metastasis of gastric cancer via AKT/GSK-3β/β-catenin pathway. Journal of experimental & clinical cancer research : CR, 38(1), 52. https://doi.org/10.1186/s13046-019-1049-7
11. Luo, Y., Ren, Z., Du, B., Xing, S., Huang, S., Li, Y., Lei, Z., Li, D., Chen, H., Huang, Y., & Wei, G. (2019). Structure Identification of ViceninII Extracted from Dendrobium officinale and the Reversal of TGF-β1-Induced Epithelial–Mesenchymal Transition in Lung Adenocarcinoma Cells through TGF-β/Smad and PI3K/Akt/mTOR Signaling Pathways. Molecules (Basel, Switzerland), 24(1), 144. https://doi.org/10.3390/molecules24010144
12. Franceschini, A., Szklarczyk, D., Frankild, S., Kuhn, M., Simonovic, M., Roth, A., Lin, J., Minguez, P., Bork, P., von Mering, C., & Jensen, L. J. (2013). STRING v9.1: protein-protein interaction networks, with increased coverage and integration. Nucleic acids research, 41(Database issue), D808–D815. https://doi.org/10.1093/nar/gks1094
13. Morris, G. M., Huey, R., Lindstrom, W., Sanner, M. F., Belew, R. K., Goodsell, D. S., & Olson, A. J. (2009). AutoDock4 and AutoDockTools4: Automated docking with selective receptor flexibility. Journal of computational chemistry, 30(16), 2785–2791. https://doi.org/10.1002/jcc.21256
14. Alexander, S. P. H., Kelly, E., Mathie, A., Peters, J. A., Veale, E. L., Armstrong, J. F., Faccenda, E., Harding, S. D., Pawson, A. J., Sharman, J. L., Southan, C., Buneman, O. P., Cidlowski, J. A., Christopoulos, A., Davenport, A. P., Fabbro, D., Spedding, M., Striessnig, J., Davies, J. A., & CGTP Collaborators (2019). THE CONCISE GUIDE TO PHARMACOLOGY 2019/20: Introduction and Other Protein Targets. British journal of pharmacology, 176 Suppl 1(Suppl 1), S1–S20. https://doi.org/10.1111/bph.14747

15. O'Boyle, N. M., Banck, M., James, C. A., Morley, C., Vandermeersch, T., & Hutchison, G. R. (2011). Open Babel: An open chemical toolbox. Journal of cheminformatics, 3, 33. https://doi.org/10.1186/1758-2946-3-33
16. Russo, A., Paret, C., Alt, F., Burhenne, J., Fresnais, M., Wagner, W., Glaser, M., Bender, H., Huprich, S., Harter, P. N., Filipski, K., Lehmann, N., Backes, N., Roth, L., Seidmann, L., Sommer, C., Brockmann, M. A., Pietsch, T., Neu, M. A., Wingerter, A., Faber, J. (2019). Ceritinib-Induced Regression of an Insulin-Like Growth Factor-Driven Neuroepithelial Brain Tumor. International journal of molecular sciences, 20(17), 4267. https://doi.org/10.3390/ijms20174267
17. Sp, N., Kang, D. Y., Kim, D. H., Park, J. H., Lee, H. G., Kim, H. J., Darvin, P., Park, Y. M., & Yang, Y. M. (2018). Nobiletin Inhibits CD36-Dependent Tumor Angiogenesis, Migration, Invasion, and Sphere Formation Through the Cd36/Stat3/Nf-Kb Signaling Axis. Nutrients, 10(6), 772. https://doi.org/10.3390/nu10060772
18. Ren, L., Mo, W., Wang, L., & Wang, X. (2020). Matrine suppresses breast cancer metastasis by targeting ITGB1 and inhibiting epithelial-to-mesenchymal transition. Experimental and therapeutic medicine, 19(1), 367–374. https://doi.org/10.3892/etm.2019.8207
19. Trott, O., & Olson, A. J. (2010). AutoDock Vina: improving the speed and accuracy of docking with a new scoring function, efficient optimization, and multithreading. Journal of computational chemistry, 31(2), 455–461. https://doi.org/10.1002/jcc.21334
20. Hart, K., Foloppe, N., Baker, C. M., Denning, E. J., Nilsson, L., & Mackerell, A. D., Jr (2012). Optimization of the CHARMM additive force field for DNA: Improved treatment of the BI/BII conformational equilibrium. Journal of chemical theory and computation, 8(1), 348–362. https://doi.org/10.1021/ct200723y
21. Justin, A. L. (2018). From proteins to perturbed Hamiltonians: a suite of tutorials for the GROMACS-2018 molecular simulation package [article v1. 0]. Living Journal of Computational Molecular Science, 1(1), 5068.
22. Kumari, R., Kumar, R., Open Source Drug Discovery Consortium, & Lynn, A. (2014). g_mmpbsa--a GROMACS tool for high-throughput MM-PBSA calculations. Journal of chemical information and modeling, 54(7), 1951–1962. https://doi.org/10.1021/ci500020m
23. Kollman, P. A., Massova, I., Reyes, C., Kuhn, B., Huo, S., Chong, L., Lee, M., Lee, T., Duan, Y., Wang, W., Donini, O., Cieplak, P., Srinivasan, J., Case, D. A., & Cheatham, T.

E., 3rd (2000). Calculating structures and free energies of complex molecules: combining molecular mechanics and continuum models. Accounts of chemical research, 33(12), 889–897. https://doi.org/10.1021/ar000033j

24. Shome, R., & Ghosh, S. S. (2021). Tweaking EMT and MDR dynamics to constrain triple-negative breast cancer invasiveness by EGFR and Wnt/β-catenin signaling regulation. Cellular oncology (Dordrecht, Netherlands), 44(2), 405–422. https://doi.org/10.1007/s13402-020-00576-8
25. Hubbard, S. R., Wei, L., Ellis, L., & Hendrickson, W. A. (1994). Crystal structure of the tyrosine kinase domain of the human insulin receptor. Nature, 372(6508), 746–754. https://doi.org/10.1038/372746a0
26. Milazzo, G., Giorgino, F., Damante, G., Sung, C., Stampfer, M. R., Vigneri, R., Goldfine, I. D., & Belfiore, A. (1992). Insulin receptor expression and function in human breast cancer cell lines. Cancer research, 52(14), 3924–3930.
27. Yang, L., Hou, Y., Yuan, J., Tang, S., Zhang, H., Zhu, Q., Du, Y. E., Zhou, M., Wen, S., Xu, L., Tang, X., Cui, X., & Liu, M. (2015). Twist promotes reprogramming of glucose metabolism in breast cancer cells through PI3K/AKT and p53 signaling pathways. Oncotarget, 6(28), 25755–25769. https://doi.org/10.18632/oncotarget.4697
28. Kawahara, R., Niwa, Y., & Simizu, S. (2018). Integrin β1 is an essential factor in vasculogenic mimicry of human cancer cells. Cancer science, 109(8), 2490–2496. https://doi.org/10.1111/cas.13693
29. Yang, X., Okamura, D. M., Lu, X., Chen, Y., Moorhead, J., Varghese, Z., & Ruan, X. Z. (2017). CD36 in chronic kidney disease: novel insights and therapeutic opportunities. Nature reviews. Nephrology, 13(12), 769–781. https://doi.org/10.1038/nrneph.2017.126
30. Pascual, G., Avgustinova, A., Mejetta, S., Martín, M., Castellanos, A., Attolini, C. S., Berenguer, A., Prats, N., Toll, A., Hueto, J. A., Bescós, C., Di Croce, L., & Benitah, S. A. (2017). Targeting metastasis-initiating cells through the fatty acid receptor CD36. Nature, 541(7635), 41–45. https://doi.org/10.1038/nature20791
31. Wang, J., & Li, Y. (2019). CD36 tango in cancer: signaling pathways and functions. Theranostics, 9(17), 4893–4908. https://doi.org/10.7150/thno.36037
32. Pitcher, C. J., Quittner, C., Peterson, D. M., Connors, M., Koup, R. A., Maino, V. C., & Picker, L. J. (1999). HIV-1-specific CD4+ T cells are detectable in most individuals with

active HIV-1 infection, but decline with prolonged viral suppression. Nature medicine, 5(5), 518–525. https://doi.org/10.1038/8400

33. Ma, X. J., Dahiya, S., Richardson, E., Erlander, M., & Sgroi, D. C. (2009). Gene expression profiling of the tumor microenvironment during breast cancer progression. Breast cancer research : BCR, 11(1), R7. https://doi.org/10.1186/bcr2222
34. Karnoub, A. E., Dash, A. B., Vo, A. P., Sullivan, A., Brooks, M. W., Bell, G. W., Richardson, A. L., Polyak, K., Tubo, R., & Weinberg, R. A. (2007). Mesenchymal stem cells within tumour stroma promote breast cancer metastasis. Nature, 449(7162), 557–563. https://doi.org/10.1038/nature06188
35. Radvanyi, L., Singh-Sandhu, D., Gallichan, S., Lovitt, C., Pedyczak, A., Mallo, G., Gish, K., Kwok, K., Hanna, W., Zubovits, J., Armes, J., Venter, D., Hakimi, J., Shortreed, J., Donovan, M., Parrington, M., Dunn, P., Oomen, R., Tartaglia, J., & Berinstein, N. L. (2005). The gene associated with trichorhinophalangeal syndrome in humans is overexpressed in breast cancer. Proceedings of the National Academy of Sciences of the United States of America, 102(31), 11005–11010. https://doi.org/10.1073/pnas.0500904102
36. Levine, R. R., Walsh, C. T., & Schwartz-Bloom, R. D. (Eds.). (2000). Pharmacology: drug actions and reactions. CRC Press.
37. de Oliveira, O. V., Rocha, G. B., Paluch, A. S., & Costa, L. T. (2021). Repurposing approved drugs as inhibitors of SARS-CoV-2 S-protein from molecular modeling and virtual screening. Journal of biomolecular structure & dynamics, 39(11), 3924–3933. https://doi.org/10.1080/07391102.2020.1772885
38. Dakir, el-H., Pickard, A., Srivastava, K., McCrudden, C. M., Gross, S. R., Lloyd, S., Zhang, S. D., Margariti, A., Morgan, R., Rudland, P. S., & El-Tanani, M. (2018). The anti-psychotic drug pimozide is a novel chemotherapeutic for breast cancer. Oncotarget, 9(79), 34889–34910. https://doi.org/10.18632/oncotarget.26175
39. Strobl, J. S., Melkoumian, Z., Peterson, V. A., & Hylton, H. (1998). The cell death response to gamma-radiation in MCF-7 cells is enhanced by a neuroleptic drug, pimozide. Breast cancer research and treatment, 51(1), 83–95. https://doi.org/10.1023/a:1006046604062

CHAPTER 3

Combination Therapy with Pimozide and Ponatinib

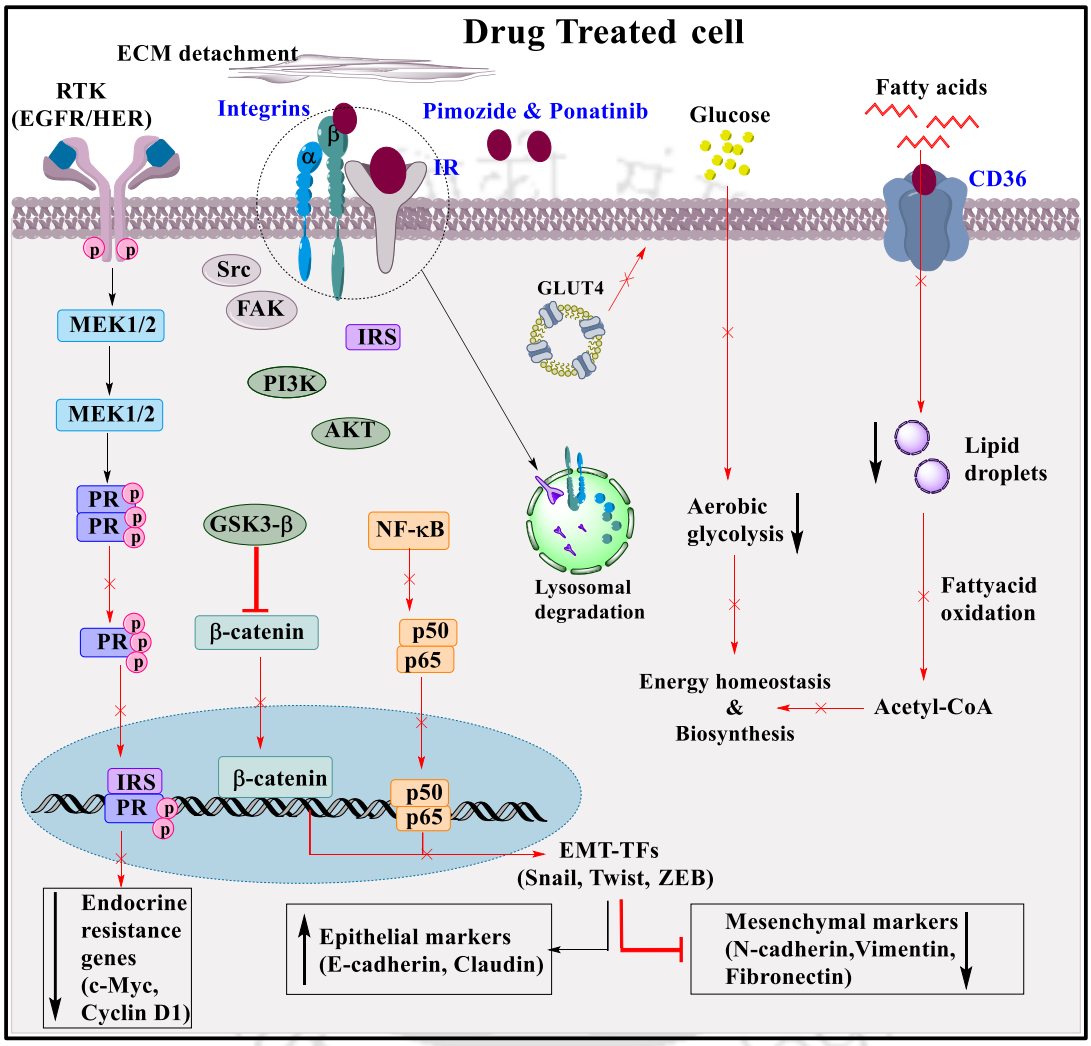

Chapter 3 investigates a synergistic drug combination of Pimozide and Ponatinib, targeting metabolic and EMT pathways to enhance apoptosis and reduce cancer stemness and metastasis, as demonstrated through in vitro studies on monolayer and spheroid models.

Journal of Cellular Biochemistry, 125(7), e30574

DOI: 10.1002/jcb.30574

CHAPTER 3

Combination Therapy with Pimozide and Ponatinib

3.1. Introduction

Energy metabolism, an essential cellular process, plays a pivotal role in cell growth and survival, irrespective of the phenotypes. Rapidly proliferating cancer cells require more energy (in the form of ATP, i.e., Adenosine triphosphate) than normal cells, which triggers the metabolic reprogramming in cancer cells [1]. The rewired metabolic pathways enable cancer cells to accelerate the generation of ATPs compared to the conventional pathways. Aerobic glycolysis, also known as the Warburg effect, is one of the prominent altered metabolisms of progressive cancers. The reaction rate of aerobic glycolysis increases in cancer cells by 15–20 times as compared to the conventional pathway in order to meet their energy demands. [2]. This enhanced reaction rate enormously depends on the glucose uptake by the cells. The study conducted by Bui T et al. confirmed the pivotal role of IR/ITGB1 complex in regulating glucose uptake [3]. The stiff extracellular matrix (ECM) collaborates with integrin receptors to recruit insulin receptors (IRs) to focal adhesions by forming integrin/IR complexes. This complex formation between ITGB1 and IR protects the IR from lysosomal degradation, subsequently enhancing the translocation of GLUT4 to the cell membrane [3]. Conversely, when cells were cultured on a soft ECM, insulin receptor (IR) degradation occurs through lysosomes, resulting in compromised AKT signaling and glucose uptake. These findings suggest that a soft ECM or reduced cell adhesion can trigger integrin degradation [3].

In addition, specific cellular conditions like epithelial to mesenchymal transition (EMT), the expression of matured ITGB1 diminishes, thereby causing the lysosomal degradation of IR. In such circumstances, cancer cells are rewired to utilize fatty acids for energy sources and biosynthesis. Fatty acid (FA) metabolism, including *de novo* synthesis, uptake, storage, and oxidation of fatty acids, represents an alternative metabolism contributing to cancer progression during stress conditions [4]. The number of ATPs generated through fatty acid oxidation is three times higher than the conventional glycolysis (36 ATPs). Fatty acid transporter proteins (FATPs, CD36), a family of transmembrane proteins, mainly assist in the transportation of fatty acids across

the membranes and subsequently enhance fatty acid metabolism. Moreover, overexpression of CD36 correlates with the poor prognosis of breast cancer patients. [4,5].

The transition of epithelial-to-mesenchymal phenotype primarily occurs during wound healing, organismal development, and tissue fibrosis. However, cancer cells hijack the EMT phenomena for tissue invasion, drug resistance, cancer stemness, and resistance to apoptosis [6]. The activation of EMT, often driven by various signaling pathways, includes EGF (Epidermal growth factor), TGFβ (transforming growth factor β), FGF (fibroblast growth factor), HGF (hepatocyte growth factor), BMP (bone morphogenic protein), canonical and non-canonical WNT pathway, Sonic Hedgehog pathway and Notch signaling pathway [7]. The interconnection between EMT and other cell survival signaling pathways drives the aggressiveness in metastatic cancers like breast cancer [8].

Several lines of evidence portrayed the interconnection and coordinated activation between metabolic reprogramming and epithelial to mesenchymal transition (EMT) signaling pathways [6, 8]. Additionally, the *in-silico* investigation revealed that concurrent inhibition of IR, CD36, and ITGB1 by Ponatinib and Pimozide perturb the interconnected functional network of energy metabolism and EMT signaling pathways [9]. In the current study, the potential of Ponatinib and Pimozide as multi-targeting agents against IR, ITGB1, and CD36 was investigated. A novel multi-component molecular dynamic simulation (MMDS) approach was employed to predict the probability of binding drugs to multiple targets in a ratio-dependent manner. Further, *in-vitro* studies demonstrated the inhibition of IR-mediated signaling, ITGB1/IR complex formation, fatty acid metabolism, and EMT activation by Ponatinib and Pimozide. In addition, the synergistic inhibitory effect of Ponatinib and Pimozide on cell proliferation, survival, migration, stemness, energy metabolism, and EMT was established in breast cancer cell lines. Furthermore, the efficacy of Pimozide, Ponatinib, and combination treatment was evaluated in *in-vitro* tumor mimic models of luminal (MCF-7) and triple-negative breast cancer (MDAMB-231) cell lines.

3.2. Experimental section

3.2.1. Multi-component molecular dynamic simulation (MMDS)

Prior to the multi-component MD simulation, the required files (PSF, CRD, PRM, and RTF) were generated using the CHARMM-GUI input generator (https://www.charmm-gui.org/). The PDB format of all three target proteins IR (PDB-ID_4IBM), ITGB1 (PDB-ID_4WK0), and CD36 (PDB-ID_5LGD) was uploaded separately under the PDB reader & manipulator option of the Input generator; without any further modifications, files required for MD simulation were generated and downloaded. Similarly, the PDB format of both drugs was uploaded under ligand reader & modeler of Input generator, and converted files were downloaded. PSF, CRD files of all three proteins, and PSF, CRD, PRM, and RTF files of ligands were uploaded under the Multi-component Assembler option of the Input generator [10]. All the settings were set as default in further steps, except the temperature is changed from 298 K to 310 K to mimic the biological environment. Finally, files required for the GROMACS simulation were downloaded with the CHARMM36 force field. Subsequently, energy minimization, NVT equilibration, and final MD simulation for 200 ns were carried out using the Gromacs 2019.6 version. After the MD simulation, the pair distance between ligands and proteins was analyzed using the "*gmx pairdist*" gromcas command and selecting respective groups for protein and ligand in subsequent steps in the Ubuntu terminal. Similarly, a snapshot of every 50 ns was extracted using the "*gmx trjconv*" gromacs command, and the whole system was selected for output PDB file generation [11].

3.2.2. Cell culture conditions

MCF-7 (luminal breast cancer) and MDA-MB-231 (Triple negative breast cancer) cell lines were obtained from the National Centre of Cell Science, Pune, India. The cell lines were cultured and maintained in DMEM media (Sigma Aldrich, St. Louis, USA), supplemented with 10% FBS and 1 % Antibiotic – Anti mycotic (Thermo Fisher Scientific, USA) at 37^0 C, 5% CO_2.

3.2.2. Cell viability by MTT assay

The efficacy of drugs affecting the cell viability in monolayer culture was assessed through MTT (3-(4,5-dimethylthiazol-2-yl)-2,5-diphenyltetrazolium-bromide) based colorimetric assay. MCF-7 and MDA-MB-231 cells were seeded in 96 well plates at 5000 cells/well and incubated for 24 h in normal maintaining conditions. In EMT induction experiments of MDA-MB-231, cells were

further serum-starved overnight in 0.5% serum media. Followed by cells treated with 40 ng/mL of EGF along with varying concentrations of selected drugs for 48 h. The drugs were dissolved with DMSO and subsequently diluted with DMEM media to ensure that the final concentration of DMSO remained below 0.25 %. Untreated cells were employed as controls in all experiments for normalization purposes. After drug treatment, 5 µL of 5 mg/mL MTT solution was added in each well with incubation of 2 h in cell culture condition. The absorbance was measured at 570 and 630 nm, and cell viability was calculated based on the below formula.

$$Cell\ viability = \left(\frac{(Abs\ 570 - Abs\ 630)treated\ cells}{(Abs\ 570 - Abs\ 630)control\ cells}\right) * 100$$

The IC_{50} concentration of respective drugs was calculated using sigmoidal dose-response curves in GraphPad Prism Version 6.0.0.

3.2.4. Determination of intracellular reactive oxygen species

The generation of intracellular reactive oxygen species after drug treatment was determined using DCFDA (2′,7′ -dichlorofluorescein diacetate) based flow cytometric analysis. Conversion of nonfluorescent DCFDA to fluorescent DCF by ROS is directly proportional to the total ROS generated upon drug treatment. MCF7 and MDA-MB-231 cells were seeded in 6 well plates at 3 x 10^5 cells/well; after 24 h, cells were treated with respective IC_{50} of selected drugs for 6 h followed by 2 µM of DCFDA for 30 min. After the incubation, cells were trypsinized and washed with PBS thrice by centrifuging at 650 rcf for 5 min at 4^0C. The fluorescence was analyzed using the FITC channel of the Beckman Coulter CytoFLEX flow cytometer.

3.2.5. Mitochondrial membrane potential determination

The change in the mitochondrial membrane potential was detected using a JC-1 dye-based flow cytometric assay. MCF-7 and MDA-MB-231 cells were seeded in 6 well plates for 24 h and treated with respective IC_{50} of drugs for 24 h, followed by 10 µM of JC-1 dye added to each well for 30 min. For positive control, cells were treated with 50 µM of CCCP (carbonylcyanide m-chlorophenylhydrazone) for 30 min. The ratio of red to green fluorescence was detected by the PE and FITC channels of the Beckman Coulter CytoFLEX flow cytometer.

3.2.6. Apoptosis assay

The apoptotic population of the treated cells was assessed by the Alexa flour™ 488 Annexin-V/Dead cell apoptosis kit (Invitrogen by Thermo Fisher Scientific). After the 48 h treatment of the desired concentration of the drugs, cells were trypsinized and processed according to the kit manual. The fluorescence data were detected using FITC and PE channel Beckman Coulter CytoFLEX flow cytometer and analyzed using Cytexpert software.

3.2.7. Scratch/wound healing assay

The effect of Pimozide and Ponatinib on migrative properties of the triple-negative breast cancer (TNBC) cell line was assessed with a scratch/wound healing assay. MDA-MB-231 cell was maintained in a 35mm plate until it reached 70 percent confluency, and scratches were made using a 10 µL pipette tip. Following this, cells were treated with respective IC_{50} of respective drugs for 18 h, and images were captured using a ZOE fluorescent imager.

3.2.8. Sphere formation assay

The sphere-forming ability of MCF-7 and MDA-MB-231 was assessed after 48 h of drug treatment based on a previously reported study [12]. The cells were collected by trypsinization and seeded in 96 well plates pre-coated with 1.5 % agarose in serum-free at 5000 cells/well. Then, 96 well plates were centrifuged at 700 rcf for 15 min to induce the sphere formation and incubated at 37^0 C for 96 h. After the incubation, images were captured using a Nikon eclipse inverted fluorescence microscope.

3.2.9. Lipid droplet detection assay

The intracellular lipid droplet formation was detected using Nile red (9-diethylamino-5H-benzo[α]phenoxazine-5- one) staining. $3x10^5$ cells were seeded in a 35 mm glass bottom plate and incubated in cell culture for 24 h, followed by overnight starvation in 0.5% serum media. After 6 h of drug treatment, cells were fixed with 4% formaldehyde and incubated with 0.01mg/mL of Nile red for 30 min in the dark, followed by 10 min of counter-staining with DAPI. Images were captured under red and blue channels using a Zeiss LSM 880 confocal microscope.

3.2.10. Fatty acid uptake assay

Fluorescent labeled Fatty acid (BODIPY™ 500/510 C1, C12 (4,4-Difluoro-5-Methyl-4-Bora-3a,4a-Diaza-s-Indacene-3-Dodecanoic Acid)) (Invitrogen by Thermo Fisher Scientific) was used to evaluate the inhibitory activity of selected drugs on target protein CD36. Inhibition of CD36 causes a significant reduction in the green fluorescent, further detected by the flow cytometer and confocal microscope. $3x10^5$ cells of MCF7 and MDA-MB-231 were cultured for 24 h in 6 well plates (for flow cytometry analysis) and 35 mm glass bottom plates (for imaging study). Cells were starved overnight in 0.5% serum media and treated with selected drugs for 6 h. Following this, 100 nM of BODIPY™ 500/510 C1, C12 was added after the treatment period and incubated for 30 min. For flow cytometric analysis, cells were trypsinized and washed with 1x PBS; the shift in the green fluorescent was measured by FITC channel Beckman Coulter CytoFLEX flow cytometer and analyzed using Cytexpert software. For the imaging study, cells were fixed with 4% formaldehyde, and images were captured under green fluorescence using a Zeiss LSM 880 confocal microscope.

3.2.11. Lysosome detection through lysotracker

LysoTracker™ Deep Red dye (Invitrogen by Thermo Fisher Scientific) was used in this study to detect the lysosome formation in MCF7 and MDA-MB-231 cell lines. $3x10^5$ cells were cultured in 6 well plates for 24 h and starved overnight in 0.5% serum media. After 6 h of drug treatment, 100 nM of LysoTracker™ Deep Red dye was added and incubated for 1 h in cell culture condition. Cells were trypsinized and washed with 1x PBS; the shift in the red fluorescence was measured by PC-5 channel in Beckman Coulter's CytoFLEX flow cytometer.

3.2.12. Immunoblotting and gene expression analysis

Immunoblotting and real-time PCR experiments were carried out, as mentioned in the previous study [12]. MCF-7 and MDA-MB-231 cells were seeded in 60 mm plates and incubated for 24 h. Subsequently, cells were treated with IC_{50} concentration of drugs for desired periods (30 min and 6 h); total protein and RNA were isolated using RIPA buffer and TRI reagent after the treatment period. The details of primer sequences and monoclonal antibodies are provided in Table 3.1 and Table 3.2.

Table 3.1: *List of primers used for real-time PCR experiments*

Sl.No	Gene name	Forward primer (5' – 3')	Reverse primer (5' – 3')
1	E-cadherin	TGGGTGAATTCGGGCTTGTT	TGAAGGTGACAGAGCCTCTGGAT
2	Fibronectin	AACATGTAACCACCAGTCTCATGTG	GGTGACACTTATGAGCGTCCTAAA
3	Vimentin	AGTCCACTGAGTACCGGAGAC	CATTTCACGCATCTGGCGTTC
4	β-actin	AAGGGACTTCCTGTAACAATGCA	CTGGAACGGTGAAGGTGACA

Table 3.2: *The list of antibodies used for protein expression study*

Antibodies	Catalog No	Manufacture
β-actin	8457S	Cell Signaling Technology, USA
IR	3025T	Cell Signaling Technology, USA
p-IR (Tyr 1146)	3021T	Cell Signaling Technology, USA
ITGB1	3407T	Cell Signaling Technology, USA
IRS-1	3407T	Cell Signaling Technology, USA
AKT	8200	Cell Signaling Technology, USA
p-AKT (T308)	9916	Cell Signaling Technology, USA
p-AKT (S473)	9271S	Cell Signaling Technology, USA
Anti-Rabbit IgG, HRP linked	7074S	Cell Signaling Technology, USA

3.2.13. Generation of MCF-7 and MDA-MB-231 tumor spheroids

Tumor spheroids of MCF-7 and MDA-MB-231 were generated from the monolayer culture via a facile and reproducible method [13]. Cells from monolayer cultures were harvested by trypsinization and counted using Tryphon blue staining. 1.5 X 10^4 cells/well for MCF-7 spheroids and 2 X 10^4 cells/well for MDA-MB-231 spheroids were seeded with 200 µL serum media and 10% FBS in 96 well plates. Prior to seeding, 96 well plates were pre-coated with 60 µL of 1.5 % agarose (in serum-free media). The plates were centrifuged at 700 rcf for 10 min and incubated at cell culture conditions (mentioned above) for 72 h. Spheroids were monitored at 12 h intervals to check their integrity using the NIKON ECLIPSE Ti microscope.

3.2.14. Cell viability assay and Live/dead cell imaging

The viability of the cells in the tumor spheroids was also assessed after 72 h of drug treatment using Alamar blue assay, and IC_{50} concentrations of drugs were calculated, as mentioned in the previous study [13]. Live/dead cell imaging after treatment with the IC_{50} concentration of drugs was carried out using Calcein AM and PI staining. Spheroids of MCF-7 and MDA-MB-231 cells were treated with drugs for 72 h and incubated with Calcein-AM (2 µm) and PI (4 µm) for 1 h, and images were captured under green and red channels using a Zeiss LSM 880 confocal

microscope. Live cells were stained with Calcein-AM (green), and dead cells were stained with PI (red).

3.2.15. Statistical analysis

All the experiments were triplicated and analyzed using GraphPad Prism software. The graphical data were expressed as mean ± SEM. Additionally, the correlations among the groups were assessed through a one-way ANOVA test, and the p-value <0.05, denoted as (*), is considered to be statistically significant, whereas $p < 0.001$, denoted as (***) and $p < 0.0001$, denoted as (****) are considered to be highly significant.

3.3. Results

3.3.1 Pimozide and Ponatinib demonstrated simultaneous interaction with IR, ITGB1, and CD36

Pimozide and Ponatinib exhibited prolonged interaction with IR, ITGB1, and CD36 independently in the previously reported MD simulation study [9]. In this study, the binding preferences of Pimozide and Ponatinib among the three target proteins were explored by a multi-component molecular dynamics simulation study. By assuming the expression of all three proteins in the cell surface as 1:1:1 ratio, the system for MD simulation was built. The total number of proteins in the system is 3 (IR, ITGB1, CD36), and the number of drug molecules in each simulation was varied. The ratio of protein to drugs in the simulation systems are as follows: 3:1 (IR/ITGB1/CD36: Pimozide), 3:1 (IR/ITGB1/CD36: Ponatinib), 3:2 (IR/ITGB1/CD36: 1 Pimozide + 1 Ponatinib), 3:3 (IR/ITGB1/CD36: 3 Pimozide), 3:3 (IR/ITGB1/CD36: 3 Ponatinib) and 3:3 (IR/ITGB1/CD36: 2 Pimozide and 1 Ponatinib). After the 200 ns MD simulation, the pair distance between the drug molecule and each target protein was measured and portrayed in **Figure 3.1A**. A pair distance of less than 0.25 nm signifies the strong interaction between drug and protein [9]. Given the conditions, in a 3:1 (drug) system, Pimozide was initially bound with CD36 up to 90 ns and shifted to IR for the rest of the simulation time. However, Ponatinib remains bound with IR throughout the simulation. In the 1 Pimozide and 1 Ponatinib system, Ponatinib remains bound with CD36, and Pimozide interacted with ITGB1 after 50 ns. To further understand the binding potential of

the drugs and proteins, the number of drug molecules equal to the number of proteins were increased.

In the 3 Pimozide system, the interaction was persistent with IR and ITGB1 but not with CD36. Similarly, Ponatinib interaction was not persistent with ITGB1. Interestingly, the system with 2 Pimozide and 1 Ponatinib exhibited prolonged interaction with all three target proteins for the entire 200 ns simulation period. Ponatinib interacted with IR, and Pimozide interacted with both CD36 and ITGB1. Studies have reported that ITGB1 has a complex forming ability with IR and CD36 [3,14, 15], which was also observed during MD simulation. It was observed that in certain simulation conditions, the distance between the drug molecule and the protein was found to be less than 0.5 nm despite the absence of any direct interaction between them. This phenomenon occurred as a result of the complex formation between the target proteins during the molecular dynamics (MD) simulation. To clarify this, the structures of each system were extracted with a 50 ns interval and portrayed them in **Figure 3.1B**. The snapshot of every 50 ns of the MD simulation reconfirms the stated observations above. Therefore, the concurrent inhibition of all three target proteins was accomplished with the 2:1 combination ratio of Pimozide and Ponatinib, indicating the synergistic outcome of the two drugs in combination. This preliminary insight from MD simulation guided further experimental investigations. In addition, findings obtained through extensive *in-vitro* studies further reconfirm the MD results, which reflect its biological significance.

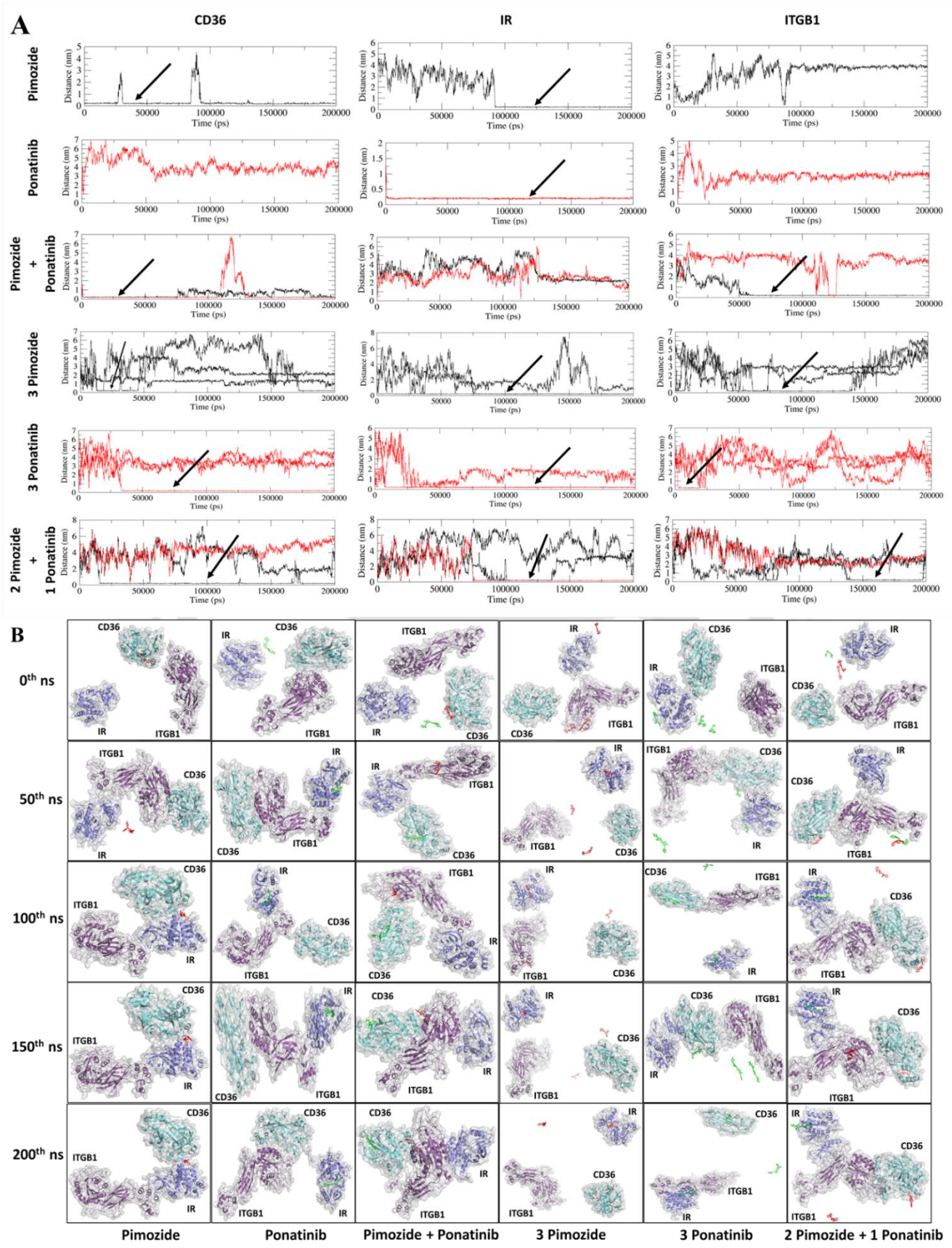

Figure 3.1: A) *Pair distance between all three target proteins and respective drugs (Pimozide in black, Ponatinib in red) obtained from the multi-component molecular dynamics simulation study. The pair distance is plotted against time on the x-axis. The black arrows indicate the time frame during which the drugs interacted with the proteins.* ***B)*** *Snapshot of MD simulation with 50 ns time interval. Pimozide is represented in red color and Ponatinib is in green color.*

3.3.2 Cellular cytotoxicity through the activation of the intrinsic pathway of apoptosis

The inhibitory effect of Pimozide and Ponatinib on breast cancer cell proliferation was assessed through an MTT assay on MCF-7 (luminal), MDA-MB-231 (triple negative breast cancer), and EGF-mediated EMT-induced MDA-MB-231 cell lines. The IC_{50} values of Pimozide, Ponatinib, and the combination treatments were evaluated after 48 h of treatment. **Figure 3.2** portrays the concentration-dependent inhibition of cell proliferation by both Pimozide and Ponatinib. Also, the IC_{50} concentration of Pimozide significantly reduced when given with half of the IC_{50} of Ponatinib (**Figure 3.2**). Isobologram analysis was carried out, and the combination index (CI) and dosage distribution cure obtained from Isobologram were portrayed in **Figure 3.2**. The CI values of the different concentrations were lesser than 1 in all three cell lines, indicating the synergism between both drugs, which is at par with the *in-silico* results (mentioned above). Furthermore, the cellular process behind the cytotoxicity of Pimozide and Ponatinib was investigated in MCF-7, MDA-MB-231, and EMT-induced MDA-MB-231 cell lines. Nutrient deprivation or metabolic stress is one of the factors for cells to undergo stress-induced intrinsic apoptosis pathway [16]. Since stress-induced intracellular ROS generation is a crucial part of the intrinsic apoptosis pathway, the increased intracellular ROS generation was assessed using DCFDA after 6 h of treatment. **Figure 3.3** depicts the fold change in intracellular ROS generation compared to untreated cells; the mean values are tabulated in **Table 3.3**. It was observed that intracellular ROS generation was higher in pimozide-treated cells than in Ponatinib and co-treatment. Moreover, during the intrinsic pathway of apoptosis induction, the generated ROS causes mitochondrial membrane depolarisation and the release of cytochrome C to the cytoplasm. Subsequently, the released cytochrome C activates the caspase 9-mediated cellular apoptosis [17]. So, the membrane potential of mitochondria was further investigated using JC1 dye and apoptotic population using Annexin V – PI (propidium iodide) stain (**Figure 3.3**). The percentage of depolarised mitochondrial membrane is provided in

Table 3.3. Notably, the fold change of generated intracellular ROS is relatively correlated with the membrane depolarization percentage after drug treatment. Moreover, Pimozide-treated cells exhibited enhanced membrane depolarisation than other treatments. However, in the case of apoptosis, cells treated with a combination of both drugs displayed more apoptotic population of cells as compared to the single drug treatment. These observations confirm that both drugs are involved in stress-induced activation of the intrinsic pathway of apoptosis, and the efficacy of combination treatment is better than single drug treatment in apoptosis induction.

Table 3.3: *Numerical values of cytotoxicity, intracellular ROS generation, mitochondrial membrane potential, and apoptotic population after drug treatment*

	Cell line	IC_{50} (µM)	Increase in the fold change of intracellular ROS	% of mitochondrial membrane depolarization	% of apoptotic cell population
Pimozide	*MCF-7*	15.18	2.7	13.15	13.66
	MDA-MB-231	19.81	1.04	76.31	25.44
	EMT- induced MDA-MB-231	8.03	16.1	59.91	17.1
Ponatinib	*MCF-7*	0.85	1.7	10.33	27.62
	MDA-MB-231	1.32	1.9	59.22	24.22
	EMT- induced MDA-MB-231	2.72	2.7	32.16	15.73
Pimozide + Ponatinib	*MCF-7*	5.6	2.4	9.79	40.85
	MDA-MB-231	8.0	6.1	6.95	36.02
	EMT- induced MDA-MB-231	0.51	7.7	95.49	12.17

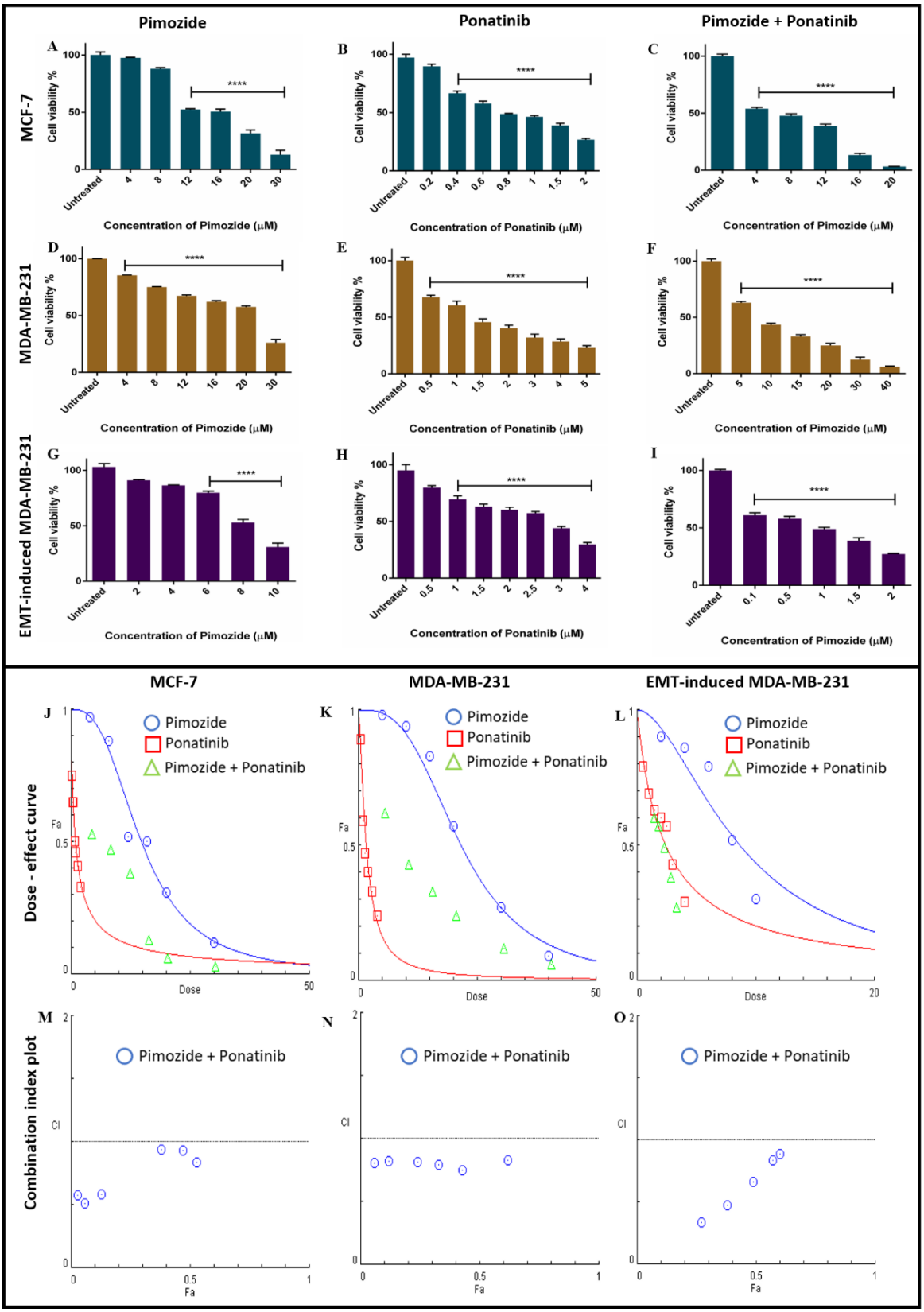

Figure 3.2: (A – I) *Dose-dependent curve of the anti-proliferative activity in monolayer culture.* ***(J – L)*** *Dose effect curve and* ***(M – O)*** *Combination index plot predicted by Isobologram.*

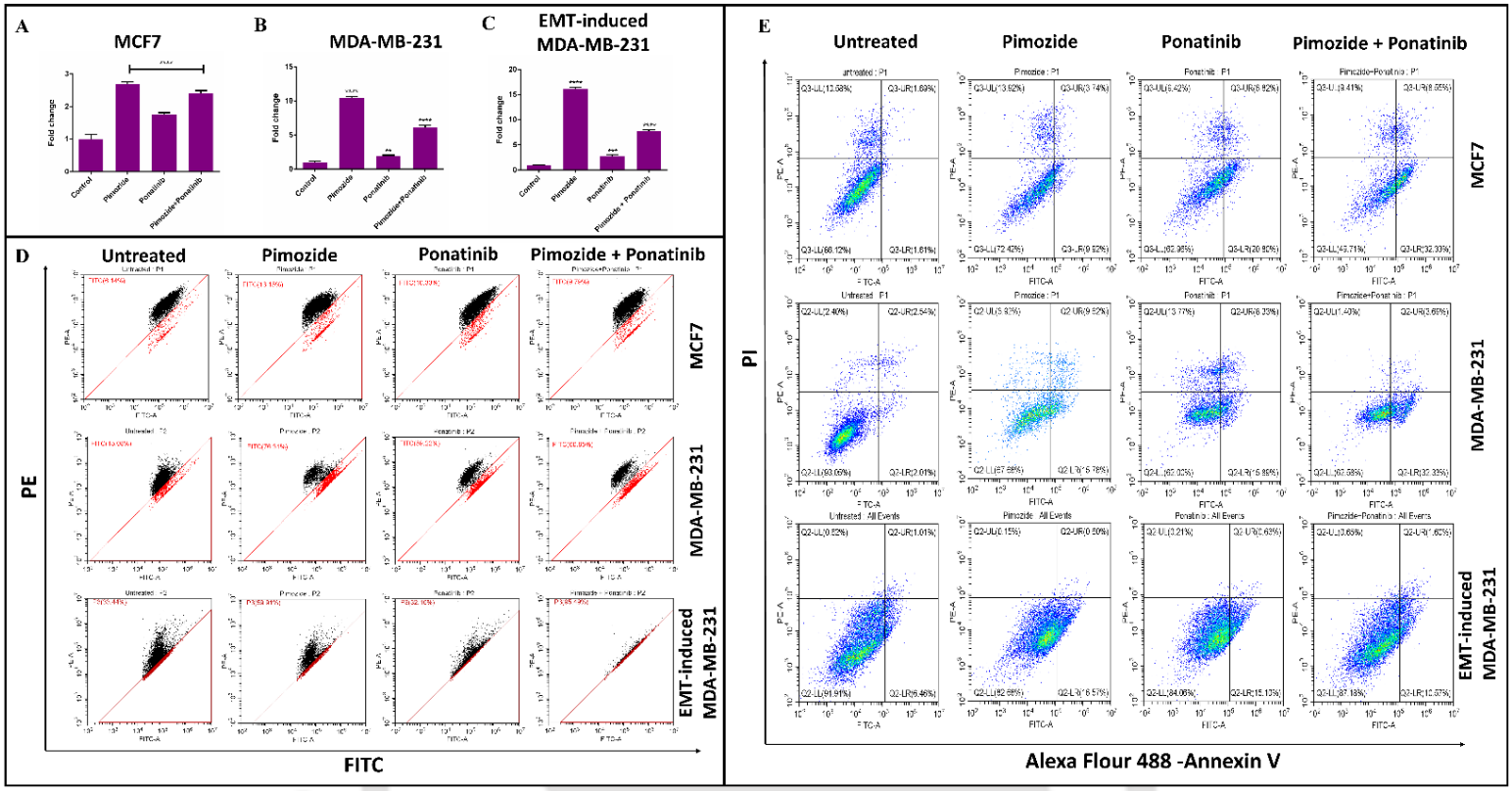

Figure 3.3: (A–C) *Intra-cellular ROS generation after 6 h of treatment in MCF-7, MDA-MB-231, and EMT-induced MDA-MB-231 cell lines.* ***D)*** *Mitochondrial membrane depolarisation by the drug treatments after 24 h.* ***E)*** *Percentage of apoptotic and necrotic cell population after 48 h of drug treatment in MCF-7, MDA-MB-231, and EMT-induced MDA-MB-231 cell lines.*

3.3.3 Deactivation of IR as competitive inhibitors for insulin inhibited IR mediated signaling

Since both drugs showed better affinity towards the insulin receptor (IR) in *in-silico* studies, their involvement in IR activation and its signaling pathways were further investigated in detail. Activation of insulin receptors begins with the autophosphorylation of a tyrosine residue at 1146/1150/1151 positions in the presence of insulin. Subsequently, IR kinase activates IRS (Insulin receptor substrate), followed by AKT-mediated translocation of GLUT4 to the cell membrane [18]. These phosphorylation events of IR occur at the early stage of insulin treatment; therefore, the proteins were isolated after 30 min of drug treatment along with the addition of 100 nM insulin [19]. The effect of drug treatments on IR, p-IR (Tyr 1146), and IRS 1 are depicted in **Figure 3.4** after western blot analysis. No significant change was observed in the protein expression level of IR after drug treatment compared to the insulin. However, phosphorylation of IR at Tyr 1146 residue decreased substantially in the drug treatment compared to insulin treatment.

The fold change in expression upon drug treatment is tabulated in **Table 3.4**. These data indicate the competitive inhibition between the drugs and insulin against insulin receptors. The downregulation of IR autophosphorylation by Pimozide is prominent in MCF-7 (luminal). A similar result was observed upon treatment with Ponatinib in the MDA-MB-231 cell line (Triple-negative breast cancer). Although both drugs have the potential to inhibit IR signaling, their efficacy was influenced by the cellular phenotype.

Moreover, the combination treatment exerted better inhibition than the single-drug treatment, irrespective of the cellular phenotype. Subsequent changes in the downstream signaling of IR were also studied by investigating IRS-1 expression and phosphorylation of AKT. IRS 1 is a primary mediator for insulin receptor signaling, assisting the maintenance of glucose homeostasis by activating PI3K/AKT-mediated pathways [18]. Earlier studies reported that upregulation of IRS-1 correlated with poor prognosis in cancer patients by inducing cancer stemness [20]. Thus, a significant reduction in IRS-1 expression (**Table 3.4**) after treatment with Pimozide and Ponatinib indicates a promising therapeutic module for breast cancer treatment by inhibiting the insulin receptor signaling pathway.

3.3.4 Complementary activity delimited the functional activation of AKT

PI3K/AKT/mTOR axis is pivotal in most RTKs (receptor tyrosine kinase) signaling pathways, including insulin receptor signaling. Emerging studies demonstrated that activation of AKT is directly linked to cell survival, cancer progression, and metabolic rewiring in breast cancer [21]. The functional activation of AKT requires the phosphorylation at two residues, threonine 308 (Thr 308) of the activation loop and serine 473 (Ser 473) of the C-terminal hydrophobic loop. The absence of phosphorylation in any of these two residues renders AKT and the PI3K/AKT/mTOR axis inactive. In this study, the expression of total AKT remained unchanged in treated cell lines compared to untreated cells. However, there was a 1.31-fold (Ponatinib treatment) and 1.96-fold (combination treatment) downregulation of total AKT observed in the EMT-induced MDA-MB-231 cell line.

Subsequent investigation demonstrated the complementary effects of Pimozide and Ponatinib on the phosphorylation state of AKT at Thr 308 and Ser 473 residues. Earlier studies reported that Ponatinib is known to activate the PI3K/AKT/mTOR pathway by upregulating the AKT phosphorylation in some of the cancer phenotypes [22]. Hence, ponatinib was either combined

with other anti-cancer drugs or not used against specific cancer types. In this study, the elevated phosphorylation of Thr 308 was observed in Ponatinib-treated MCF-7 cell lines (luminal breast cancer type), not in the triple-negative breast cancer type (MDA-MB-231). Also, the phosphorylation status of Ser 473 was reduced in MCF-7 and MDA-MB-231 and remained unchanged in EMT-induced MDA-MB-231 (**Figure 3.4**).

Conversely, Pimozide exhibited promising downregulation of Thr 308 phosphorylation in MCF-7, MDA-MB-231, but no significant change in Ser 473 phosphorylation was observed. Further, in combination treatment, overall functional activation of AKT was restricted by downregulating Ser 473 phosphorylation in luminal breast cancer type (MCF-7) and by downregulating Thr 308 phosphorylation in triple-negative breast cancer type (MDA-MB-231) (**Figure 3.4**). Thus, the complementing action makes both Pimozide and Ponatinib act as effective co-therapy modules against both luminal and triple-negative breast cancer types.

Table 3.4: *Fold change in the expression of proteins after 30 min of drug treatments. Blue shade denotes the downregulation in fold change, green shade denotes the upregulation in fold change, and white denotes no significant change in the expression.*

	Drug name	p-IR (Y1146)	IR	IRS-1	p-AKT (T308)	p-AKT (S473)	AKT
MCF-7	*Pimozide*	2.04	1.17	1.69	1.49	1.02	1.56
	Ponatinib	1.47	1.20	2.12	1.35	1.29	1.35
	Pimozide+Ponatinib	2.12	1.02	2.00	1.50	1.78	1.21
MDA-MB-231	*Pimozide*	1.49	1.01	2.04	3.57	1.51	1.01
	Ponatinib	1.69	1.49	3.03	1.08	1.61	1.05
	Pimozide+Ponatinib	2.12	1.26	2.5	3.33	1.01	1.38
EMT induced MDA-MB-231	*Pimozide*	1.25	1.04	1.03	1.16	1.19	1.09
	Ponatinib	2.00	1.20	1.19	1.72	1.25	1.31
	Pimozide+Ponatinib	2.17	2.38	1.56	2.38	1.04	1.96

Table 3.5: *Fold change in the expression of ITGB1 and IR after 6 h of drug treatments. Blue shade denotes the downregulation in fold change, and white denotes no significant change in the expression.*

	Drug name	MCF-7	MDA-MB-231	EMT-induced MDA-MB-231
ITGB1	*Pimozide*	1.51	1.17	1.19
	Ponatinib	2.12	1.08	1.08
	Pimozide+Ponatinib	3.12	1.11	1.38
IR	*Pimozide*	1.96	1.28	2.08
	Ponatinib	2.04	1.29	1.08
	Pimozide+Ponatinib	1.69	2.17	1.14

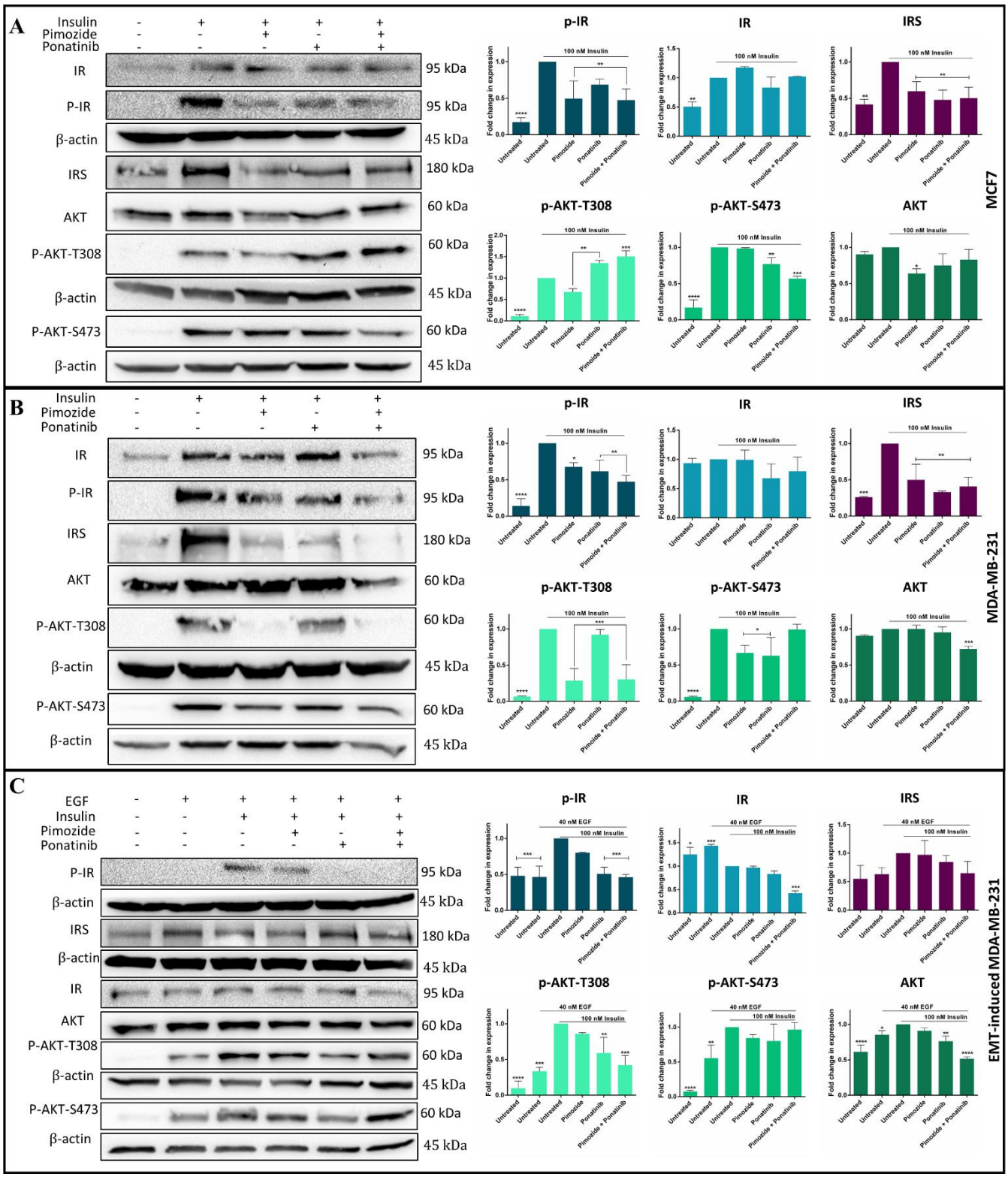

Figure 3.4: *Western blot analysis of IR-mediated signaling proteins after 30 min of Pimozide, Ponatinib, and Combination treatment* ***A)*** *MCF-7,* ***B)*** *MDA-MB-231,* ***C)*** *EMT-induced MDA-MB-231.*

3.3.5 Co-treatment promotes the lysosomal degradation of IR via ITGB1 inhibition

ITGB1 helps traffic the IR to the focal adhesion sites and avoids lysosomal degradation by forming the ITGB1/IR complex. It is also involved in the EMT-mediated metabolic reprogramming of cancer cells. Studies reported a reduced expression of matured ITGB1 in mesenchymal phenotype in comparison to epithelial, thereby causing detachment from ECM [23]. This detachment from ECM induces the lysosomal degradation of the ITGB1/IR complex and metabolic reprogramming of aerobic glycolysis to fatty acid oxidation. ITGB1 is one of the target proteins for both Pimozide and Ponatinib, based on previous *in-silico* studies. Hence, the protein expression profile of ITGB1 and IR was investigated after 6 h of treatment with the respective drugs.

Interestingly, in the MCF-7 cell line, the protein expression of both ITGB1 and IR downregulated significantly (**Figure 3.5**). It was also observed that the lower band of ITGB1 (a matured form of ITGB1) is more prominent than the upper band (precursor form of ITGB1) in MCF-7 (epithelial phenotype). Vice versa, in MDA-MB-231 (mesenchymal phenotype), the upper band is more prominent than the lower band (**Figure 3.5**). These findings support that during EMT, the expression of matured ITGB1 reduces and causes detachment-triggered IR degradation. Consistent with this observation, the efficacy of both drugs against ITGB1 in the MDA-MB-231 (mesenchymal) cell line was also subdued because of the lower expression level of matured ITGB1. The fold change in the expression of ITGB1 and IR after treatment compared to untreated cells was tabulated in **Table 3.5**.

Further, the effect of Pimozide and Ponatinib treatment on lysosome formation was examined via lysotracker staining. After 6 h of treatment, cells were stained with Lysotracker, and the fluorescence was measured using a flow cytometer. As expected, elevated levels of lysosome formation were observed in treated MCF-7 and MDA-MB-231 cells, especially in combination treatment 2-fold induction was detected (**Figure 3.5**). In EMT-induced conditions, fold change in lysosomal formation and the degradation of IR was subtler compared to the other two cell lines. This data demonstrates that degradation in the protein expression of IR and ITGB1 is the result of elevated lysosomal activity. Moreover, integrins play a pivotal role in cancer invasion and metastasis via focal adhesion, so the loss of ITGB1 on the migratory property of TNBC (MDA-MB-231) cells was evaluated by wound healing/scratch assay. The migration rate of cells toward the wounded/scratched region signifies their potential for metastasis. A significant reduction in the

wound-healing ability was observed in the treated MDA-MB-231 cells (**Figure 3.6A**). The efficacy of the treatment on the migratory property is represented from higher to lower as follows: combination, Ponatinib, and Pimozide treatment. Additionally, to confirm the viability of structurally modified cells post-drug treatment, live/dead staining was conducted in MDA-MB-231 cells **(Figure 3.6B)**. This analysis revealed that the treated-cells maintained viability, further supporting the observed reduction in migratory ability following loss of ITGB1 expression.

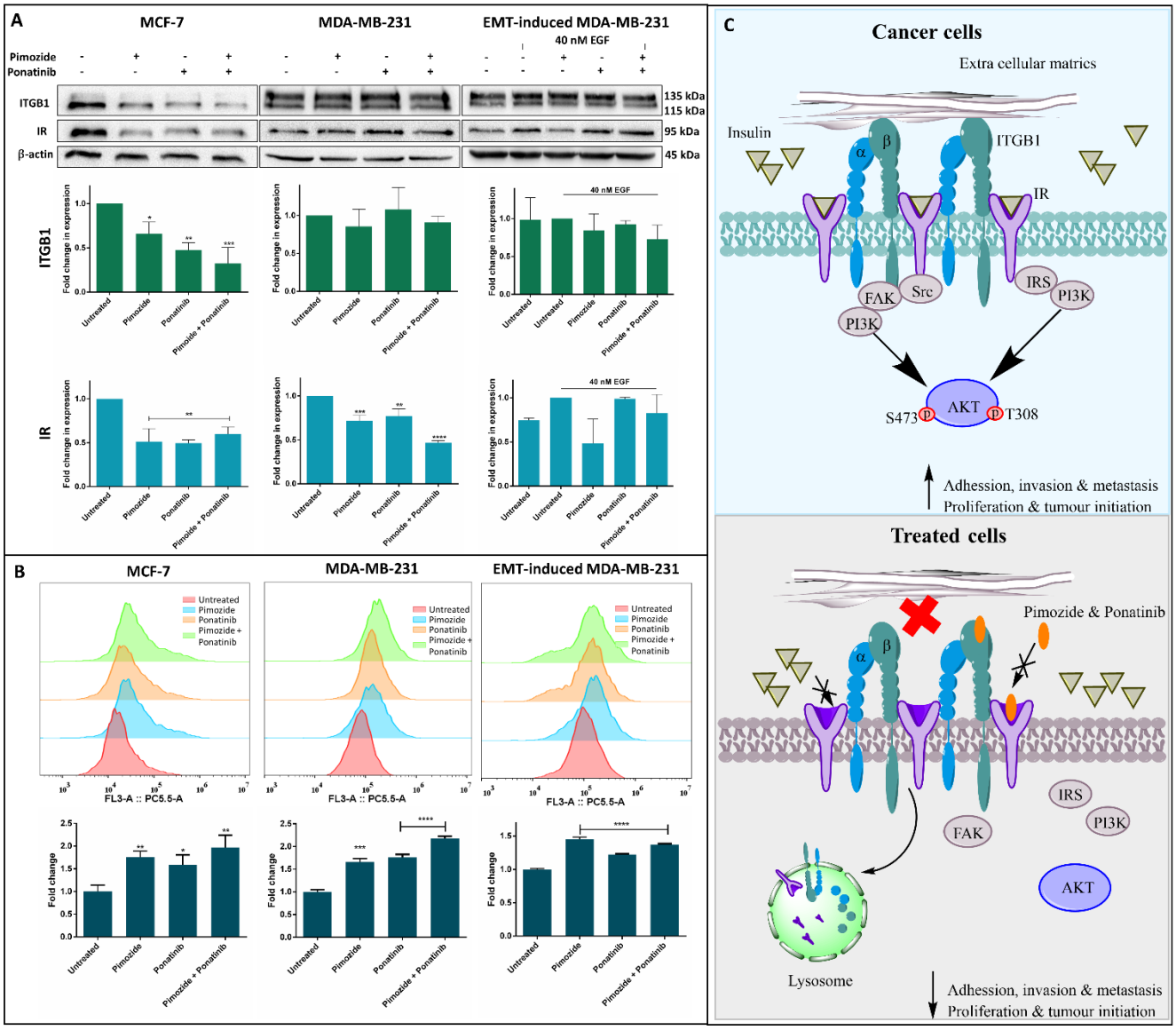

Figure 3.5: ***A)*** *Protein expression analysis of ITGB1 and IR after 6 h of treatment by western blot.* ***B)*** *Detection of lysosomes using Lysotracker.* ***C)*** *Graphical representation of ITGB1/IR complex in cancer progression.*

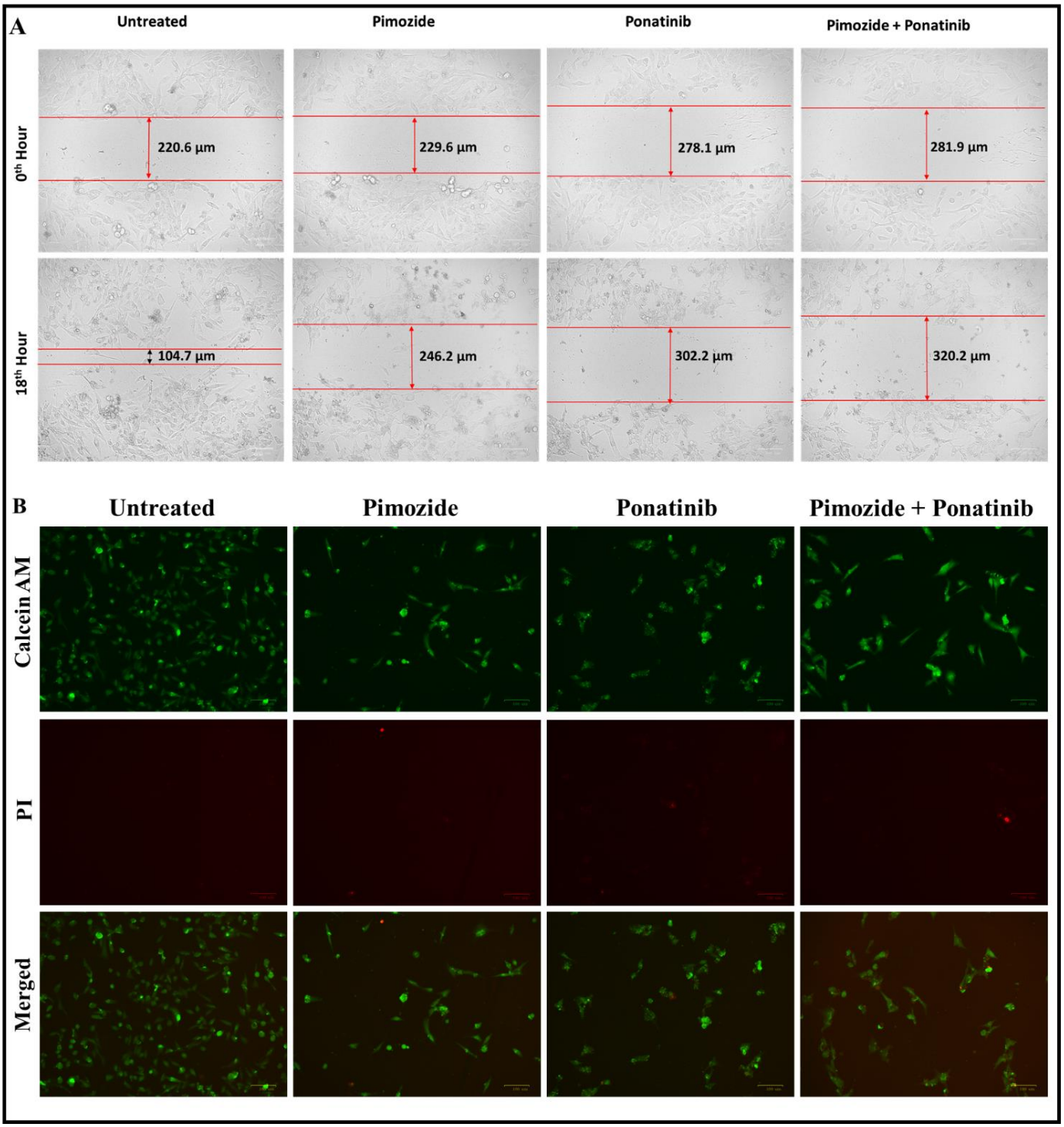

Figure 3.6: ***A)*** *Wound healing/scratch assay to assess the migratory property of MDA-MB-231 cell line after drug treatment.* ***B)*** *Live/dead cell imaging of MDA-MB-231 cell line after 48 h drug treatment using Calcein AM and PI staining (Scale – 100 µm).*

3.3.6 Inhibition of CD36 activity impeded the exogenous uptake and endogenous storage of fatty acids in TNBC cells.

Metabolic reprogramming of fatty acids plays a crucial role in malignant transformation, migration, and invasion. Increased exogenous fatty acid uptake, storage, and β-oxidation were observed in several cancers, including breast cancer cells, during stress conditions [5]. Typically, breast cancer cells obtain exogenous fatty acids from cancer-associated adipocytes. The amplified metabolic reprogramming meets the energy demand of highly proliferating cancer cells and biosynthesis of cellular components [5]. Since CD36 is one of the multi-target proteins for both drugs and is involved in fatty acid metabolism, the effect of drug treatment on the exogenous uptake and endogenous storage of fatty acids was investigated. The uptake study was assessed by fluorescently labeled BODIPY™ 500/510 C1, C12 fatty acids in MCF-7 and MDA-MB-231 cells. The images were captured after 6 h treatment of both drugs to assess the potential downstream effects of drug binding to CD36 and minimize the likelihood of false-positive results arising from non-specific interactions (**Figure 3.7**). It was observed that Pimozide reduced the exogenous uptake by blocking CD36 in MCF-7 and Ponatinib in MDA-MB-231 (both standard and EMT-induced conditions). However, the combination therapy exhibited an inhibitory effect against CD36 only in EMT-induced MDA-MB-231.

In addition, this study also investigated the cell population in which CD36 function was fully inhibited due to the drug treatments. Fluorescent-labeled fatty acids were detected using the FITC channel in the flow cytometer, and cell populations were gated with respect to unstained cells (no fluorescent-labeled fatty acids). Moreover, 8 to 20 percent of the cell population of treated cells was observed under unstained regions, whereas only 0 to 3 percent in untreated cells. This data indicates the inhibition of CD36 activity by Pimozide and Ponatinib in MCF-7 and MDA-MB-231 cell lines. The efficacy of CD36 inhibition, as demonstrated by the reduced uptake of fluorescent-labeled fatty acids, varied across cellular types and conditions, highlighting the complexity of CD36-mediated processes and the importance of context-dependent effects.

Additionally, the lipid droplets (LD) were stained using Nile red in both MCF-7 (epithelial phenotype) and MDA-MB-231 (mesenchymal phenotype). Interestingly, the lipid droplet accumulation was more abundant in MDA-MB-231 cells than in the MCF-7 (**Figure 3.7**). Studies have reported that an abundance of lipid droplet accumulation leads to aggressiveness of cancer,

especially in TNBCs. Pimozide and Ponatinib significantly reduced LD accumulation in MDA-MB-231 (normal and EMT-induced conditions). Comparatively, Ponatinib exerted better activity than Pimozide in disrupting the endogenous storage of fatty acids (**Figure 3.7**). In the case of MCF-7 cells, LD accumulation was shallow in both untreated and treated conditions.

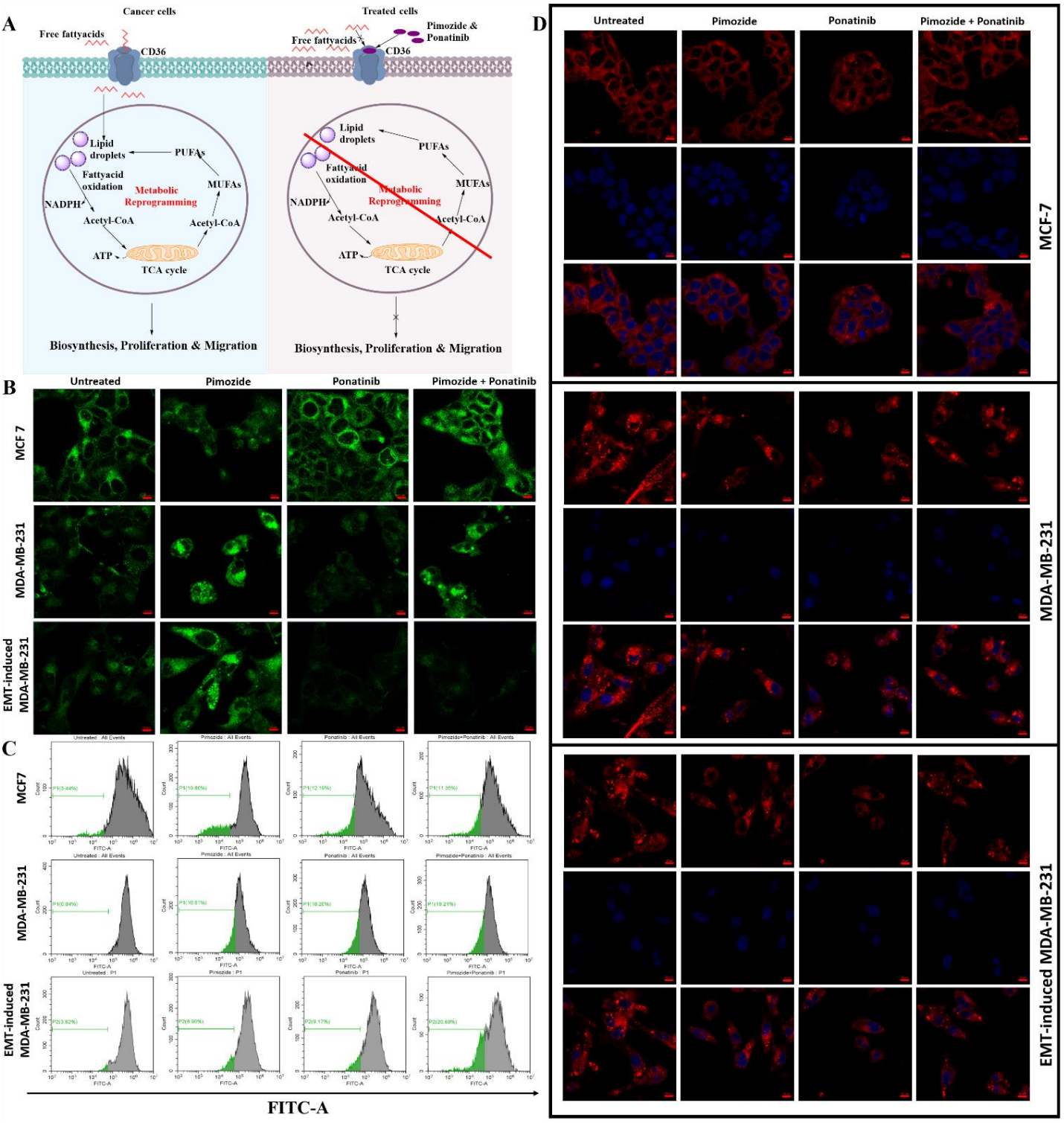

Figure 3.7: ***A)*** *Graphical representation of the role of CD36 in metabolic reprogramming.* ***B)*** *Fluorescently labeled fatty acid uptake assay after 6 h of treatment with respective drugs (Scale – 10 µm).* ***C)*** *Flowcytometric analysis of fluorescently labeled fatty acid uptake after 6 h of respective drug treatment.* ***D-F)*** *Lipid droplet staining by Nile red after 6 h of respective drug treatment (Scale – 10 µm).*

3.3.7 Downregulation of IRS-1 expression suppressed the IRS1/PR mediated stemness in MCF-7 and MDA-MB-231 cell lines

The crucial role of the IR/IRS1 pathway in endocrine resistance breast cancer and their link to upregulated cancer stem cell (CSC) growth were recently reported by Dwyer, A.R et, al. [24]. They also mentioned that the downregulation of IRS1 reduces the formation of phospho-PR and IRS1 complex, thereby reducing the tumor sphere formation. In this study, Pimozide and Ponatinib treatment demonstrated a significant reduction in the protein level expression of IRS1 (**Figure 3.8**). In continuation, the sphere-forming ability of both MCF-7 and MDA-MB-231 cells after the 48h treatment was also investigated. It was observed that Pimozide inhibited the CSC core formation in both MCF-7 and MDA-MB-231 cell lines, whereas Ponatinib treatment reduced the size of sphere formation (**Figure 3.8**). Moreover, the combination treatment portrayed better efficacy by blocking the CSC core formation as well as disrupting the tumor sphere. These findings suggest that the combination of Pimozide and Ponatinib might be a better therapeutic module for endocrine-resistant breast cancer in which reoccurrence of the tumor is a major concern.

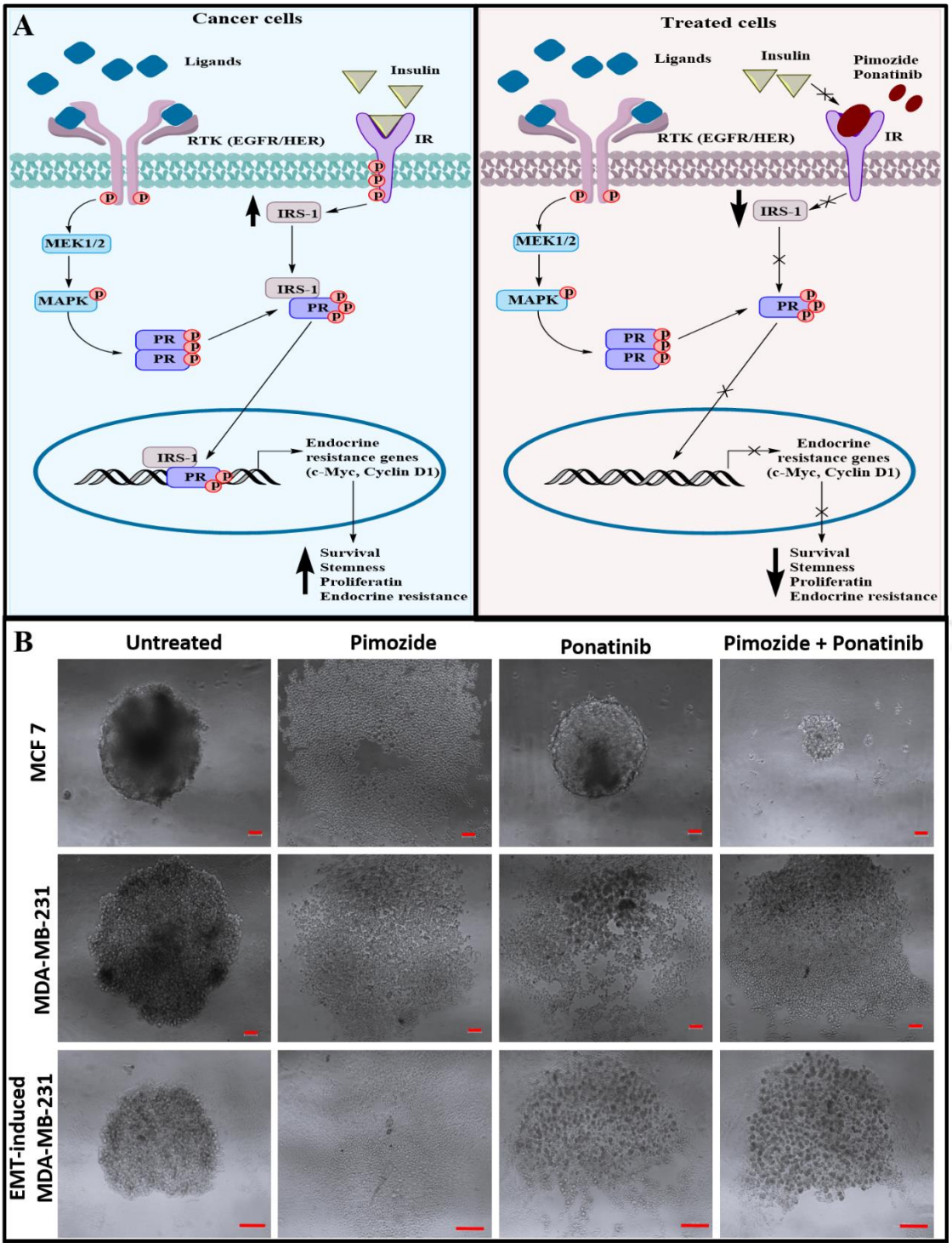

Figure 3.8: A) Graphical representation of IRS-1 mediated cancer stemness activation ***B)*** *Sphere formation assay to assess the effect of drug treatment on self-renewal/stemness property of breast cancer cells (Scale – 50 µm in MCF-7, MDA-MB-231 and 100 µm in EMT-induced MDA-MB-231)*

3.3.8 Inhibition of IR inhibits the EMT activation by altering E-cadherin and vimentin expression in TNBC cells

Metabolic reprogramming and EMT activation are the two emerging fields of study in cancer therapeutics. Understanding the interconnection between metabolic reprogramming and EMT activation paves a path to novel therapeutic targets. Previous study established the interconnected network of metabolic proteins and EMT signaling [9]. IR is one of the metabolic proteins that assists aerobic glycolysis by transporting GLUT4 to the cell membrane via AKT activation. In addition, IR also activates the AKT-mediated translocation of β-catenin and p50/p65 complex to the nucleus for the transcription of EMT transcription factors such as Snail, ZEB, and TWIST [7]. Transcription of EMT transcription factors upregulates the mesenchymal markers (Vimentin, N-cadherin, and fibronectin) and downregulates epithelial markers (E-cadherin and claudin). Since both Pimozide and Ponatinib exerted inhibitory activity against IR, the expression level of E-cadherin, Vimentin, and fibronectin were studied after 6 h of treatment (**Figure 3.9**). After drug treatment, a significant increase in the mRNA level of the epithelial marker gene (E-cadherin) and a reduction in the mesenchymal markers (Vimentin and Fibronectin) was observed. No significant reduction of mesenchymal marker genes was observed in Pimozide treatment after 6 h. In addition, the protein level expression of the mesenchymal marker also exhibited the same trend as the m-RNA level for both Pimozide and Ponatinib (**Figure 3.9**). It is also observed that compared to untreated and ponatinib-treated groups, the protein expression of Vimentin is significantly reduced in combination treatment (**Figure 3.9**). This observation portrays the efficacy of combination treatment in EMT reduction.

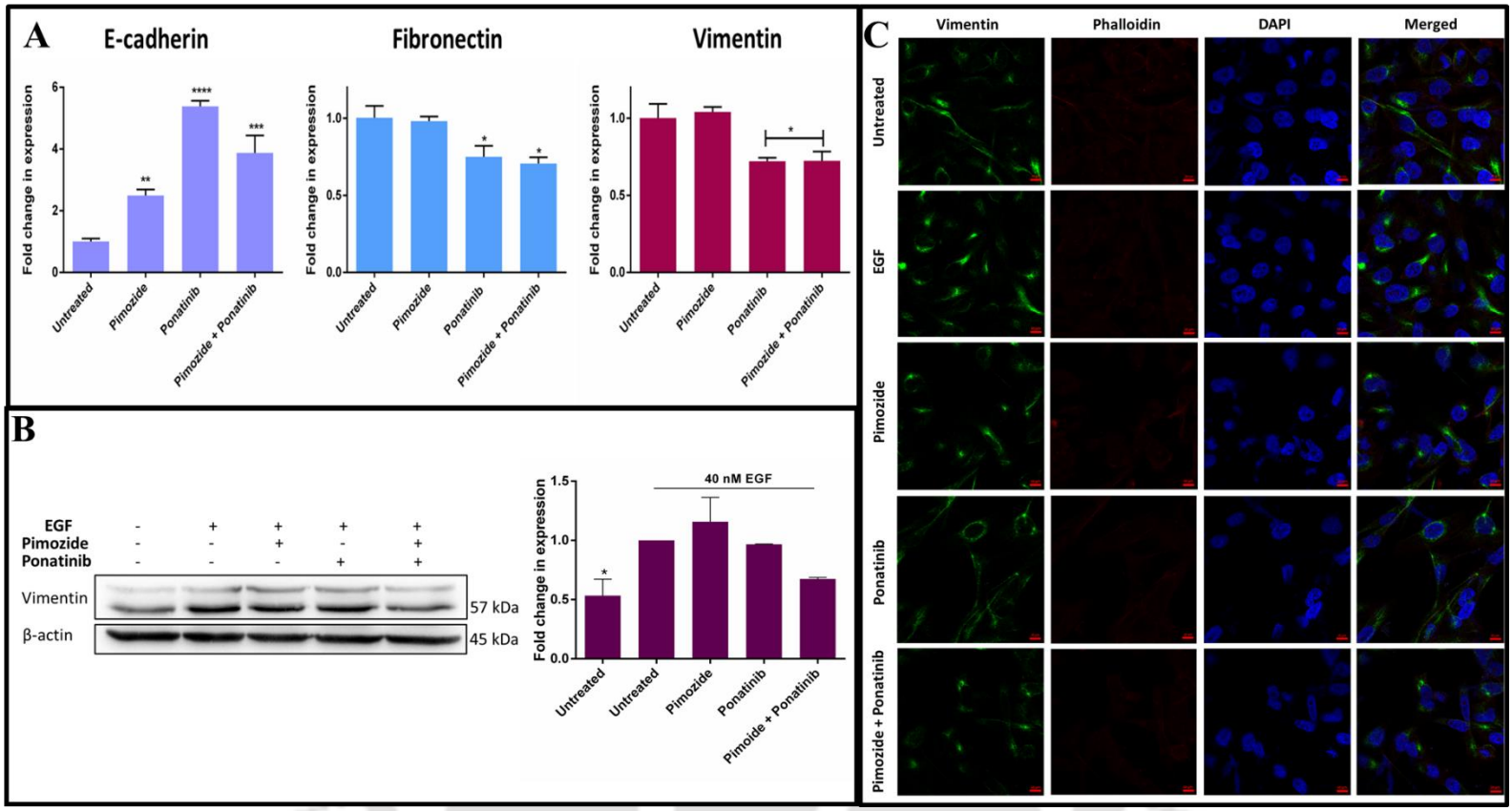

Figure 3.9: ***A)*** *Gene expression analysis of EMT markers by real-time PCR in EMT-induced MDA-MB-231 cells after 6 h of treatment.* ***B****) Western blot analysis of Vimentin in EMT-induced MDA-MB-231 cells after 6 h of drug treatment.* **C)** *Immunocytochemistry analysis of Vimentin in EMT-induced MDA-MB-231 cells after 6 h of drug treatment (Scale – 10 µm).*

3.3.9 Concurrent inhibition of IR, ITGB1, and CD36 demonstrated enhanced cytotoxicity in *in-vitro* tumor mimic models

The cytotoxic effect of Pimozide and ponatinib on MCF-7 and MDA-MB-231 tumor spheroids was investigated through an Almarblue assay. As stated in the methods section, tumor spheroids were generated in 96 well plates and monitored every 24 h. After 72 h of incubation, compact spheroids measuring 600 µm in MCF-7 and 800 µm in MDA-MB-231 were formed. Subsequently, spheroids were treated with increasing concentrations of Pimozide and Ponatinib; in the case of EMT-induced MDA-MB-231, drugs were treated along with 40 nM EGF in 0.5 % serum media. A dose-dependent decrease in cell viability was observed after 72 h of drug treatments in MCF-7, MDA-MB-231, and EMT-induced MDA-MB-231 spheroids (**Figure 3.10**). The IC_{50} values of Pimozide, Ponatinib, and combination treatments were 16.21 µM, 1.65 µM, 7.41 µM in MCF-7 and 5.51 µM, 3.32 µM, 4.05 µM in MDA-MB-231 respectively. It was evident that the combination of Pimozide with Ponatinib significantly reduced the IC_{50} of Pimozide in both MCF7 and MDA-MB-231 spheroids.

Furthermore, live/dead cell imaging of tumor spheroids was carried out using Calcein AM and PI staining. The tumor spheroids were treated with respective IC_{50} concentrations for 72 h and stained with Calcein AM and PI for 1 h. Subsequent reduction of green fluorescence (live cells) and an increase of red fluorescence (dead cells) were observed in the drug treatment with respect to untreated spheroids. The combination treatment of Pimozide and Ponatinib exerted higher dead cell populations in MCF-7 and MDA-MB-231 spheroids (**Figure 3.10**). A similar effect was observed in EMT-induced MDA-MB-231 spheroid as well (**Figure 3.10**). This study on *in-vitro* tumor mimicking might assist in the dosage optimization of drugs in the future for *in-vivo* models.

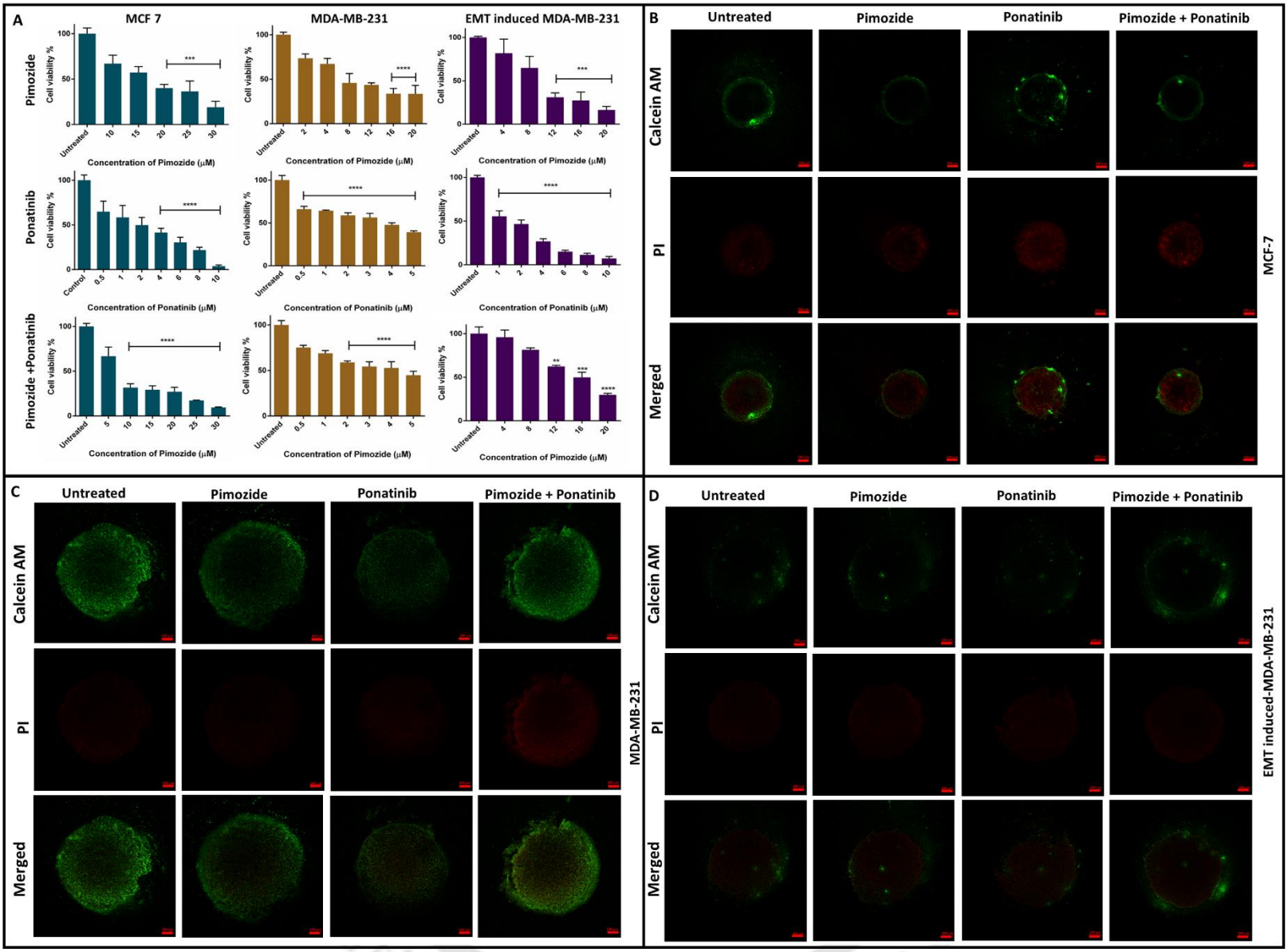

Figure 3.10: A) *Dose-dependent cytotoxic effect of Pimozide, Ponatinib, and combination in tumor spheroids of MCF-7, MDA-MB-231and EMT-induced MDA-MB-231. Live/dead cell imaging of* ***B)*** *MCF-7,* ***C)*** *MDA-MB-231 and* ***D)*** *EMT-induced MDA-MB-231 tumor spheroids by Calcein AM / PI staining (Scale – 200 µm). Images were captured after 72 h of treatment with* IC_{50} *concentration of drugs.*

3.4. Discussions

The intricate interplay between cancer cell proliferation and metabolic reprogramming underscores the significance of understanding the underlying mechanisms driving cancer progression. Cancer cells exhibit heightened energy demands, leading to the rewiring of conventional metabolic pathways [25]. In this context, emerging evidence highlights the association between metabolic reprogramming and epithelial-mesenchymal transition (EMT), a process crucial for tumor aggressiveness and metastasis [26]. While aerobic glycolysis predominates in epithelial phenotypic cancer cells, mesenchymal phenotype cells rely on fatty acid metabolism and autophagy to meet their energy requirements.

Recognizing the pivotal role of metabolic-EMT interconnection in cancer progression, this study targeted a comprehensive network of 70 proteins encompassing metabolic and EMT signaling pathways. Specifically, a multi-component molecular dynamics simulation study was employed to evaluate the multi-targeting ability of Ponatinib and Pimozide against three key proteins: insulin receptor (IR), integrin beta1 (ITGB1), and CD36. Notably, this study simulates three target proteins with various drug combinations. This culminated in the concurrent inhibition of all three targets achieved through a 2:1 ratio of Pimozide and Ponatinib, corroborated by *in-vitro* cytotoxicity assays.

Initial assessments of drug cytotoxicity on luminal and TNBC cells revealed lower inhibitory concentrations (IC_{50}) with Ponatinib treatment compared to Pimozide alone. Remarkably, co-treatment with Ponatinib significantly reduced the IC_{50} of Pimozide, indicating synergistic effects between the two drugs. Mechanistically, this study elucidated the cellular processes underlying the cytotoxic effects of Pimozide and Ponatinib, demonstrating intracellular reactive oxygen species (ROS) generation, mitochondrial membrane depolarization, and apoptotic cell death. These observations underscore the activation of the intrinsic pathway of apoptosis through oxidative stress-mediated cytochrome C release from mitochondria [17].

Furthermore, current research investigated the inhibitory efficacy of Pimozide, Ponatinib, and combination treatment on the interconnected metabolic-EMT network from various perspectives. Firstly, the IR-mediated AKT activation was examined, which is crucial for energy metabolism and EMT signaling. Protein expression studies revealed significant reductions in p-IR, IRS-1, and

p-AKT levels following drug treatments, indicating functional AKT inactivation by Pimozide and Ponatinib.

Subsequently, the impact of Pimozide and Ponatinib on energy metabolism was evaluated, focusing on ITGB1-mediated IR stability and fatty acid metabolism, as well as CD36-mediated fatty acid uptake and lipid droplet accumulation. The findings demonstrated inhibition of aerobic glycolysis and fatty acid metabolism in epithelial and mesenchymal phenotypic cells, underscoring the dual inhibitory effects of Pimozide and Ponatinib on cancer cell metabolism.

Moreover, the modulation of EMT marker genes by Pimozide and Ponatinib was observed, revealing significant downregulation of mesenchymal markers (Vimentin and Fibronectin) and upregulation of the epithelial marker (E-cadherin). Additionally, the impact of drug treatments on cancer stemness was elucidated, highlighting the complete inhibition of cancer stem cell (CSC) core formation in luminal and TNBC cell lines through the disruption of IRS-1 and PR complex formation.

Overall, this study provides comprehensive mechanistic insights into the inhibitory activity of Pimozide and Ponatinib against the interconnected network of energy metabolism and EMT signaling in breast cancer cells. These findings attribute the therapeutic potential of targeting multiple nodes within this network and pave the way for further preclinical and clinical investigations to validate the translational relevance of these findings in breast cancer therapy.

3.5. Conclusion

In brief, co-administration of anti-cancer drug with anti-psychotic drug demonstrated better efficacy in terms of cytotoxicity in breast cancer cell lines. Combined treatment of Pimozide with Ponatinib facilitated the activation of the intrinsic pathway of apoptosis by inducing ROS generation and mitochondrial membrane depolarization. As per *in-silico* as well as *in-vitro* findings, co-therapy exerted substantial inhibition of all three target proteins (IR/ITGB1/CD36). It eventually suppressed the activation of AKT, along with inhibition of the complex formation of IRS1/PR and ITGB1/IR. The functional inactivation of AKT subsequently downregulated the expression of mesenchymal markers by impeding GSK3β and NF-κB signaling. In addition to that, the downregulation of IRS-1 and ITGB1 ultimately reduced the CSC core formation and migratory ability of the breast cancer cells. Moreover, co-therapy exhibited a significant cytotoxic

effect in *in-vitro* tumor mimic models constituting breast cancer cells. Therefore, the co-therapeutic module comprising Pimozide and Ponatinib denotes a promising approach to perturb the interconnected functional network of energy metabolism and EMT in the realm of breast cancer therapy.

3.6. References

1. Schiliro, C., & Firestein, B. L. (2021). Mechanisms of metabolic reprogramming in cancer cells supporting enhanced growth and proliferation. Cells, 10(5), 1056. https://doi.org/10.3390/cells10051056
2. Vander Heiden, M. G., Cantley, L. C., & Thompson, C. B. (2009). Understanding the Warburg effect: the metabolic requirements of cell proliferation. science, 324(5930), 1029-1033. https://doi.org/10.1126/science.1160809
3. Bui, T., Rennhack, J., Mok, S., Ling, C., Perez, M., Roccamo, J., & Muller, W. J. (2019). Functional redundancy between β1 and β3 integrin in activating the IR/Akt/mTORC1 signaling axis to promote ErbB2-driven breast cancer. Cell reports, 29(3), 589-602. https://doi.org/10.1016/j.celrep.2019.09.004
4. Koundouros, N., & Poulogiannis, G. (2020). Reprogramming of fatty acid metabolism in cancer. British journal of cancer, 122(1), 4-22. https://doi.org/10.1038/s41416-019-0650-z
5. Liang, Y., Han, H., Liu, L., Duan, Y., Yang, X., Ma, C., & Chen, Y. (2018). CD36 plays a critical role in proliferation, migration and tamoxifen-inhibited growth of ER-positive breast cancer cells. Oncogenesis, 7(12), 98. https://doi.org/10.1038/s41389-018-0107-x
6. Georgakopoulos-Soares, I., Chartoumpekis, D. V., Kyriazopoulou, V., & Zaravinos, A. (2020). EMT factors and metabolic pathways in cancer. Frontiers in oncology, 10, 499. https://doi.org/10.3389/fonc.2020.00499
7. Gonzalez, D. M., & Medici, D. (2014). Signaling mechanisms of the epithelial-mesenchymal transition. Science signaling, 7(344), re8-re8. https://doi.org/10.1126%2Fscisignal.2005189
8. Georgakopoulos-Soares, I., Chartoumpekis, D. V., Kyriazopoulou, V., & Zaravinos, A. (2020). EMT factors and metabolic pathways in cancer. Frontiers in oncology, 10, 499. https://doi.org/10.3389%2Ffonc.2020.00499

9. Kandasamy, T., Sen, P., & Ghosh, S. S. (2022). Multi-targeted drug repurposing approach for breast cancer via integrated functional network analysis. Molecular Informatics, 41(8), 2100300. https://doi.org/10.1002/minf.202100300
10. Jo, S., Kim, T., Iyer, V. G., & Im, W. (2008). CHARMM-GUI: a web-based graphical user interface for CHARMM. Journal of computational chemistry, 29(11), 1859-1865. https://doi.org/10.1002/jcc.20945
11. Lemkul, J. (2018). From proteins to perturbed Hamiltonians: a suite of tutorials for the GROMACS-2018 molecular simulation package [article v1. 0]. LiveCoMS 1 (1): 5068. https://doi.org/10.33011/LIVECOMS.1.1.5068
12. Sen, P., Kandasamy, T., & Ghosh, S. S. (2023). Multi-targeting TACE/ADAM17 and gamma-secretase of notch signalling pathway in TNBC via drug repurposing approach using Lomitapide. Cellular Signalling, 102, 110529. https://doi.org/10.1016/j.cellsig.2022.110529
13. Arora, N., Shome, R., & Ghosh, S. S. (2019). Deciphering therapeutic potential of PEGylated recombinant PTEN-silver nanoclusters ensemble on 3D spheroids. Molecular Biology Reports, 46, 5103-5112. https://doi.org/10.1007/s11033-019-04965-7
14. Samovski, D., Dhule, P., Pietka, T., Jacome-Sosa, M., Penrose, E., Son, N. H., & Abumrad, N. A. (2018). Regulation of insulin receptor pathway and glucose metabolism by CD36 signaling. Diabetes, 67(7), 1272-1284. https://doi.org/10.2337%2Fdb17-1226
15. Heit, B., Kim, H., Cosío, G., Castaño, D., Collins, R., Lowell, C. A., & Grinstein, S. (2013). Multimolecular signaling complexes enable Syk-mediated signaling of CD36 internalization. Developmental cell, 24(4), 372-383. https://doi.org/10.1016/j.devcel.2013.01.007
16. Redza-Dutordoir, M., & Averill-Bates, D. A. (2016). Activation of apoptosis signalling pathways by reactive oxygen species. Biochimica et Biophysica Acta (BBA)-Molecular Cell Research, 1863(12), 2977-2992. https://doi.org/10.1016/j.bbamcr.2016.09.012
17. Elmore, S. (2007). Apoptosis: a review of programmed cell death. Toxicologic pathology, 35(4), 495-516. https://doi.org/10.1080/01926230701320337
18. Boucher, J., Kleinridders, A., & Kahn, C. R. (2014). Insulin receptor signaling in normal and insulin-resistant states. Cold Spring Harbor perspectives in biology, 6(1), a009191. https://doi.org/10.1101/cshperspect.a009191

19. Tsuchiya, A., Kanno, T., & Nishizaki, T. (2013). Stearic acid serves as a potent inhibitor of protein tyrosine phosphatase 1B. Cellular physiology and biochemistry, 32(5), 1451-1459. https://doi.org/10.1159/000356582
20. Kaewlert, W., Sakonsinsiri, C., Lert-Itthiporn, W., Ungarreevittaya, P., Pairojkul, C., Pinlaor, S., & Thanan, R. (2023). Overexpression of Insulin Receptor Substrate 1 (IRS1) Relates to Poor Prognosis and Promotes Proliferation, Stemness, Migration, and Oxidative Stress Resistance in Cholangiocarcinoma. International Journal of Molecular Sciences, 24(3), 2428. https://doi.org/10.3390/ijms24032428
21. Paplomata, E., & O'Regan, R. (2014). The PI3K/AKT/mTOR pathway in breast cancer: targets, trials and biomarkers. Therapeutic advances in medical oncology, 6(4), 154-166. https://doi.org/10.1177/1758834014530023
22. Liu, C., Mu, X., Wang, X., Zhang, C., Zhang, L., Yu, B., & Sun, G. (2019). Ponatinib inhibits proliferation and induces apoptosis of liver cancer cells, but its efficacy is compromised by its activation on PDK1/Akt/mTOR signaling. Molecules, 24(7), 1363. https://doi.org/10.3390/molecules24071363
23. Tixi, W., Maldonado, M., Chang, Y. T., Chiu, A., Yeung, W., Parveen, N., & Shih, H. P. (2023). Coordination between ECM and cell-cell adhesion regulates the development of islet aggregation, architecture, and functional maturation. Elife, 12, e90006. https://doi.org/10.7554/elife.90006
24. Dwyer, A. R., Truong, T. H., Kerkvliet, C. P., Paul, K. V., Kabos, P., Sartorius, C. A., & Lange, C. A. (2021). Insulin receptor substrate-1 (IRS-1) mediates progesterone receptor-driven stemness and endocrine resistance in oestrogen receptor+ breast cancer. British Journal of Cancer, 124(1), 217-227. https://doi.org/10.1038/s41416-020-01094-y
25. Pavlova, N. N., & Thompson, C. B. (2016). The emerging hallmarks of cancer metabolism. Cell metabolism, 23(1), 27-47. https://doi.org/10.1016/j.cmet.2015.12.006
26. Sciacovelli, M., & Frezza, C. (2017). Metabolic reprogramming and epithelial-to-mesenchymal transition in cancer. The FEBS journal, 284(19), 3132-3144. https://doi.org/10.1111/febs.14090

CHAPTER 4

Drug Cocktail Strategy for Enhanced Efficacy

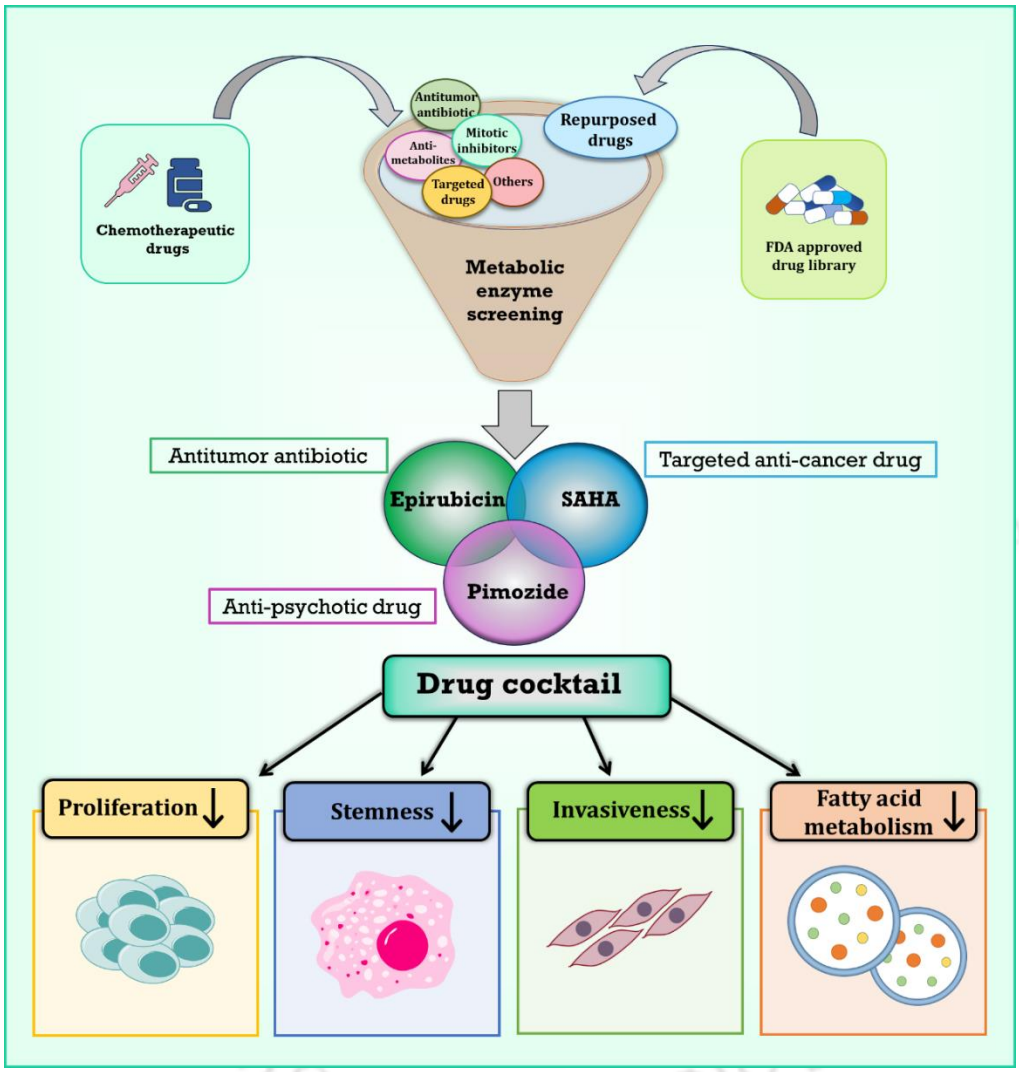

Chapter 4 explores a drug cocktail strategy to enhance therapeutic efficacy by optimizing metabolic compatibility among selected drugs. The Pimozide-Epirubicin-SAHA (ESP) combination is developed, which substantially lowers the IC50 of Pimozide and induces robust apoptosis through ROS generation and intrinsic apoptotic pathways. This approach offers a more potent and lower-toxicity option for breast cancer treatment, addressing challenges associated with traditional therapies.

IUBMB life, 77(5), e70020

DOI: 10.1002/iub.70020

CHAPTER 4

Drug Cocktail Strategy for Enhanced Efficacy

4.1. Introduction

Breast cancer remains one of the most prevalent and challenging malignancies to treat, with a variety of therapeutic approaches developed over the years [1]. Current treatment strategies include surgery, radiation therapy, and systemic therapies such as chemotherapy, targeted therapy, and hormone therapy [1]. Chemotherapeutic agents, currently used in breast cancer treatment, span a broad range of drug classes, each with its own mechanisms and limitations [2]. For instance, anti-tumor antibiotics like Doxorubicin and Epirubicin are widely used due to their ability to intercalate DNA, inhibiting replication. However, their cumulative use is associated with dose-dependent cardiotoxicity, which severely limits long-term use [2, 3]. Alkylating agents like Cyclophosphamide and Cisplatin are another class that function by cross-linking DNA strands, but they also cause severe side effects such as bone marrow suppression and nephrotoxicity [2, 3]. Similarly, anti-metabolites like Capecitabine and Gemcitabine interfere with nucleotide synthesis and DNA replication but are associated with significant hematological and gastrointestinal toxicities [2, 3]. Topoisomerase inhibitors like Irinotecan and Topotecan hinder enzymes that regulate DNA winding, leading to the interruption of DNA transcription and replication [2, 3]. These drugs, however, are not without their own drawbacks, including diarrhea and myelosuppression. While effective at killing cancer cells, this chemotherapeutics are often plagued by dose-limiting toxicities, narrow therapeutic windows, and the inevitable emergence of drug resistance, where cancer cells adapt and become less responsive to the treatment [2, 3]. Moreover, non-specificity in targeting both cancerous and healthy cells result in systemic toxicity, leading to further complications. These significant drawbacks emphasize the need for novel therapeutic strategies that improve treatment efficacy while minimizing adverse effects.

In recent years, drug repurposing has emerged as a promising approach in cancer therapy. Drugs originally developed for non-cancer conditions, such as antipsychotics and antihypertensives, have shown potential for treating various cancers, including breast cancer [4]. Antipsychotic drugs, particularly Pimozide, have emerged as an unexpected yet promising avenue in cancer therapy. Initially developed to treat psychiatric conditions such as schizophrenia and Tourette syndrome,

antipsychotic agents have been found to possess anti-cancer properties [5]. These drugs often modulate pathways involved in cell proliferation, survival, and apoptosis, which are crucial in the development and progression of cancer. Pimozide, a typical antipsychotic, has gained attention due to its ability to inhibit multiple signaling pathways critical in cancer biology, including those involved in cell proliferation and migration [5]. Specifically, Pimozide has been shown to target the Wnt/β-catenin and STAT3 pathways, both of which are key regulators of cancer stem cell behavior and epithelial-to-mesenchymal transition (EMT), processes that are associated with cancer metastasis and therapy resistance [6].

Preclinical studies have demonstrated that Pimozide exhibits cytotoxic effects against a range of cancer cell lines, including breast cancer cells, by inducing apoptosis and inhibiting cell migration and invasion [6, 7, 8]. In breast cancer, Pimozide has been reported to downregulate the expression of cyclin D1, a protein essential for cell cycle progression, thereby halting the proliferation of cancer cells [6]. Additionally, Pimozide has been found to reduce vascular endothelial growth factor (VEGF) levels, thereby impeding angiogenesis, a critical process for tumor growth and metastasis [7]. This multifaceted mechanism of action positions Pimozide as a compelling candidate for breast cancer therapy, particularly in cases where conventional chemotherapeutics have failed or resulted in drug resistance. Despite its potential, however, Pimozide, like many repurposed drugs, faces challenges in clinical application. Higher doses are often required to achieve therapeutic levels in cancer treatment, which can result in significant off-target effects and toxicity, especially since the drug is not originally designed for oncological use [4, 5]. Moreover, the limited cancer-specific targeting of Pimozide increases the likelihood of adverse side effects, particularly in long-term treatment scenarios. To address the limitations of both chemotherapeutic and repurposed drugs, combination or cocktail therapies have been explored.

Combination and cocktail therapies involve using two or more drugs to target different cancer pathways simultaneously, aiming to improve efficacy and reduce resistance. For example, a study reported that a triple-chemotherapy drug cocktail combining doxorubicin, all-trans retinoic acid (ATRA), and Entinostat (EAD) in triple-negative breast cancer led to a 90% reduction in tumor sphere formation by enhancing differentiation and drug sensitivity [9]. However, conventional combination approaches, while effective in some cases, are often hindered by drug interactions and overlapping drug metabolism pathways [10]. This overlap can increase the metabolic burden

on key drug-metabolizing enzymes, such as cytochrome P450 enzymes, leading to adverse effects and limiting the therapeutic potential of the combination [11]. Drug-metabolizing enzymes play a crucial role in determining the efficacy and safety of combination treatments. When multiple drugs are metabolized by the same enzyme, the competition for metabolic processing can lead to enzyme saturation, resulting in altered drug pharmacokinetics, increased toxicity, and reduced therapeutic efficacy [10, 11]. This highlights the importance of carefully selecting drug combinations based on their metabolic profiles to minimize these risks.

In this study, a cocktail approach was employed, where more than two drugs are combined with careful consideration of their metabolic pathways, presents a significant advantage over traditional combination therapies. By selecting drugs that do not share metabolizing enzymes, the cocktail approach not only reduces the metabolic load on individual enzymes but also enhances the overall therapeutic efficacy while minimizing toxicity. This strategy offers a more refined and effective way to repurpose drugs and optimize chemotherapeutic regimens for breast cancer therapy.

4.2. Experimental section

4.2.1. Identification of metabolizing enzymes of drugs

Identification of the metabolizing enzymes (cytochrome P450) involved in the metabolism of corresponding drugs were carried out using the Drug Bank database. Metabolizing enzymes of each drugs were compared with those of the repurposed drug Pimozide to identify potential drug combinations that do not share metabolic pathways, thereby reducing the risk of metabolic competition and associated toxicity.

4.2.2. Drug-drug interaction analysis

The STITCH (Search Tool for Interactions of Chemicals) database was employed to assess potential drug-drug interactions among the selected drugs. STITCH provides insights into interactions between chemicals and proteins, which helped ensure that the chosen drugs do not exhibit significant interactions that could impact their combined use.

4.2.3. Cell culture conditions

MCF-7 (luminal) and MDA-MB-231 (triple-negative breast cancer, TNBC) cell lines were obtained from the National Centre for Biological Sciences (NCBS), Pune, India. The cells were

cultured in Dulbecco's Modified Eagle Medium (DMEM, Sigma) supplemented with 10% fetal bovine serum (FBS, Gibco) and 1% antibiotic-antimycotic solution (Gibco). Cell cultures were maintained in a humidified incubator with 5% CO_2 at 37°C.

4.2.4. Cellular cytotoxicity assay

To evaluate the cytotoxic effects of the drug combinations, cellular cytotoxicity assays were performed using the MCF-7 and MDA-MB-231 cell lines. Cells were seeded in a 96-well plate at a density of 5×10^3 cells/well for MCF-7 and MDA-MB-231. After 24 h of incubation under standard cell culture conditions (5% CO_2, 37°C), cells were treated with varying concentrations of the selected drugs. Following 48 h of drug treatment, 0.25 mg/mL of MTT was added to respective wells for 2 h to assess cell viability. The resulting formazan crystals were dissolved by adding dimethyl sulfoxide (DMSO), and the absorbance was measured at 570 nm and 630 nm. The IC_{50} concentration of respective drugs and combinations were calculated using sigmoidal dose-response curves in GraphPad Prism Version 6.0.0 as reported earlier [8]. The synergism between the drug combinations were analysed using Compusyn version 1.0.

4.2.5. Intracellular reactive oxygen species (ROS) measurement

To assess intracellular ROS levels, MCF-7 and MDA-MB-231 cells were seeded at a density of 3×10^5 cells/well in 6-well plates. After 24 h of incubation at 37°C in a humidified atmosphere with 5% CO_2, cells were treated with the respective IC_{50} concentrations of individual drugs or drug combinations. Following a 6-h treatment period, 2 µM of 2',7'-dichlorofluorescein diacetate (DCFDA) was added to the cells and incubated for 30 minutes in the dark. Fluorescent images were captured using the ZOE Fluorescence Imager (BioRad). The fluorescence intensity of DCFDA, indicative of ROS levels, was quantified using ImageJ software, and the fold changes in ROS production were calculated. Data were plotted and analyzed using GraphPad Prism software (version 6.0.0).

4.2.6. Apoptosis assay

To evaluate drug-induced apoptosis, MCF-7 and MDA-MB-231 cells were seeded at a density of 3×10^5 cells/well in 6-well plates. After 24 h of incubation, cells were treated with the IC_{50} concentrations of drugs or drug combinations for 48 h. At the end of the treatment period, cells were trypsinized, collected, and washed twice with phosphate-buffered saline (PBS) by

centrifugation at 650 rcf for 5 minutes at 4°C. Cells were then resuspended in 1X binding buffer and stained with Alexa Fluor™ 488 Annexin-V and propidium iodide (PI) for 15 minutes at room temperature in the dark. Apoptotic populations were analyzed using a BD FACS Melody flow cytometer. The collected data were processed and analyzed using FlowJo software (version 10), and the percentage of early and late apoptotic cells was quantified.

4.2.7. Live/dead staining of monolayer and tumor spheroids

The cell viability and death in both monolayer and 3D spheroid cultures were assessed through live/dead staining. For monolayer cultures, MCF-7 and MDA-MB-231 cells were seeded in 6-well plates at a density of 3×10^5 cells/well and treated with IC_{50} concentrations of individual drugs or drug combinations for 48 h. Following the treatment, cells were stained with 2 µM Calcein-AM (to stain live cells) and 4 µM propidium iodide (PI, to stain dead cells) for 30 minutes. Images were captured using the ZOE Fluorescence Imager (BioRad). For tumor spheroid cultures, 2×10^4 cells/well of MCF-7 or MDA-MB-231 cells were seeded in 96-well plates pre-coated with 1.5% agarose to promote non-adherent conditions. After seeding, the plates were centrifuged at 700 rcf for 10 minutes at 25°C to facilitate spheroid formation. The plates were incubated for 72 h at 37°C in 5% CO_2 to allow spheroid formation. Once the spheroids were established, they were treated with the IC_{50} concentrations of drugs and combinations. After 72 h of treatment, spheroids were stained with 2 µM Calcein-AM and 4 µM PI for 1 h. Confocal images of live and dead cells were captured using a Zeiss LSM 880 confocal microscope. Calcein-AM stained live cells in green, while PI stained dead cells in red.

4.2.8. Western blot analysis

The alterations in the expression of protein markers after drug treatment were analysed using western blot method. After 24 h of drug treatment (or 48 h for apoptosis markers), total proteins were isolated using RIPA buffer and protease inhibitor cocktail. The quantification of total protein was carried out by the BCA protein quantification kit. Equal amounts of protein were used for Western blot experiment following standard protocols [12]. The bands were visualized using ECL detection, and quantified using ImageJ, with β-actin used as the loading control.

Table 4.1: *The list of antibodies used for protein expression study*

Antibodies	Catalog No	Manufacture
β-actin	8457	Cell Signaling Technology, USA
β-tubulin	2146	Cell Signaling Technology, USA
Cleaved PARP	5625	Cell Signaling Technology, USA
P53	32532	Cell Signaling Technology, USA
SOD2	13141	Cell Signaling Technology, USA
AKT	8200	Cell Signaling Technology, USA
NRF2	12721	Cell Signaling Technology, USA
P21	2947	Cell Signaling Technology, USA
Anti-Rabbit IgG, HRP linked	7074S	Cell Signaling Technology, USA

4.2.9. Lipid droplet staining by Nile red

The Nile red staining method was used to study the accumulation of endogenous lipid droplets in cells. Both cells were seeded at a density of 3×10^5 cells/well in 35 mm glass-bottom dishes. After allowing 24 h for cell adhesion, the cells were treated with IC_{50} concentrations of the drugs or drug combinations for 6 h. Following treatment, the cells were stained with Nile red (0.01 mg/mL) for 30 minutes at 37°C in the dark and fixed with 4% formaldehyde. The fluorescence intensity of lipid droplets (stained red by Nile Red) was visualized and captured using a Zeiss LSM 880 confocal microscope, and intensity measurements were quantified using ImageJ software.

4.2.10. Fatty acid uptake assay

The exogenous uptake of fatty acids was measured using a fluorescent labelled fatty acid. MCF-7 and MDA-MB-231 cells were seeded in 35 mm glass-bottom dishes at the same density of 3×10^5 cells/well and treated with IC_{50} concentrations of the drugs or drug combinations for 6 h. Following treatment, the cells were stained with 100 nM of BODIPY™ 500/510 C1, C12 fluorescently labeled fatty acid (Invitrogen by Thermo Fisher Scientific) for 30 min in the dark. Cells were then washed with PBS and fixed with 4% formaldehyde for 15 min. The fatty acid uptake, visualized by green fluorescence, was imaged using the Zeiss LSM 880 confocal microscope. Quantification of the fluorescent intensity was performed using ImageJ software to determine the extent of fatty acid uptake in treated cells.

4.2.11. Sphere formation assay

To assess the impact of drug treatments on cancer stemness, a sphere formation assay was conducted. MCF-7 and MDA-MB-231 cells were seeded in 6-well plates at a density of 3×10^5

cells per well for MCF-7 and 8×10^5 cells per well for MDA-MB-231. After 24 h of incubation, cells were treated with the IC_{50} concentrations of individual drugs or drug combinations for 48 h, following the same protocol as described in the apoptosis assay. After treatment, cells were isolated, and 2×10^4 cells were seeded in 96-well plates pre-coated with 1.5% agarose to promote sphere formation. After seeding, the plates were centrifuged at 700 rcf for 10 min at 25°C to facilitate spheroid formation. The plates were incubated for 96 h at 37°C in 5% CO_2. Spheres were imaged using a Nikon Eclipse inverted fluorescence microscope, and their diameters were measured using ImageJ software. Fold changes in sphere formation were calculated by comparing treated groups with untreated controls.

4.2.12. Matrigel invasion assay

The invasiveness of TNBC cells following drug treatments was assessed using an Matrigel invasion assay. MDA-MB-231 cells were seeded in 6-well plates at a density of 3×10^5 cells and treated with the IC_{50} concentrations of individual drugs or drug combinations for 48 h. After 48 h of drug treatment, cells were isolated, and 2×10^4 cells were seeded into the upper chamber of 24-well Transwell inserts coated with Matrigel, using serum-free media. The lower chamber contained media with 10% FBS to act as a chemoattractant. After 18 h of incubation, non-invasive cells on the upper surface of the membrane were removed, and the invaded cells on the lower surface were fixed with 4% formaldehyde for 15 min. Cells were stained with 1 µM DAPI, and images were captured using a confocal microscope. The fluorescence intensity was measured using ImageJ software to quantify cell invasion, and fold changes in invasion were calculated by comparing the treated and untreated control groups.

4.2.13. Statistical analysis

All experiments were performed in triplicate, and the results were expressed as mean ± SEM. Statistical significance between groups was determined using one-way ANOVA followed by post hoc tests for multiple comparisons. A p-value of less than 0.05 was considered statistically significant. Data analysis and graph generation were performed using GraphPad Prism version 6.0.

4.3. Results

4.3.1. Comparative analysis of drug metabolizing enzymes

Enhancing the efficacy of breast cancer treatments while minimizing toxicity is a critical focus in oncological research. This study aimed to achieve therapeutic efficacy by identifying drug combinations that do not share metabolizing enzymes with the repurposed drug Pimozide there by reducing metabolic load and potential toxicity. Study began by comparing the metabolizing enzymes of 31 drugs commonly used in breast cancer treatment. **Figure 4.1A** details the corresponding metabolizing enzymes of the selected drugs. From this comparison, it was found that 8 drugs did not overlap with metabolic enzymes of Pimozide. The 8 selected drugs span various classes of chemotherapeutic agents. These include Vorinostat, Epirubicin, Mitomycin C, Chlorambucil, Cisplatin, Capecitabine, Gemcitabine, and Cladribine. Vorinostat is a targeted anti-cancer drug. Epirubicin and Mitomycin C are anti-tumor antibiotics. Chlorambucil and Cisplatin are alkylating agents. Capecitabine, Gemcitabine, and Cladribine are anti- metabolites. In addition, a drug-drug interaction analysis was conducted using the STITCH database, which helps identify potential interactions between drugs. **Figure 4.1B** portrays that there were no significant interactions among Vorinostat, Epirubicin, Chlorambucil, and Gemcitabine. These findings suggest that these drugs can be combined with Pimozide without increasing the risk of adverse effects due to interactions. Further *in-vitro* experiments were carried out using the selected drugs in combination with pimozide to identify potential drug cocktail for breast cancer therapy.

4.3.2. Identification of potent synergistic anti-cancer drugs for Pimozide combination

Determining the cytotoxic potential of individual drugs is a crucial step in optimizing combination therapy for breast cancer, as it helps to select drugs that can enhance therapeutic efficacy while minimizing toxicity. Cytotoxicity assay was performed to establish the IC_{50} values of Chlorambucil, Epirubicin, Gemcitabine, Pimozide, and Vorinostat (SAHA) in both MCF-7 and MDA-MB-231 cell lines. In MCF-7 cells, the IC_{50} values were 27.9 µM for Chlorambucil, 0.4 µM for Epirubicin, 0.13 µM for Gemcitabine, 16.45 µM for Pimozide, and 5.86 µM for Vorinostat. Similarly, in MDA-MB-231 cells, the IC_{50} values were >200 µM for Chlorambucil, 2.20 µM for Epirubicin, 15 µM for Gemcitabine, 17.5 µM for Pimozide, and 8 µM for Vorinostat. The results indicated that, except for Chlorambucil, all other drugs exhibited lower IC_{50} values than Pimozide in both cell lines. Since one of the objectives is to reduce drug concentrations in therapy to

minimize toxicity, Epirubicin, Gemcitabine, and Vorinostat were selected for the combination studies with Pimozide. Drugs with higher IC_{50} values than Pimozide were excluded to avoid a cumulative increase in drug dosage and toxicity. **Figure 4.2** depicts the dose dependent decrease in the cell viability with respect to the selected drugs in both MCF-7 and MDA-MB-231 cell lines. Further, the synergistic potential of Pimozide in combination with Epirubicin, Gemcitabine, and Vorinostat was evaluated through a series of subsequent assays.

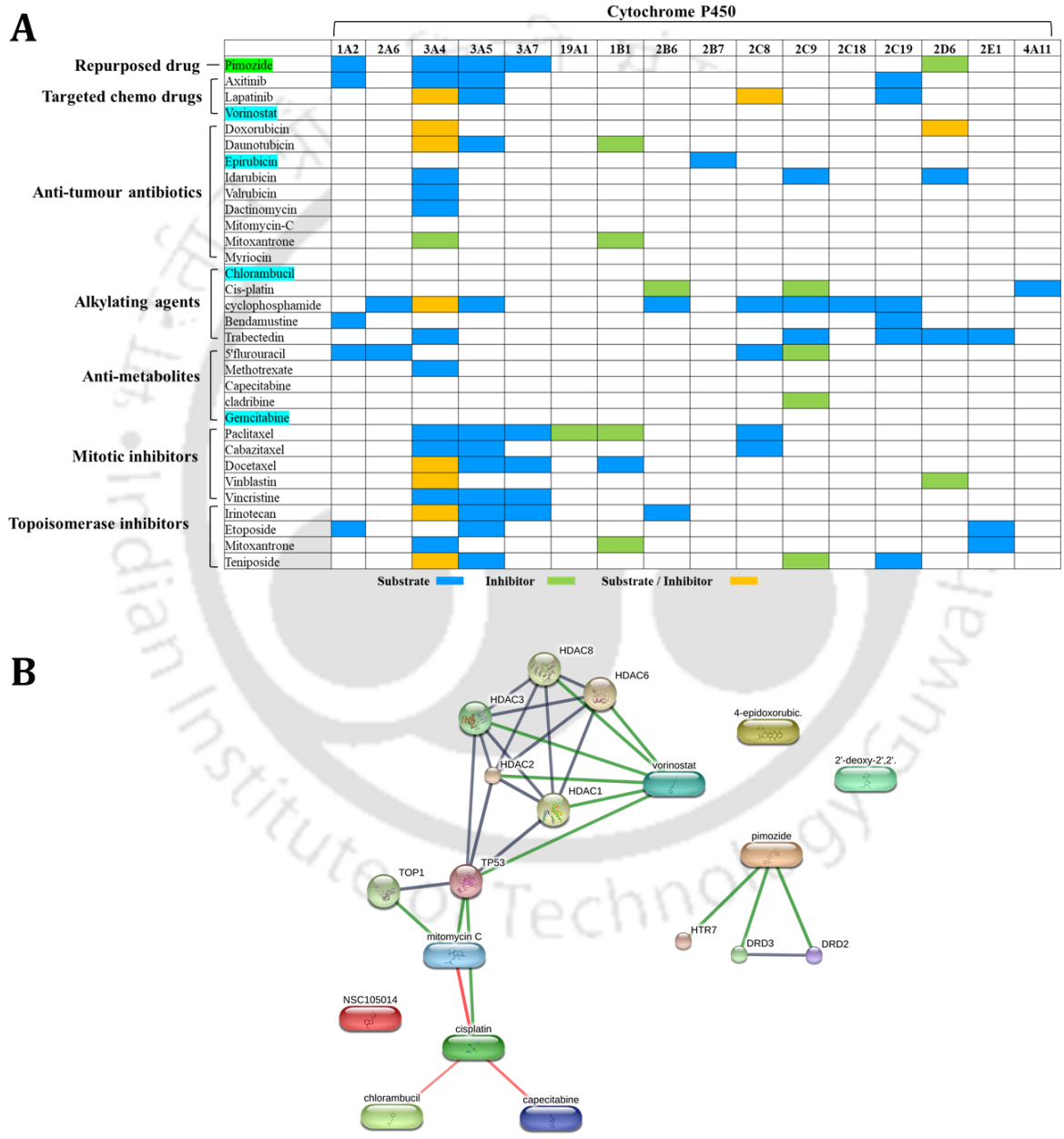

Figure 4.1: ***A)*** *Chemotherapeutic drugs used in breast cancer and their corresponding metabolizing enzymes.* ***B)*** *Drug-Drug and Drug-Protein interaction profile from STICH database*

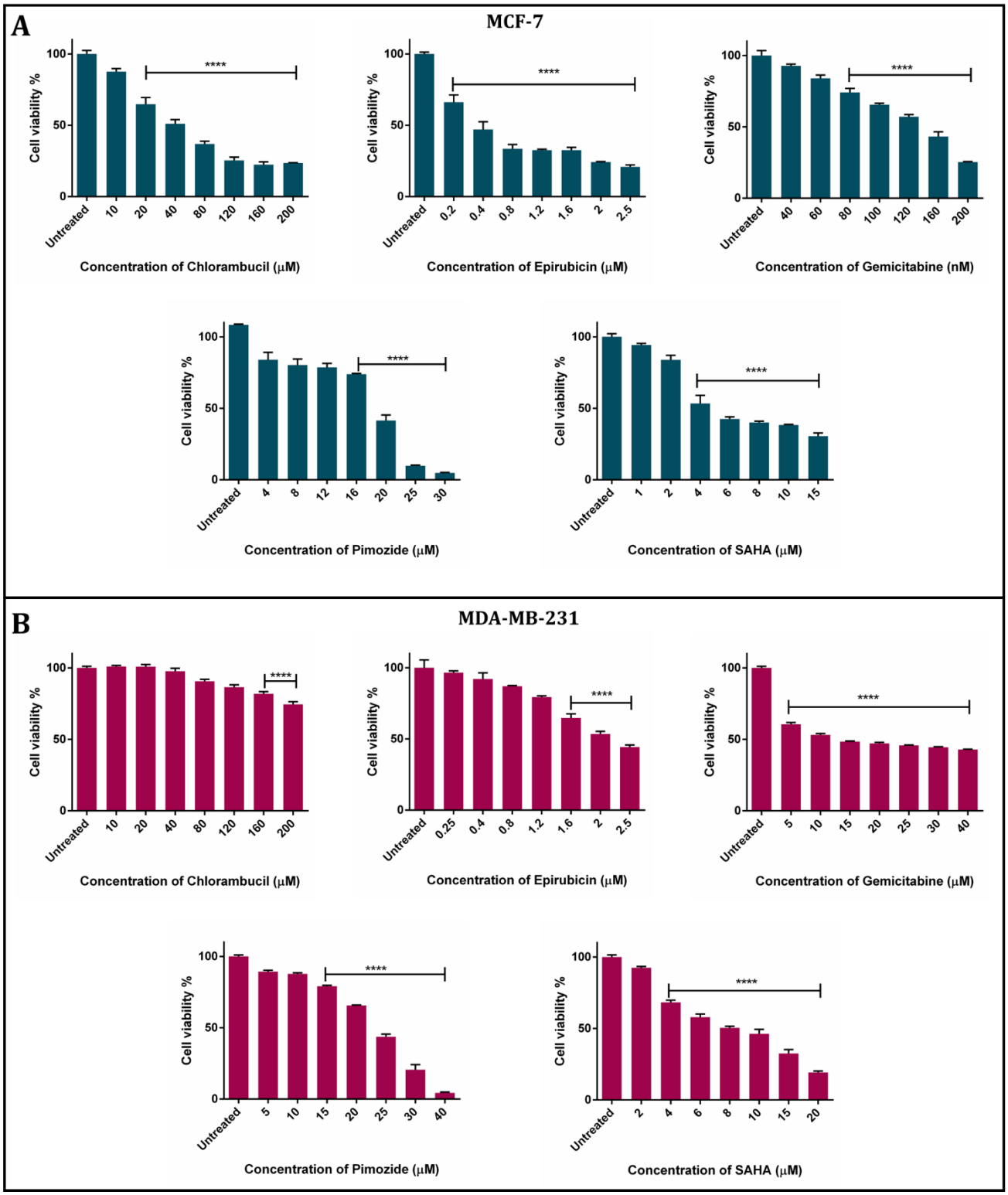

Figure 4.2: *Dose dependent decrease in the cell viability after 48 h treatment with respective drugs* ***A)*** *MCF-7* ***B)*** *MDA-MB-231.*

4.3.3. Synergistic evaluation of Pimozide in combination with chemotherapeutic drugs

Further assessment of the synergistic potential among Pimozide and the selected chemotherapeutic drugs was carried out with various drug combinations. This study included six different drug combinations in both MCF-7 and MDA-MB-231 cell lines: Epirubicin (E) + Pimozide (P), SAHA (S) + Pimozide, Gemcitabine (G) + Pimozide, Epirubicin + SAHA, Gemcitabine + SAHA, and Gemcitabine + Epirubicin. For each combination, the concentration of one drug was kept constant (half of its IC_{50}), while the concentration of the other drug was varied to assess dose-dependent changes in cell viability. Notably, the drug with the lower IC_{50} was kept constant to minimize cumulative drug toxicity. The IC_{50} values for the combination treatments in MCF-7 cells were as follows: 1.65 µM for Epirubicin + Pimozide, 2.13 µM for SAHA + Pimozide, 18.11 µM for Gemcitabine + Pimozide, 4.07 µM for Epirubicin + SAHA, 5.38 µM for Gemcitabine + SAHA, and 0.37 µM for Gemcitabine + Epirubicin. In MDA-MB-231 cells, the IC_{50} values were 12.56 µM for Epirubicin + Pimozide, 9.13 µM for SAHA + Pimozide, 19.59 µM for Gemcitabine + Pimozide, 0.94 µM for SAHA + Gemcitabine, 3.80 µM for Epirubicin + SAHA, and >20 µM for Gemcitabine + Epirubicin (**Figure 4.3 A-B**).

subsequently, a combination index (CI) of the treatments were analysed using Compusyn software to evaluate the nature of interactions between the drugs. In MCF-7 cells, the combinations of Gemcitabine + Pimozide, Gemcitabine + SAHA, and Gemcitabine + Epirubicin had CI values greater than 1, indicating antagonism (**Figure 4.3D**). In MDA-MB-231 cells, Gemcitabine + Pimozide and Gemcitabine + Epirubicin also showed CI values greater than 1, further suggesting antagonism (**Figure 4.3D**). However, all other combinations in both cell lines exhibited CI values of less than 1, indicating synergism, particularly between Epirubicin, SAHA, and Pimozide. Given these results, the combination of Epirubicin, SAHA, and Pimozide (ESP) was proceeded for further studies. Since both Epirubicin and SAHA had lower IC_{50} values compared to Pimozide, the one-fourth of their concentrations were kept at constant and varied the Pimozide concentration. The IC_{50} values of Pimozide in the ESP combination were significantly reduced to 0.57 µM for MCF-7 cells and 3.35 µM for MDA-MB-231 cells (**Figure 4.3C**). The CI value of the ESP combination was also less than 1 in both cell lines, confirming a strong synergistic effect (**Figure 4.3D**). Notably, the IC_{50} of Pimozide in the ESP combination was significantly reduced compared to Pimozide alone, with a fold change reduction of 28-fold in MCF-7 cells and 5.2-fold in MDA-

MB-231 cells (**Figure 4.3E**). These promising results set the foundation for further assays, focusing on the mechanistic insights of the observed synergy in Pimozide combinations.

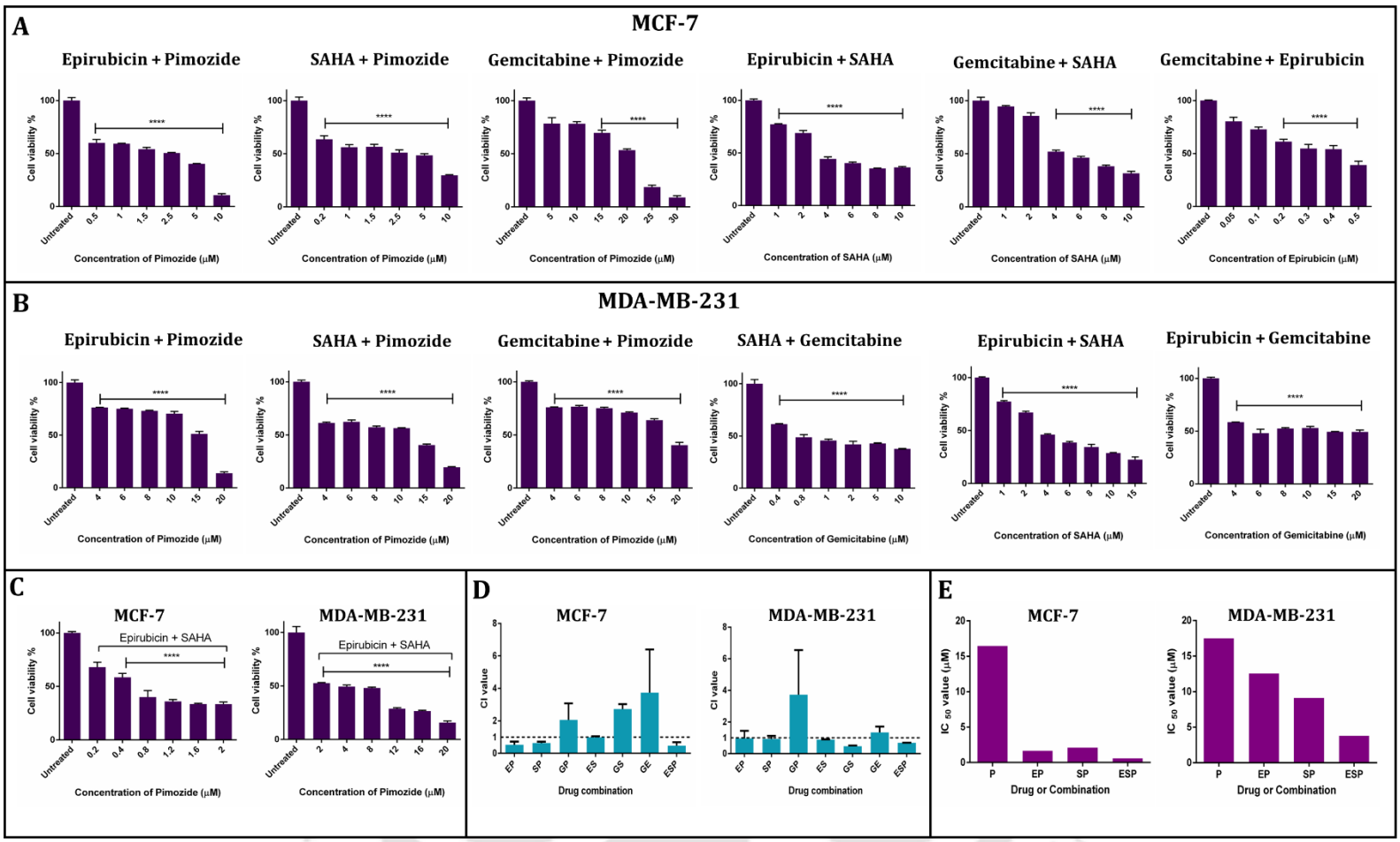

Figure 4.3: *Dose dependent decrease in the cell viability after 48 h treatment with respective drugs* combinations ***A)*** *MCF-7,* ***B)*** *MDA-MB-231,* ***C)*** *ESP combination in MCF-7 and MDA-MB-231* ***D)*** *Combination Index value of different combinations in MCF-7 and MDA-MB-231* ***E)*** *comparative analysis of* IC_{50} *value of Pimozide in different combinations.*

4.3.4. Investigating the cellular mechanisms of cytotoxicity in the ESP combination

Following the identification of the synergistic combination of Epirubicin (E), SAHA (S), and Pimozide (P), the underlying cellular mechanism behind this cytotoxicity was explored further. Most chemotherapeutic drugs are known to induce cellular stress, leading to cell death [13, 14]. For instance, Epirubicin is reported to cause DNA damage, while SAHA inhibits histone deacetylases (HDACs), leading to altered gene expression and cell cycle arrest [15, 16]. Pimozide,

on the other hand, is known to induce metabolic stress, subsequently triggering the intrinsic apoptotic pathway via targeting IR, ITGB1 and CD36 [8, 17]. To validate whether the ESP combination could activate the intrinsic pathway of apoptosis, a series of assays were performed: intracellular ROS measurement using DCFDA, apoptosis detection using Annexin V-PI staining, and Western blot analysis to examine cleaved PARP expression. The results demonstrated a significant increase in intracellular ROS generation following 6 h of ESP treatment. Similar increases in ROS were also observed with Pimozide, EP, and SP combinations, suggesting that all three drugs possess the ability to elevate intracellular ROS levels, contributing to oxidative stress in the cells **(Figure 4.4A)**.

Apoptotic populations were analyzed after 48 h of treatment with the respective IC_{50} concentrations. In MCF-7 cells, the EP and ESP combinations induced more than 30% apoptosis, surpassing the apoptotic effect of Pimozide or EP treatments alone **(Figure 4.4B)**. In MDA-MB-231 cells, both Pimozide and ESP treatments resulted in over 30% apoptosis, while other combinations also showed a significant increase compared to untreated controls **(Figure 4.4B)**. This demonstrates the effectiveness of the ESP combination in promoting apoptosis, particularly via the intrinsic apoptotic pathway. To further confirm this, the expression of cleaved PARP, a hallmark of apoptosis, was evaluated after 24 h of treatment **(Figure 4.4C)**. In MCF-7 cells, all three combinations (EP, SP, and ESP) led to approximately a 10-fold increase in cleaved PARP expression. However, in MDA-MB-231 cells, only the ESP combination induced a similar increase in cleaved PARP as MCF-7 and EP combination exerted approximately 5-fold increase in the expression of cleaved PARP. Interestingly, a reduction in β-tubulin as well as β-actin expression was also observed, indicating potential structural damage caused by the combination treatment. The investigation of lysosomal degradation of proteins under stress conditions was carried out using the lysotracker assay. After 24 h of treatment, increased lysosomal activity was observed in combination treatments, including EP, SP, and ESP (**Figure 4.4D**). This suggests that lysosomal degradation of proteins may also contribute to the cytotoxic effects of these combinations, particularly the reduction in actin and tubulin expression. Overall, these findings suggest that the ESP combination induces intrinsic apoptosis and enhances lysosomal activity, contributing to its cytotoxic effects in both luminal and TNBC breast cancer cells.

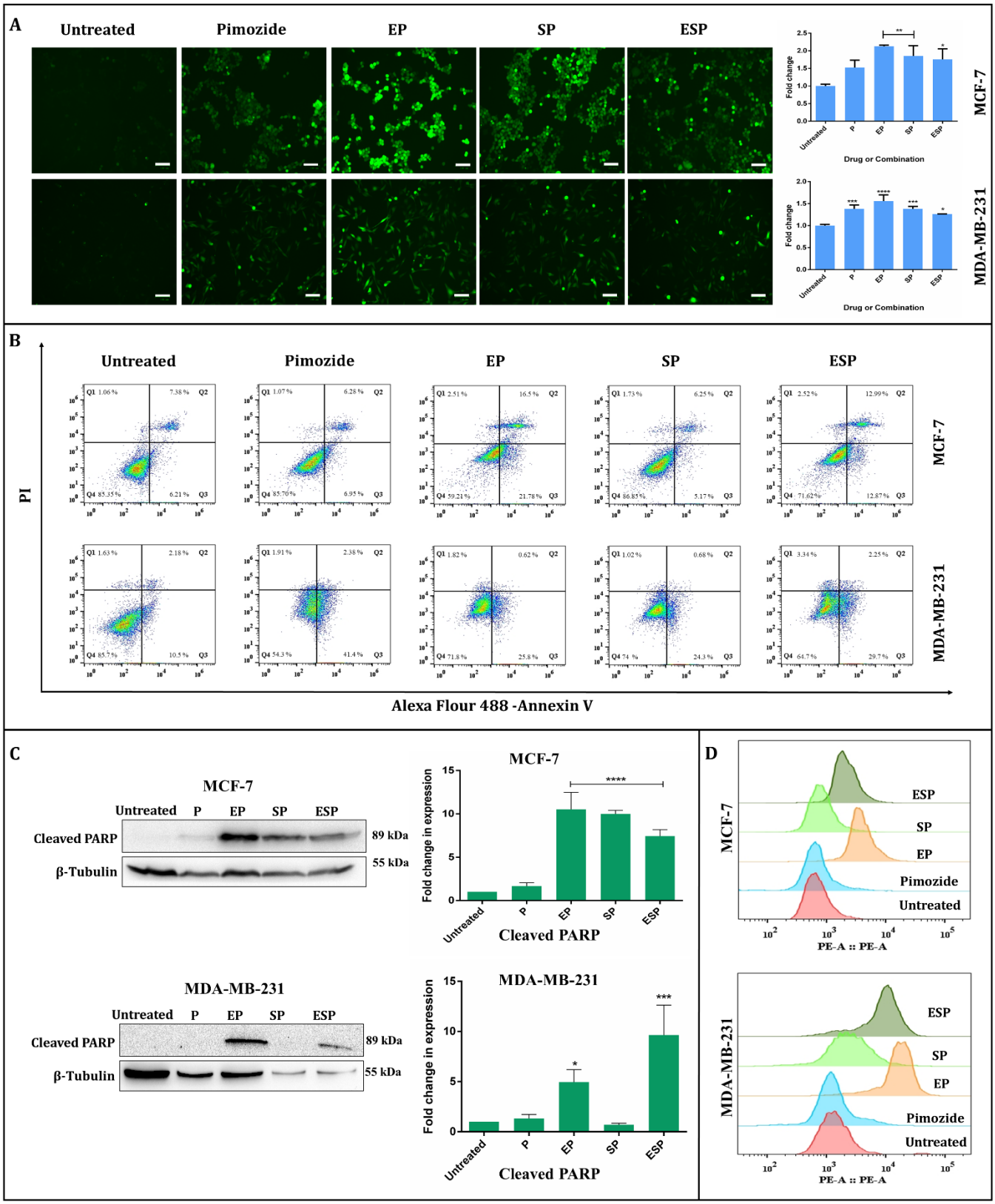

Figure 4.4: A) *Intra cellular ROS generation in MCF-7 and MDA-MB-231 cell lines after 6 h treatment with respective drug combinations (Scale 100 µm).* ***B)*** *percentage of apoptotic population in MCF-7 and MDA-MB-231 cell lines after 48 h treatment with respective drug combinations.* ***C)*** *Change in the expression of cleaved PARP in MCF-7 and MDA-MB-231 cell lines after 24 h treatment with respective drug combinations.* ***D)*** *Flowcytometric analysis of lysosomal activity using Lysotracker deep red dye after 24 h of drug treatment.*

4.3.5. ESP combination significantly increases cell death in both monolayer and 3D tumor spheroids of breast cancer cells

To assess the effect of the ESP combination on both 2D monolayer and 3D tumor spheroids, live/dead analysis was carried out in MCF-7 and MDA-MB-231 cell lines. Monolayer cultures were treated with Pimozide, EP (Epirubicin + Pimozide), SP (SAHA + Pimozide), and ESP (Epirubicin + SAHA + Pimozide) combinations for 48 h (**Figure 4.5 A-B**). In both cell lines, a significant increase in red fluorescence was observed, indicating dead cells, across all treated groups compared to untreated controls. Similarly, in the tumor spheroids, a pronounced increase in red fluorescence was also seen in treated groups after 72 h of the treatment, confirming the cytotoxic efficacy of the ESP combination in 3D models (**Figure 4.5 C-D**). These results highlight the potent cytotoxic effect of the ESP combination in both monolayer and 3D tumor spheroids, demonstrating its potential to target cells in different tumor architectures.

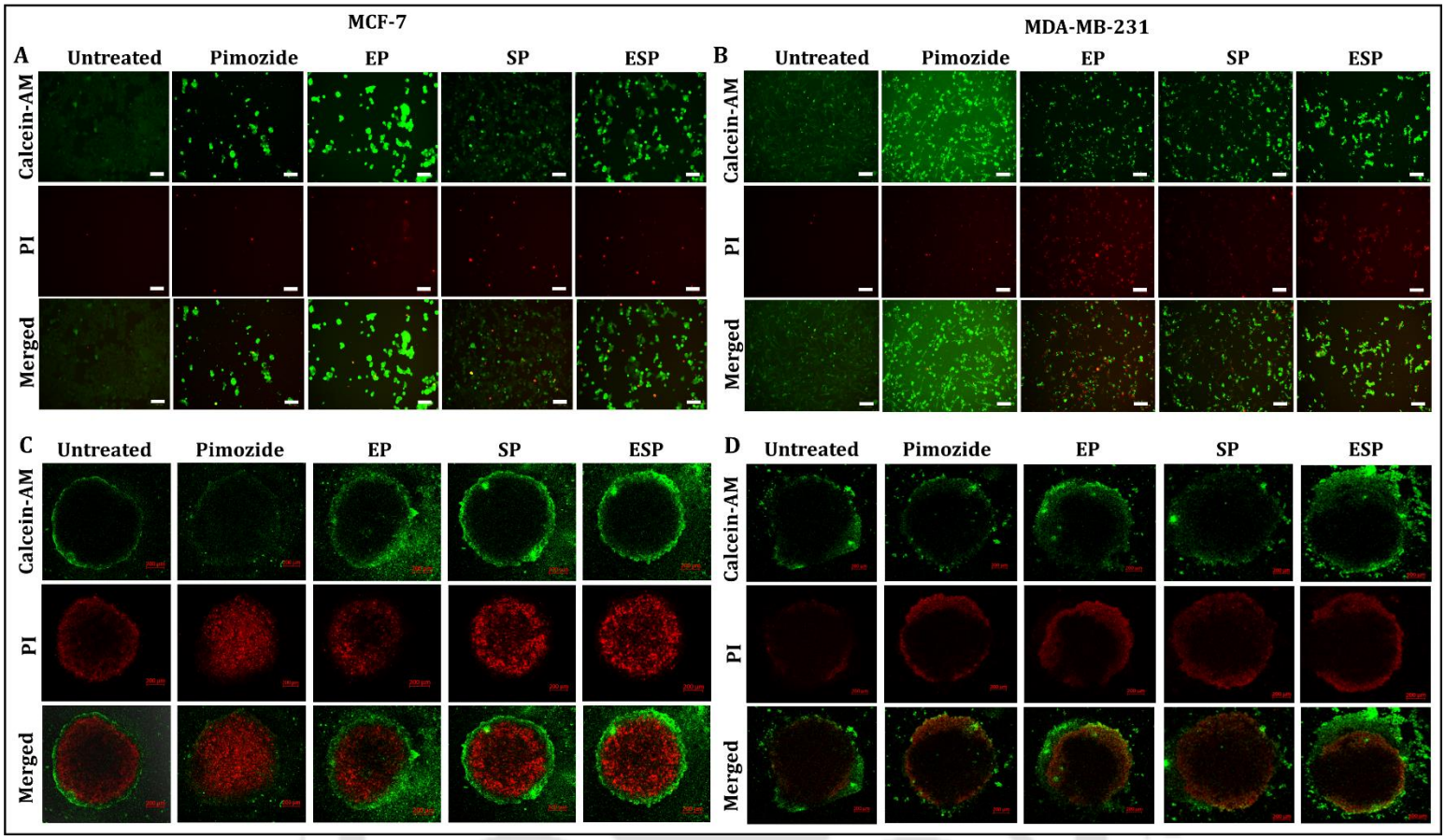

Figure 4.5: *Live/dead cells imaging of monolayer culture after 48 h treatment with drug combinations **A)** MCF-7, **B)** MDA-MB-231 (Scale 100 µm). Live/dead cells staining of 3D tumor spheroids after 72 h treatment with drug combinations **C)** MCF-7, **D)** MDA-MB-231 (Scale 200 µm).*

4.3.6. Differential modulation of oxidative stress and apoptotic signaling by ESP combination in luminal and TNBC cells

To further investigate the cellular effects of the ESP combination (Epirubicin + SAHA + Pimozide), key signaling molecules involved in stress response, apoptosis, and cell cycle regulation were analyzed in both luminal (MCF-7) and TNBC (MDA-MB-231) cell lines. The proteins assessed included NRF2 (nuclear factor erythroid 2-related factor 2), SOD2 (superoxide dismutase 2), P53, AKT, and P21, which play significant roles in oxidative stress response, apoptosis regulation, and cell cycle progression [18, 19]. In MCF-7 cells, the expression of NRF2 and SOD2 remained largely unchanged across most treatments (**Figure 4.6A**). However, the SP combination (SAHA + Pimozide) led to a notable 5.4-fold increase in SOD2 expression, indicating

a specific oxidative stress response induced by this combination (**Figure 4.6A**). Regarding apoptosis-related proteins, there was a significant reduction in P53 (7.14-fold) and AKT (3.44-fold) expression after treating with ESP combination (**Figure 4.6A**). The reduction in P53 suggests a dampened DNA damage response, while the decrease in AKT points toward reduced cell survival signaling. Notably, P21 expression was markedly increased by 7.5-fold in SP and 1.5-fold in ESP combination, indicating enhanced cell cycle arrest following treatment (**Figure 4.6A**). In MDA-MB-231 cells, the ESP combination resulted in an increase in SOD2 expression by 1.9-fold, without any change in NRF2 levels (**Figure 4.6B**). Unlike MCF-7, MDA-MB-231 cells exhibited a 2-fold increase in P53 expression and a substantial 9.3-fold increase in P21 expression, reinforcing the activation of cell cycle arrest pathways in ESP combination (**Figure 4.6B**). Additionally, AKT expression was significantly reduced by 2.4-fold in ESP combination, indicating inhibition of pro-survival signaling pathways (**Figure 4.6B**).

Further, the impact of the ESP combination on different cellular processes was elucidated using a preliminary proteomics analysis in MCF-7 cells after 48 h of treatment. This analysis identified 357 differentially expressed proteins (DEPs), which provided insights into the molecular mechanisms underlying the observed effects. These DEPs were categorized into three major cellular processes: metabolism, cellular stress, and apoptosis. The interaction networks between these DEPs are illustrated in **Figure 4.6C**, which portrays their involvement across these critical cellular processes. 101 proteins were found to be involved in metabolic pathways, highlighting the effect of the ESP combination on disrupting cancer cell metabolism. Followed by 92 proteins were involved in stress responses, indicating an activation of stress pathways that could contribute to the cytotoxicity observed. Total of 15 proteins were directly involved in apoptotic signaling, reinforcing the role of the ESP combination in inducing apoptosis through intrinsic pathways. A detailed Venn diagram in the figure also depicts the overlap and unique contributions of proteins involved in metabolism, stress response, and apoptosis, offering a comprehensive view of how the ESP combination disrupts cancer cell function at the proteomic level (**Figure 4.6D)**.

These findings suggest that the ESP combination activates distinct signaling mechanisms in luminal and TNBC breast cancer cells, particularly through the modulation of oxidative stress responses, the p53-P21 axis, and the inhibition of AKT signaling. This differential regulation may contribute to the enhanced cytotoxic effects of the ESP combination across both cell lines. The

proteomics data further support the notion that the combination therapy impacts multiple cellular processes, providing a multifaceted attack on cancer cell survival.

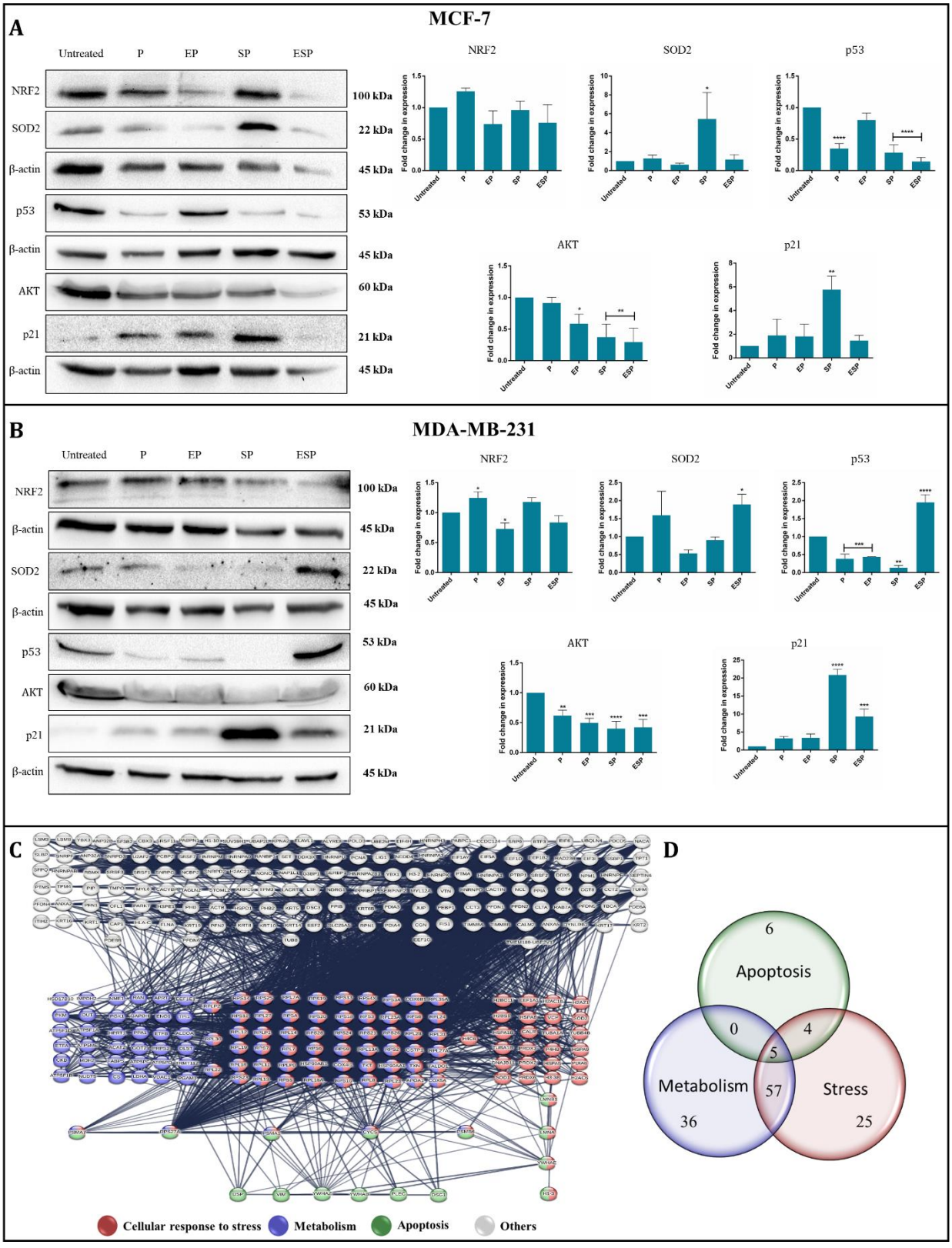

Figure 4.6: *Protein expression analysis of NRF2, SOD2, p53, AKT and p21 after 24 h treatment with drug combinations with* **A)** *MCF-7,* ***B)*** *MDA-MB-231cells.* ***C)*** *Functional interaction network of differentially expressed proteins (DEPs) in MCF-7 after treatment with ESP combination for 48 h.* ***D)*** *Ven diagram depicting the proteins involved in metabolism, stress response, and apoptosis.*

4.3.7. ESP combination effectively reduces cancer stemness and invasiveness in breast cancer cells

The effect of the ESP combination on cancer stemness and invasiveness was investigated through sphere formation and Matrigel invasion assays [20]. After 48 h of drug treatment, both MCF-7 and MDA-MB-231 cells lost the ability to form tumor spheres, with a significant reduction in sphere size observed, especially in the ESP combination group (**Figure 4.7 A-B**). This suggests a potent inhibition of cancer stemness by the ESP combination. In addition, the invasive properties of MCF-7 and MDA-MB-231 cells were evaluated using a Matrigel Transwell assay after 48 hours of treatment. The ESP combination consistently reduced invasiveness by approximately 2-fold in both cell lines, demonstrating its robust anti-invasive potential. In contrast, the effects of other combinations, including EP, varied depending on the cell type, suggesting a differential response to treatment. These findings highlight the superior ability of the ESP combination to effectively inhibit cancer cell invasion across different breast cancer subtypes (**Figure 4.7 C-D**).

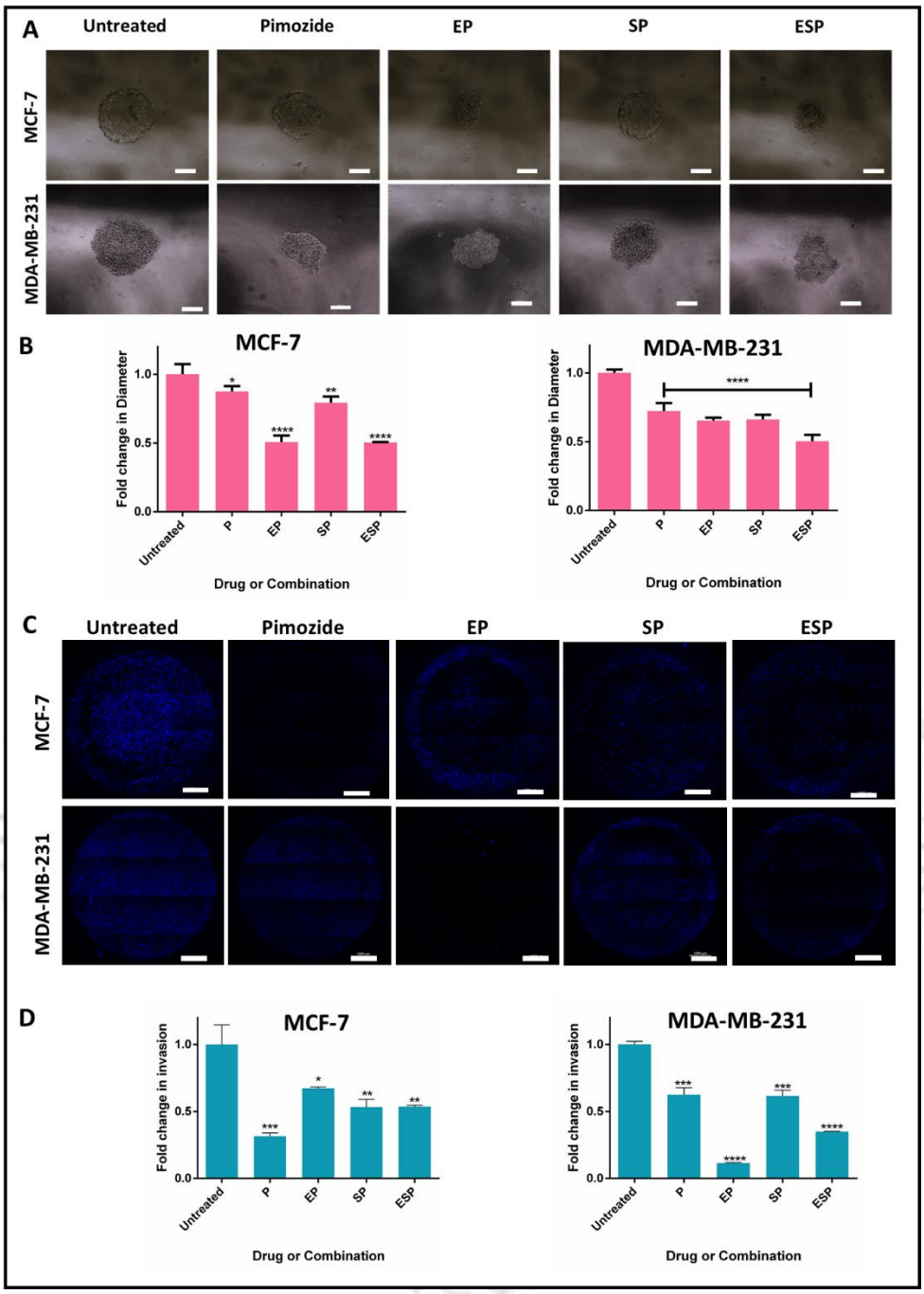

Figure 4.7: ***A)*** *Sphere forming ability of MCF-7 and MDA-MB-231 cells after treatment with respective drug combinations (Scale 100 µm).* ***B)*** *Fold change in the sphere size after drug treatment in MCF-7 and MDA-MB-231 cell lines.* ***C)*** *Invasive property of MCF-7 and MDA-MB-231 cells after treatment with respective drug combinations (Scale 1000 µm).* ***D)*** *fold change in the invasive property of MCF-7 and MDA-MB-231 cells after drug treatment.*

4.3.8. ESP combination inhibits fatty acid uptake and modulates lipid droplet accumulation in breast cancer cells

Fatty acid metabolism is vital for cancer cell survival, supplying both energy and structural components essential for tumor growth and proliferation. Aberrant fatty acid uptake and lipid droplet accumulation have been linked to enhanced cancer cell survival, metastasis, and resistance to therapy [21]. Targeting these metabolic processes can, therefore, impair cancer progression, making them an attractive therapeutic strategy. To investigate the impact of the ESP combination on fatty acid metabolism, both exogenous fatty acid uptake and endogenous lipid droplet accumulation were assessed in MCF-7 and MDA-MB-231 cells. After 6 h of drug treatment, cells were stained with fluorescently labeled fatty acids. A significant reduction in fatty acid uptake was observed in both cell lines, indicating that the ESP combination effectively disrupts fatty acid metabolism. Interestingly, while the EP combination showed no effect on fatty acid uptake in MCF-7 cells, all other combinations, including ESP, markedly inhibited fatty acid uptake (**Figure 4.8 A-B**).

In parallel, lipid droplet accumulation was also assessed using Nile red staining. After 6 h of treatment, a significant reduction in lipid droplet accumulation was observed in both cell lines, further supporting the ability of the ESP combination to interfere with lipid metabolism (**Figure 4.8 C-D**). Notably, the EP combination resulted in increased lipid droplet accumulation in MDA-MB-231 cells. This could be due to Epirubicin-induced metabolic reprogramming, which may drive lipid storage as a protective mechanism against oxidative stress or drug-induced cellular stress, enhancing cell survival in these aggressive cancer cells [22]. Overall, the ESP combination showed a robust inhibitory effect on fatty acid metabolism by reducing both fatty acid uptake and lipid droplet accumulation. This disruption of metabolic pathways could be a critical factor in its cytotoxic efficacy, particularly in breast cancer cells that rely heavily on fatty acid metabolism for growth and survival.

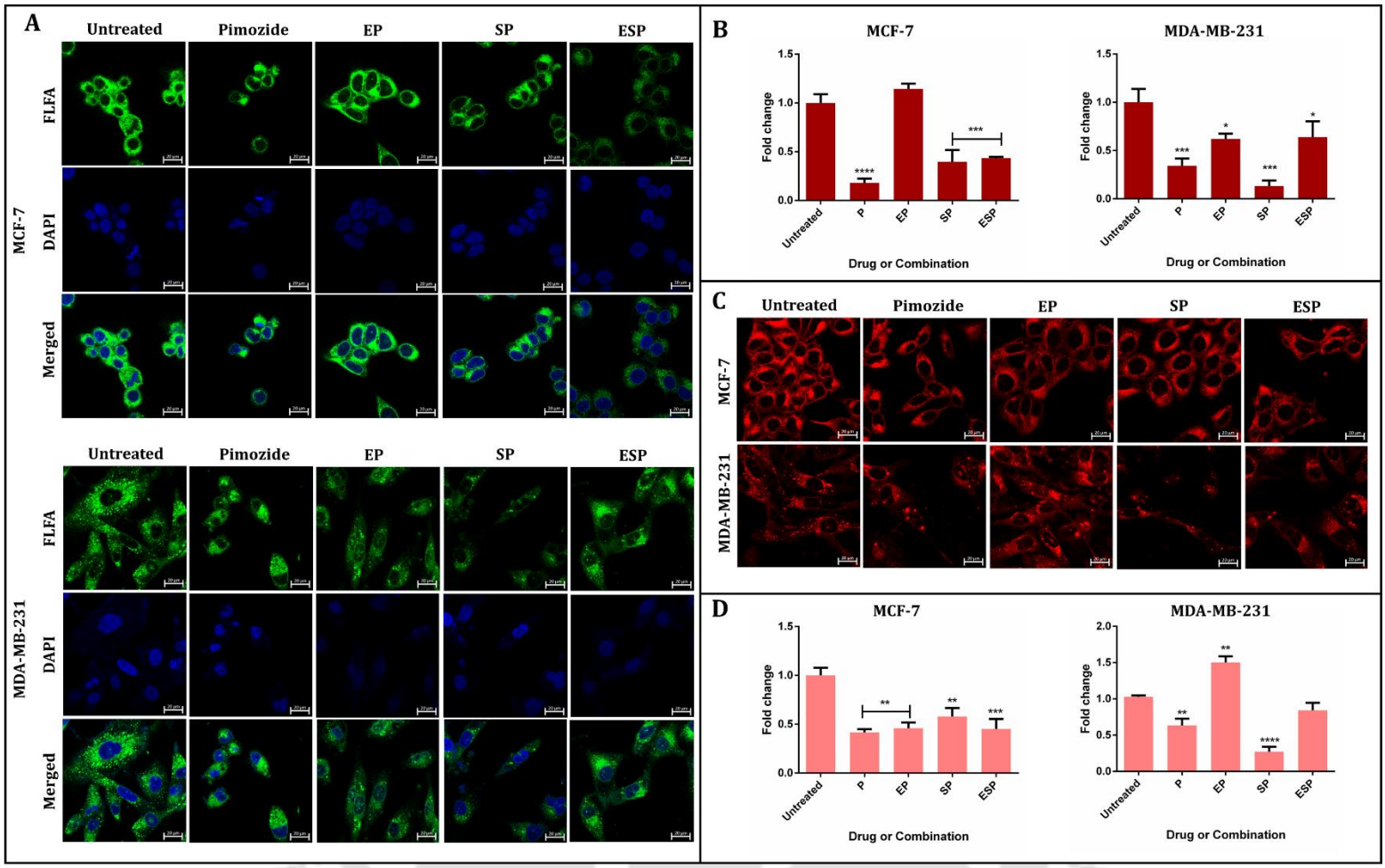

Figure 4.8: ***A)*** *Fluorescent labelled fatty acid (FLFA) uptake by MCF-7 and MDA-MB-231 cells after treatment with respective drug combinations (Scale 20 µm).* ***B)*** *Graphical representation of fold change in the fatty acid uptake.* ***C)*** *Lipid droplet accumulation in MCF-7 and MDA-MB-231 cells after treatment with respective drug combinations (Scale 20 µm).* ***D)*** *Graphical representation of fold change in the lipid droplet accumulation.*

4.4. Discussions

The current study aimed to identify and evaluate the synergistic effects of Pimozide in combination with standard chemotherapeutic agents and the underlying mechanisms driving their cytotoxicity in breast cancer cells. Specifically, it focused on the combinations of Pimozide with Epirubicin, Gemcitabine, and Vorinostat (SAHA), and subsequently elucidated their effects on cellular mechanisms, oxidative stress, apoptosis, cancer stemness, invasiveness, and fatty acid metabolism in both luminal (MCF-7) and triple-negative breast cancer (TNBC) (MDA-MB-231) cell lines.

The combination treatment of Pimozide, Epirubicin, and Vorinostat (SAHA) demonstrated significant potential in enhancing the therapeutic efficacy against breast cancer cells, as observed through various assays and mechanistic evaluations. Initial IC_{50} studies in both luminal MCF-7 and TNBC MDA-MB-231 cells revealed that except for Chlorambucil, all other tested chemotherapeutic drugs showed lower IC_{50} values than Pimozide, allowing for the selection of Epirubicin, Gemcitabine, and SAHA for combination studies with Pimozide. Among these, the ESP combination emerged as the most effective, significantly reducing the IC_{50} of Pimozide in both cell lines, particularly in MCF-7 cells. This substantial reduction of IC_{50} of Pimozide in the ESP combination, especially in MCF-7 cells compared to MDA-MB-231, suggests that the luminal subtype may be more sensitive to this combination treatment. The cytotoxicity assay with different drug combinations demonstrated varying degrees of synergism, particularly with the ESP combination. Importantly, the combination index (CI) values confirmed the synergistic interaction of ESP in both cell lines, with marked improvements in reducing the cumulative drug concentrations required for cytotoxic effects. The ability of ESP to significantly lower IC_{50} of Pimozide highlights its potential for reducing drug toxicity while enhancing efficacy, a crucial factor in optimizing cancer therapies. In parallel, the live-dead assays conducted in both monolayer and 3D spheroid models confirmed that the ESP combination induces a robust cytotoxic response in both cancer models. The enhanced red fluorescence in treated cells, indicating increased cell death, reinforces the efficacy of the ESP combination in both 2D monolayer and 3D spheroids, further validating its potential to target cancer cells in more physiologically relevant models like tumor spheroids.

Mechanistic insights into the cytotoxic effects of the ESP combination revealed that the treatment induced significant intracellular ROS generation, which is a key driver of stress-mediated cell death [23]. The observation of elevated ROS levels across all combinations, including Pimozide alone, reinforces the role of oxidative stress in the cytotoxicity of these drugs. Notably, in MCF-7 cells, both EP and ESP combinations induced substantial apoptotic populations, further supported by the elevated expression of cleaved PARP. In MDA-MB-231, the ESP combination was particularly effective in inducing apoptosis, with increased cleaved PARP levels and reduced β-tubulin expression, suggesting a structural degradation of the cytoskeleton, potentially driven by lysosomal degradation processes [24], as confirmed by the Lysotracker assay. This increase in

lysosomal activity further supports the hypothesis that the combination treatment accelerates autophagy and degradation processes, contributing to cellular apoptosis.

Notably, western blot analysis also revealed significant alterations in key signaling molecules that regulate cell survival and apoptosis. In MCF-7 cells, the ESP combination led to a pronounced downregulation of p53 and AKT expression, while upregulating p21, a known cell cycle regulator. This pattern indicates that the ESP combination may induce cell cycle arrest and inhibit survival signaling pathways, thereby enhancing the apoptotic response. In contrast, in TNBC cells, the ESP combination significantly increased p53 and p21 expression while also reducing AKT levels. The differential modulation of p53 between the two cell lines may reflect the divergent reliance of these cancer types on p53-related pathways for cell death regulation. Further, the proteomic analysis provided additional insights into the cellular mechanisms affected by the ESP combination. The identification of 357 differentially expressed proteins (DEPs) involved in metabolism, cellular stress, and apoptosis underscores the broad impact of this combination on fundamental cancer cell processes. Notably, the large number of DEPs associated with cellular metabolism and stress suggests that the ESP combination disrupts these processes, leading to cancer cell death. The intricate network of these proteins, particularly those involved in apoptosis, as portrayed in the interaction analysis, highlights the synergistic nature of the combination.

Cancer stemness and invasiveness, critical properties of aggressive cancers, were also effectively targeted by the ESP combination. Sphere formation assays revealed a marked reduction in tumor sphere size, particularly in the ESP-treated groups, in both luminal and TNBC cells. The reduced ability of MDA-MB-231 cells to invade after ESP treatment further underscores its potential in targeting metastatic traits, a vital factor in combating TNBC, which is notoriously invasive. Finally, the modulation of fatty acid metabolism, a critical survival pathway for cancer cells [21, 22], was evident in ESP-treated cells. Both exogenous fatty acid uptake and endogenous lipid droplet accumulation were significantly reduced following ESP treatment in both cell lines. This disruption of lipid metabolism likely contributes to the overall cytotoxic effect, as cancer cells rely on these metabolic processes for energy and growth. Interestingly, the increase in lipid droplet accumulation with the EP combination in MDA-MB-231 cells suggest an adaptive survival mechanism or altered metabolic regulation, warranting further investigation.

In summary, the ESP combination demonstrates enhanced efficacy in luminal cells, as reflected by the significantly lower IC_{50} of Pimozide in MCF-7 compared to MDA-MB-231, positions this combination as a promising therapeutic strategy, particularly for luminal breast cancer. The enhanced efficacy of the ESP combination can be attributed to the interconnected modulation of several key signaling pathways. The downregulation of AKT and p53 pathways, combined with the upregulation of p21, leads to the inhibition of cell survival and promotion of apoptosis. Additionally, the increase in ROS generation intensifies oxidative stress, further driving cell death through mitochondrial damage. The ESP combination effectively modulates these pathways, leading to a cumulative effect that disrupts cancer cell proliferation, survival, and metabolic reprogramming, ultimately enhancing its therapeutic efficacy against breast cancer. These findings provide a strong rationale for further exploration of the ESP combination in preclinical and clinical settings to optimize breast cancer treatment.

4.5. Conclusion

Breast cancer treatment continues to pose significant challenges due to tumor heterogeneity and resistance to conventional therapies. This study focused on identifying a synergistic combination of drugs to enhance therapeutic efficacy and reduce side effects associated with high-dose chemotherapy. A potent synergistic combination of Epirubicin, SAHA (Vorinostat), and Pimozide (ESP) was developed that exhibits enhanced cytotoxicity in both luminal and TNBC cells. This combination effectively reduced the IC_{50} of Pimozide, particularly in MCF-7 cells, highlighting its potential for lowering drug doses while maintaining efficacy. Mechanistically, the ESP combination induces oxidative stress, disrupts fatty acid metabolism, and activates intrinsic apoptotic pathways, as confirmed by increased ROS generation, altered lipid metabolism, and upregulation of cleaved PARP expression. The combination also significantly impaired cancer stemness and invasive potential, which are key factors contributing to tumor aggressiveness and recurrence. These results indicate that the ESP combination modulates several critical signaling pathways, including p53, AKT, and p21, which regulate cell survival and apoptosis. The differential responses observed between luminal and TNBC cells accentuate the importance of tailoring therapeutic strategies to specific cancer subtypes. Furthermore, the ability of ESP combination to induce cell death in both monolayer and 3D tumor spheroids supports its potential to overcome tumor microenvironment-related resistance mechanisms. Overall, this study provides

strong evidence for the therapeutic potential of the ESP combination in breast cancer cells, particularly in addressing the challenges posed by drug resistance and tumor heterogeneity. These findings lay the groundwork for further preclinical evaluation and development of ESP (Epirubicin, SAHA, and Pimozide) combination as a promising strategy for improving outcomes in breast cancer treatment.

4.6. References

1. Wang, J., & Wu, S. G. (2023). Breast cancer: an overview of current therapeutic strategies, challenge, and perspectives. Breast Cancer: Targets and Therapy, 721-730. https://doi.org/10.2147%2FBCTT.S432526
2. Anand, U., Dey, A., Chandel, A. K. S., Sanyal, R., Mishra, A., Pandey, D. K., & de la Lastra, J. M. P. (2023). Cancer chemotherapy and beyond: Current status, drug candidates, associated risks and progress in targeted therapeutics. Genes & Diseases, 10(4), 1367-1401. https://doi.org/10.1016%2Fj.gendis.2022.02.007
3. van den Boogaard, W. M., Komninos, D. S., & Vermeij, W. P. (2022). Chemotherapy side-effects: not all DNA damage is equal. *Cancers*, *14*(3), 627. https://doi.org/10.3390/cancers14030627
4. Ajmeera, D., & Ajumeera, R. (2024). Drug repurposing: A novel strategy to target cancer stem cells and therapeutic resistance. Genes & Diseases, 11(1), 148-175. https://doi.org/10.1016%2Fj.gendis.2022.12.013
5. Vlachos, N., Lampros, M., Voulgaris, S., & Alexiou, G. A. (2021). Repurposing antipsychotics for cancer treatment. Biomedicines, 9(12), 1785. https://doi.org/10.3390/biomedicines9121785
6. Li, J., Qu, P., Zhou, X. Z., Ji, Y. X., Yuan, S., Liu, S. P., & Zhang, Q. G. (2022). Pimozide inhibits the growth of breast cancer cells by alleviating the Warburg effect through the P53 signaling pathway. Biomedicine & Pharmacotherapy, 150, 113063. https://doi.org/10.1016/j.biopha.2022.113063
7. Dakir, E. H., Pickard, A., Srivastava, K., McCrudden, C. M., Gross, S. R., Lloyd, S., & El-Tanani, M. (2018). The anti-psychotic drug pimozide is a novel chemotherapeutic for breast cancer. Oncotarget, 9(79), 34889. https://doi.org/10.18632%2Foncotarget.26175

8. Kandasamy, T., Sarkar, S., Sen, P., Venkatesh, D., & Ghosh, S. S. (2024). Concurrent inhibition of IR, ITGB1, and CD36 perturbated the interconnected network of energy metabolism and epithelial-to-mesenchymal transition in breast cancer cells. Journal of Cellular Biochemistry. https://doi.org/10.1002/jcb.30574
9. Merino, V. (2022, December 9). Three-drug cocktail shows efficacy in triple-negative breast cancer. Pharmacy Times. https://www.pharmacytimes.com/view/threedrug-cocktail-shows-efficacy-in-triplenegative-breast-cancer
10. Teo, Y. L., Ho, H. K., & Chan, A. (2015). Metabolism-related pharmacokinetic drug− drug interactions with tyrosine kinase inhibitors: current understanding, challenges and recommendations. British journal of clinical pharmacology, 79(2), 241-253. https://doi.org/10.1111%2Fbcp.12496
11. Zhao, M., Ma, J., Li, M., Zhang, Y., Jiang, B., Zhao, X., & Qin, S. (2021). Cytochrome P450 enzymes and drug metabolism in humans. International journal of molecular sciences, 22(23), 12808. https://doi.org/10.3390%2Fijms222312808
12. Mahmood, T., & Yang, P. C. (2012). Western blot: technique, theory, and trouble shooting. North American journal of medical sciences, 4(9), 429. https://doi.org/10.4103%2F1947-2714.100998
13. Milner, A. E., Palmer, D. H., Hodgkin, E. A., Eliopoulos, A. G., Knox, P. G., Poole, C. J., & Young, L. S. (2002). Induction of apoptosis by chemotherapeutic drugs: the role of FADD in activation of caspase-8 and synergy with death receptor ligands in ovarian carcinoma cells. Cell Death & Differentiation, 9(3), 287-300. https://doi.org/10.1038/sj.cdd.4400945
14. Ricci, M. S., & Zong, W. X. (2006). Chemotherapeutic approaches for targeting cell death pathways. The oncologist, 11(4), 342-357. https://doi.org/10.1634%2Ftheoncologist.11-4-342
15. Olinski, R., Jaruga, P., Foksinski, M., Bialkowski, K., & Tujakowski, J. (1997). Epirubicin-induced oxidative DNA damage and evidence for its repair in lymphocytes of cancer patients who are undergoing chemotherapy. Molecular pharmacology, 52(5), 882-885. https://doi.org/10.1124/mol.52.5.882
16. Natarajan, U., Venkatesan, T., Radhakrishnan, V., Samuel, S., Rasappan, P., & Rathinavelu, A. (2019). Cell cycle arrest and cytotoxic effects of SAHA and RG7388 mediated through

p21WAF1/CIP1 and p27KIP1 in cancer cells. Medicina, 55(2), 30. https://doi.org/10.3390%2Fmedicina55020030

17. Kandasamy, T., Sen, P., & Ghosh, S. S. (2022). Multi-targeted drug repurposing approach for breast cancer via integrated functional network analysis. Molecular informatics, 41(8), 2100300. https://doi.org/10.1002/minf.202100300
18. Hammad, M., Raftari, M., Cesário, R., Salma, R., Godoy, P., Emami, S. N., & Haghdoost, S. (2023). Roles of oxidative stress and Nrf2 signaling in pathogenic and non-pathogenic cells: a possible general mechanism of resistance to therapy. Antioxidants, 12(7), 1371. https://doi.org/10.3390%2Fantiox12071371
19. Engeland, K. (2022). Cell cycle regulation: p53-p21-RB signaling. Cell Death & Differentiation, 29(5), 946-960. https://doi.org/10.1038/s41418-022-00988-z
20. Sen, P., Kandasamy, T., & Ghosh, S. S. (2023). Multi-targeting TACE/ADAM17 and gamma-secretase of notch signalling pathway in TNBC via drug repurposing approach using Lomitapide. Cellular Signalling, 102, 110529. https://doi.org/10.1016/j.cellsig.2022.110529
21. Mallick, R., Bhowmik, P., & Duttaroy, A. K. (2023). Targeting fatty acid uptake and metabolism in cancer cells: A promising strategy for cancer treatment. Biomedicine & Pharmacotherapy, 167, 115591. https://doi.org/10.1016/j.biopha.2023.115591
22. Jin, H. R., Wang, J., Wang, Z. J., Xi, M. J., Xia, B. H., Deng, K., & Yang, J. L. (2023). Lipid metabolic reprogramming in tumor microenvironment: from mechanisms to therapeutics. Journal of Hematology & Oncology, 16(1), 103. https://doi.org/10.1186/s13045-023-01498-2
23. Checa, J., & Aran, J. M. (2020). Reactive oxygen species: drivers of physiological and pathological processes. Journal of Inflammation research, 1057-1073. https://doi.org/10.2147%2FJIR.S275595
24. Huff, L. M., Sackett, D. L., Poruchynsky, M. S., & Fojo, T. (2010). Microtubule-disrupting chemotherapeutics result in enhanced proteasome-mediated degradation and disappearance of tubulin in neural cells. Cancer research, 70(14), 5870-5879. https://doi.org/10.1158/0008-5472.CAN-09-4281

CHAPTER 5

Targeted Delivery of Pimozide Using ZIF-8

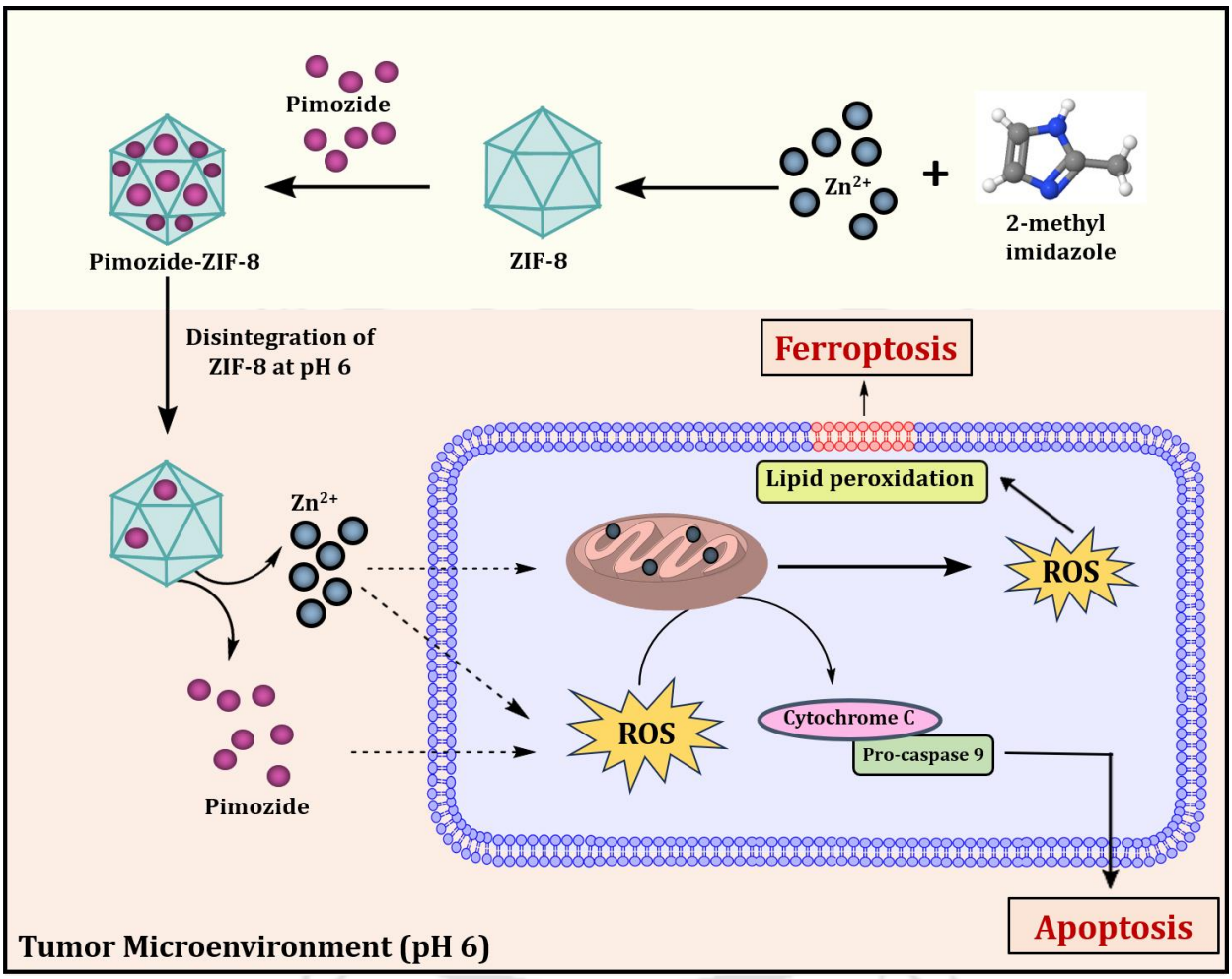

Chapter 5 delves into the targeted delivery of Pimozide using a pH-responsive ZIF-8 framework, designed to release the drug specifically in tumor microenvironment mimic conditions. By encapsulating Pimozide within ZIF-8, this system achieves controlled, targeted release, which minimizes systemic toxicity and maximizes local therapeutic efficacy. Additionally, the synergistic activity of this delivery approach supports drug repurposing strategies, potentially enhancing the overall impact of Pimozide in breast cancer treatment.

Chemistry & Biodiversity, e202402883

DOI: 10.1002/cbdv.202402883

CHAPTER 5

Targeted Delivery of Pimozide Using ZIF-8

5.1. Introduction

Metal ions have garnered significant attention in the field of cancer therapy due to their multifaceted roles in cellular processes, including the generation of reactive oxygen species (ROS), disruption of cellular metabolism, and induction of apoptosis [1]. Among the various metal ions, zinc (Zn), iron (Fe), copper (Cu), and platinum (Pt) have demonstrated particular promise in cancer treatment. These metal ions can be integrated into therapeutic strategies to enhance the efficacy of conventional drugs through synergistic effects, targeted delivery, and controlled release mechanisms [1, 2]. Zinc ions, in particular, have shown considerable potential due to their involvement in various cellular functions, including DNA synthesis, repair, and cell division [2]. Zinc is essential for the function of numerous enzymes and transcription factors, and its dysregulation has been implicated in the progression of various cancers. Zn ions can also induce ferroptosis, a type of programmed cell death characterized by iron-dependent lipid peroxidation, which has emerged as a novel target for cancer therapy [3, 4]. By promoting oxidative stress within cancer cells, Zn ions can potentiate the anticancer effects of chemotherapeutic agents [5].

Metal-organic frameworks (MOFs), particularly Zeolitic Imidazolate Framework-8 (ZIF-8), have emerged as innovative drug delivery systems due to their unique properties, including high surface area, tunable porosity, and chemical stability [6, 7, 8]. ZIF-8, composed of zinc ions coordinated with imidazole ligands, exhibits pH-responsive behavior, making it an ideal candidate for targeted drug delivery within the tumor microenvironment (TME) [9]. The acidic pH of the TME (pH 6-6.5) as compared to normal tissues (pH 7.2-7.4) can be exploited to achieve selective drug release, thereby minimizing off-target effects and enhancing therapeutic efficacy [10]. In addition to their structural role in MOFs, zinc ions themselves contribute to the therapeutic potential of these nanocarriers. By leveraging the inherent properties of Zn, ZIF-8 can deliver therapeutic agents in a controlled manner while simultaneously exerting direct anticancer effects through the induction of oxidative stress and ferroptosis [9, 11]. This dual functionality of ZIF-8, as both a carrier and an active agent, represents a significant advancement in the field of nanomedicine.

Drug repurposing has become an attractive strategy in oncology to accelerate the development of effective treatments and reduce the high clinical attrition rates associated with novel drug discovery [12]. Antipsychotic drugs, for example, have been repurposed for cancer treatment due to their ability to modulate signaling pathways that are critical for cancer cell survival and proliferation [13, 14, 15, 16]. Pimozide, an antipsychotic drug traditionally used for the treatment of Tourette's Disorder, has shown potential as an anticancer agent. It targets the PI3K/AKT pathway and modulates the Warburg effect, both of which are crucial for the metabolic adaptation of cancer cells [17, 18]. However, the clinical application of repurposed antipsychotic drugs like Pimozide is often hampered by the need for high doses and the associated off-target effects. To overcome these challenges, nano-mediated targeted drug delivery systems have been explored to enhance the specificity and efficacy of these drugs [19].

This study aims to develop a novel therapeutic strategy by integrating the therapeutic potential of Zn ions, the advanced drug delivery capabilities of ZIF-8, and the repurposing of Pimozide. Unlike previous studies that focus solely on the drug delivery capabilities of ZIF-8, this study explores the unique synergistic mechanisms of Zn ions and Pimozide, thereby offering a promising avenue for future cancer treatments.

5.2. Experimental section

5.2.1. Chemicals and Reagents

All chemicals and reagents used in this study were obtained from commercial sources. Zinc nitrate hexahydrate and 2-methyl imidazole were purchased from Sigma-Aldrich, Merck Life Science Pvt. Ltd., Mumbai, India. Methanol was procured from Sisco Research Laboratories Pvt. Ltd. (SRL), Mumbai, India. DMEM high glucose media powder was obtained from Sigma-Aldrich, Merck Life Science Pvt. Ltd., Mumbai, India. Fetal bovine serum (FBS) and anti-mycotic & anti-biotic solution (100X) were sourced from Gibco, Thermo Fisher Scientific India Pvt. Ltd., Mumbai, India. MTT powder was purchased from HiMedia Laboratories Pvt. Ltd., Mumbai, India. DCFDA and Calcein AM were obtained from Sigma-Aldrich, Merck Life Science Pvt. Ltd., Mumbai, India. BODIPY™ 581/591 C11 was procured from Thermo Fisher Scientific India Pvt. Ltd., Mumbai, India. Propidium Iodide (PI) was obtained from Sigma-Aldrich, Merck Life Science Pvt. Ltd., Mumbai, India.

5.2.2. Synthesis of ZIF-8 and Pimozide-ZIF-8

Synthesis of ZIF-8 particles was carried out with a single-step optimized protocol reported earlier by Tiwari et al [11]. Zinc nitrate hexahydrate (450 mg) was dissolved in 15 mL of MilliQ water, and 990 mg of 2-methyl imidazole (2-MI) was dissolved in 30 mL of methanol separately to form a clear solution. In the case of Pimozide encapsulated ZIF-8 formation, 3.5 mg of Pimozide was dissolved along with 2-MI in 30 ml of methanol. The synthesis of ZIF-8 and Pimozide – ZIF-8 particles was carried out by mixing two reactant solutions in stirring condition (300 rpm) for 15 min at room temperature. The formed ZIF-8 particles were separated by centrifuging at 11000 rpm for 30 min at room temperature, followed by a three-time methanol wash at the same centrifugation conditions. At last, the pellets were dried at room temperature and collected for further characterization studies.

5.2.3. Characterization studies of ZIF-8 and Pimozdie-ZIF-8

5.2.3.1.X-ray diffraction analysis

The crystallinity of synthesized ZIF-8 and Pimozide-ZIF-8 particles were analyzed using a 9KW Powder X-Ray Diffraction (XRD) System, Rigaku Technologies, Japan. The powder form of Pimozide, ZIF-8, and Pimozide-ZIF-8 was used in this analysis. The X-ray diffraction analysis was carried out using Cu Kα monochromatized radiation with a wavelength of 1.5405 Å and 2θ range of 5^0 - 40^0. The obtained XRD patterns data were blotted using Xmgrace software and verified with published ZIF-8 XRD data.

5.2.3.2. Field-emission scanning electron microscopy imaging

The structure of synthesized ZIF-8 particles was further analyzed using Field-emission scanning electron microscopy (FESEM), Zesis, Sigma-300. The diluted concentration of ZIF-8 was prepared in methanol. The sample was sonicated for 5 min in an Ultrasonic bath and drop cast in silica plates. The images were captured with EHT of 5 KV and magnification of 200K and 500K. The size of the synthesized ZIF-8 was measured using ImageJ and blotted using Graph pad Prism 6.0.

5.2.3.3. Field-emission transmission electron microscopy imaging

Field-emission transmission electron microscopy (FE-TEM) imaging was utilized for morphology and elemental analysis studies of the synthesized ZIF-8 particles. The analysis was conducted using a JEOL, 2100F field emission transmission electron microscope. The diluted sample was drop cast onto the TEM copper grids.

5.2.3.4. Atomic force microscope imaging

The surface smoothness of synthesized ZIF-8 and Pimozide ZIF-8 particles were analyzed using Cypher S Atomic force microscope (AFM), Oxford Instruments. Diluted solutions of ZIF-8 and Pimozide-ZIF-8 were drop cast in silica plates. Images were captured in tapping mode at a scanning rate of 0.9 Hz.

5.2.3.5. Dynamic light scattering analysis

The size distribution of synthesized ZIF-8 in the solution state was analyzed using Malvern Zetasizer Nano ZS. The synthesized ZIF-8 was dispersed in methanol and sonicated using an Ultrasonic bath for 5 min to make a homogeneous mixture.

5.2.3.6. Fourier-transform infrared (FTIR) spectroscopy

FTIR spectra analysis was employed to analyze the characteristic peaks corresponding to ZIF-8 functional groups and molecular vibrations. The powder form of ZIF-8, Pimozide, and Pimozide-ZIF-8 was used for the analysis. The spectra were recorded by FTIR spectrophotometer (PerkinElmer Spectrum Two) with a wavenumber range from 400 to 4000 cm^{-1}.

5.2.4. Drug encapsulation and release study

The amount of Pimozide loaded into the 1 mg of ZIF-8 was measured using the UV-visible spectroscopy method. Initially, 1 mg of Pimozide encapsulated ZIF-8 was decomposed with 50 µL of 2 M hydrochloric acid for 5 min and diluted with methanol up to 1 mL. The diluted solution was examined by UV-visible spectroscopy at a wavelength of 482 nm and compared with the standard graph of Pimozide. The drug loading capacity (DLC) and drug loading efficiency (DLE) were determined using the following equations.

DLC (%) = ((Amount of loaded drugs) / (Amount of ZIF-8)) X 100

DLE (%) = ((Amount of loaded drugs) / (Total amount of drugs added)) X 100

A drug release study of Pimozide encapsulated ZIF-8 was carried out in a solution of Phosphate buffer saline (PBS) and tween 20 (0.5 v/v %) with physiological pH 7.5 and acidic pH 6.0. Initially, 5 mg of Pimozide-ZIF-8 powder was dissolved in 5 mL of buffer solutions and incubated at 37^0 C with shaking (180 rpm). After the desired time intervals, 0.5 mL of solution was collected by centrifuge and replaced with an equal volume of buffer. The amount of Pimozide released in buffer solutions was measured by UV-spectroscopy at a wavelength of 482 nm and analyzed with the calibration curve.

5.2.5. In-vitro studies of Pimozide loaded ZIF-8.

5.2.5.1. Cell culture conditions

Luminal breast cancer cell line MCF-7 was procured from NCCS (National Centre for Cell Sciences) Pune, India. Cells were maintained in DMEM media with 10% FBS (fetal bovine serum) and 1% anti-mycotic, anti-biotic solution in a humidified CO_2 incubator at 37^0 C.

5.2.5.2. Cellular cytotoxicity assay

Cellular cytotoxicity assay was performed in two different pH conditions that are pH 7.5 (physiological) and pH 6 (tumour microenvironment). DMEM media with pH 6 was prepared by the addition of 2N hydrochloric acid and filtered using a 0.2 µm filter. A total of 3000 cells/well were seeded in 96 well plates in physiological pH conditions and allowed to adhere for 24 h in a CO_2 incubator. Cells were treated with varying concentrations of ZIF-8 and Pimozide-ZIF-8 in both pH conditions for 48 h. After the treatment period, 5mg/ml of MTT (3- (4, 5-dimethylthiazol-2-yl) -2, 5- diphenyl tetrazolium bromide) was added to each well and incubated for 90 min. Followed by 120 µL of DMSO was added to each well, and absorbance was measured at 570 and 630 nm.

5.2.5.3. Determination of intracellular ROS generation

Intracellular ROS generation was determined by DCFDA in MCF-7 breast cancer cell lines with different time intervals. Approximately $3x10^5$ cells were seeded in a 35 mm dish and incubated for 24 h. Cells were treated with the IC_{50} concentration of Pimozide-ZIF-8 and free Pimozide (Concentration relative to encapsulated Pimozide) for 3, 6, 12, and 24 h. The increased green fluorescence corresponding to intracellular ROS was captured using a ZOE fluorescent imager.

The images were further analyzed using ImageJ software to measure the mean grey values of the fluorescence. The fold changes were normalized using untreated controls, and graphs were plotted using GraphPad Prism Version 6.0.0.

5.2.5.4. Mitochondrial Membrane Potential (MMP) Detection by JC-1 Staining

MCF-7 cells were seeded at a density of 3×10^5 cells per 35 mm dish and incubated for 24 hours to allow adherence. Following incubation, cells were treated with the IC_{50} concentration of Pimozide-ZIF-8 and the relative concentration of free Pimozide in pH 6 media for 48 hours. After treatment, the culture medium was removed, and cells were incubated with 2.5 µM JC-1 dye for 30 minutes at 37°C in the dark. Subsequently, cells were washed with PBS, and fluorescence images were captured using the ZOE Fluorescence Cell Imager to assess mitochondrial membrane depolarization.

5.2.5.5. Apoptosis assay

The apoptotic population of the untreated and treated cells was assessed utilizing flowcytometric based Alexa flour™ 488 Annexin-V/Dead cell apoptosis kit (Invitrogen by Thermo Fisher Scientific). This method distinguishes between live, early apoptotic, and late apoptotic/necrotic cell populations based on Annexin V and PI (Propidium Iodide) fluorescence profiles. Approximately $3x10^5$ cells of MCF-7 were seeded in 35 mm dishes and incubated for 24 h. Subsequently, cells were treated with the IC_{50} concentration of Pimozide-ZIF-8 and free Pimozide (Concentration relative to encapsulated Pimozide) for 48 h. Further sample processing for flow cytometric analysis was carried out by following the instructions from the Kit manual. The fluorescence was detected using the FITC and PE channel of BD FACSMelody™ Cell Sorter and analyzed using Flowjo V.10 software.

5.2.5.6. Gene Expression Analysis by qRT-PCR

MCF-7 cells were seeded at a density of 3×10^5 cells per 35 mm dish and incubated at 37°C with 5% CO_2 for 24 hours to allow cell attachment. Following incubation, cells were treated with Pimozide-ZIF-8 (at its IC50 concentration) and an equivalent concentration of free Pimozide for 24 hours under pH 6 conditions. Untreated cells served as the control group. After treatment, total RNA was extracted using TRIzol reagent (Sigma-Aldrich, USA) following the manufacturer's protocol. The concentration and purity of the isolated RNA were assessed using a NanoDrop

spectrophotometer (Thermo Fisher Scientific, USA). 1 µg of RNA was reverse transcribed into complementary DNA (cDNA) using the iScript cDNA Synthesis Kit (Bio-Rad, USA). Quantitative real-time PCR (qRT-PCR) was performed using the iTaq Universal SYBR Green Supermix (Bio-Rad, USA). The gene-specific primers for P21, P53, and ALOX15 were designed using Primer-BLAST and synthesized commercially. β-Actin was used as an internal control for normalization. The relative gene expression levels were calculated using the $2^{-}\Delta\Delta Ct$ method.

5.2.5.7. Lipid peroxidation assay

Investigation of lipid peroxidation-mediated ferroptosis was carried out using BODIPY™ 581/591 C11 (Lipid Peroxidation Sensor). It is a radiometric fluorescent sensor for lipid peroxidation, which shifts its fluorescence emission from red to green upon oxidation. MCF-7 cells were seeded in a 35 mm dish at the density of $3x10^5$ cells/plate and incubated for 24 h. Subsequently, 5µM of BODIPY™ 581/591 C11 were added along with drug treatments. The shift in the fluorescence was captured after 48 h using a ZOE fluorescent imager. The images were further analyzed using ImageJ software to measure the mean grey values of the fluorescence, and the red/green ratio was calculated. The fold changes were normalized using untreated controls, and par graphs were plotted using GraphPad Prism Version 6.0.0.

5.2.5.8. Live/dead cell staining of monolayer culture

Live dead staining of Pimozide and Pimozide-ZIF8 treated cells was performed using Calcein Am and PI staining. MCf-7 cells were seeded in a 35 mm dish with a density of $3x10^5$ cells/plate and incubated for 24 h. After the cells were attached, IC_{50} concentration of Pimozide-ZIF-8 and free Pimozide (Concentration relative to encapsulated Pimozide) were added and incubated for 48 h. Subsequently, Calcein-AM and PI were added to the cells with the final concentrations of 2 µM and 4 µM. After a 30 min incubation, images were captured using a ZOE fluorescent imager.

5.2.5.9. Live/dead cell staining of tumor spheroid

Tumor spheroids composed of MCF-7 cells were generated from a monolayer culture. The cells were collected from the monolayer cultures through trypsinization. Ninety-six-well plates were coated in advance with 60 µL of 1.5% agarose in serum-free media. Subsequently, 2 $x10^4$ cells/well were seeded with 200 µL of serum media containing 10% FBS. The plates were then centrifuged at 700 rcf for 10 minutes and placed in cell culture conditions for 72 hours [17, 20].

Following this, the spheroids were treated with Pimozide and Pimozide-ZIF-8 for another 72 hours. Staining was performed using 2 µM of Calcein-AM and 4 µM of PI, and images were captured using a Zeiss LSM 880 confocal microscope.

5.2.6. In-silico analysis

5.2.6.1. Network analysis by STITCH

The drug-protein interaction data for Zinc ions (Zn) and Pimozide were retrieved from the STITCH database (http://stitch.embl.de/), which provides a comprehensive collection of known and predicted interactions between various biological entities. The interactions included both direct and indirect connections, allowing for a holistic view of the molecular networks involving Zn ions and Pimozide**.** The SMILE format of both Pimozide and Zn ion was given as query, minimum required interaction score was set to highest (0.900) and max number of interactors were set to 50. The resulted network of drug and proteins were downloaded in high resolution images.

5.2.6.2. Toxicity prediction by ProTox-II

In silico toxicity predictions for Pimozide and ZIF-8 were conducted using the ProTox-II web server (https://tox.charite.de/protox3/). The 2D structures of both compounds were generated with ChemDraw software, and their SMILES representations were obtained: for Pimozide, the SMILES string is (C1CN(CCC1N2C3=CC=CC=C3NC2=O)CCCC(C4=CC=C(C=C4)F)C5=CC=C(C=C5)F). For a single unit of Zn (II) coordinated by two 2-methylimidazole molecules, the SMILES string is [Zn+2].[nH]1cnc(c1C)C.[nH]1cnc(c1C)C. The ProTox-II tool assesses toxicity through a series of predictive models, including hepatotoxicity, neurotoxicity, nephrotoxicity, immunotoxicity, and interactions with cytochrome P450 enzymes, with parameters set to include various toxicity endpoints.

5.2.7. Statistical analysis

All the experiments were carried out in triplicate, and the graphical data were expressed as mean ± SEM. Additionally, the correlations between the groups were assessed through a one-way ANOVA test, and the p-value <0.05, denoted as (*), is considered to be statistically significant, whereas $p < 0.001$, denoted as (***) and $p < 0.0001$, denoted as (****) are considered to be highly significant.

5.3. Results & Discussion

5.3.1. Physicochemical characterization of ZIF-8 and Pimozide-ZIF-8

Synthesis of ZIF-8 and Pimozide-ZIF-8 was carried out using a single-step room temperature protocol, following established procedures [11]. The morphology, crystallinity, and chemical composition of the synthesized materials were analyzed using a combination of characterization techniques, including FE-SEM, FE-TEM, AFM, XRD, and FTIR.

FE-SEM micrographs revealed well-defined octahedral structures of ZIF-8 crystals with a uniform size distribution, consistent with previous reports [11] (**Figure 5.1 A-B**). The average particle size of synthesized ZIF-8 was approximately 40 nm (**Figure 5.1C**). FE-TEM analysis further confirmed the internal structure and morphology of ZIF-8 nanoparticles, depicting characteristic octahedral crystals (**Figure 5.1 D-E**). The selected area electron diffraction (SAED) pattern and energy dispersive X-ray spectroscopy (EDX) analysis from FE-TEM also confirm the crystallinity and composition of synthesized ZIF-8 (**Figure 5.2**). Dynamic light scattering analysis indicated an average size of hydrated ZIF-8 particles as 155 nm (**Figure 1 F**) and zeta potential of -10.6 mV (**Figure 5.2**). This zeta potential value suggests a relatively low surface charge, which may result in reduced colloidal stability. However, the low absolute value of the zeta potential is advantageous for cellular uptake, as particles with minimal charge are less likely to be repelled by the negatively charged cell membranes, potentially enhancing their internalization into cancer cells. Further, insights into the surface morphology, showing occasional protrusions corresponding to individual ZIF-8 crystals, were obtained through AFM analysis (**Figure 5.3**). Upon encapsulation of Pimozide, an increase in surface roughness was observed. The mean root-mean-square (RMS) roughness values are measured to be 12.78 nm for ZIF-8 and 31.47 nm for Pimozide-ZIF-8. This increased surface roughness in Pimozide-ZIF-8 indicates the encapsulation of drug molecules in the ZIF-8 framework.

Further, the crystallinity of ZIF-8 after drug loading was ensured with the help of the XRD pattern. The XRD patterns of both ZIF-8 and Pimozide-ZIF-8 exhibited sharp peaks corresponding to characteristic crystallographic planes of ZIF-8 [21, 22, 23], with peaks observed at 2θ values around 7.3°, 10.4°, 12.9°, 16.7°, 18.6°, and 23.7° (**Figure 5.3**). These obtained XRD peaks were properly aligned with the standard ZIF-8 peaks from Joint Committee on Powder Diffraction Standards (JCPDS) (**Figure 5.4**). Although the intensity of peaks in Pimozide-ZIF-8 was slightly

reduced due to drug incorporation. However, the overall crystalline structure remained unchanged. Further, FTIR spectra of ZIF-8 displayed characteristic peaks corresponding to the stretching vibrations of imidazole rings and metal–nitrogen bonds. The peak at 1583 cm^{-1} is attributed to the C=N stretching mode, while the peaks at 1450-1550 cm^{-1} and 1200-1300 cm^{-1} correspond to the stretching vibrations of C–N and C–H bonds, respectively (**Figure 5.3**). These results confirm the successful formation of ZIF-8 and the presence of expected chemical bonds [21, 22]. In Pimozide-ZIF-8, the same peaks were observed with less intensity due to the masking of peaks associated with framework vibrational modes by the encapsulated drug molecules. In summary, the physicochemical characterization confirms the successful synthesis and drug encapsulation in ZIF-8, providing crucial insights into its structural and chemical properties.

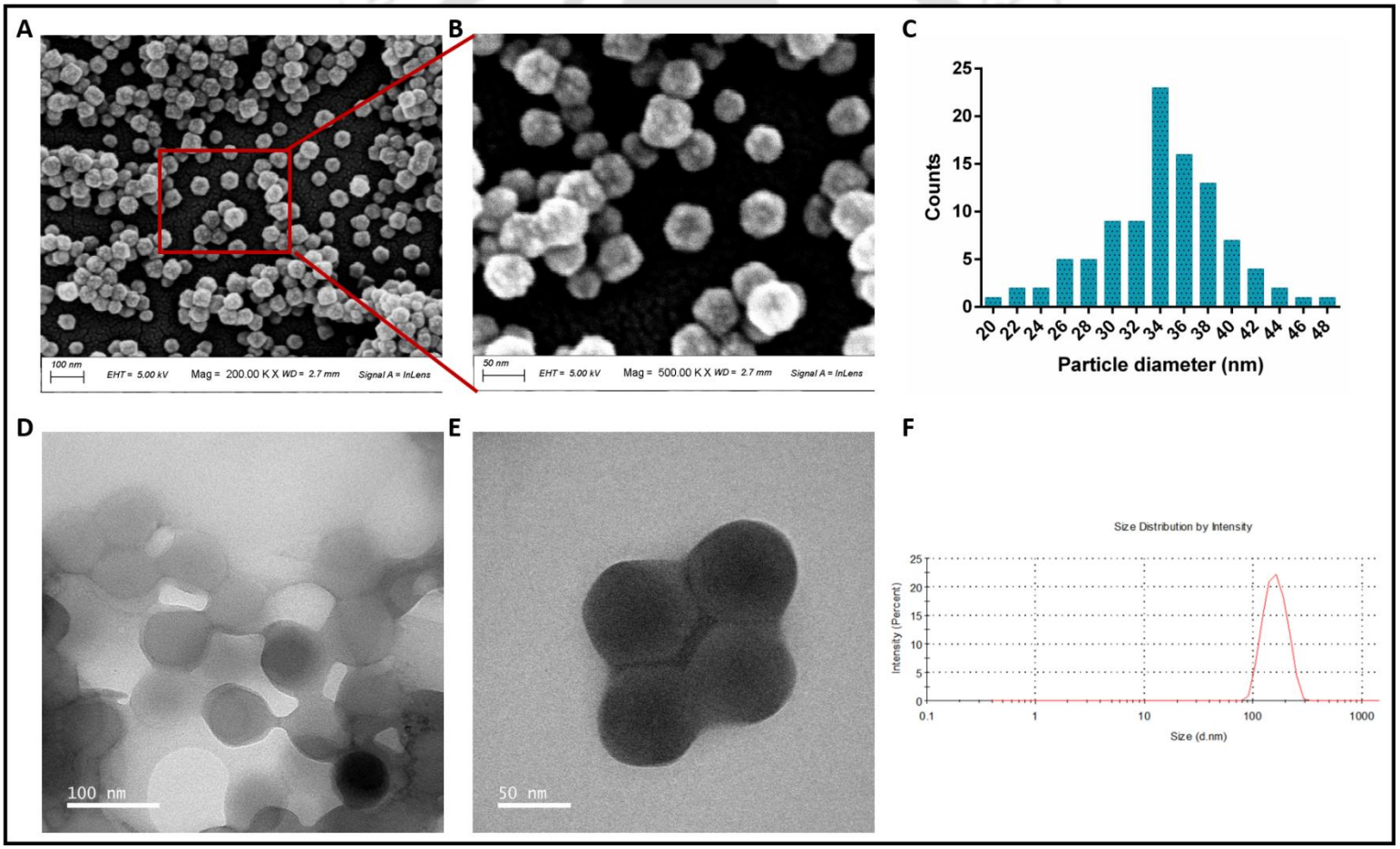

Figure 5.1: A-B) *FE-SEM image of synthesized ZIF-8.* ***C)*** *Size distribution graph of synthesized ZIF-8 based on FE-SEM image.* ***D-E)*** *FE-TEM imaging of synthesized ZIF-8.* ***F)*** *Hydrodynamic diameter of Synthesized ZIF-8 by DLS method*

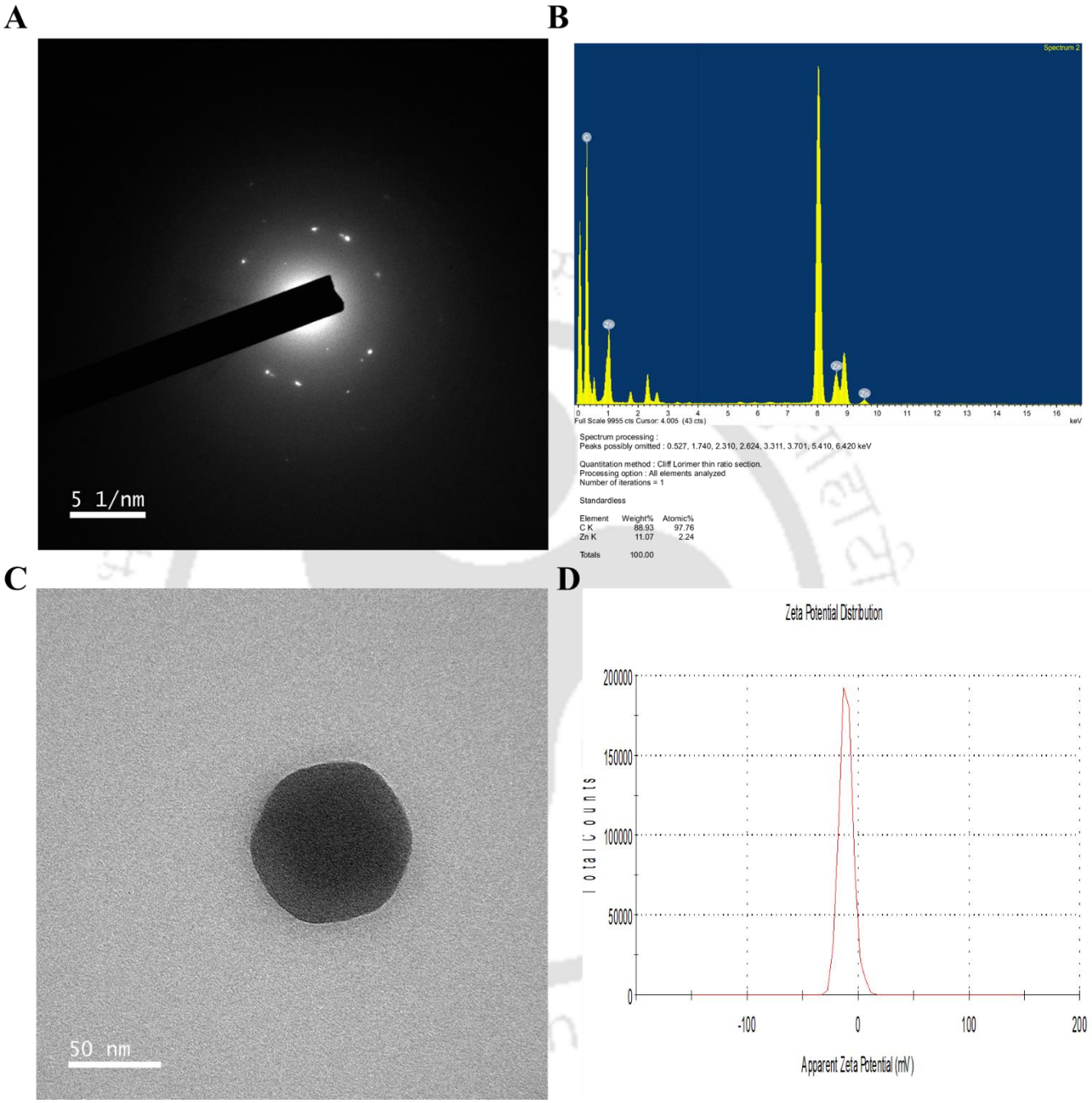

Figure 5.2: ***A)*** *SAD pattern* ***B)*** *Elemental analysis of ZIF-8 using FE-TEM* ***C)*** *Morphology of single unit ZIF-8 from FE-TEM analysis* ***D)*** *zeta potential distribution curve of synthesized ZIF-8*

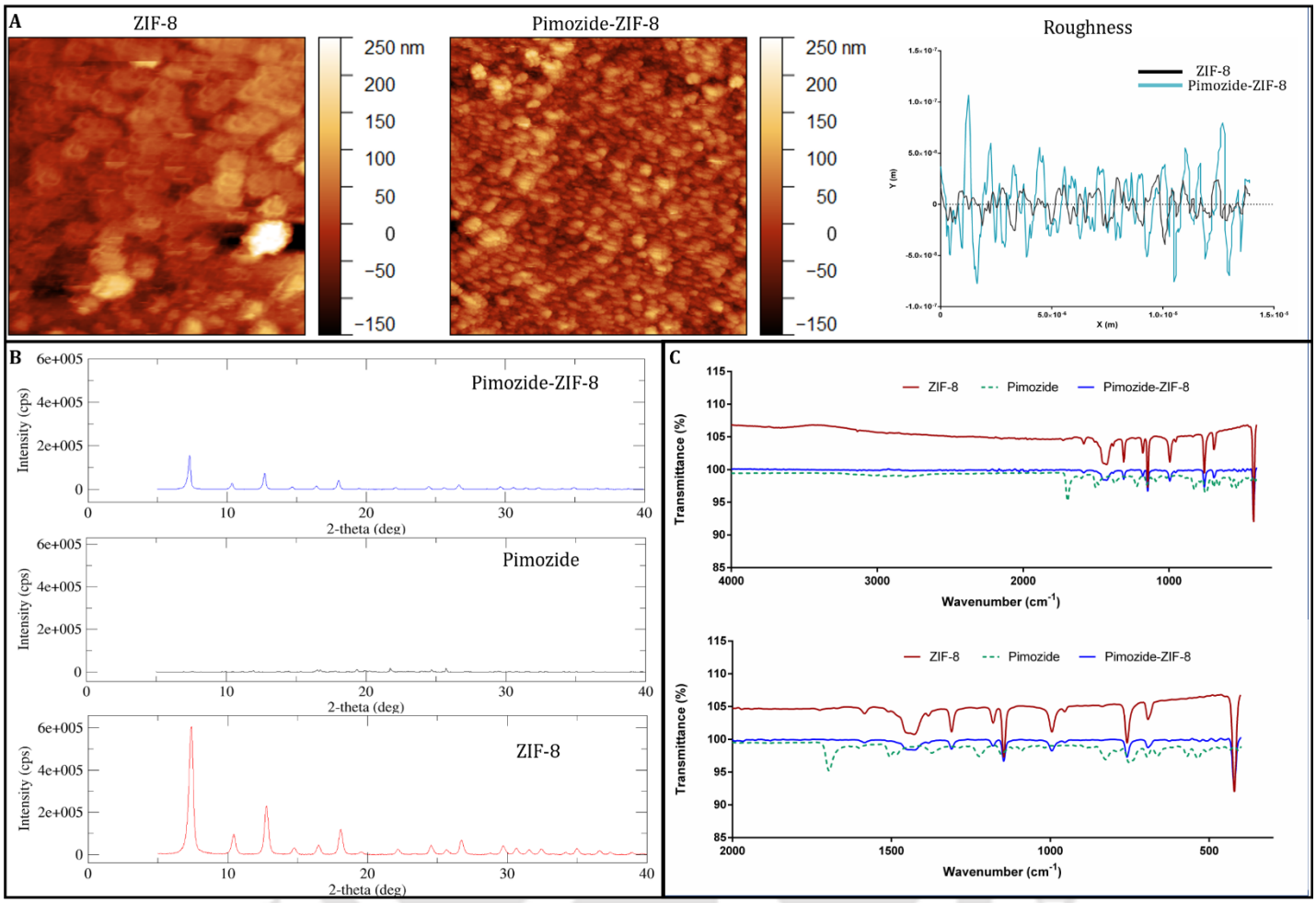

Figure 5.3: A) *AFM analysis of synthesized ZIF-8 and Pimozide-ZIF-8.* ***B)*** *XRD analysis of ZIF-8, Pimozide and Pimozide-ZIF-8.* ***C)*** *FTIR analysis of ZIF-8, Pimozide and Pimozide-ZIF-8*

PDF Card No.: 00-062-1030 Quality:S

Sub-File Name:	Organic
Formula:	(C H3 C3 H2 N2)2 Zn
Name:	Basolite Z1200T, ZIF-8, activated I/Ic (RIR)= 10.77
Crystal System:	Cubic Space Group: I-43m(217) Dmeas:
Cell Parameters:	a= 17.0116 b= 17.0116 c= 17.0116
	Alpha= 90.000 Beta= 90.000 Gamma= 90.000
	Volume= 4923.081 Z= 12
Reference:	Kaduk, J. A., Poly Crystallography Inc., Naperville, IL, USA; Wong-Ng, W., NI...
Radiation:	Sync Wavelength= 0.41221
2Theta range:	7.34 - 65.83
Database comments:	General Comments: Contains 0.7 wt.% ZnO impurity. Processing Information: Rietveld refinement. Sample Preparation: A solid mixture of 2,5-dihydroxy-1,4-benzenedicarboxylic acid and zinc nitrate tetrahydrate was dissolved in a mixture of DMF, 2-propanol, water and placed in a Pyrex tube, which was then frozen in a liquid nitrogen bath, evacuated, flame sealed and heated to 378 K at 275 K per minute, held for 20 hours and then cooled to room

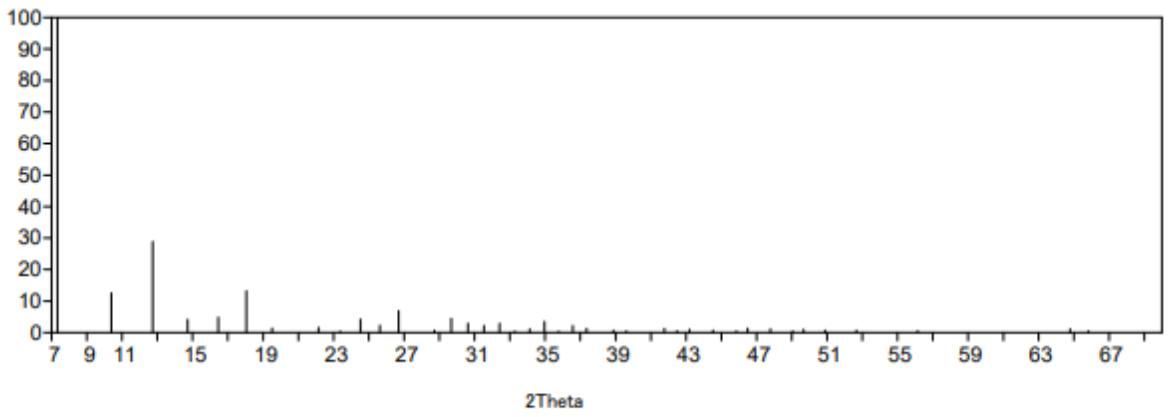

No.	2Theta	d-Value	Intensity	h	k	l	No.	2Theta	d-Value	Intensity	h	k	l
1	7.34	12.029	100.0	1	1	0	21	35.77	2.508	0.4	6	3	1
2	10.39	8.506	12.6	2	0	0	22	36.57	2.455	2.2	4	4	4
3	12.74	6.945	28.9	2	1	1	23	37.35	2.406	1.3	5	4	3
4	14.72	6.015	4.1	2	2	0	24	38.87	2.315	0.7	7	2	1
5	16.46	5.380	4.9	3	1	0	25	39.61	2.273	0.5	6	4	2
6	18.05	4.911	13.2	2	2	2	26	41.78	2.160	1.3	6	5	1
7	19.51	4.547	1.4	3	2	1	27	42.48	2.126	0.6	8	0	0
8	22.15	4.010	1.6	4	1	1	28	43.19	2.093	1.0	7	4	1
9	23.37	3.804	0.4	4	2	0	29	44.52	2.033	0.7	6	5	3
10	24.52	3.627	4.2	3	3	2	30	45.85	1.978	0.5	8	3	1
11	25.63	3.472	2.3	4	2	2	31	46.50	1.951	1.4	6	6	2
12	26.70	3.336	6.9	4	3	1	32	47.78	1.902	1.1	8	4	0
13	28.72	3.106	0.7	5	2	1	33	49.04	1.856	0.5	8	4	2
14	29.68	3.007	4.5	4	4	0	34	49.66	1.834	1.0	9	2	1
15	30.62	2.917	2.9	4	3	3	35	50.88	1.793	0.7	7	5	4
16	31.53	2.835	2.2	4	4	2	36	52.67	1.736	0.7	8	4	4
17	32.42	2.760	2.9	6	1	1	37	56.14	1.637	0.6	10	2	2
18	33.28	2.690	0.4	6	2	0	38	64.79	1.438	1.1	10	6	2
19	34.13	2.625	1.1	5	4	1	39	65.83	1.418	0.5	8	8	4
20	34.96	2.565	3.5	6	2	2							

Note: 2theta are calculated with wavelength = 1.54059

Figure 5.4: *Simulated XRD peaks of ZIF-8 from JCPDS database*

5.3.2. pH-responsive nature of ZIF-8 led to an enhanced release of Pimozide at pH 6 over 48h

ZIF-8 is a metal-organic framework known for its high surface area, controllable pore size, and pH-responsive nature [24]. A single-step room temperature synthesis approach was employed to trap Pimozide molecules within the ZIF-8 framework effectively, which led to the formation of stable composite material ideal for drug delivery applications [11]. Further, spectroscopy analysis demonstrated that encapsulation efficiency and loading capacity of Pimozide within ZIF-8 was 52.21 ± 1.86 % and 2.53 ± 0.09 %, respectively. This indicates the efficient loading of drug molecules into the porous structure of the ZIF-8. Subsequently, evaluation of the drug release profile revealed an intriguing pattern: a notably enhanced release of Pimozide was observed at pH 6 compared to physiological pH conditions 7.5 (**Figure 5.5**). This pH-dependent release behavior suggests that the acidic environment facilitated the liberation of Pimozide from the ZIF-8 composite [25]. The maximum drug release was observed at 48 h for pH 6 and 120 h for pH 7.5. The percentage of drug release after 48 h was 84.13 % for pH 6 and 40.5 % for pH 7.5. The sustained release of Pimozide from the composite material for 48 h accentuates its potential as a platform for controlled drug delivery. The prolonged-release kinetics offer advantages such as reduced dosing frequency and improved patient compliance, which are crucial factors in the management of chronic conditions requiring long-term medication. This release profile is consistent with recent reports on drug release kinetics from ZIF-8-based nanocarriers. For instance, Nguyen et al. 2024 reported 70-85% release of quercetin from ZIF-8 under acidic conditions over 48 hours, while Pham et al. 2024 demonstrated 80-90% release of carboplatin [6, 7]. The slight variations in release percentages may be attributed to differences in drug encapsulation efficiency, ZIF-8 particle size, and drug-ZIF-8 interactions. Overall, the successful encapsulation of Pimozide within ZIF-8 and the enhanced drug release observed at pH 6 demonstrate the potential of the Pimozide-ZIF-8 composite for targeted and sustained drug delivery applications. Further, the *in-vitro* efficacy of pH-dependent drug release was explored in breast cancer cell lines.

5.3.3. The complementary effect of decomposed ZIF-8 and Pimozide enhanced the efficacy of Pimozide-ZIF-8 formulation at pH 6

The investigation of the cytotoxic effects of Pimozide-ZIF-8 was carried out in MCF-7 cells under conditions mimicking the tumor microenvironment (pH 6) and compared with physiological

conditions (pH 7.5). Our findings revealed a notable enhancement in cytotoxicity when MCF-7 cells were treated with Pimozide-ZIF-8 at pH 6 compared to pH 7.5 (**Figure 5.5**). The IC_{50} concentrations obtained were 23.58 µg/ml and 36.65 µg/ml for pH 6 and pH 7.5, respectively. The relative concentration of Pimozide in Pimozide-ZIF-8, calculated from DLC, was 0.6 µg/ml, which is ~7-fold lower than the IC_{50} of free Pimozide (4.46 µg/ml) at pH 6. The comparative analysis of the cytotoxicity of Pimozide-ZIF-8 and the relative concentration of free Pimozide is also portrayed in **Figure 5.5 G**. It was also evident that no significant cytotoxicity was attained for free Pimozide up to the concentration of 1 µg/ml at both pH 6 and pH 7.5 **(Figure 5.5 E).** This enhancement in the cytotoxicity of Pimozide after ZIF-8 encapsulation suggests a complementary effect of the decomposed ZIF-8 framework and Pimozide under acidic conditions. The acidic microenvironment facilitates the decomposition of ZIF-8, leading to the release of metal ions and ligands (Butonova et al. 2021, Ettlinger et al. 2019; Tran and Lee 2021). Zn ions, in particular, play a crucial role in this process. Several studies have demonstrated the ability of Zn ions in the induction of ferroptosis, a form of programmed cell death characterized by iron-dependent lipid peroxidation (Chen et al. 2021; Zhang et al. 2020; Chen and Chi 2021). This dual mechanism, involving both the drug and the released metal ions, contributes significantly to the observed increase in cytotoxicity at pH 6.

Further the cytotoxicity of Pimozide-ZIF-8 in a more aggressive breast cancer subtype was evaluated using MDA-MB-231 (TNBC) cells. The IC_{50} values obtained for MDA-MB-231 were 39.15 µg/ml at pH 6 and greater than 50 µg/ml at pH 7.5, indicating a considerably lower sensitivity compared to MCF-7 cells (**Figure 5.6**). Notably, the IC_{50} of free Pimozide in MDA-MB-231 cells was 11.22 µg/ml, which is significantly higher than the IC_{50} observed in MCF-7 (4.46 µg/ml) (**Figure 5.6)**. This confirms that Pimozide itself is inherently more effective against luminal breast cancer than TNBC. The lower sensitivity of MDA-MB-231 to both free and encapsulated Pimozide may be attributed to differences in drug uptake, metabolic adaptation, and resistance mechanisms characteristic of TNBC. Given that MCF-7 cells exhibited significantly higher sensitivity, further mechanistic studies were focused on this cell line to explore the full therapeutic potential of Pimozide-ZIF-8 in luminal breast cancer. In addition, the selective toxicity of Pimozide-ZIF-8 toward cancer cells while minimizing potential toxicity to normal cells were assessed by performing cytotoxicity studies on HEK293 cells at pH 7.5. The results demonstrated no significant cytotoxicity up to 50 µg/ml, confirming the biocompatibility of the formulation

under normal physiological conditions (**Figure 5.6)**. This highlights the enhanced toxicity of Pimozide-ZIF-8 predominantly observed in the acidic tumor microenvironment.

Furthermore, combination index (CI) analysis of Pimozide-ZIF-8 at pH 6 and pH 7.5, portrayed in **Figures 5.4 H and 5.4 I**, respectively, supports the synergistic activity at pH 6. CI values all treated concentrations of Pimozide-ZIF-8 at pH 6 were less than 1, indicating synergism. In contrast, at pH 7.5, Pimozide-ZIF-8 concentrations of 5, 10, and 20 µg/ml showed CI values of less than 1 but did not exhibit significant cytotoxicity at these concentrations. However, at concentrations of 30 and 40 µg/ml, the CI values were greater than 1, indicating antagonism. This suggests that while lower concentrations of Pimozide-ZIF-8 may show some synergistic potential at neutral pH, higher concentrations exhibit antagonistic effects, reducing overall efficacy. The reduced cytotoxicity at pH 7.5 could be attributed to the slower release rate of Pimozide from the ZIF-8 carrier under physiological conditions, resulting in decreased exposure of cancer cells to the drug. Additionally, the neutral environment at pH 7.5 might have attenuated the decomposition of ZIF-8, leading to diminished cytotoxicity.

Overall, these results highlight the importance of considering the complementary effect of decomposed ZIF-8 and released Pimozide in pH-responsive drug delivery systems for targeted cancer therapy. The integration of Zn ions not only enhances the efficacy of the drug but also introduces a novel approach to inducing ferroptosis, further contributing to the therapeutic potential of this system.

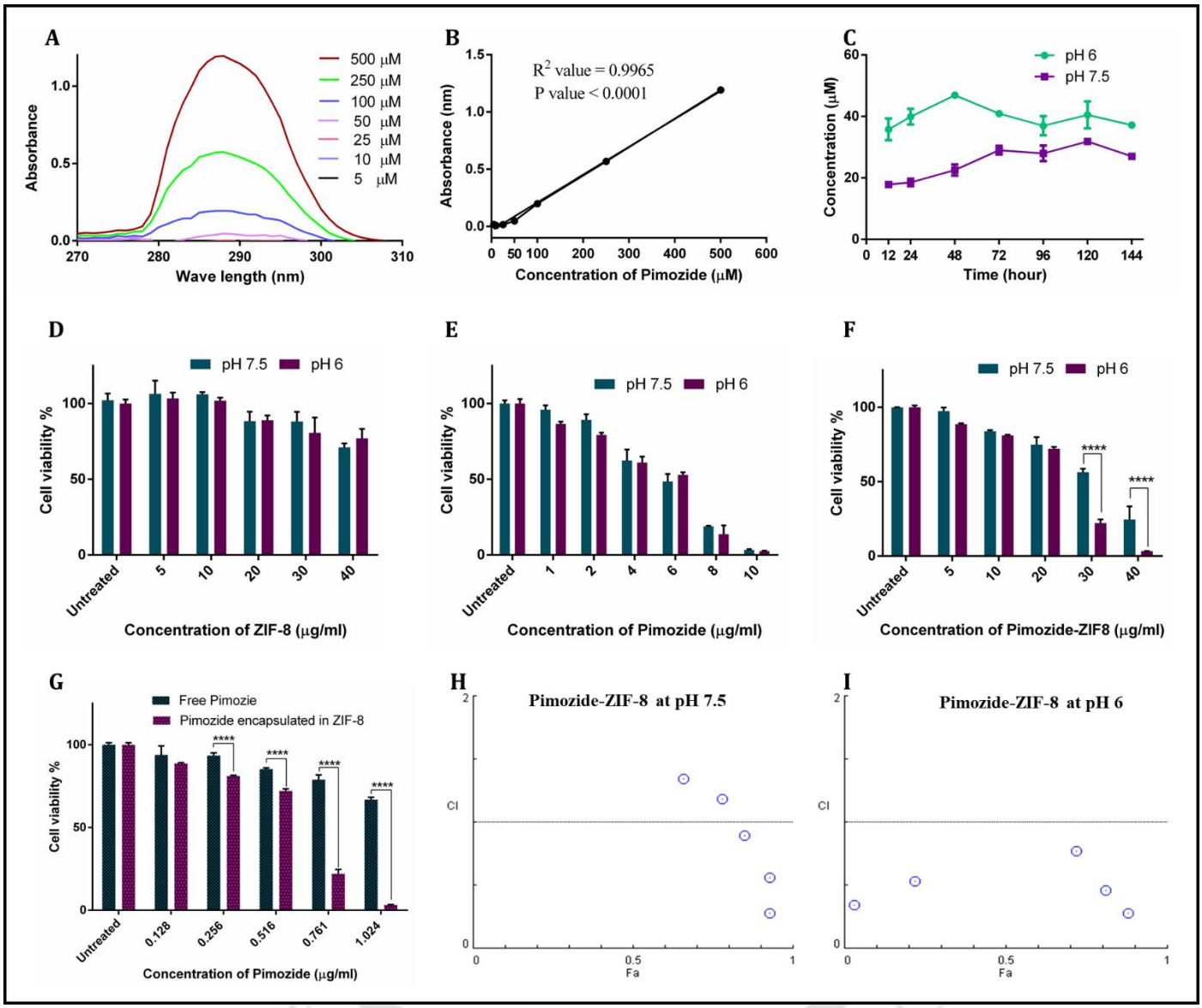

Figure 5.5: A) *UV-visible absorbance spectra of Pimozide standard curve* ***B)*** *Standard graph of Pimozide by UV-visible spectroscopy.* ***C)*** *Drug release study of Pimozide encapsulated ZIF-8 at pH 6 and pH 7.5* ***D-F)*** *Comparative cytotoxicity analysis of ZIF-8, Pimozide, and Pimozide-ZIF8 at pH 6 Vs. pH 7.5 on MCF-7 cell line* ***G)*** *Comparative cytotoxicity analysis of Pimozide encapsulated ZIF-8 Vs. Relative concentrations of free Pimozide in MCF-7 cell line.* ***H&I)*** *Combination Index graph of Pimozide-ZIF-8 on MCF-7 at pH 7.5 and 6.*

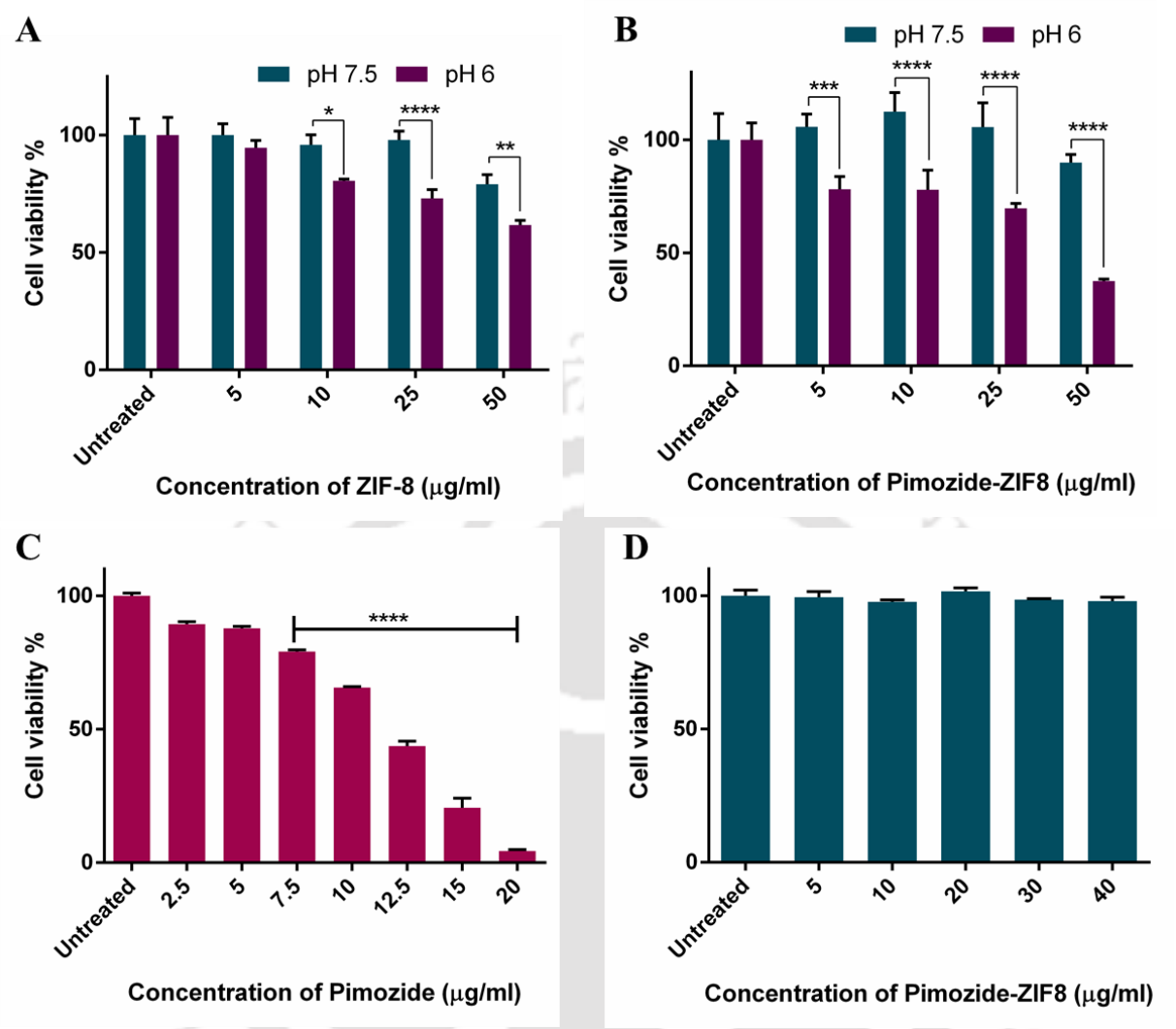

Figure 5.6: ***(A-B)*** *Comparative cytotoxicity analysis of ZIF-8 and Pimozide-ZIF-8 in MDA-MB-231 cells under pH 6 and pH 7.5 conditions, highlighting the pH-dependent effects of the formulations.* ***(C)*** *Cytotoxicity analysis of free Pimozide in MDA-MB-231 cells at pH 7.5, demonstrating its dose-dependent effects.* ***(D)*** *Cytotoxicity analysis of Pimozide-ZIF-8 in HEK293 cells, assessing its biocompatibility in non-cancerous cells.*

5.3.4. The ZIF-8 formulation of Pimozide retained its inherent ability to activate intrinsic apoptotic pathways.

In line with a recent study, Pimozide activates the intrinsic pathway of apoptosis via intracellular ROS generation and mitochondrial dysfunction in breast cancer cells (Kandasamy et al. 2024). Therefore, apoptosis inducing potential of Pimozide-ZIF-8 nanoparticles was further investigated through extensive *in-vitro* studies.

Determination of the fold change of intracellular ROS generation of free Pimozide and Pimozide-ZIF-8 using DCFDA dye in the MCF-7 cell line was carried out under an acidic environment. The increase in fold change of ROS after free Pimozide treatment with IC_{50} concentration as well as relative concentration were portrayed in **Figure 5.7 & Figure 5.8**. Remarkably, the findings portrayed the gradual increase of intracellular ROS levels up to 12 h of free Pimozide treated with relative concentration similar to IC_{50} concentration (**Figure 5.8 A-C**). The increase in fold changes is 3.2-fold at 3 h, 4-fold at 6 hr, and a maximum of 6.67-fold at 12 hr. Whereas, in the case of Pimozide-ZIF-8, there was no significant ROS generation was observed after 3 h and 6 h of treatment. After 12 h of treatment, the ROS generation was obtained to be maximum, which was 2.43-fold (**Figure 5.8 D**). These observations indicate the slow release of Pimozide and also confirm that encapsulation did not compromise the ROS-inducing property of Pimozide.

Further, mitochondrial dysfunction was analyzed using JC-1 staining to assess mitochondrial membrane potential (MMP). Under normal conditions, mitochondria maintain a high membrane potential, resulting in JC-1 dye aggregation and red fluorescence. Following treatment with Pimozide-ZIF-8, a significant increase in membrane depolarization was observed, as indicated by a higher green/red fluorescence ratio (**Figure 5.9)**. The disruption of MMP is a direct consequence of increased ROS levels induced by Pimozide-ZIF-8, leading to mitochondrial damage. This loss of mitochondrial integrity is a crucial step in the activation of the intrinsic apoptosis pathway.

In addition, the apoptotic population of Pimozide-ZIF8 and free Pimozide-treated MCF-7 cells at pH 6 was determined. **Figure 5.8 E-H** portrays that the total apoptotic population percentage was similar for both free Pimozide (17.12 %) and Pimozide-ZIF8 (16.42 %). This validates the retention of the intrinsic apoptosis-inducing property of Pimozide within the ZIF-8 formulation. To further validate the activation of apoptosis, we analyzed the gene expression of P21 and P53, two key regulators of the apoptotic pathway. The results revealed a 1.55-fold upregulation of P21

and a 1.71-fold upregulation of P53 in Pimozide-ZIF-8-treated MCF-7 cells at pH 6 compared to untreated controls **(Figure 5.10)**. This confirms the activation of apoptosis, consistent with the findings from ROS generation, mitochondrial membrane depolarization, and apoptotic cell population analysis. These findings collectively suggest that Pimozide-ZIF-8 effectively induces apoptosis via mitochondrial dysfunction, ROS generation, and activation of apoptotic signaling pathways, while maintaining the apoptotic potential of free Pimozide.

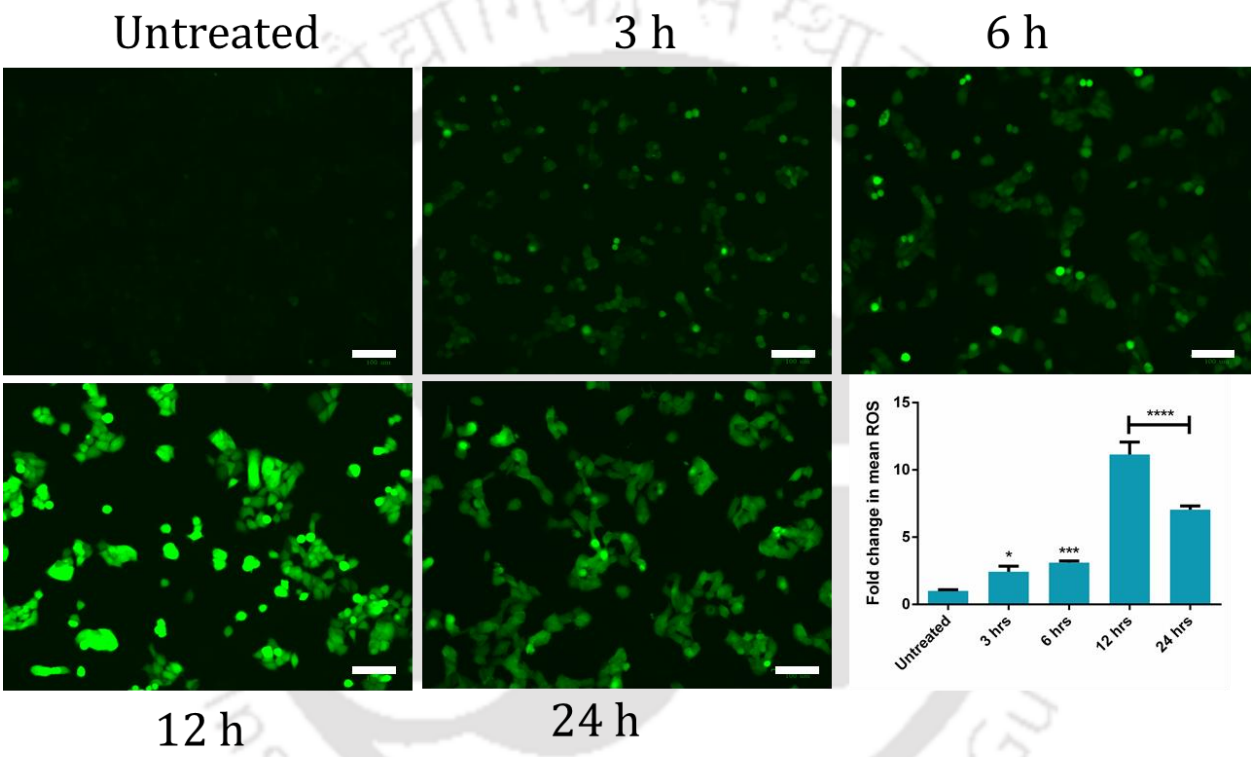

Figure 5.7: *Generation of intracellular ROS by free Pimozide with IC_{50} concentration in MCF-7 cell line at pH 6. Scale 100 µm.*

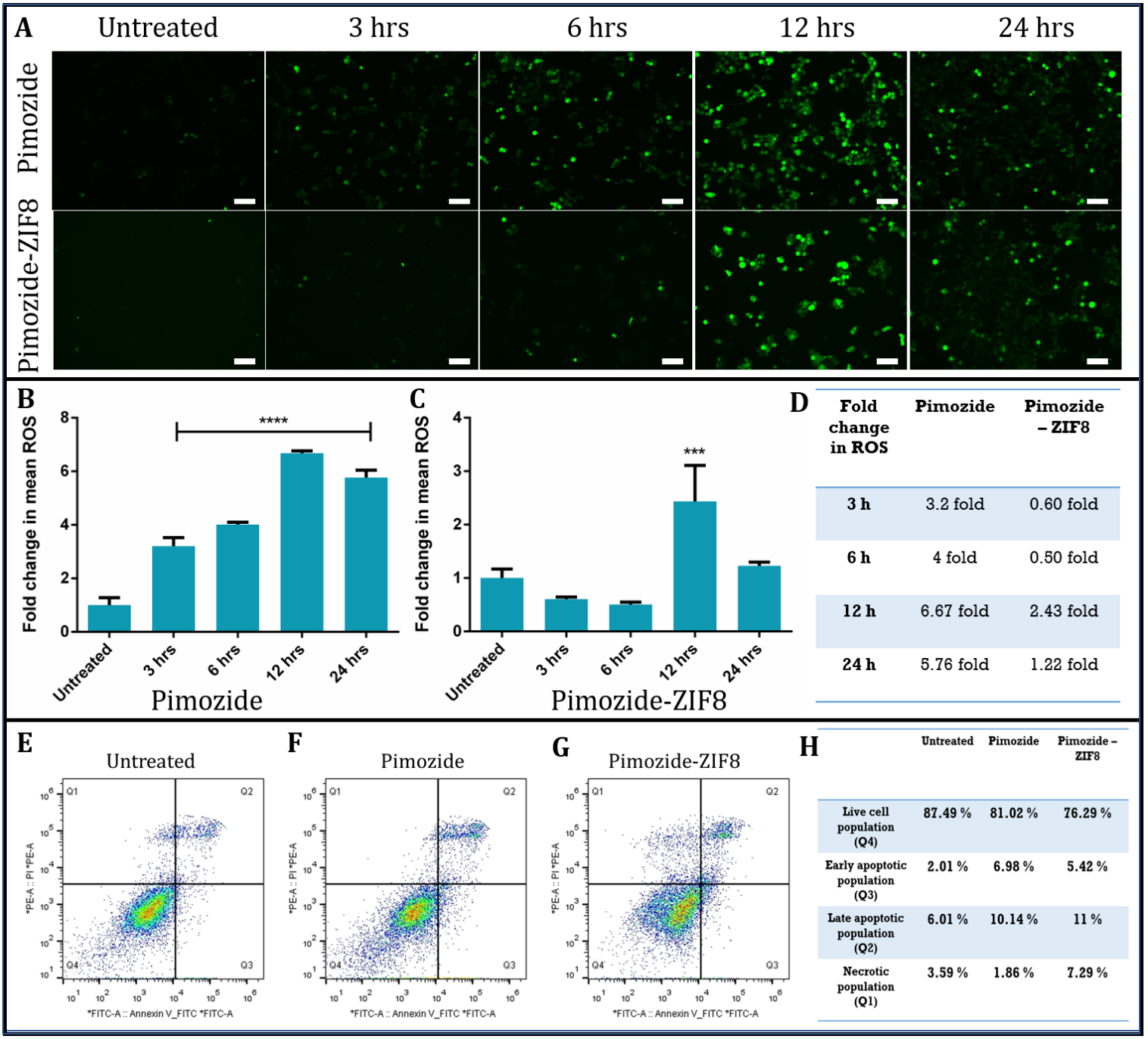

D

Fold change in ROS	Pimozide	Pimozide – ZIF8
3 h	3.2 fold	0.60 fold
6 h	4 fold	0.50 fold
12 h	6.67 fold	2.43 fold
24 h	5.76 fold	1.22 fold

H

	Untreated	Pimozide	Pimozide – ZIF8
Live cell population (Q4)	87.49 %	81.02 %	76.29 %
Early apoptotic population (Q3)	2.01 %	6.98 %	5.42 %
Late apoptotic population (Q2)	6.01 %	10.14 %	11 %
Necrotic population (Q1)	3.59 %	1.86 %	7.29 %

Figure 5.8: A) *Determination of intracellular ROS generation by Pimozide-ZIF-8 using DCFDA dye in MCF-7 cell line at pH 6.* ***B-D)*** *Fold change in the intracellular ROS in the MCF-7 cell line.* ***E-H)*** *Determination of apoptotic population after treatment with Pimozide and Pimozide-ZIF-8 at pH 6. Scale 100 µm.*

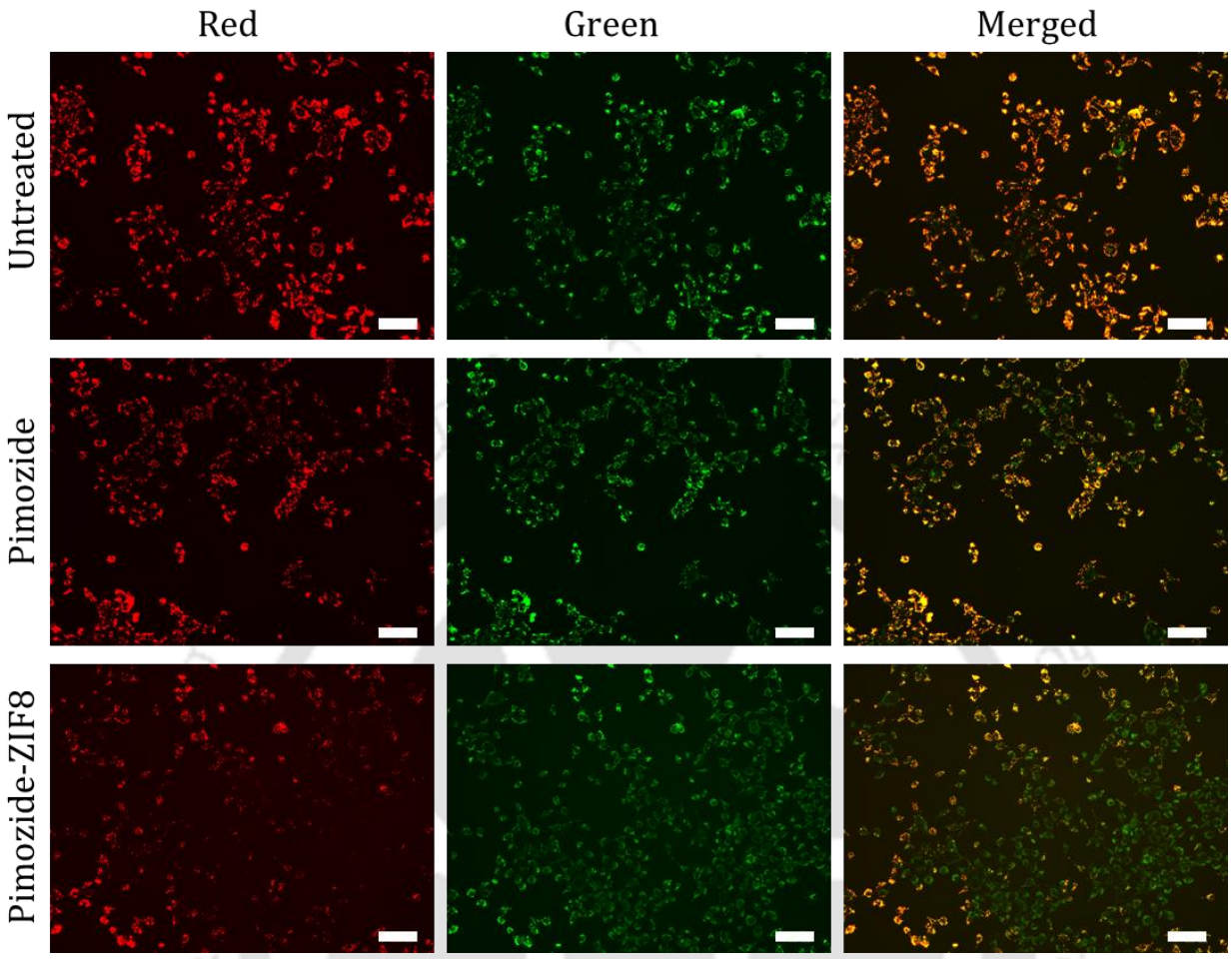

Figure 5.9: *Mitochondrial membrane potential of MCF-7 cell line by JC-1 staining after 24 h treatment with IC_{50} concentration of Pimozide and Pimozide-ZIF8. Scale 100 µm.*

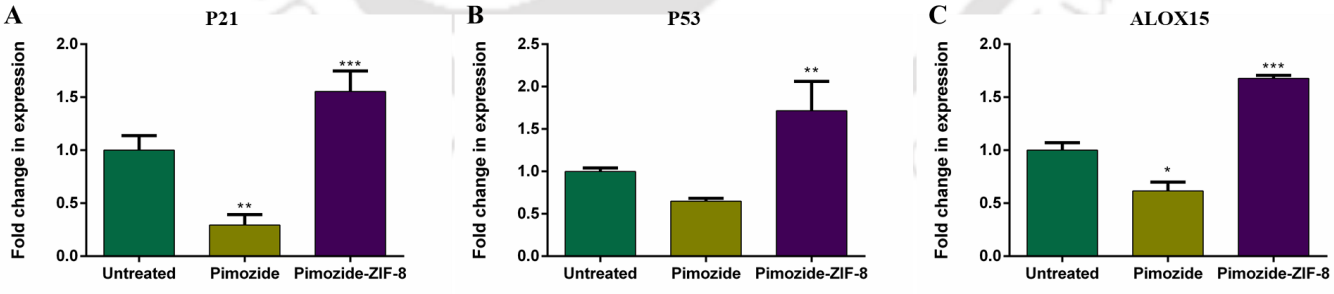

Figure 5.10: (A-B) *Gene expression analysis of apoptosis marker genes P21 and P53 in MCF-7 cells, demonstrating their upregulation following treatment with Pimozide-ZIF-8 compared to untreated cells.* ***(C)*** *Gene expression analysis of the ferroptosis marker gene ALOX15, showing significant upregulation in Pimozide-ZIF-8-treated cells, indicating ferroptosis activation.*

5.3.5. Decomposed ZIF-8 accentuates the efficacy of Pimozide by inducing ferroptosis

Ferroptosis is often characterized as programmed necrosis caused by the oxidized phospholipids in the cell membrane (Shan et al. 2020). The potential of ZIF-8 to enhance cellular cytotoxicity by inducing ferroptosis in MCF-7 cells was further evaluated under acidic conditions (pH 6). It was found that cells treated with Pimozide-ZIF8 had a significant increase in the necrotic cell population (7.29%) compared to free Pimozide-treated cells (1.86%) (**Figure 5.8 H**). This indicates a plausible effect of Zn ions released from the decomposed ZIF-8 nanoparticles.

A Plethora of evidence demonstrated that Zn ions induce ferroptosis through the peroxidation of polyunsaturated fatty acids in the cell membrane (Chen et al. 2021; Chen and Chi 2021). Therefore, using BODIPY™ 581/591 C11 (a fluorescent sensor sensitive to oxidative stress), the lipid peroxidation state of Pimozide-ZIF-8 treated cells was evaluated. **Figure 5.11 A** demonstrated that cells treated with pimozide-ZIF-8 exhibited a substantial rise in green fluorescence, which is evidence of elevated lipid peroxidation and ferroptosis. In addition, fluorescence images with lower magnification, capturing a greater number of cells, were obtained for quantification purposes (**Figure 5.12**). The quantification of red and green fluorescence intensity from these images was performed using ImageJ software, and the resulting data are presented in graph form in **Figure 5.11 B**. The ratio of red to green fluorescence was also reduced significantly compared to untreated cells (**Figure 5.11 B**). These findings confirm the Zn ion from decomposed ZIF-8 induced ferroptosis in tumor microenvironment mimic condition (**Figure 5.11 C**). Further confirmation of the involvement of ferroptosis, was analysed by the checking the expression of ALOX15 (a key enzyme implicated in lipid peroxidation-driven ferroptosis). ALOX15 expression was significantly upregulated (1.67-fold) in Pimozide-ZIF-8-treated MCF-7 cells (**Figure 5.10**), whereas no substantial change was observed in free Pimozide-treated cells compared to untreated controls at pH 6. This result corroborates the lipid peroxidation findings and provides molecular evidence that Pimozide-ZIF-8 induces ferroptosis via the activation of the ALOX pathway. The absence of a similar effect in free Pimozide-treated cells further reinforces that the Zn ions released from ZIF-8 play a crucial role in driving ferroptosis, aligning with previous studies highlighting the impact of Zn on ferroptotic cell death. Collectively, these findings confirm that Pimozide-ZIF-8 formulation not only enhances lipid peroxidation but also triggers ferroptosis-specific molecular responses in the tumor microenvironment.

Furthermore, Live/dead staining of monolayer culture and tumor spheroids of MCF-7 cells was performed to assess the cellular cytotoxicity. The staining revealed that significant increase in dead cells stained with propidium iodide (PI) and a decrease in live cells stained with Calcein AM (**Figure 5.13**). In addition, live/dead staining of Pimozide treated with IC_{50} concentration also confirmed the cytotoxic nature of Pimozide under acidic pH (**Figure 5.14**). These findings emphasize the enhanced cellular cytotoxicity of Pimozide-ZIF-8 mediated by the ferroptosis induction. Importantly, the enhanced cytotoxicity was more distinct in the acidic tumor microenvironment (pH 6), which underlines the pH-responsive nature of decomposed ZIF-8 nanoparticles and their potential for targeted cancer therapy (**Figure 5.5**). Altogether, these findings demonstrated that Zn ions, released from the decomposed ZIF-8 framework in a tumor microenvironment mimic condition, induce ferroptosis by promoting lipid peroxidation and altering iron metabolism. Meanwhile, the released Pimozide triggers apoptosis through its established mechanisms, primarily via mitochondrial dysfunction and caspase activation. Pimozide has been previously reported to induce apoptosis in breast cancer cells [8], and this effect is retained in the Pimozide-ZIF-8 formulation. The interplay between ferroptosis and apoptosis contributes to the enhanced cytotoxicity observed with the Pimozide-ZIF-8 system. While ferroptosis leads to oxidative membrane damage and necrotic-like cell death, apoptosis ensures programmed cell death via caspase-dependent pathways. The simultaneous activation of both cell death mechanisms allows a more effective therapeutic outcome by overcoming potential resistance mechanisms. This dual mechanism of ferroptosis and apoptosis activation highlights the synergistic anti-cancer effects of the Pimozide-ZIF-8 system, further strengthening its therapeutic potential in breast cancer treatment.

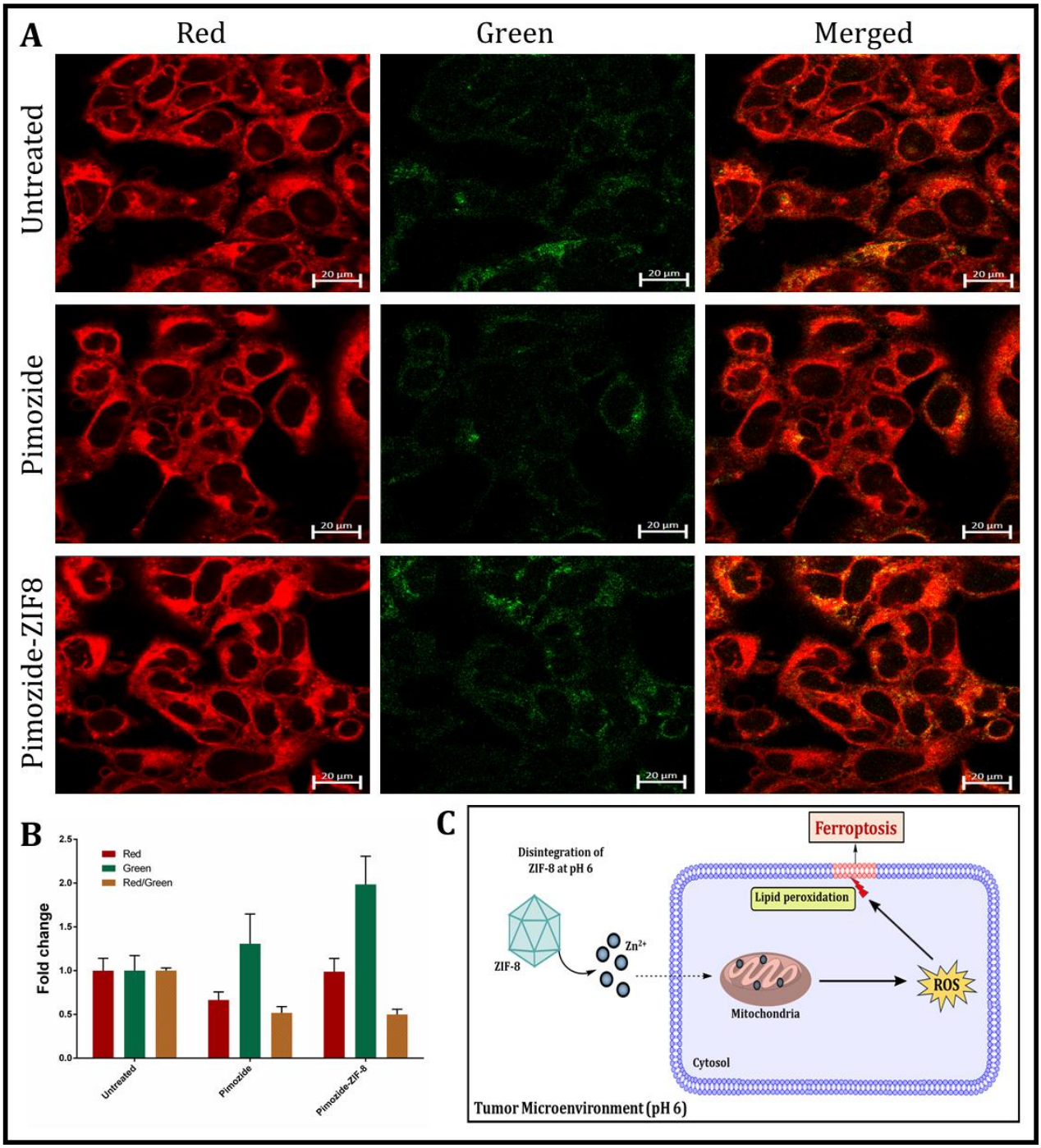

Figure 5.11: (A) *Representative fluorescence images showing lipid peroxidation in MCF-7 cells after 48 h treatment with Pimozide-ZIF-8 at pH 6, assessed using BODIPY™ 581/591 C11 staining. An increase in green fluorescence indicates elevated lipid peroxidation, confirming ferroptosis induction (Scale: 20 µm).* ***(B)*** *Quantification of red-to-green fluorescence intensity shift, representing the extent of lipid peroxidation after treatment.* ***(C)*** *Schematic representation illustrating the proposed mechanism of Zn^{2+} ion-mediated ferroptosis induction.*

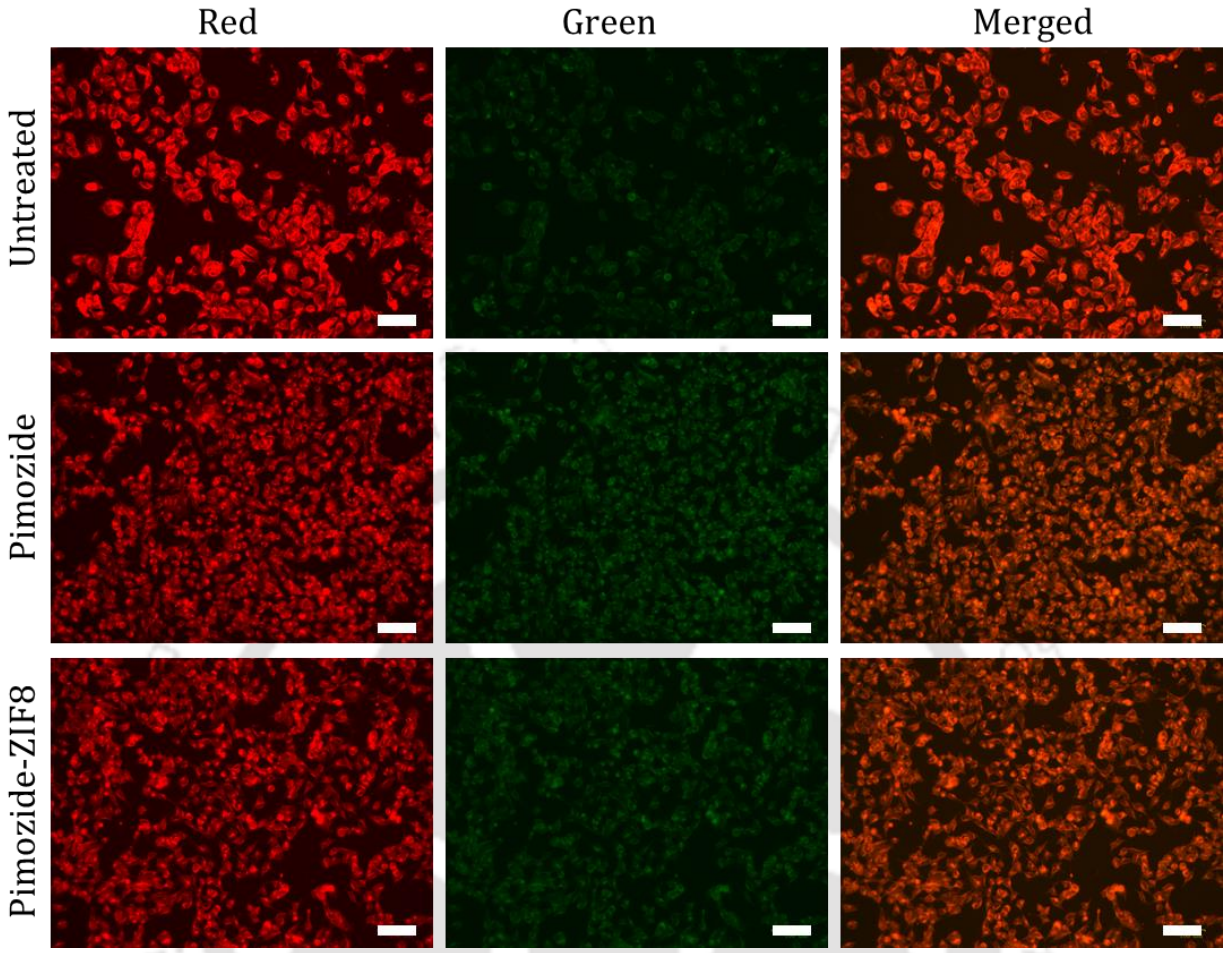

Figure 5.12: *Lipid peroxidation study to confirm the induction of ferroptosis in MCF-7 after treatment with Pimozide-ZIF-8 at pH 6. Scale 100 µm.*

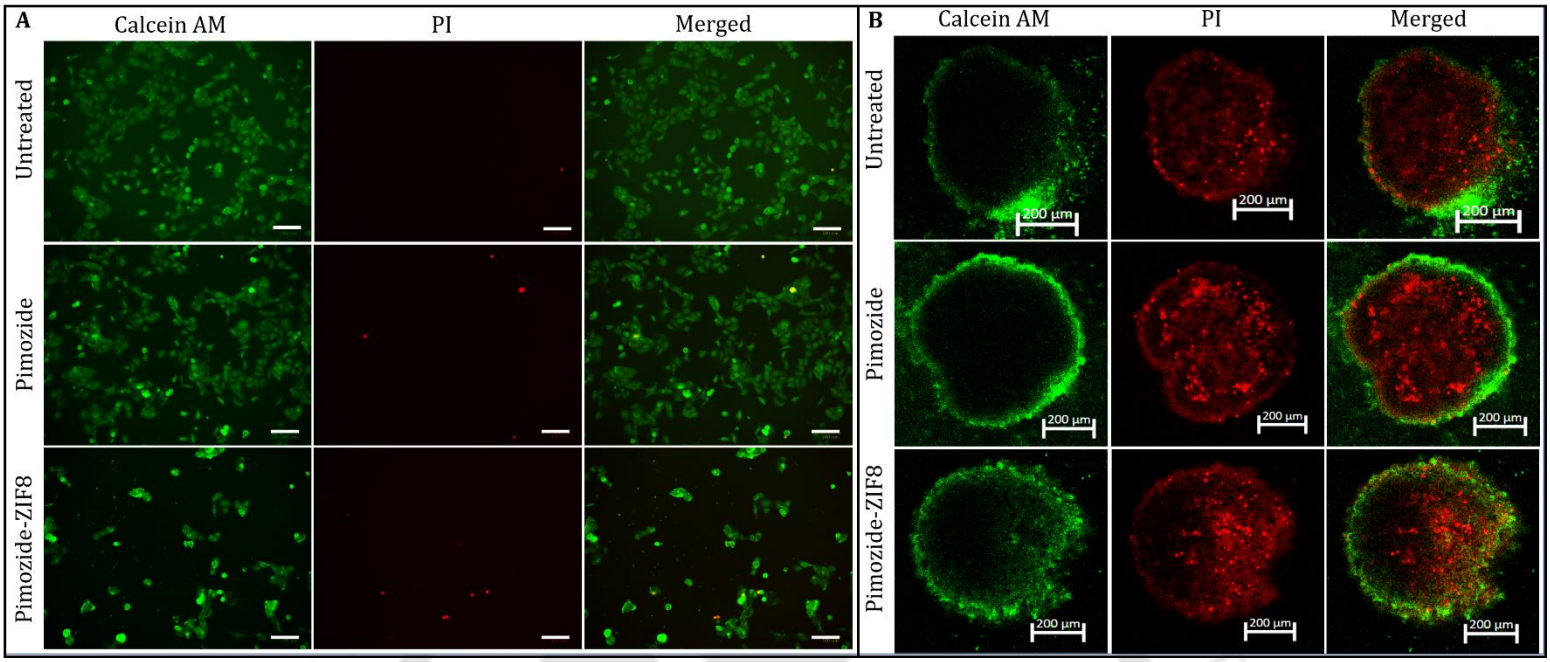

Figure 5.13: *Live/dead cell staining of MCF-7 cells treated with Pimozide-ZIF-8 for 48 h using Calcein AM (live cells, green) and propidium iodide (PI) (dead cells, red).* ***(A)*** *Fluorescence images of treated cells in monolayer culture, demonstrating the viability status of the cells (Scale: 100 µm).* ***(B)*** *Live/dead staining of tumor spheroids post-treatment, highlighting the effect of Pimozide-ZIF-8 in a 3D culture model (Scale: 200 µm).*

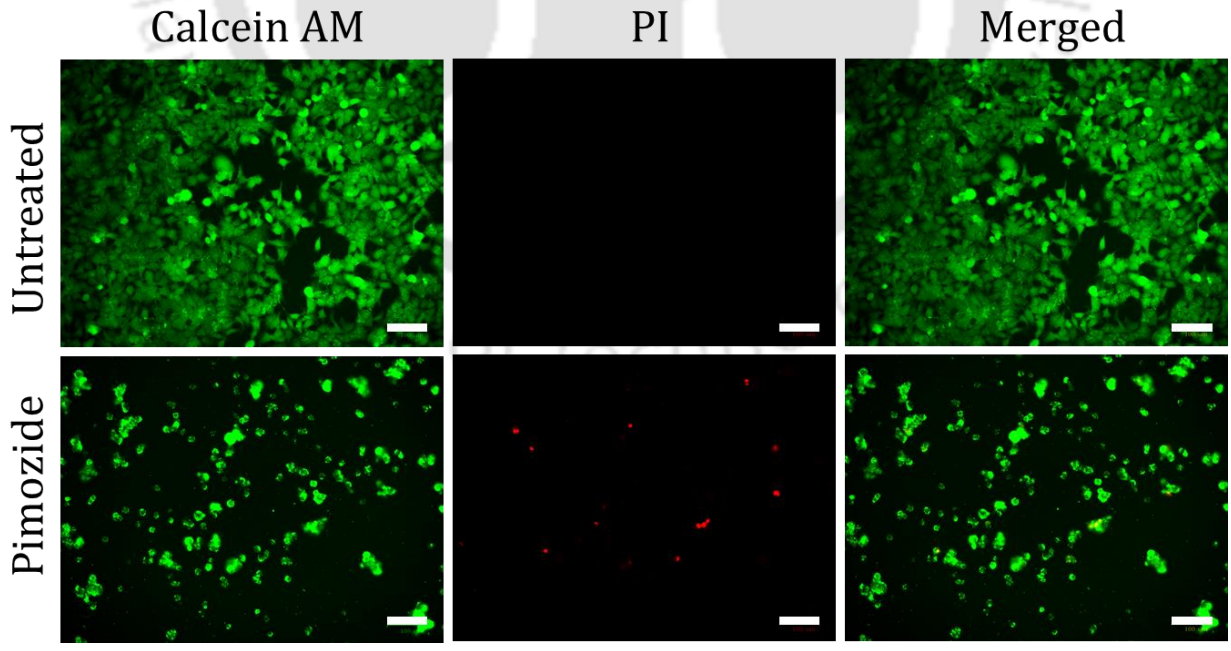

Figure 5.14: *Live/dead cell imaging of MCF-7 cell line after 48 h treatment with IC_{50} concentration of free Pimozide. Scale 100 µm.*

5.3.6. Network analysis of Zn ion and Pimozide interactions

Further, to better understand the molecular interactions and biological targets of both Zn ions and Pimozide, a network analysis was conducted. The STITCH database analysis yielded a network of 50 prominent protein interactions for Zn ions and Pimozide, illustrating distinct yet potentially complementary mechanisms (**Figure 5.15**). Zn ions interacted with 47 proteins, focusing on pathways related to oxidative stress regulation, apoptosis, and metal ion transport. In contrast, Pimozide specifically interacted with the dopaminergic and serotonergic receptors DRD2, DRD3, and HTR7, alongside its known inhibition of insulin receptor (IR), integrin beta-1 (ITGB1), and CD36 (Kandasamy et al. 2024). Notably, the two compounds do not share interactors, highlighting distinct targets that may produce a synergistic effect when used in combination. Zn ions demonstrated interactions with proteins central to oxidative stress management, apoptosis, and ion transport, including SOD1 and SOD3 (superoxide dismutases), CASP3 (caspase-3), and SLC30A1 (a zinc transporter). These proteins are crucial for inducing oxidative stress and apoptosis in cancer cells, which could lead to cancer cell death. The interactions of Zn with catalase (CAT) and thioredoxin (TXN) further point to its involvement in redox balance and the potential to disrupt cellular homeostasis in tumor environments. The association with HSP90AA1 and SNAP25 suggests the role of Zn in impacting protein folding and neurotransmitter signalling, respectively, further broadening its mechanistic pathways relevant to cancer therapeutics. The interactions of Pimozide with DRD2, DRD3, and HTR7 highlight its influence on dopaminergic and serotonergic pathways, potentially inhibiting cancer cell survival through receptor-mediated signaling. Additionally, the known inhibitory effects of Pimozide on IR, ITGB1, and CD36 suggest additional mechanisms relevant to cancer progression. IR inhibition may disrupt cancer cell metabolism, while ITGB1 impacts cell adhesion and migration, and CD36 relates to lipid metabolism and fatty acid uptake, key components in the metastatic process of cancer cells.

The distinct and non-overlapping targets of Zn and Pimozide suggest a potential for synergistic anti-cancer effects. The role of Zn in inducing oxidative stress and promoting apoptosis complements the modulation of signaling pathways critical to cancer survival and metastasis by Pimozide. By disrupting cellular redox balance and triggering apoptotic pathways, Zn may enhance the efficacy of Pimozide in inhibiting receptors and signaling networks. This complementary interaction strategy supports a multi-targeted approach for breast cancer treatment,

aiming to hinder survival pathways at multiple levels and potentially reduce the likelihood of resistance development.

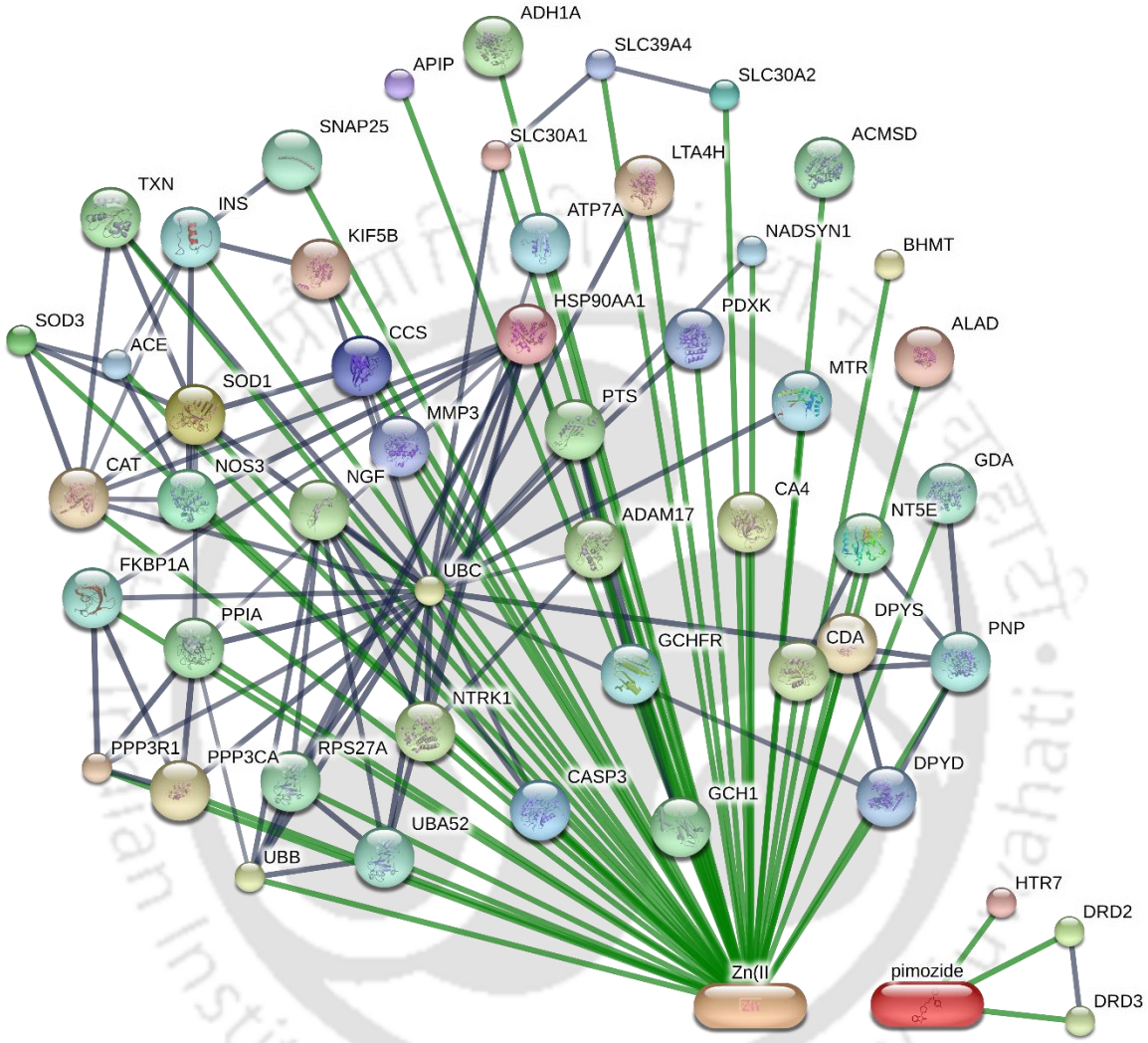

Figure 5.15. *Network analysis of Zn ion and Pimozide with cellular proteins by STITCH database*

5.3.7. In-Silico Toxicity Evaluation of Pimozide and ZIF-8

The *in-silico* toxicity prediction using the ProTox-II platform provided detailed toxicity profiles for both Pimozide and ZIF-8, aiding in the assessment of their compatibility and safety for use in targeted breast cancer therapy. Pimozide demonstrated significant risks in multiple toxicity categories, including neurotoxicity, hepatotoxicity, nephrotoxicity, and cardiotoxicity (**Figure 5.16 A-B**). The prediction results confirm that Pimozide carries a high potential for off-target side effects, particularly within cardiovascular and central nervous system tissues. Additionally,

Pimozide exhibited inhibitory effects on key cytochrome P450 enzymes (CYP3A4, CYP2D6, CYP1A2), which could increase the risk of adverse interactions if combined with other drugs metabolized by these pathways. This profile aligns with clinical observations of Pimozide toxicity, emphasizing the importance of a controlled delivery approach to mitigate systemic exposure (Finder et al., 1976).

In contrast to Pimozide, ZIF-8 exhibited a low-risk toxicity profile, showing no significant risks in neurotoxicity, immunotoxicity, or hepatotoxicity and minimal interaction with CYP450 enzymes (**Figure 5.16 C-D**). The low cytotoxicity of ZIF-8 at neutral pH supports its role as a safe carrier for targeted drug delivery, particularly as its acid-sensitive framework facilitates drug release predominantly in the acidic tumor microenvironment (TME). The biocompatibility and minimal interaction with drug-metabolizing enzymes underscore suitability of ZIF-8 as a nanocarrier, reducing the likelihood of metabolic competition with Pimozide and allowing for a more targeted and sustained delivery within cancerous tissues.

The complementary toxicity profiles of Pimozide and ZIF-8 highlight the potential advantages of using ZIF-8 to encapsulate Pimozide. Encapsulation may alleviate some of the systemic risks associated with Pimozide by ensuring controlled, localized release in the TME. The absence of CYP450 inhibition by ZIF-8 also reduces the risk of metabolic interactions, allowing Pimozide to be delivered effectively within the acidic TME while minimizing off-target toxicity. The *in-silico* toxicity assessment supports the feasibility of using ZIF-8 as a safe, effective nanocarrier for Pimozide. To further mitigate the potential neurotoxic effects of Pimozide, strategies such as dose optimization and sustained release formulations can be employed to limit peak plasma concentrations and reduce systemic exposure. Additionally, targeted delivery through ZIF-8 ensures that Pimozide is preferentially released in the tumor site rather than normal tissues, lowering the risk of neurological side effects. These mitigation strategies reinforce the therapeutic potential of Pimozide-ZIF-8 while addressing key safety concerns. This computational analysis aligns with the experimental cytotoxicity studies, underscoring the promise of this targeted delivery approach in breast cancer therapy.

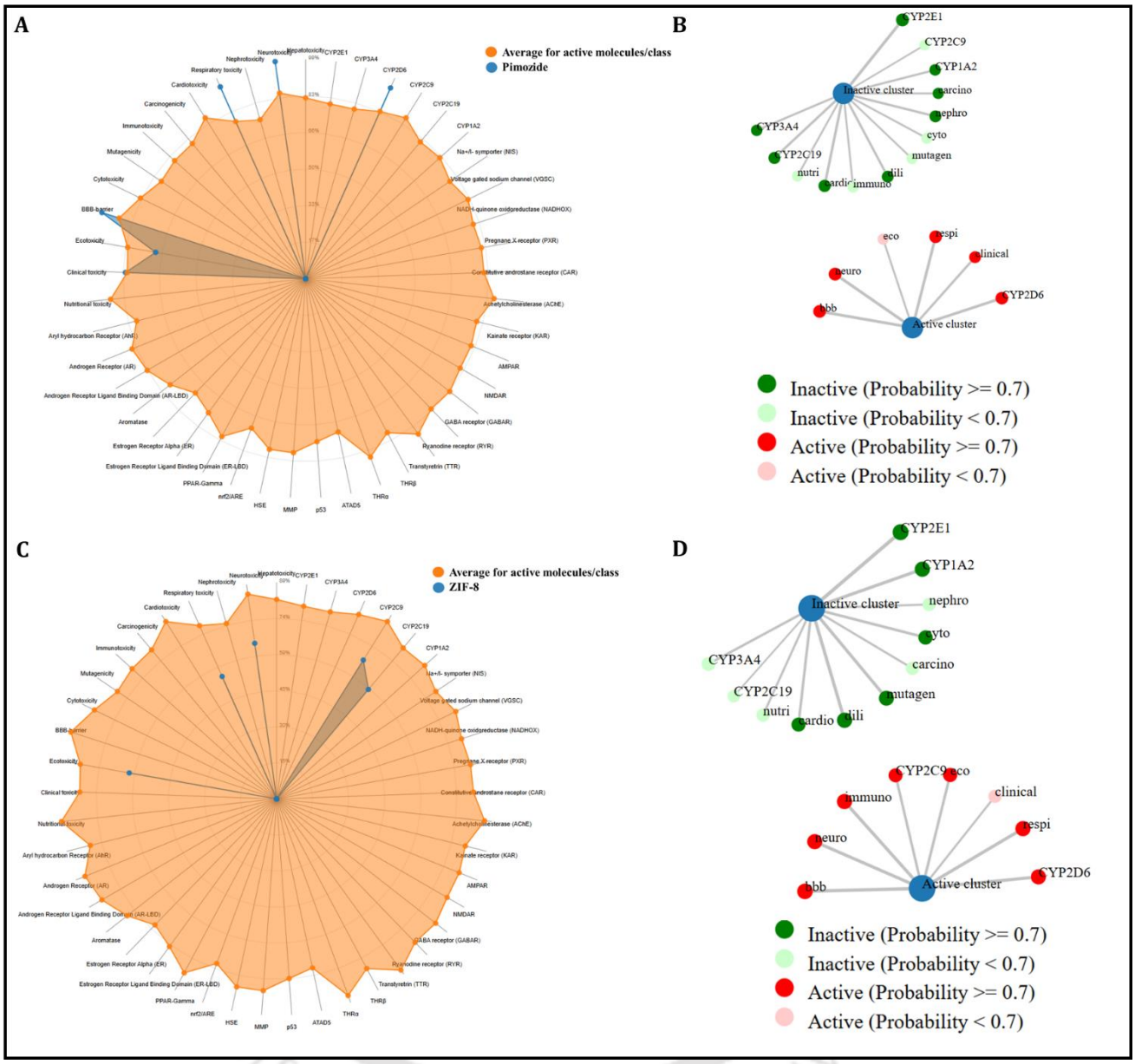

Figure 5.16. *In silico toxicity assessment of Pimozide and ZIF-8.* ***(A)*** *Radar chart depicting the toxicity profile of Pimozide, summarizing its predicted effects on hepatotoxicity, neurotoxicity, nephrotoxicity, immunotoxicity, and its interactions with cytochrome P450 enzymes.* ***(B)*** *Molecular interaction network of Pimozide showing interactions with key biomolecules and associated toxicological endpoints.* ***(C)*** *Radar chart representing the toxicity profile of ZIF-8, highlighting toxicity predictions for hepatic, renal, neuro, and immune systems, as well as interactions with cytochrome P450 enzymes.* ***(D)*** *Interaction network of ZIF-8 with potential biomolecular targets, emphasizing its predicted toxicity pathways and possible implications in biomedical applications.*

5.4. Discussion

The complex nature of breast cancer and resistance to conventional treatments highlight the urgent need for synergistic therapeutic approaches that go beyond monotherapy. In this study, a dual-action approach was explored by encapsulating Pimozide, a repurposed antipsychotic drug, within ZIF-8 nanoparticles. The drug delivery abilities of ZIF-8 was utilized to create a synergistic therapeutic effect between the released Zn ions and Pimozide. This approach addresses the challenges of targeted drug delivery while simultaneously amplifying anticancer activity through combined mechanisms.

The comprehensive physicochemical characterization of ZIF-8 and Pimozide-ZIF-8 provided crucial insights into the development and encapsulation of the Nano-framework. Further, the pH-responsive characteristics of ZIF-8 triggered the maximum release of Pimozide under conditions mimicking the TME. Subsequent *in-vitro* experiments demonstrated enhanced cytotoxicity of Pimozide-ZIF-8 against MCF-7 cells through lowering the IC_{50} concentration compared to free Pimozide. Cellular assays confirmed increased intracellular ROS generation and apoptotic population. Additionally, ZIF-8 frameworks were found to induce lipid peroxidation-mediated ferroptosis under acidic conditions.

The exploration of the combinatory effect of ZIF-8 with the released Pimozide makes this study unique, unlike previous studies that focus solely on the drug delivery capabilities of ZIF-8. Moreover, the synergistic enhancement of therapeutic efficacy was emphasized through the dual mechanisms of pharmacological activity by Pimozide and the unique mode of cell death induced by decomposed ZIF-8. The integration of Zn ions released from ZIF-8 is particularly significant as they not only contribute to the structural integrity of ZIF-8 but also enhance the efficacy of the drug by inducing ferroptosis. This process complements the apoptotic pathways activated by Pimozide, demonstrating a potent synergistic effect. To better understand the molecular interactions and biological targets of both Zn ions and Pimozide, a network analysis was conducted. This analysis highlighted that Pimozide uniquely interacts with DRD2, DRD3, IR, ITGB1, CD36 and HTR7, while Zn ions engage a broad spectrum of proteins involved in oxidative stress regulation, apoptosis, and cell survival pathways. The network analysis underscores the distinct and complementary roles of Zn ions and Pimozide, suggesting that their combined action within the ZIF-8 framework may maximize therapeutic effects through multi-targeted interactions.

This insight into the multi-targeted interactions enhances the understanding of how ZIF-8-encapsulated Pimozide achieves its efficacy, as it addresses multiple cancer-related pathways concurrently.

Additionally, *in-silico* toxicity predictions were performed to assess the safety profile of the Pimozide-ZIF-8 formulation. The results aligned with clinically observed toxicities of Pimozide, confirming known neurotoxic and hepatotoxic risks while underscoring the need for careful monitoring in therapeutic applications. These findings highlight that while ZIF-8 holds promise as a drug carrier, attention to potential toxicity is essential to its safe implementation. To mitigate these risks, strategies like dose optimization, surface modification, and controlled release can be employed to improve biocompatibility and reduce toxicity *in vivo.* Unlike conventional ZIF-8-based systems that primarily focus on passive drug delivery, our Pimozide-ZIF-8 formulation offers multiple advantages, including higher encapsulation efficiency, enhanced stability, and a controlled pH-responsive release that ensures minimal premature drug leakage. Furthermore, it uniquely integrates the therapeutic effects of both Pimozide and Zn ions, leading to a significant reduction in IC50 and a dual-mode mechanism of apoptosis and ferroptosis, surpassing the efficacy of existing ZIF-8 drug delivery platforms. Importantly, Pimozide-ZIF-8 maintained its structural and functional integrity for at least three months, as confirmed by XRD, AFM, FTIR and FETEM analyses and retained biological activities for cytotoxicity, ROS, apoptosis assays. The long-term stability of our formulation aligns with reported studies on ZIF-8, further supporting its potential for extended storage and clinical applications.

Altogether, this study demonstrates the potential of ZIF-8 to act as a multifunctional platform for breast cancer therapy, facilitating synergistic drug-nanoparticle interactions. By integrating Zn-induced ferroptosis with apoptosis-driven effects by Pimozide, ZIF-8-Pimozide constructs may serve as an effective and targeted therapy against breast cancer, encouraging further exploration of metal-organic frameworks in cancer treatment.

5.5. Conclusion

In conclusion, the Pimozide-ZIF-8 formulation shows significant promise as an advanced drug delivery system with targeted anti-cancer activity. The structural and physicochemical analyses confirmed successful encapsulation of Pimozide within the ZIF-8 matrix, resulting in a pH-responsive delivery platform capable of releasing the drug preferentially in the acidic tumor microenvironment. This controlled release is critical for enhancing the efficacy of Pimozide while minimizing potential off-target effects in normal physiological conditions. The *in vitro* studies demonstrated that Pimozide-ZIF-8 exhibits increased cytotoxicity at pH 6, with synergistic effects that are likely attributed to the release of Zn ions, which further contribute to cell death through mechanisms like ferroptosis. This dual mechanism of action – combining the intrinsic apoptotic effects of Pimozide with the ferroptosis induced by Zn ions – provides a unique approach to overcome resistance in cancer cells and improve therapeutic outcomes. Furthermore, the Pimozide-ZIF-8 formulation maintained the capacity of Pimozide to induce reactive oxygen species (ROS) generation, which is a key factor in promoting apoptosis. The increased lipid peroxidation observed in treated cells also confirms the role of ferroptosis, offering an additional pathway to target cancer cells. These findings suggest that Pimozide-ZIF-8 could be particularly effective against solid tumors where the acidic microenvironment and elevated ROS levels create conditions conducive to the proposed mechanism of action. Overall, Pimozide-ZIF-8 represents a novel strategy that leverages the benefits of pH-sensitive drug release, enhanced cytotoxicity, and the induction of both apoptotic and ferroptosis cell death pathways.

5.6. References

1. Xiao, P., Li, C., Liu, Y., Gao, Y., Liang, X., Liu, C., & Yang, W. (2024). The role of metal ions in the occurrence, progression, drug resistance, and biological characteristics of gastric cancer. Frontiers in Pharmacology, 15, 1333543. https://doi.org/10.3389%2Ffphar.2024.1333543
2. Wang, Y., Gao, F., Zhao, L., Wu, Y., Li, C., Li, H., & Jiang, Y. (2024). Enhancing cancer treatment via “Zn2+ interference” with Zn-based nanomaterials. Coordination Chemistry Reviews, 500, 215535. http://dx.doi.org/10.1016/j.ccr.2023.215535
3. Chen, P. H., & Chi, J. T. (2021). Unexpected zinc dependency of ferroptosis: what is in a name?. Oncotarget, 12(12), 1126. https://doi.org/10.18632%2Foncotarget.27951

4. Chen, P. H., Wu, J., Xu, Y., Ding, C. K. C., Mestre, A. A., Lin, C. C., & Chi, J. T. (2021). Zinc transporter ZIP7 is a novel determinant of ferroptosis. Cell death & disease, 12(2), 198. https://doi.org/10.1038/s41419-021-03482-5
5. Zhang, C., Liu, Z., Zhang, Y., Ma, L., Song, E., & Song, Y. (2020). "Iron free" zinc oxide nanoparticles with ion-leaking properties disrupt intracellular ROS and iron homeostasis to induce ferroptosis. Cell Death & Disease, 11(3), 183. https://doi.org/10.1038/s41419-020-2384-5
6. Nguyen, H. V. T., Pham, S. N., Mirzaei, A., Mai, N. X. D., Nguyen, C. C., Nguyen, H. T., & Doan, T. L. H. (2024). Surface modification of ZIF-8 nanoparticles by hyaluronic acid for enhanced targeted delivery of quercetin. Colloids and Surfaces A: Physicochemical and Engineering Aspects, 696, 134288. https://doi.org/10.1016/j.colsurfa.2024.134288
7. Pham, T. Q., Nguyen, T. T., Van Nguyen, H., Do, H. H., Linh, T. H., Pham, H. T. T., & Doan, T. L. H. (2024). Nanoscale ZIF-8 as an efficient carboplatin carrier for targeted cancer therapy. Inorganic Chemistry Communications, 165, 112567. https://doi.org/10.1016/j.inoche.2024.112567
8. Nguyen, D. T., Nguyen, L. D. T., Pham, Q. T., Le, T. M., Le, B. Q. G., Mai, N. X. D., & Nguyen, L. H. T. (2021). Zeolitic imidazolate frameworks as an efficient platform for potential curcumin-based on/off fluorescent chemosensor. Microporous and Mesoporous Materials, 327, 111445. https://doi.org/10.1016/j.micromeso.2021.111445
9. Zhang, S., Li, J., Yan, L., You, Y., Zhao, F., Cheng, J., & Li, Y. (2023). Zeolitic imidazolate framework-8 (ZIF-8) as a drug delivery vehicle for the transport and release of telomerase inhibitor BIBR 1532. Nanomaterials, 13(11), 1779. https://doi.org/10.3390/nano13111779
10. Lopes, C. M., Barata, P., & Oliveira, R. (2018). Chapter 5. Stimuli-responsive nanosystems for drugtargeted delivery. Drug Targeting and Stimuli Sensitive Drug Delivery Systems, William Andrew Publishing, 55-209. https://doi.org/10.1016/B978-0-12-813689-8.00005-7
11. Tiwari, A., Singh, A., Garg, N., & Randhawa, J. K. (2017). Curcumin encapsulated zeolitic imidazolate frameworks as stimuli responsive drug delivery system and their interaction with biomimetic environment. Scientific reports, 7(1), 12598. https://doi.org/10.1038/s41598-017-12786-6

12. Vlachos, N., Lampros, M., Voulgaris, S., & Alexiou, G. A. (2021). Repurposing antipsychotics for cancer treatment. Biomedicines, 9(12), 1785. https://doi.org/10.3390/biomedicines9121785
13. Navari, R. M. (2016). Olanzapine for the prevention of chemotherapy-induced nausea and vomiting. Management of Chemotherapy-Induced Nausea and Vomiting: New Agents and New Uses of Current Agents, 107-120. https://doi.org/10.1056/NEJMoa1515725
14. Chopko, T. C., & Lindsley, C. W. (2018). Classics in chemical neuroscience: risperidone. ACS chemical neuroscience, 9(7), 1520-1529. https://doi.org/10.1021/acschemneuro.8b00159
15. Prommer, E. (2017). Aripiprazole: a new option in delirium. American Journal of Hospice and Palliative Medicine®, 34(2), 180-185. https://doi.org/10.1177/1049909115612800
16. Schmid, C. L., Streicher, J. M., Meltzer, H. Y., & Bohn, L. M. (2014). Clozapine acts as an agonist at serotonin 2A receptors to counter MK-801-induced behaviors through a βarrestin2-independent activation of Akt. Neuropsychopharmacology, 39(8), 1902-1913. https://doi.org/10.1038/npp.2014.38
17. Kandasamy, T., Sarkar, S., Sen, P., Venkatesh, D., & Ghosh, S. S. (2024). Concurrent inhibition of IR, ITGB1, and CD36 perturbated the interconnected network of energy metabolism and epithelial-to-mesenchymal transition in breast cancer cells. Journal of cellular biochemistry. https://doi.org/10.1002/jcb.30574
18. Li, J., Qu, P., Zhou, X. Z., Ji, Y. X., Yuan, S., Liu, S. P., & Zhang, Q. G. (2022). Pimozide inhibits the growth of breast cancer cells by alleviating the Warburg effect through the P53 signaling pathway. Biomedicine & Pharmacotherapy, 150, 113063. https://doi.org/10.1016/j.biopha.2022.113063
19. Yao, Y., Zhou, Y., Liu, L., Xu, Y., Chen, Q., Wang, Y., & Shao, A. (2020). Nanoparticle-based drug delivery in cancer therapy and its role in overcoming drug resistance. Frontiers in molecular biosciences, 7, 193. https://doi.org/10.3389%2Ffmolb.2020.00193
20. Arora, N., Shome, R., & Ghosh, S. S. (2019). Deciphering therapeutic potential of PEGylated recombinant PTEN-silver nanoclusters ensemble on 3D spheroids. Molecular Biology Reports, 46(5), 5103-5112. https://doi.org/10.1007/s11033-019-04965-7
21. Park, K. S., Ni, Z., Côté, A. P., Choi, J. Y., Huang, R., Uribe-Romo, F. J., & Yaghi, O. M. (2006). Exceptional chemical and thermal stability of zeolitic imidazolate frameworks.

Proceedings of the National Academy of Sciences, 103(27), 10186-10191. https://doi.org/10.1073/pnas.0602439103

22. Pan, Y., Liu, Y., Zeng, G., Zhao, L., & Lai, Z. (2011). Rapid synthesis of zeolitic imidazolate framework-8 (ZIF-8) nanocrystals in an aqueous system. Chemical Communications, 47(7), 2071-2073. https://doi.org/10.1039/c0cc05002d
23. Schejn, A., Balan, L., Falk, V., Aranda, L., Medjahdi, G., & Schneider, R. (2014). Controlling ZIF-8 nano-and microcrystal formation and reactivity through zinc salt variations. CrystEngComm, 16(21), 4493-4500. https://doi.org/10.1039/C3CE42485E
24. Butonova, S. A., Ikonnikova, E. V., Sharsheeva, A., Chernyshov, I. Y., Kuchur, O. A., Mukhin, I. S., & Morozov, M. I. (2021). Degradation kinetic study of ZIF-8 microcrystals with and without the presence of lactic acid. RSC advances, 11(62), 39169-39176. https://doi.org/10.1039/D1RA07089D
25. Ettlinger, R., Moreno, N., Volkmer, D., Kerl, K., & Bunzen, H. (2019). Zeolitic imidazolate framework-8 as pH-sensitive nanocarrier for "Arsenic Trioxide" drug delivery. Chemistry–A European Journal, 25(57), 13189-13196. https://doi.org/10.1002/chem.201902599
26. Tran, V. A., & Lee, S. W. (2021). pH-triggered degradation and release of doxorubicin from zeolitic imidazolate framework-8 (ZIF8) decorated with polyacrylic acid. RSC advances, 11(16), 9222-9234. https://doi.org/10.1039%2Fd0ra10423j
27. Shan, X., Li, S., Sun, B., Chen, Q., Sun, J., He, Z., & Luo, C. (2020). Ferroptosis-driven nanotherapeutics for cancer treatment. Journal of controlled release, 319, 322-332. https://doi.org/10.1016/j.jconrel.2020.01.008
28. Finder, R. M., Brogden, R. N., Sawyer, P. R., Speight, T. M., Spencer, R., & Avery, G. S. (1976). Pimozide: a review of its pharmacological properties and therapeutic uses in psychiatry. Drugs, 12, 1-40. https://doi.org/10.2165/00003495-197612010-00001

Conclusion & Future prospects

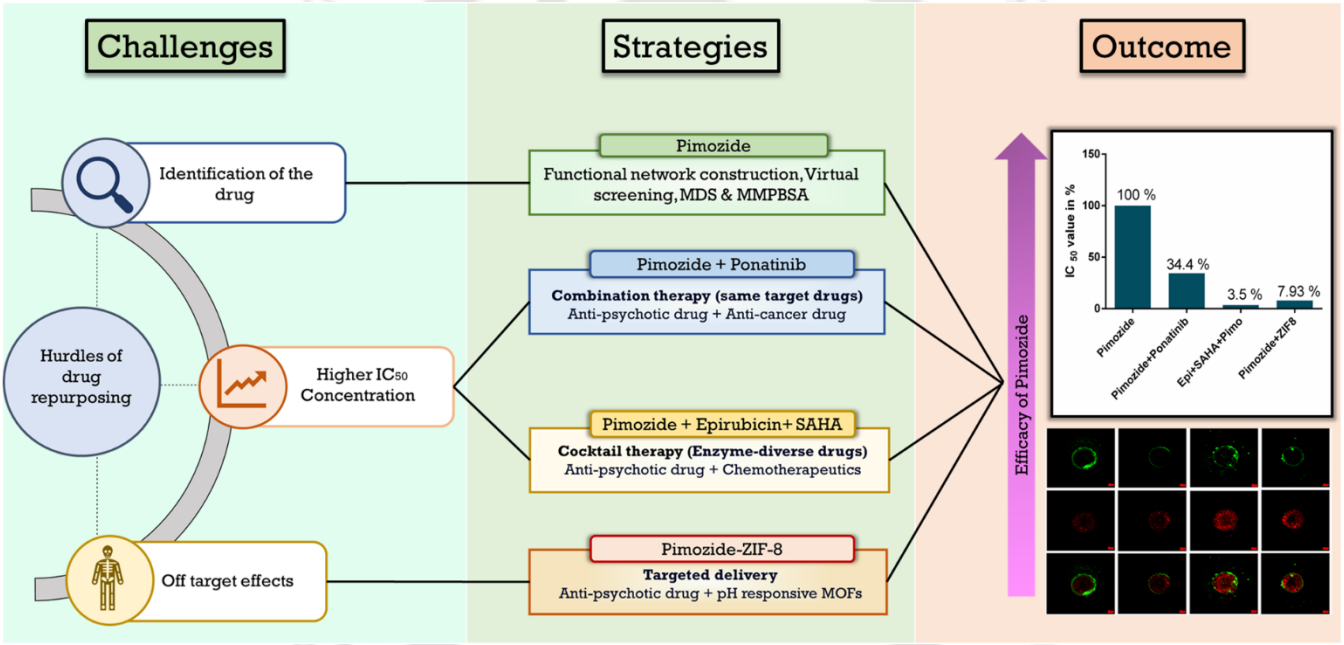

The artwork summarizes the important findings and the possible future prospects of the thesis work.

Conclusion & Future prospects

The current thesis work presents a multi-faceted approach to breast cancer therapy, addressing complex aspects of tumor progression, resistance mechanisms, and treatment efficacy through innovative repurposing, combination strategies, and advanced delivery methods. By targeting the interlinked metabolic and epithelial-to-mesenchymal transition (EMT) pathways, the research underscores the importance of disrupting key processes that contribute to metastasis, resistance, and tumor resilience. Findings across each chapter illustrate the potential of combining repurposed drugs and innovative delivery platforms to increase treatment efficacy while minimizing systemic toxicity, addressing key challenges in current breast cancer therapies.

In the initial phase, computational studies were pivotal in identifying Insulin Receptor (IR), Integrin Beta 1 (ITGB1), and CD36 as significant targets in the metabolic and EMT network, leading to the discovery of potential inhibitors such as Pimozide and Ponatinib. Further *in vitro* experiments confirmed the effectiveness of Pimozide in reducing breast cancer cell proliferation and its promising selectivity for EMT phenotypes. The synergistic combination of Pimozide and Ponatinib demonstrated substantial inhibition of cancer cell metabolism and EMT, highlighting the therapeutic potential of this dual-drug approach. Moreover, the ESP (Epirubicin, SAHA, and Pimozide) cocktail therapy reduced the IC_{50} of Pimozide and induced apoptosis through both ROS production and intrinsic pathways, achieving enhanced efficacy and lower toxicity. The final phase of this study focused on ZIF-8, a pH-sensitive drug delivery system, which successfully encapsulated Pimozide and released it in the acidic tumor microenvironment mimic conditions. The ZIF-8 and Pimozide combination exhibited synergistic activity, as the ZIF-8 matrix not only enhanced the controlled release of Pimozide at the tumor site but also amplified its therapeutic action while reducing systemic toxicity.

Comparing these strategies, the ESP cocktail therapy emerged as the most effective, due to its substantial IC_{50} reduction, robust apoptotic effects, and superior efficacy in luminal breast cancer cells, establishing it as the top-ranked approach. Following this, the Pimozide-Ponatinib combination ranks second for its significant inhibition of EMT and cancer metabolism, though it presents dosing challenges. Finally, ZIF-8-mediated delivery of Pimozide ranks third, demonstrating targeted release and reduced toxicity, although its therapeutic effects are less

pronounced alone. Together, these results suggest that a multi-targeted approach that combines the unique strengths of repurposed drugs, combination therapies, and advanced delivery mechanisms offers a promising avenue for breast cancer treatment. This research paves the way for future studies to further optimize these strategies, ultimately contributing to more effective and safer therapeutic options in breast cancer care.

Furthermore, this multi-pronged therapeutic approach may hold immunological implications, particularly in the context of immunologically "cold" tumors like triple-negative breast cancer. EMT is a key driver of immune evasion via upregulation of PD-L1 and downregulation of antigen presentation machinery. The reversal of EMT through the proposed therapies could therefore mitigate immune suppression and enhance responsiveness to immune checkpoint blockade. Additionally, the induction of ferroptosis by the ZIF-8-Pimozide formulation suggests potential for immunogenic cell death (ICD), supported by Zn-mediated oxidative stress and lipid peroxidation. The role of ZIF-8 in modulating macrophage polarization and inflammasome signaling also opens translational opportunities in immuno-oncology. These perspectives position the developed strategies as not only anti-proliferative but also immuno-sensitizing, laying the foundation for future combination with cancer immunotherapies

Future Prospects

1. **Refinement of Computational Screening Approaches**: Enhancing computational approaches for identifying drug targets and synergistic compounds could improve drug discovery and optimization. Integrating machine learning algorithms and large datasets could lead to the identification of even more effective drug combinations and their potential off-target effects.
2. **Clinical Validation of Repurposed Drug Combinations**: Building on the promising preclinical data, future studies should focus on advancing these drug combinations, particularly the Pimozide-Ponatinib and ESP combinations, through clinical trials. Evaluating their efficacy and safety in patients will provide insight into their potential for routine clinical use in breast cancer treatment.
3. **Mechanistic Studies on Metabolic and EMT Pathways**: Further studies on the interplay between metabolic reprogramming and EMT in various breast cancer subtypes could help tailor targeted therapies to patient-specific tumor biology, enhancing treatment precision and efficacy.
4. **Integration with Immunotherapy Platforms:** Future work should explore the integration of EMT-reversing and ferroptosis-inducing strategies with existing immunotherapies. Specifically, evaluating biomarkers of immunogenic cell death (e.g., calreticulin, HMGB1) and the influence of ZIF-8 nanoparticles on innate immune pathways such as macrophage polarization could provide deeper insights into their potential in immuno-oncology.
5. **Expansion to Other Cancer Types**: Given the broad role of metabolic and EMT signaling in other cancers, these findings could inform similar therapeutic approaches beyond breast cancer, laying a foundation for broader oncology applications.
6. **Long-term Toxicity and Resistance Studies**: Investigating the long-term effects of these therapies, particularly any potential for resistance development, will be essential to understanding their feasibility for long-term use and exploring modifications to counteract resistance mechanisms if they arise.

Publications

From thesis work

1. **Thirukumaran Kandasamy.,** Shilpi Sarkar., Azar Zochedh, Thandavarayan Kathiresan & Siddhartha Sankar Ghosh. (2025). Synergistic Effects of Epirubicin-Vorinostat-Pimozide Drug Cocktail on Proliferation, Stemness, Invasiveness, and Fatty Acid Metabolism in Breast Cancer Cells. ***IUBMB life,*** 77(5), e70020. https://doi.org/10.1002/iub.70020
2. **Thirukumaran Kandasamy.,** Shilpi Sarkar., & Siddhartha Sankar Ghosh. (2025). Synergistic Therapeutic Effects of Zn Ions and Pimozide in Breast Cancer Cells. ***Chemistry & Biodiversity***, e202402883. https://doi.org/10.1002/cbdv.202402883
3. **Thirukumaran Kandasamy.,** Shilpi Sarkar., & Siddhartha Sankar Ghosh. (2024). Harnessing Drug Repurposing to Combat Breast Cancer by Targeting Altered Metabolism and Epithelial-to-Mesenchymal Transition Pathways. ***ACS Pharmacology & Translational Science.*** https://doi.org/10.1021/acsptsci.4c00545
4. **Thirukumaran Kandasamy.,** Shilpi Sarkar., Plaboni Sen., Dheepika Venkatesh., & Siddhartha Sankar Ghosh. (2024). Concurrent inhibition of IR, ITGB1, and CD36 perturbated the interconnected network of energy metabolism and epithelial-to-mesenchymal transition in breast cancer cells. ***Journal of Cellular Biochemistry***. https://doi.org/10.1002/jcb.30574
5. **Thirukumaran Kandasamy.,** Plaboni Sen., & Siddhartha Sankar Ghosh. (2022). Multi-targeted drug repurposing approach for breast cancer via integrated functional network analysis. ***Molecular Informatics,*** 41(8), 2100300. https://doi.org/10.1002/minf.202100300

From Collaborative Work

1. Shilpi Sarkar., **Thirukumaran Kandasamy,** & Siddhartha Sankar Ghosh. (2025). Inhibition of the MLL1-WDR5 interaction modulates Epithelial to mesenchymal transition and metabolic pathways in triple-negative breast cancer cells. ***Biochemical and Biophysical Research Communications,*** 151559. https://doi.org/10.1016/j.bbrc.2025.151559
2. Sayantani Mukhopadhyay, **Thirukumaran Kandasamy,** Siddhartha S. Ghosh, & Parameswar Krishnan Iyer. Deciphering Therapeutic Targeting of Cathepsin B using Repurposed Drug Darifenacin. ***ChemMedChem,*** e202500117. https://doi.org/10.1002/cmdc.202500117
3. Dheepika Venkatesh, Shilpi Sarkar, **Thirukumaran Kandasamy**, and Siddhartha Sankar Ghosh. (2024). In-silico identification and validation of Silibinin as a Dual inhibitor for ENO1 and GLUT4 to curtail EMT Signaling and TNBC Progression. ***Computational Biology and Chemistry,*** 108312. https://doi.org/10.1016/j.compbiolchem.2024.108312
4. Shilpi Sarkar., **Thirukumaran Kandasamy,** & Siddhartha Sankar Ghosh. (2024). Imatinib Impedes EMT and Notch Signalling by Inhibiting p300 Acetyltransferase in Breast Cancer Cells. ***Molecular Carcinogenesis,*** 10.1002/mc.23848. Advance online publication. https://doi.org/10.1002/mc.23848
5. Priyam Ghosh, Sayantani Mukhopadhyay, **Thirukumaran Kandasamy**, Subrata Mondal, Parameswar K. Iyer, and Siddhartha Sankar Ghosh. (2025). Multifunctional Hydroxyquinoline-Derived Turn-on Fluorescent Probe for Alzheimer's Disease Detection and Therapy. ***Journal of Materials Chemistry B***. https://doi.org/10.1039/D4TB01740D
6. Shilpi Sarkar, Dheepika Venkatesh, **Thirukumaran Kandasamy**, and Siddhartha Sankar Ghosh. (2024). Epigenetic Modulations in Breast Cancer: An Emerging Paradigm in Therapeutic Implications. ***Frontiers in Bioscience-Landmark,*** 29(8), 287. https://doi.org/10.31083/j.fbl2908287
7. Parijat Dutta, Plaboni Sen, **Thirukumaran Kandasamy**, and Siddhartha Sankar Ghosh. (2024). Targeting AR-positive breast cancer cells via drug repurposing approach. ***Computational Biology and Chemistry,*** 108, 108007. https://doi.org/10.1016/j.compbiolchem.2023.108007

8. Arupam Patra, **Thirukumaran Kandasamy.,** Siddhartha Sankar Ghosh, & Gurvinder Kaur Saini . (2024). In vitro anticancer effects of recombinant anisoplin through activation of SAPK/JNK and downregulation of NFκB. ***Toxicology in Vitro,*** 94, 105737. https://doi.org/10.1016/j.tiv.2023.105737
9. Priyam Ghosh., Kamal Shokeen, Subrata Mondal, **Thirukumaran Kandasamy**, Sachin Kumar, Siddhartha Sankar Ghosh, and Parameswar Krishnan Iyer. (2024). Amyloid Targeting Red Emitting AIE Dots for Diagnostic and Therapeutic Application against Alzheimer's Disease. ***ACS Chemical Neuroscience,*** 15(2), 268-277. https://doi.org/10.1021/acschemneuro.3c00473
10. Arindam Sain., Dipshikha Khamrai, **Thirukumaran Kandasamy**, and Debdut Naskar (2023). Apigenin exerts anti-cancer effects in colon cancer by targeting HSP90AA1. ***Journal of Biomolecular Structure and Dynamics,*** 1-13. https://doi.org/10.1080/07391102.2023.2299305
11. Anjela Xalxo., Ujjwal Jyoti Goswami, Shilpi Sarkar, **Thirukumaran Kandasamy**, Kriti Mehta, Siddhartha S. Ghosh, Prasad V. Bharatam, and Abu T. Khan. (2023). Synthesis of 3-sulfenylindole derivatives from 4-hydroxy-2H-chromene-2-thione and indole using oxidative cross-dehydrogenative coupling reaction and anti-proliferative activity study of some of their sulfone derivatives. ***Bioorganic Chemistry,*** 141, 106900. https://doi.org/10.1016/j.bioorg.2023.106900
12. Shilpi Sarkar., **Thirukumaran Kandasamy,** Rajib Shome, and Siddhartha Sankar Ghosh. (2023). In silico screening and identification of potential drug against p300 acetyltransferase activity in breast cancer via drug repurposing approach. ***Journal of Biomolecular Structure and Dynamics,*** 1-12. https://doi.org/10.1080/07391102.2023.2270086
13. Suchandra Roy Acharyya., Plaboni Sen, **Thirukumaran Kandasamy,** and Siddhartha Sankar Ghosh. (2023). Designing of disruptor molecules to restrain the protein–protein interaction network of VANG1/SCRIB/NOS1AP using fragment-based drug discovery techniques. ***Molecular Diversity,*** 27(3), 989-1010. https://doi.org/10.1007/s11030-022-10462-0
14. Plaboni Sen., **Thirukumaran Kandasamy,** and Siddhartha Sankar Ghosh. (2023). Multi-targeting TACE/ADAM17 and gamma-secretase of notch signalling pathway in TNBC via

drug repurposing approach using Lomitapide. ***Cellular Signalling,*** 102, 110529. https://doi.org/10.1016/j.cellsig.2022.110529

15. Arindam Sain., **Thirukumaran Kandasamy,** and Debdut Naskar. (2023). Targeting UNC-51-like kinase 1 and 2 by lignans to modulate autophagy: Possible implications in metastatic colorectal cancer. ***Molecular Diversity,*** 27(1), 27-43. https://doi.org/10.1007/s11030-022-10399-4
16. Sundaramahalingam, M. A., Amrutha, C., Rajeshbanu, J., **Thirukumaran Kandasamy**., Manibalan, S., Ashokkumar, M., & Sivashanmugam, P. (2023). In silico approach for enhancing innate lipid content of Yarrowia lipolytica, by blocking the acyl-CoA oxidase-1 enzyme, using various analogous compounds of lipids. ***Journal of Biomolecular Structure and Dynamics***, 41(2), 511-524. https://doi.org/10.1080/07391102.2021.2008498
17. Plaboni Sen., **Thirukumaran Kandasamy,** and Siddhartha Sankar Ghosh. (2022). In-silico evidence of ADAM metalloproteinase pathology in cancer signaling networks. ***Journal of Biomolecular Structure and Dynamics,*** 40(22), 11771-11786. https://doi.org/10.1080/07391102.2021.1964602
18. Arindam Sain., **Thirukumaran Kandasamy,** and Debdut Naskar. (2022). In silico approach to target PI3K/Akt/mTOR axis by selected Olea europaea phenols in PIK3CA mutant colorectal cancer. ***Journal of Biomolecular Structure and Dynamics,*** 40(21), 10962-10977. https://doi.org/10.1080/07391102.2021.1953603
19. Suchandra Roy Acharyya., Plaboni Sen, **Thirukumaran Kandasamy,** and Siddhartha Sankar Ghosh. (2022). Dual therapeutic approach to modulate Glycogen Synthase kinase−3 beta (GSK-3B) and inhibitor of nuclear factor kappa kinase-beta (IKK-β) receptors by in silico designing of inhibitors. ***Journal of Molecular Graphics and Modelling,*** 115, 108225. https://doi.org/10.1016/j.jmgm.2022.108225
20. Arindam Sain., Dipshikha Khamrai, **Thirukumaran Kandasamy**, and Debdut Naskar (2022). Targeting protein tyrosine phosphatase 1B in obesity-associated colon cancer: Possible role of sweet potato (Ipomoea batatas). ***Proteins: Structure, Function, and Bioinformatics,*** 90(6), 1346-1362. https://doi.org/10.1002/prot.26316
21. Soumen Barman, Anirban Roy, Ishita Bardhan, **Thirukumaran Kandasamy,** Shivani Shivani, and Babu Sudhamalla (2021). Insights into the molecular mechanisms of histone

code recognition by the BRPF3 bromodomain. ***Chemistry–An Asian Journal***, 16(21), 3404-3412. https://doi.org/10.1002/asia.202100793

22. Arun Baskaran Jayaraman., **Thirukumaran Kandasamy**., Dilip Venkataraman., & Meenakshisundaram, S. (2021). Rational design of Shewanella sp. L-arabinose isomerase for D-galactose isomerase activity under mesophilic conditions. ***Enzyme and Microbial Technology,*** 147, 109796. https://doi.org/10.1016/j.enzmictec.2021.109796
23. Manibalan, S., **Thirukumaran Kandasamy**., Varshni, M., Shobana, A., & Achary, A. (2020). Report on biopharmaceutical profile of recent biotherapeutics and insilco docking studies on target bindings of known aptamer biotherapeutics. ***Biotechnology and Genetic Engineering Reviews,*** 36(2), 57-80. https://doi.org/10.1080/02648725.2020.1858395
24. Manibalan, Subramaniyan, Ayyachamy Shobana, Manickam Kiruthika, Anant Achary, Madasamy Swathi, Renganathan Venkatalakshmi, Kandasamy **Thirukumaran Kandasamy**. Suhasini, and Sharon Roopathy. (2020) Protein network studies on PCOS biomarkers with S100A8, druggability assessment, and RNA aptamer designing to control its cyst migration effect. ***Frontiers in bioengineering and biotechnology***, 8, 328. https://doi.org/10.3389/fbioe.2020.00328

Workshops/Conferences Attended

1. **Participated** in SCIENTIFIQUE; ORAL PRESENTATION entitled "*Perturbation of metabolic and EMT networks in breast cancer cells: A polypharmacological approach*" in Research and Industrial Conclave 2024 during 9th -11th August, 2024; organized by IIT Guwahati.
2. **Participated** in SCIENTIFIQUE; 3 MINUTE THESIS PRESENTATION entitled "*Multi-faceted approach for breast cancer therapy: Drug repurposing, synergistic combinations and pH responsive delivery*" in Research and Industrial Conclave 2024 during 9th -11th August, 2024; organized by IIT Guwahati.
3. **Participated** in POSTER PRESENTATION entitled "*pH-controlled release of a repurposed drug within breast cancer tumor microenvironment mimic conditions using Nano frameworks*" in InJaNa 2024 during 23rd - 25th April, 2024; organized by IIT Roorkee. [**Best Poster award**]
4. **Participated** in POSTER PRESENTATION entitled "*Therapeutic targeting of EMT and metabolic pathways in breast cancer via drug repurposing approach*" in Research and Industrial Conclave 2023 during 14th -16th May 2023; organized by IIT Guwahati. [**Best Poster award]**
5. **Resource person** at the offline workshop titled **"Hands-on workshop on basic flow cytometry"** conducted by BioNEST, IIT Guwahati Technology Innovation and Development foundation on January 18th, 2023.

Rights & Permissions

RightsLink

Harnessing Drug Repurposing to Combat Breast Cancer by Targeting Altered Metabolism and Epithelial-to-Mesenchymal Transition Pathways

ACS Publications
Most Trusted. Most Cited. Most Read.

Author: Thirukumaran Kandasamy, Shilpi Sarkar, Siddhartha Sankar Ghosh
Publication: ACS Pharmacology & Translational Science
Publisher: American Chemical Society
Date: Dec 1, 2024

PERMISSION/LICENSE IS GRANTED FOR YOUR ORDER AT NO CHARGE

This type of permission/license, instead of the standard Terms and Conditions, is sent to you because no fee is being charged for your order. Please note the following:

- Permission is granted for your request in both print and electronic formats, and translations.
- If figures and/or tables were requested, they may be adapted or used in part.
- Please print this page for your records and send a copy of it to your publisher/graduate school.
- Appropriate credit for the requested material should be given as follows: "Reprinted (adapted) with permission from {COMPLETE REFERENCE CITATION}. Copyright {YEAR} American Chemical Society." Insert appropriate information in place of the capitalized words.
- One-time permission is granted only for the use specified in your RightsLink request. No additional uses are granted (such as derivative works or other editions). For any uses, please submit a new request.

If credit is given to another source for the material you requested from RightsLink, permission must be obtained from that source.

BACK CLOSE WINDOW

JOHN WILEY AND SONS LICENSE
TERMS AND CONDITIONS

Dec 20, 2024

This Agreement between Thirukumaran Kandasamy ("You") and John Wiley and Sons ("John Wiley and Sons") consists of your license details and the terms and conditions provided by John Wiley and Sons and Copyright Clearance Center.

License Number	5933051017402
License date	Dec 20, 2024
Licensed Content Publisher	John Wiley and Sons
Licensed Content Publication	Molecular Informatics
Licensed Content Title	Multi-targeted Drug Repurposing Approach for Breast Cancer via Integrated Functional Network Analysis
Licensed Content Author	Siddhartha Sankar Ghosh, Plaboni Sen, Thirukumaran Kandasamy
Licensed Content Date	Mar 11, 2022
Licensed Content Volume	41
Licensed Content Issue	8
Licensed Content Pages	17
Type of use	Dissertation/Thesis
Requestor type	Author of this Wiley article
Format	Print and electronic
Portion	Full article
Will you be translating?	No
Title of new work	A Multi-faceted Approach for Targeting Metabolic and EMT Networks in Breast Cancer Cells
Institution name	Indian Institute of Technology, Guwahati

JOHN WILEY AND SONS LICENSE
TERMS AND CONDITIONS

Dec 20, 2024

This Agreement between THIRUKUMARAN KANDASAMY ("You") and John Wiley and Sons ("John Wiley and Sons") consists of your license details and the terms and conditions provided by John Wiley and Sons and Copyright Clearance Center.

License Number	5907490049779
License date	Nov 14, 2024
Licensed Content Publisher	John Wiley and Sons
Licensed Content Publication	Journal of Cellular Biochemistry
Licensed Content Title	Concurrent inhibition of IR, ITGB1, and CD36 perturbated the interconnected network of energy metabolism and epithelial-to-mesenchymal transition in breast cancer cells
Licensed Content Author	Thirukumaran Kandasamy, Shilpi Sarkar, Plaboni Sen, et al
Licensed Content Date	May 5, 2024
Licensed Content Volume	125
Licensed Content Issue	7
Licensed Content Pages	19
Type of use	Dissertation/Thesis
Requestor type	Author of this Wiley article
Format	Print and electronic
Portion	Full article
Will you be translating?	No
Title of new work	A Multi-faceted Approach for Targeting Metabolic and EMT Networks in Breast Cancer Cells

JOHN WILEY AND SONS LICENSE
TERMS AND CONDITIONS

May 15, 2025

This Agreement between Thirukumaran Kandasamy ("You") and John Wiley and Sons ("John Wiley and Sons") consists of your license details and the terms and conditions provided by John Wiley and Sons and Copyright Clearance Center.

License Number	6030220439955
License date	May 15, 2025
Licensed Content Publisher	John Wiley and Sons
Licensed Content Publication	IUBMB Life
Licensed Content Title	Synergistic Effects of Epirubicin-Vorinostat-Pimozide Drug Cocktail on Proliferation, Stemness, Invasiveness, and Fatty Acid Metabolism in Breast Cancer Cells
Licensed Content Author	Thirukumaran Kandasamy, Shilpi Sarkar, Azar Zochedh, et al
Licensed Content Date	Apr 30, 2025
Licensed Content Volume	77
Licensed Content Issue	5
Licensed Content Pages	16

JOHN WILEY AND SONS LICENSE
TERMS AND CONDITIONS

May 15, 2025

This Agreement between Thirukumaran Kandasamy ("You") and John Wiley and Sons ("John Wiley and Sons") consists of your license details and the terms and conditions provided by John Wiley and Sons and Copyright Clearance Center.

License Number	6030220747933
License date	May 15, 2025
Licensed Content Publisher	John Wiley and Sons
Licensed Content Publication	Chemistry & Biodiversity
Licensed Content Title	Synergistic Therapeutic Effects of Zn Ions and Pimozide in Breast Cancer Cells
Licensed Content Author	Thirukumaran Kandasamy, Shilpi Sarkar, Siddhartha Sankar Ghosh
Licensed Content Date	Mar 21, 2025
Licensed Content Volume	0
Licensed Content Issue	0
Licensed Content Pages	15